

Development of a novel photocatalytic reactor for the treatment of polycyclic aromatic hydrocarbons.

GBADAMOSI, T.G.

2019

The author of this thesis retains the right to be identified as such on any occasion in which content from this thesis is referenced or re-used. The licence under which this thesis is distributed applies to the text and any original images only – re-use of any third-party content must still be cleared with the original copyright holder.

**DEVELOPMENT OF A NOVEL PHOTOCATALYTIC
REACTOR FOR THE TREATMENT OF POLYCYCLIC
AROMATIC HYDROCARBONS**

TAIYE GBENGA GBADAMOSI

PhD

2019

DEVELOPMENT OF A NOVEL PHOTOCATALYTIC REACTOR FOR THE TREATMENT OF POLYCYCLIC AROMATIC HYDROCARBONS

TAIYE GBENGA GBADAMOSI

A thesis submitted in partial fulfilment of the requirements of the Robert
Gordon University for degree of Doctor of Philosophy

February 2019

DECLARATION

I declare that the thesis has been composed solely by myself and presented herein is mine except where otherwise acknowledged, and this has not been submitted in any previous application degree or qualification at any other academic institution.

ACKNOWLEDGEMENT

My sincere gratitude to my wife (Olanike Gbadamosi) and mother (Lola Gbadamosi) for their support both emotional and financial towards this PhD

I like to thank my supervisors: Dr. Cathy McCullagh, Prof. Linda Lawton, Dr. Kyari Yates and Dr. Morgan Adams for their support, guidance, advice and supervision during this PhD.

TABLE OF CONTENTS

DECLARATION.....	2
ACKNOWLEDGEMENT	3
TABLE OF CONTENTS	4
LIST OF ABBREVIATIONS.....	9
LIST OF FIGURES	11
LIST OF TABLES	16
ABSTRACT	18
CHAPTER 1	20
1.0. WATER POLLUTION AND TREATMENTS.....	20
1.1. Introduction.....	20
1.2. Produced water discharge.....	21
1.2.1. Constituents of produced water.....	23
1.2.2. Produced water waste management	25
1.2. Polycyclic aromatic hydrocarbon	27
1.3.1. Discharge Limits and Legislation	29
1.3.1. Environmental Impact	30
1.4. Chitosan Biopolymer	31
1.4.1. Application of chitosan in pollutant remediation	34
1.5. Photocatalysis	35
1.5.1. Mechanism of photocatalysis	36
1.5.2. Photocatalytic application in water treatment.....	39
1.6 Photocatalytic photoreactor.....	39
1.6.1 Suspended photocatalyst reactor	41
1.6.2 Immobilized photocatalyst reactor.....	42
1.6.3 Suspended and Immobilized photocatalyst reactor comparison	44

1.7. Scope and Aim of research	46
1.7.1. Scope	46
1.7.2. Aim of Research.....	48
1.7.3. Structure of the thesis	48
CHAPTER 2	51
2.0. METHOD DEVELOPMENT.....	51
2.1. Introduction	51
2.1.1. Analytical quantification system	51
2.1.2. Sampling Integrity	52
2.2. PAHs extraction and sampling in water	52
2.2.1 Justification of analytical system	54
2.3. Experimental methods and materials.....	55
2.3.1. Material	55
2.3.2. Method	56
2.3.3. Method validation.....	56
2.4. Result and discussion	59
2.4.1. Identification of PAHs in water	59
2.4.2. Effect of UV quantification wavelength on PAH identification	61
2.4.3. Validation of identification and quantification method	63
2.4.4. PAH Quantification	66
2.4.5. Limit of detection (LOD) and Limit of Quantification (LOQ)	68
2.5. Conclusion	71
CHAPTER 3	73
3.0. POLYCYCLIC AROMATIC HYDROCARBON REMEDIATION USING CHITOSAN	73
3.1. Introduction	73
3.1.1. Efficiency of Chitosan as a coagulant	74
3.2. Experimental.....	76

3.2.1 Materials and method	76
3.2.2 Chitosan as a coagulant in PAH removal in water	77
3.3. Results and discussion.....	80
3.3.1. Effect of Powder chitosan on the removal of naphthalene water	80
3.3.3 Effect of settling time of naphthalene and phenanthrene removal using powder chitosan	84
3.4 Conclusion	85
CHAPTER 4	87
4.0. PHOTOCATALYSIS DEVELOPMENT FOR THE REMEDIATING OF PAH....	87
4.1. Introduction	87
4.2. Photocatalysis method design and development.....	88
4.2.1 Basis of design.....	88
4.2.2 Theoretical governing equations.....	90
4.3. Experimental.....	91
4.3.1 Analytical materials and methods.....	91
4.3.2 PAH preparation.....	92
4.3.3 Photocatalytic reactor design and setup	93
4.3.4 Photocatalysis procedure.....	96
4.4 Results and Discussion	98
4.4.1 Photocatalytic degradation of Naphthalene	98
4.4.2 Photocatalytic degradation of Phenanthrene	101
4.4.3 Photocatalytic degradation of Fluorene.....	103
4.5 Photocatalytic degradation effect on multiple PAHs in water	105
4.6 Effect of Acetone on PAH photocatalytic reaction rate	107
4.6.1 Naphthalene and phenanthrene preparation in acetone.....	107
4.6.2 Influence of solvent on photocatalytic degradation	108
4.7 Effect of TiO ₂ loading on photocatalysis	110
4.8 TiO ₂ particle limitation to photocatalysis	112

4.9 Conclusion	112
CHAPTER 5	115
5.0. DESIGN AND DEVELOPMENT OF A NOVEL PHOTOCATALYTIC REACTOR FOR PAH PHOTOCATALYSIS	115
5.1. Introduction	115
5.2. Immobilised photocatalyst design and development	117
5.2.1. Stage 1 Design: Static Immobilized Photocatalytic Reactor (SPR)..	117
5.2.2. Stage 2 Design: Flow Through Immobilized Photocatalytic Reactor (FTIPR)	119
5.2.2.1 Flow Through Immobilized Photocatalytic Reactor (FTIPR) design components.....	122
5.3. Sol gel preparation and glass tube coating	129
5.3.1. TiO ₂ sol gel preparation.....	129
5.3.2. Glass tube coating – Sol gel deposition	129
5.3.4 Characterization of TiO ₂ on glass tubes	131
5.3.5 Photocatalytic Procedure	131
5.4 SEM/EDXA analysis of TiO ₂ coated glass	132
5.5 Naphthalene photocatalysis using SIPR	135
5.6. Phenanthrene photocatalysis using SIPR	137
5.7. Fluorene photocatalysis using SIPR.....	139
5.8. Effect on multiple PAHs photodegradation using SIPR.....	141
5.9. FTIPR photoactivity testing and optimization of naphthalene photocatalysis.....	142
5.10. Model X ₄ FTIPR for photodegrading Phenanthrene and fluorene ..	150
5.11. Model X ₄ FTIPR photodegradation of three PAHs	151
5.12. Photocatalysis of PAH in sea water	153
5.12.1. FTIPR Photodegradation of Naphthalene in seawater.....	154
5.12.2. FTIPR Photodegradation of 7 PAH in seawater.	156

5.13. Conclusion	159
CHAPTER 6	161
6.0. CONCLUSION, CONTRIBUTION AND RECOMMENDATION FOR FUTURE OF WORK	161
6.1. Conclusion	161
6.2 Contribution.....	165
6.2.1 Experimental approach	165
6.2.2 Optimizing of TiO ₂ immobilized on glass tube.....	165
6.2.3 PAH photocatalytic efficiency	165
6.2.4 FTIPR design	166
6.3 Recommendation for future work.....	166
REFERENCES.....	167
APPENDIX A.....	179
APPENDIX B.....	188

LIST OF ABBREVIATIONS

AOPs	Advanced Oxidation Processes
BTEX	Benzene, toluene, ethylbenzene and xylenes
Boe	Barrel of oil equivalent
BEIS	Business, Energy and Industrial Strategy
DPR	Department for petroleum resource
EGASPIN	Environmental guideline and standards for petroleum industry in Nigeria
EPA	Environmental protection agency
FTIR	Fourier transform infrared spectroscopy
FTIPR	Flow through Immobilized Photocatalytic Reactor
GC-MS	Gas Chromatography with mass spectrometry
LOD	Limit of detection
LOQ	Limit of quantification
HPLC	High performance liquid chromatography
PAHs	Polycyclic aromatic hydrocarbons
ppm	Parts-per-million
ppb	Parts-per-billion
PW	Produced water
rpm	Revolution per minutes
SPME	Solid phase micro-extraction
SPR	Suspended photocatalytic reactor

SIPR	Static immobilized photocatalytic reactor
SEPA	Scottish environment protection agency
TiO ₂	Titanium dioxide
UV	Ultra violet
UN	United Nations

LIST OF FIGURES

Figure 1.1: Produced water discharged and reinjected globally	22
Figure 1.2: EPA Priority PAHs	28
Figure 1.2: Chemical structure of chitin and chitosan	33
Figure 1.3: Photocatalysis process	36
Figure 1.4: Photocatalytic oxidation with the use of TiO ₂ photocatalyst	38
Figure 1.5: Model of suspended photocatalyst reactor agitated mechanically and by air	41
Figure 1.6: Model of immobilized photocatalyst reactor agitated mechanically.	43
Figure 2.1: 18 EPA PAHs chromatogram showing PAH peaks separated under conditions described in table 2.1.....	60
Figure 2.2 : UV adsorption spectra of naphthalene showing max of 220.2 nm	61
Figure 2.3: UV adsorption spectra of phenanthrene showing max of 250.8 nm	61
Figure 2.4: Analysis of 18 EPA PAHs by reverse phase chromatograph (1000 ppb) showing the chromatogram at 300 nm	62
Figure 2.5: Analysis of 18 EPA PAHs by reverse phase chromatograph (1000 ppb) showing the chromatogram at 254 nm	62
Figure 2.6: Analysis of 18 EPA PAHs by reverse phase chromatograph (1000 ppb) showing the chromatogram at 220 nm	63
Figure 2.7: Capacity factor calculated for analytical method	64
Figure 2.8: Selectivity factor calculated for analytical method	64
Figure 2.9: Chromatographic column efficiency calculated for analytical method	65
Figure 2.10: Calibration curve for naphthalene. Mobile phase in HPLC-UV system; acetonitrile:water. Flow rate; 1.5 mL/min, UV detection at 220nm. n=3	67

Figure 3.1: Flocs formation through positive and negative charge adsorbent and species	73
Figure 3.3 – Experimental protocol for powder chitosan for the adsorption of PAHs in water.....	78
Figure 3.4 : Experimental setup of coagulation-flocculation method	78
Figure 3.5 : Chitosan settled in naphthalene solution	79
Figure 3.6 – Experimental steps using solubilized chitosan for the adsorption of PAHs in water.....	80
Figure 3.7: The effect of powder chitosan (12.5, 25 and 50ppm) on the removal of naphthalene in water.....	81
Figure 3.8: The effect of chitosan on the removal of Naphthalene and phenanthrene in deionized water	83
Figure 3.9: The effect of chitosan (1.25 and 2.5ppm) on the removal of naphthalene in deionized water at settling time: 0.5, 24, 48 & 120 hours.	84
Figure 4.2: Reactor setup of suspended TiO ₂ photoreactor	94
Figure 4.3: Photocatalysis degradation of PAHs alongside the test control.....	93
Figure 4.4: Photocatalytic degradation of naphthalene; (1)Under UV light & TiO ₂ (2)Under UV light & No TiO ₂ (3)No UV light& TiO ₂ . TiO ₂ :1000ppm	99
Figure 4.5: Photocatalytic degradation of phenanthrene; (1)Under UV light & TiO ₂ (2)Under UV light & No TiO ₂ (3)No UV light& TiO ₂ . TiO ₂ :1000 ppm	102
Figure 4.6: Photocatalytic degradation of fluorene; (1)Under UV light & TiO₂ (2)Under UV light & No TiO ₂ (3)No UV light& TiO ₂ . TiO ₂ :1000 ppm	104
Figure 4.7:Photocatalytic degradation of naphthalene, phenantharene and fluorene; (1)Under UV light & TiO₂ TiO ₂ :1000ppm	106
Figure 4.8: Photocatalytic degradation of naphthalene in acetone; (1)Photocatalysis (2)Photolysis (3)Dark Adsorption. TiO ₂ loading:1000 ppm .	109

Figure 4.9: Photocatalytic degradation of phenanthrene in acetone; (1)Photocatalysis (2)Photolysis (3)Dark Adsorption. TiO ₂ loading:1000 ppm	110
Figure 4.10: Rate Constant of phenanthrene at TiO ₂ loading: 1000, 800, 600, 400 and 200 ppm	111
Figure 5.1:SIPR reactor vessel	118
Figure 5.2: SIPR photocatalytic degradation process	119
Figure 5.3: Flow process of FTIPR reactor setup using 480 W UV Lamp	120
Figure 5.4: Image of FTIPR reactor setup using 480 W UV Lamp	121
Figure 5.5: Flow process of FTIPR reactor setup using 4 50 W UV Lamp	121
Figure 5.6: Image of FTIPR reactor using four 50 W UV Lamp	122
Figure 5.7: Pressure can for driving PAH solution through the reactor	123
Figure 5.8: FTIPR reactor vessel single pass.....	125
Figure 5.9: FTIPR reactor vessel double chamber.....	126
Figure 5.10: UV illumination configuration for 480 W UV LAMP at 250 mm irradiation distance - Model X ₁	127
Figure 5.11: UV illumination configuration for four 50 W UV LAMP at 50 mm irradiation distance - Model X ₂	127
Figure 5.12: UV illumination configuration for 480 W UV LAMP at 100 mm irradiation distance - Model X ₃	128
Figure 5.13: UV illumination configuration for 480 W UV LAMP at 250 mm irradiation distance (double reactor chamber) - Model X ₄	128
Figure 5.14: Coated glass tubes using sol gel A and B	130
Figure 5.15: SEM image of uncoated glass tube surface.....	133
Figure 5.16: SEM image of coated glass tube surface coated using TiO ₂ sol gel A	133
Figure 5.17: SEM of coated glass tube surface coated using TiO ₂ sol gel B ...	133

Figure 5.18: EDAX spectrum confirming the presence of Titanium & oxygen on the glass surface when coated with sol gel A	134
Figure 5.19:EDAX spectrum confirming the presence of Titanium & oxygen on the glass surface when coated with sol gel B	135
Figure 5.20:Photocatalytic degradation of naphthalene in immobilized photoreactor (1)Sol gel A (2)Sol gel B.....	137
Figure 5.21: Photocatalytic degradation of phenanthrene in immobilized photoreactor (1)Sol gel A (2)Sol gel B.....	138
Figure 5.22:Photocatalytic degradation of Fluorene in immobilized photoreactor (1)Sol gel A (2)Sol gel B.....	140
Figure 5.23: Photocatalytic degradation of naphthalene, phenanthrene and fluorene; (1)Under UV light & TiO ₂ , TiO ₂ :100 mg,water:100 mL.	142
Figure 5.24: Test control of naphthalene in the presence of immobilized TiO ₂ and absence of UV light in FTIPR	144
Figure 5.25: Photocatalytic degradation of naphthalene in Model X ₁ FTIPR. Photoreactor conditions: UV lamp: 480 W and irradiation distance: 250 mm ..	145
Figure 5.26: Photocatalytic degradation of naphthalene Model X ₂ FTIPR. Photoreactor conditions: UV lamp: four 50 W and irradiation distance: 50 mm	147
Figure 5.28: Photocatalytic degradation of naphthalene Model X ₄ FTIPR. Photoreactor conditions: UV lamp: 480 W and irradiation distance: 100 mm , double chamber.....	149
Figure 5.29: Photocatalytic degradation of phenanthrene (blue) in Model X ₄ FTIPR with control test (orange)	151
Figure 5.30: Photocatalytic degradation of fluorene (blue) in Model X ₄ FTIPR with control test (orange)	151

Figure 5.31: Photocatalytic degradation of naphthalene, phenanthrene, fluorene in a mixture; immobilized TiO ₂ and UV light (480 W and 100 mm), double reactor chamber.....	152
Figure 5.32: Photocatalytic degradation of naphthalene (blue) in seawater using Model X ₄ FTIPR and test control (orange).....	156
Figure 5.33: Degradation of 7 PAHs in seawater using Model X ₄ FTIPR. Initial concentration: orange, 1st sampling (60 minutes): blue, 2nd sampling (120 minutes): green	158

LIST OF TABLES

Table 2.1: HPLC-UV operating conditions for the quantification and identification of PAHs in water	58
Table 2.2 – Capacity factor, selectivity factor, column efficiency and resolution value of HPLC system.....	66
Table 2.3: HPLC-UV system calibration data for 18 PAH. Regression equation and linearity generated from calibration curve.	68
Table 2.4: 18 PAH LOD and LOQ for HPLC-UV system.	70
Table 4.1 : Chemical structure of naphthalene, phenanthrene and fluorene	89
Table 4.2: Rate constant, degradation time and degradation efficiency of	104
naphthalene, phenanthrene and fluorene in suspended TiO ₂	104
Table 4.3: Photodegradation of naphthalene and fluorene, and dark adsorption.	107
Table 5.2: Stages involved in photocatalytic reactor optimization and degradation efficiency	143
Table 5.3: Stage 1 involved in FTIPR optimization showing system loss	144
Table 5.4: Stage 1-2 involved in FTIPR optimization showing degradation efficiency	146
Table 5.5: Stage 1-3 involved in FTIPR optimization showing degradation efficiency	147
Table 5.6: Stage 1-3 involved in FTIPR optimization showing degradation efficiency	148
Table 5.7: Stage 1-5 involved in FTIPR optimization showing degradation efficiency	150

Table 5.8: Naphthalene, phenantharene and fluorene photodegradation efficiency using FTIPR.....	153
Table 5.9: Ionic elemental composition of instant ocean salt and North Pacific	154
Table 5.10: 7 PAHs photodegradation efficiency using Model X ₁ FTIPR.....	158

ABSTRACT

Water pollution through the discharge of contaminated water into the environment has been a major problem both to humans and the aquatic environment. This has received major attention due to the potential effects it imposes. In industry, a group of contaminants still facing challenges with regards to effective remediation are the Polycyclic Aromatic Hydrocarbons (PAH) present in water. These PAHs impose significant risk due to their carcinogenic, mutagenic and teratogenic potential. 18 of these PAHs are classified as high priority by the EPA due to their toxic and harmful nature. This research investigated two remediation methods which includes coagulation-flocculation and photocatalysis for the remediation of these 18 PAHs in water. In each remediation method investigated, preliminary works were first carried out on 3 PAHs: naphthalene, phenanthrene and fluorene, before then applying the established remediation method to the other 15 PAHs.

Coagulation-flocculation remediation method was investigated as it has been proven from past literature to be an effective method in the adsorption of pollutants from water. Also in the investigation powder and solubilized (in acetone) chitosan were used as an adsorbent to remove the PAHs in water. Results from this investigation showed little significance in the removal of PAHs with a removal efficiency of 15% attained for phenanthrene using powder chitosan (25 ppm) at 30 minutes contact time. An increase in contact time to 120 hours increased the removal efficiency to 88%. To attain sustainable removal from an industrial treatment point of view, a fast and effective remediation method is required. This method shows a slow removal of 120 hours resulting in the further investigation of a rapid and effective removal of PAHs in water. This in turn led to the investigation of the photocatalysis remediation method.

Investigation carried out using the photocatalytic remediation method involved the design and construction of photocatalytic reactor. Preliminary work was first carried out in a constructed batch suspended photocatalytic reactor to investigate the photodegradation of naphthalene, phenanthrene and fluorene to confirm the photocatalytic ability of TiO_2 to photodegrade PAH under the influence of UV light. A high removal efficiency of 99% was achieved but with limitation of TiO_2 secondary removal requirement. Due to the secondary treatment required to remove TiO_2 after treatment an immobilized photocatalyst reactor was then further investigated. Preliminary works was first carried out on a batch immobilized TiO_2 coated photoreactor to confirm the ability of PAH to be photodegrade using immobilized photoreactor. The batch immobilized TiO_2 coated photoreactor achieved significant result achieving 83% removal of naphthalene from water over 20 minutes. This resulted to the design and construction of a flow through photocatalytic reactor. A designed and constructed novel flow through photocatalytic reactor was therefore carried with the optimization of the immobilized TiO_2 photocatalyst and the UV light radiation. A high removal of 84% was achieved using the flow through photocatalytic reactor in the removal of naphthalene in water. Further investigation also carried out with PAH present synthesized sea water achieved a high removal rate of 77%. This novel flow through photocatalytic reactor provides a solution to the challenge for the effective removal of the PAHs in water.

Polycyclic Aromatic Hydrocarbons, Photocatalysis, Photodegradation, Photocatalytic reactor, Titanium dioxide, Advanced Oxidation Process, UV ray, Coagulation, Flocculation, Chitosan

CHAPTER 1

1.0. WATER POLLUTION AND TREATMENTS

1.1. Introduction

Water pollution is referred to as a factor producing a condition which impacts negatively on the beneficial use of a given water body which is as a result of the presence of chemical, physical and biological components. The measure of water pollution depends on the ability of the water to be used for other useful purposes and the impact it has on human and aquatic life. Water pollution is subjected to the source of the contaminant introduced to the given water body (Shi et al., 2016, Yang et al., 2016, Yandong et al., 2018). Although major water pollution is as a result of human activities, nature also has a contributing factor. Contaminants pollute water either through point sources or nonpoint sources. Contaminants attributed to point source pollution are mainly from industrial activities such as refineries, factories, power plants and treatment plants. In contrast, nonpoint sources can be attributed to diffuse contaminants from diverse sources of pollutants, such as contamination within a watershed resulting in similar levels of pollution (Wang and Yang 2016, Jiabiao et al., 2018).

An increase in the amount of wastewater generated over the years has been recorded. The United Nations (UN) has estimated the annual world production of wastewater to be 1,500 km³ which is equivalent to more than six times the total amount of water in all the rivers in the world. Water pollution from industries has added significantly to this figure. Studies carried out by UN-Water on developing countries shows that 70% of waste is disposed into the water untreated. The constant introduction of contaminants into water bodies has increased the concern of the

adverse effects it has on humans. An average of 2.2 million people die annually due to water pollution related causes (WHO and UNICEF 2000) with 15% accounted for children although much of this is through microbial contribution.

Waste water generated from the oil and gas industry mainly consists of dissolved organic materials, inorganic materials, process chemicals, heavy metals and suspended solids. The main source of this waste water is from discharged produced water present in subsurface formation which are drilled during oil and gas production. Waste water can also be produced from unconventional sources such as water waste from gas shale. The waste water is not always treated to required standards therefore contributing significantly to water pollution. The waste water concentration from produced water sources depends on the source, which is influenced by the geographical formation and location of the oil and gas reservoir generating the produced water (Daniela et al., 2013). Oil and gas reservoirs generate different volumes of produced water. As a result of the higher compressibility and sorption capacity of gas, gas reservoirs tend to generate less produced water compared to oil reservoirs (Daniela et al., 2011, Paul et al., 2015). Over time as oil and gas is drilled, more produced water is generated which can be attributed to the reinjected produced water which subsequently increases the water-to-oil ratio.

1.2. Produced water discharge

Produced water accounts for on average one seventh of the total amount of drilled fluid. As a result of this it generated the largest volume of waste water in the oil and gas industry (Marzieh et al., 2018). Due to the amount of waste water it generates, emphasis is more on the disposal rather than the beneficial use. The way it has been managed, treated and discharged into the environment has been of great concern due to the harmful substances present in it. Subsurface reinjection has been one of

the most preferable methods of produced water management (Siagian et al., 2018). Other disposal methods employed by the oil and gas industry is through the direct discharge into the environment but the produced water must be of good quality. Regulated discharge limits are imposed on this so as to limit the effect it has on the environment (Chen et al 2016). Due to this reason, most of the oil and gas industry prefer to reinject the produced waste water. Based on the recent statistics released by Oil and Gas UK environmental report 2016 (figure 1.1), in 2003 alone an estimated 250 million barrels of produced water was discharged into the environment, reducing to 180 million barrels in 2013 which shows a significant (28%) reduction over a 10 year period. When compared to the amount of reinjected water from 40 million barrels in 2013, the amount of discharged water from produced water, discharged water is still significantly high. Following on from the year 2013 there has been a steady increase in the amount of produced water still being discharged into the environment. For this reason there has been more focus on the treatment of produced water in order to regulate the contaminant level discharged into the environment (EEMS July 2016).

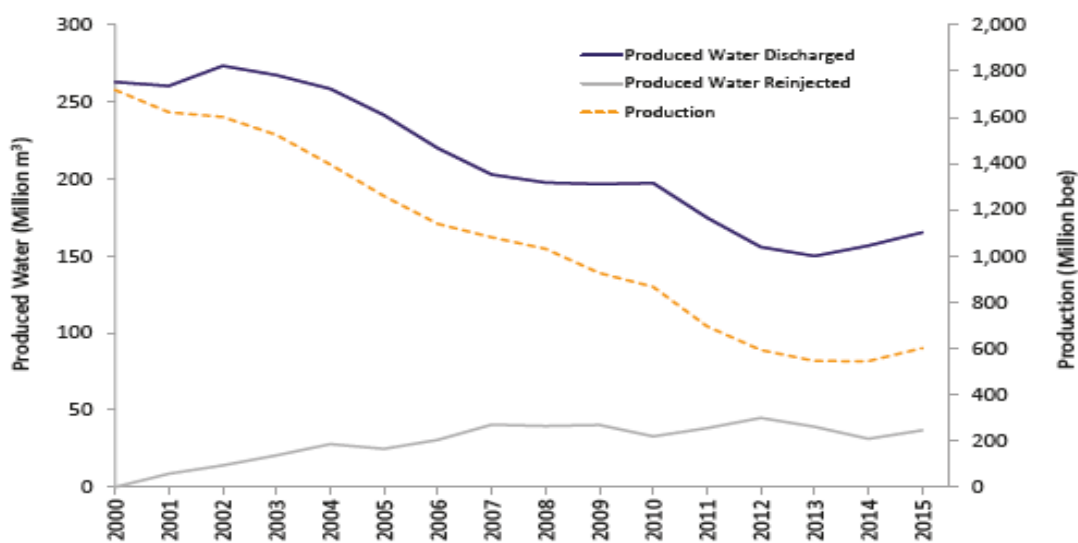


Figure 1.1 – Produced water discharged and reinjected globally
(Source: EEMS July 2016)

1.2.1. Constituents of produced water

The constituents of produced water are significantly influenced by the geographical location of their source field, extraction process and type of hydrocarbon present in the reservoir (Ahmadun et al., 2009; Dores et al., 2012). Produced water has the chemical constituent of the hydrocarbon it has been in contact with in the reservoir and it can vary over the life time of the reservoir lifespan. Produced water generated in gas wells is more toxic than that generated in oil wells, this can be as high as 10 times more toxic in most cases due to the dissolved contaminants (Camus et al., 2015). Produced water majorly consists of; salts (mostly referred to as total dissolved solid), oil and grease, BTEX (benzene, toluene, ethylbenzene and xylenes), polycyclic aromatic hydrocarbons (PAHs), phenol, organic acids, natural organic and inorganic compounds (table 1.1).

Regulatory policies in the oil and gas industry focus on the regulation of oil content in the discharged produced water, both dissolved and dispersed oil. The oil content in produced water depends on various factors such as salinity, pH, temperature and oil-to-water ratio (Pitre 2013).

Dispersed oil:

Dispersed oil is mostly made up of heavy alkyl phenols ($C_6 - C_9$ alkylated phenols) which are much less soluble in produced water. Also high molecular weight PAHs are also found in dispersed oil. They are present in droplets of oil which are suspended in produced water (Arthur et al., 2011)

Dissolved oil:

Dissolved oil is mainly water soluble organic compounds such as: PAHs, BTEX, phenol, low molecular weight aromatic compounds and carboxylic acid (Bostick and

Luo 2001). During extraction the pH, temperature and pressure influences their water solubility thereby increasing their concentration in the reservoir, therefore the amount of dissolved oil depends greatly on the pH, temperature and pressure (Daigle 2012)

Category	Components	Concentration (ppm)
PAHs	Naphthalene	0.194 – 3.21
	Acenaphthylene	0.0026 – 0.0045
	Acenaphthene	0.0003 – 0.015
	Fluorene	0.0041 – 0.067
	Phenanthrene	0.009 – 0.365
	Anthracene	0.26 – 0.45
	Fluoranthene	0.01 – 0.51
	Pyrene	0.01 – 0.94
	Benzo(a)anthracene	0.01 – 0.74
	Chrysene	0.02 – 3.6
	Benzo(b)fluoranthene	0.01 – 0.61
	Benzo(k)fluoranthene	0.006 – 0.15
	Benzo(a)pyrene	0.01 - 0.38
	Dibenzo(a,h)anthracene	0.012 – 0.21
	Benzo(g,h,l)perylene	0.01 – 0.23
	Indeno(1,2,3-cd)pyrene	0.022 – 0.23
BTEX	Benzene	0.032 – 14.97
	Toluene	0.058 – 5.86
	Ethylbenzene	0.086 – 0.57
	Xylenes	0.074 – 0.34
Inorganic compounds	Na	0 – 150000
	Cl	0 – 250000
	Ba	0 – 850
	Sr	0 – 6250
	SO ₄ ²⁻	0 - 15000
	Ti	0.01 – 0.7
	Zn	0.01 – 35
	As	0.005 – 0.3
	Pb	0.008 – 0.88
Phenols		0.009 - 23
Total Dissolved Solids	TDS	100 - 400000
Total Suspended Solids	TSS	1.2 - 1000
Total Organic Carbon	TOC	0 - 1500
Total Oil and Grease	O&G	2 - 560

Table 1.1: Produced water constituent (*Nelf et al., 2011*)

1.2.2. Produced water waste management

Management of produced water waste depends on the factors such as end-use, chemical and physical properties of the produced water, the regulation limits set by regulatory bodies (Dores et al., 2012). Oil and gas industries focus on the factors with greater emphasis on meeting the regulations set. The most common management strategy used in the oil and gas industry is the recycling (reinjection) and the disposal. Prior to this produced water has to be first treated but the extent of treatment depends greatly on the end-use. Recycling management strategy requires less treatment compared to when the produced water is to be disposed into the environment.

Due to the high concentration of contaminants present in produced water, most treatment systems involve the use of different treatment techniques either used alone or in a combined system. Treatment techniques can be classified into three major categories; physical, chemical and biological treatment (Younker and Walsh 2014). This can then be further classified based on the level of advancement in each technique: primary, secondary and advanced treatment. The treatment technology included are hydro-cyclone, centrifuge, adsorption filtration, oxidation, UV disinfection, skimming tanks, and air flotation, which are further classified as shown in table 1.2. Each of these methods have varying efficiency on the contaminant to be treated.

Treatment level	Treatment technology	Field mostly utilizing treatment technology	Substance treatment/removed
Primary treatment	Hydro-cyclone	Offshore and Onshore	• Suspended solids
	Skimming	Onshore	• Dispersed oil
	Dissolved air flotation	Onshore	• Inorganic salts
	Induced gas flotation	Onshore	• Microorganisms
	Centrifuge	Onshore	
Secondary treatment	Gas flotation (with flocculants)	Offshore	• Metal ions,
	Adsorption filtration	Offshore and Onshore	• Some Polycyclic aromatic hydrocarbon (PAHs) • BTEX – Benzene , toluene, ethylbenzene, xylene • Heavy metals
	Corrugated plate separator	Onshore	• Suspended solids
Advanced/tertiary treatment	Membrane filter	Offshore and Onshore	• Dispersed oil • Metal ions, • Polycyclic aromatic hydrocarbon (PAHs)
	Steam stripping	Offshore	• Polycyclic aromatic hydrocarbon (PAHs) • BTEX – Benzene , toluene, ethylbenzene, xylene • Dispersed oil • Demulsifies
	Biological treatment (aerobic degradation)	Offshore	• BTEX – Benzene , toluene, ethylbenzene, xylene • Dispersed oil and some metals

Table 1.2 – Treatment method for remediation of toxic substances in produced water (*Scurtu 2009*)

1.2. Polycyclic aromatic hydrocarbon

Crude oil present in reservoirs contains a mixture of hydrocarbons which contains more than 1000 compounds. Among these compounds are a group of substances called polycyclic aromatic hydrocarbons (PAHs). These hydrocarbons have two to eight aromatic rings. Also present in their chemical structure are a range of substituents such as nitro, alkyl and amino group. Atoms such as sulfur, nitrogen and oxygen can be added into their aromatic rings. Steroids are precursors of PAHs that can be naturally found in crude oil (Daniela et al., 2013).

PAHs mostly present in aquatic environments consist of two types which are the petrogenic and pyrogenic. Pyrogenic PAHs are PAHs formed from the incomplete combustion of organic compounds. Their aromatic rings are much larger than that of petrogenic PAHs. Petrogenic PAHs are found in crude oil and coal. These PAHs enter the aquatic environment through oil spills, oil seeps and produced water which are discharged into the environment. Sixteen of these petrogenic PAHs are classified as priority PAH pollutants by the US Environmental Protection Agency and also included as hazardous substances for surface water under the European Union Water Framework Directive 2000/60/EC due to their carcinogenic and mutagenic nature. They are referred to as 16 EPA PAHs (figure 1.2). Produced water which is the major source of PAHs entering the environment has received much attention due to its potential for being harmful. PAHs vary in concentration present in produced water depending on the oil reservoirs sources (table 1.3)

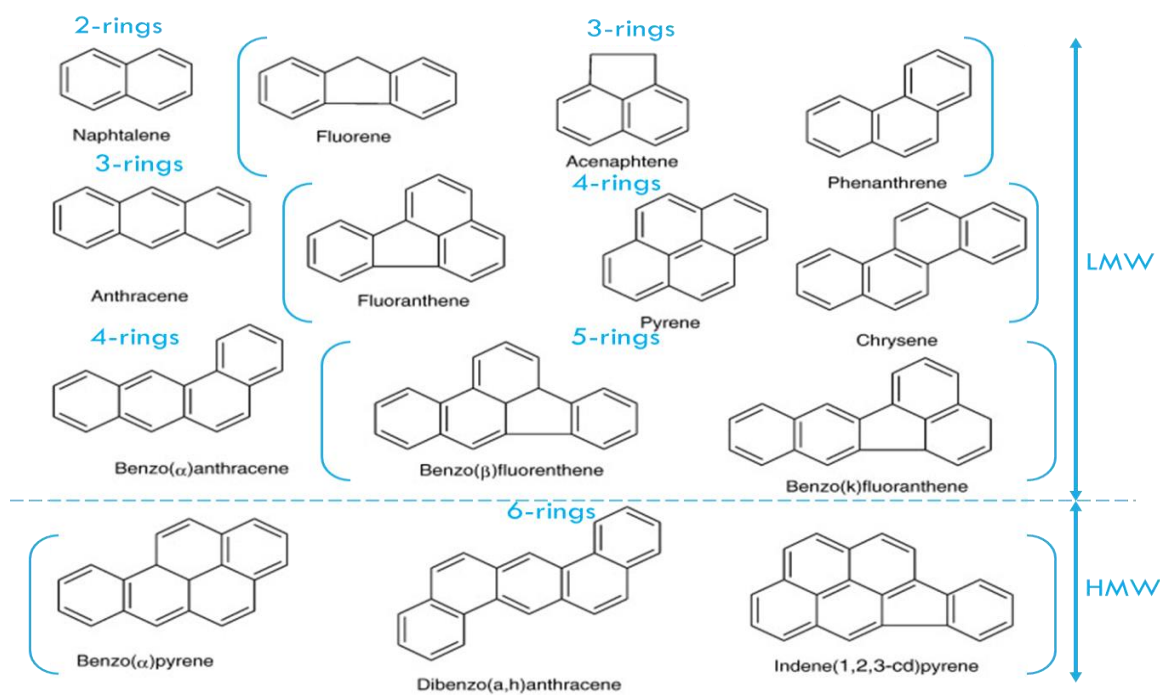


Figure 1.2: EPA Priority PAHs

Naphthalene which is the only EPA priority PAH that has 2 aromatic rings possess significant risk when discharged into the environment. Its high solubility, toxic nature and abundance in produced water (table 1.3) imposes a significant health impact on humans and aquatic life. Naphthalene was therefore selected as a model PAH in the investigation of PAH removal.

PAH	North Sea (ppb)	Gulf of Mexico (ppb)	Grands Bank (ppb)	Scotia Shelf (ppb)
Naphthalene	237-394	5.3-90.2	131	1512
Acenaphthylene	ND	ND-1.1	2.3	1.3
Acenaphthene	0.37-4.1	ND-0.1	ND	ND
Fluorene	2.6-21.7	0.06-2.8	16.5	13
Phenanthrene	1.3-32.0	0.11-8.8	29.3	4
Anthracene	ND	ND-0.45	ND	0.26
Fluoranthene	0.01-1.1	ND-0.12	0.51	0.39
Pyrene	0.03-1.9	0.01-0.29	0.94	0.36
Benzo(a)anthracene	0.01-0.74	ND-0.20	0.60	0.32
Chrysene	0.02-2.4	ND-0.85	3.6	ND
Benzo(b)fluoranthene	0.01-0.54	ND-0.03	0.61	ND
Benzo(k)fluoranthene	0.006-0.15	ND-0.07	ND	ND
Benzo(a)pyrene	0.01-0.41	ND-0.09	0.38	ND
Dibenzo(a,h)anthracene	0.012-0.10	ND-0.02	0.21	ND
Benzo(g,h,i)perylene	0.01-0.28	ND-0.03	0.17	ND
Indeno(1,2,3-cd)pyrene	0.022-0.23	ND-0.01	ND	ND

Table 1.3 : PAHs Concentration in produced water in various oil reservoirs
(Nelf et al., 2011) ND- Not detected

1.3.1. Discharge Limits and Legislation

Various countries through their regulatory bodies have legislation limits (table 1.4) in place to control the concentration of oil in produced water that can be discharged into the environment (Arthur et al., 2004). In Scotland, United Kingdom, the Water Framework Directive (WFD) helps to regulate the discharge of wastewater into the water system. Scottish Environment Protection Agency (SEPA) highlights the discharge limits of contaminants such as PAHs in the SEPA supporting guidance (WAT-SG-53). In the United States, this is regulated under the Federal Clean Water Act with specific discharge standards (Arthur et al., 2004). Also in Nigeria, discharge

limits are regulated by the Department for petroleum resource, environmental guideline and standards for petroleum industry in Nigeria (DPR-EGASPIN).

The discharge limits of the PAHs (table 1.4) used in this research will be based on the discharge limit guideline stated by Scottish Environment Protection Agency (SEPA) and the United States Environment Protection Agency (US EPA)

PAHs	Maximum allowable Discharge Concentration (ppb)
Naphthalene	130
Fluorene ¹	6.15
Anthracene	0.1
Phenanthrene ¹	1.7
Acenaphthene	1.68
Benzo(a)pyrene	0.27
Benzo(b)fluoranthene	0.017
Benzo(k)fluoranthene	0.017
Pyrene	0.43
Benzo(ghi)perylene	0.0082
Fluoranthene	0.12

Table 1.4: PAHs discharge limits in Marine water (*SEPA WAT-SG-53 2018*)
1 : US EPA: 440/5-86-001,

1.3.1. Environmental Impact

Due to the abundant potential of PAHs in aquatic environment and the risk they may pose on aquatic life and humans there has been an increased need to quantify and determine the extent of the risk on human life. In order to fully understand the effect of PAHs on aquatic life, studies have been carried out to determine the PAH distribution in aquatic life. High concentration of PAHs have been found in aquatic life close to offshore platform and oil vessel transport routes (Law et al., 1997). Most

countries have set up monitoring programmes to monitor discharge of PAHs from platform into the aquatic body. In the North Sea the Water Column Monitoring programme was set up in 2001 to monitor PAHs discharged.

Over the years studies (Xu et al., 2013, Wen-Jing et al., 2012, Long et al., 2014, Hussein et al., 2016, Lawal et al., 2017) have been carried out to provide evidence of PAHs presence in humans. The concentration of PAHs in aquatic life has been investigated and reported by several researcher also (Huang et al., 2012, Sabate et al., 2001; Wang et al., 2011) with all researcher coming to the conclusion that the accumulation and persistence of PAHs can be harmful to aquatic life and human. Most PAHs found in humans are as a result of occupational activities with workers on oil rigs (Ainhua et al., 2014) although exposure through other routes are also of concern. Polyaromatic compounds which PAHs fall under the category of have been associated with kidney cancer, lung cancer, bladder and skin cancer (Vela et al., 2012).

1.4. Adsorption using Coagulation-flocculation

Coagulation is a conventional method of treatment, which is utilized in the treatment of produced water. It involves negatively charged suspended particles present in the wastewater being adsorbed by a coagulant introduced into the wastewater thereby forming flocs. Inorganic coagulant and metal salts are the most widely used coagulants due to their rapid hydrolysis in water forming cationic species which helps in adsorbing the negatively charged particles (Chai et al., 2014).

Flocculation is also a conventional treatment method used in the treatment of produced water. It involves the introduction of flocculants into a stream of oily wastewater which also aids coagulation thereby neutralizing the negatively charged particles present in the wastewater and thereafter creating floc by collecting the neutralized particles (Chai et al., 2014). Over the years flocculants have been

modified in an effort to improve its treatment efficiency. Organic synthetic flocculants like polyacrylic acid, polyethylene amine (Shih et al., 2001), polyacrylamide and polydiallyl dimethyl ammonium chloride (PDADMAC) and natural source bio flocculants: chitosan, tannin and cellulose (Chai et al., 2014) have been widely used due to their favourable chemical and physical properties which include biodegradability, non-toxicity and high adsorption rate (Islam et al., 2011).

Research on more effective coagulants for wastewater remediation has been developed over the last decade. Coagulants such as palm oil mill boiler (POMB) bottom ash, ferric chloride and aluminium electrodes has been proven to have a treatment efficiency of 99% TSS removal (Chang et al., 2009), 62% COD removal (Younker et al., 2011) and 98.8% suspended solid removal (Sekman et al., 2011) respectively. The use of polymer inorganic mixture has also been widely researched as an effective way of treating oily wastewater. An example of this is aluminium sulphate chitosan (a mixture of polymer: chitosan and inorganic substance: aluminium sulphate) and anionic tannin as a flocculant resulted in a treatment efficiency of 99% colour removal (Roussy et al., 2005).

Due to the significant result achieved in literature this method was investigated for the remediation of PAHs in water.

1.4.1 Chitosan Biopolymer

Over the years there has been an increase in research on the application of biopolymers in water treatment due to their environmentally friendly characteristics. Polymers can also be generated from synthesized petroleum based chemicals. Synthetic biopolymers are expensive and have the potential of creating secondary pollution thus limiting their application in produced water treatment. Also natural sourced biopolymers are polymers generated from sources such as animals, plants

and microorganisms, which are biodegradable. Examples of natural source biopolymers are chitosan, tannin, cellulose, alginate, gums, and mucilage (Taylor et al., 2015). Research on the application of chitosan in water treatment has increased over the last decade for example it has been used in the removal of dyes (Ngaha et al., 2011), methyl orange (Wong et al., 2004), heavy metals (Chintana 2002), copper ion (Nabel et al., 2015) and mercury ions (Zeinali et al., 2014) from wastewater

Chitosan belongs to the polysaccharide family which are found on the exoskeleton of crustaceans. Chitosan which is derived from chitin, consists of a linear β -(1-4)-2-amino-2-deoxy-D-glucopyranose unit (figure 1.2). It is a linear polymer made up of D-glucosamine and acetyl-D-glucosamine which is produced by the deacetylation of chitin (Ran et al., 2016). The percentage of D-glucosamine is also referred to as the degree of deacetylation (DDA) of chitosan. Professor C. Rouget first discovered chitosan in 1981 by cooking chitin in alkali (Chintana 2002) and from then chitosan has had significant application in different fields. Chitosan undergoes demineralization and removal of the protein process before it is been produced (figure 1.2) (Islam et al., 2011).

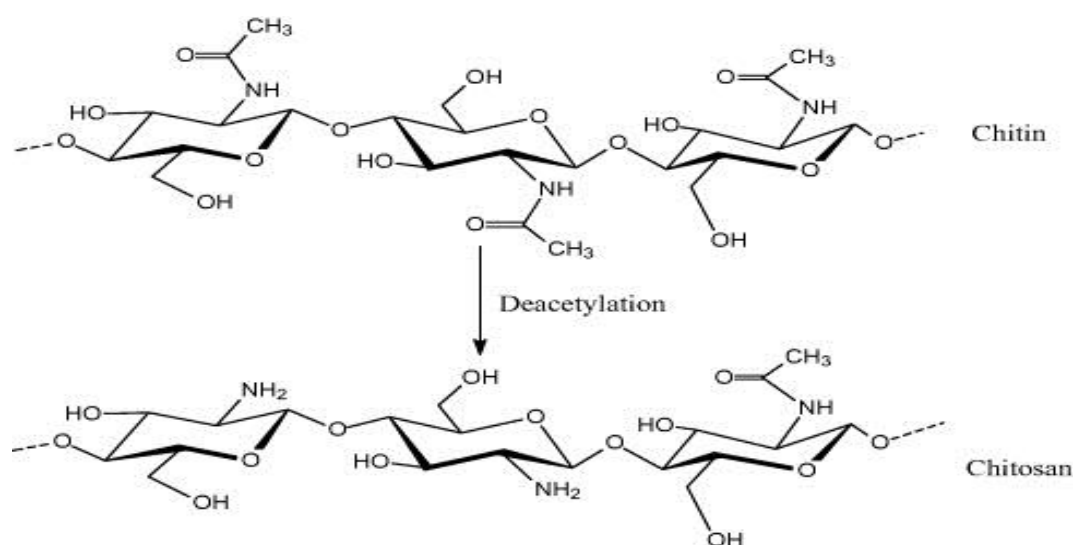


Figure 1.2 – Chemical structure of chitin and chitosan

The present global estimate of harvested seafood is 29.9 million tonnes yearly (Jozef et al., 2003), which shows a significant amount of chitosan available to be utilized. Presently USA and Japan are the leading producers of chitosan with an estimated global production of 240,000 tonnes produced yearly (Joanna 2010). Chitosan costs can vary from \$20 per kilogram to as high as \$1,000 per kilogram depending on its quality (Ensymm UG & Co. KG).

1.4.1. Application of chitosan in pollutant remediation

Chitosan has been utilized for over three decades for the purification of wastewater (Johnson et al., 1984; Coughlin et al., 1990; Delben et al., 1994; Strand et al., 2003; Guibal et al., 2005; Miranda et al., 2013; Perez et al., 2016). Due to high porosity it has seen significant achievement in the removal of metals ions such as copper, chromium, cadmium, mercury and lead, oil, grease and fine particles in wastewater. It has also been utilized in the cleaning up of oil spills by helping to bind the oil together for easy clean up.

Zeinali et al. (2014) investigated the impact chitosan coated in magnetite nano-particle (Fe_3O_4) has on the removal of Hg^{2+} ions in oily sample water. Due to the absence of any functional group enabling chitosan to bind directly onto the iron oxide nanoparticle, chitosan was carboxymethylated and after covalently bound onto the nanoparticle. The diameter of the chitosan coated nanoparticle was 10 nm. The best removal results were achieved using 8 mg ml^{-1} of the chitosan coated nanoparticles in an aqueous solution of 2 ppm (pH 3) giving a 90.98% removal of Hg^{2+} .

Nabel et al. (2014) conducted a study on the removal of Cu^{2+} ions and Co^{2+} ions from water using natural chitosan, chitosan in chloroacetic acid and chitosan in glycine. The adsorption efficiencies were also investigated in neutral and alkaline medium at various contact times. The study results showed that at pH 9 it gave maximum Co^{2+} ions removal efficiency of natural chitosan (0.27 mg L^{-1}), chitosan-chloroacetic acid

(46.3 mg L⁻¹) and chitosan-glycine (4.3 mg L⁻¹) to be 99.9%, 81.48% and 98.28% respectively at 20 minutes contact time. Also in the removal of Cu²⁺ ions at pH 9 a maximum removal efficiency of chitosan (2 mg L⁻¹), chitosan-chloroacetic acid (92.5 mg L⁻¹) and chitosan-glycine (88.0 mg L⁻¹) to be 99.2%, 62.99% and 64.80% respectively at 20 minutes contact time.

Wipawen et al. (2014) investigated the use of chitosan flakes in the removal of pollutants present in biodiesel water. The pollutants that were investigated were oil and grease and also high biological oxygen demand (BOD) and chemical oxygen demand (COD). Results showed that using 3.5 g L⁻¹ chitosan a removal efficiency of 59.3%, 87.9% and 66.2% of oil & grease, BOD and COD respectively was achieved at pH 4.0.

Chitosan application is not only limited to wastewater treatment. Other industrial applications of chitosan involve fat stabilization during food preparation, bacterial immobilizer, cosmetic additive, ion exchange media and flavour stabilizer. The health sector utilize chitosan in weight lost medicines, wound healing, antacids, blood pressure control, bone repair and also dental recovery (Wipada et al., 2014; Vitor et al., 2016). In the beverage industry it is used in the clarification and deacidification of beverages (Akile et al., 2016) and the agriculture industry in soil treatment (Mao et al., 2014).

1.5. Photocatalysis

Recent research has shown that specific pollutants cannot fully be remediated using the conventional treatment method as a result of their mineralization resistance and strong chemical stability. The use of a stronger reactive system to overcome this is therefore employed which is referred to as Advanced oxidation process. The production of reactive OH radicals during the oxidation process as a more reactive

agent to degrade the pollutant gives it a unique capability as a more efficient treatment method. Advanced oxidation process is classified based on the non-selectivity of the pollutant degraded and the mechanism by which the OH radicals are generated (Garcia-Martinez et al., 2005).

Specific types of catalyst have been used to speed up the generation of OH radicals. Heterogeneous photocatalysis, advanced oxidation process, involves photo-induced reaction transformation which occurs on the surface of the photocatalyst. After the oxidation process, the photocatalyst remains unchanged during continuous transfer of energy to the pollutant. Semiconductors such as TiO_2 have been proven to be a suitable photocatalyst as it does not have a continuum of electron states but a void region referred to as band gap having no energy level from the top valence band to the bottom conduction band (Manariotis et al., 2011).

1.5.1. Mechanism of photocatalysis

Photocatalysis is governed by the activation of a photocatalyst (semiconductor) surface through the radiation of UV. The semiconductor generates electrons from its valence band and holes due to the adsorption of photons equal or greater than the semiconductors bandgap. The electrons and holes then react with the dissolved oxygen in water to degrade the organic compounds present in the water (figure 1.3).

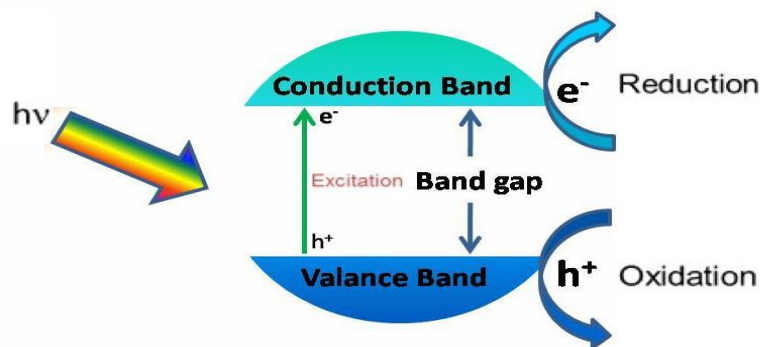


Figure 1.3 – Photocatalysis process

Titanium dioxide (TiO_2) a naturally occurring oxide of titanium has been widely reviewed on its potential as a photocatalyst. The high photocatalytic activity of titanium dioxide makes it more applicable when compared to other semiconductors such as ZnO , WO_3 , MoS_3 , BiVO_4 and CdS . A drawback in the application of TiO_2 comes from the wide band gap between the conduction and valence band thereby only allowing photons to be absorbed in the UV range and not in visible light. This has therefore lead to increased research in the application of TiO_2 with the use of UV light. Other semiconductors such as ZnO and CdS have a much smaller band gap but are unstable with the potential of degrading over time leading to photocorrosion. Due to this TiO_2 is more preferable as it is resistant to photocorrosion and also has high photostability

In the 1900s, TiO_2 was investigated as a photocatalyst in the remediation of pollutants in water. In 1972, Fujishima and Honda used an n-type semiconductor TiO_2 electrode with ultraviolet (UV) light to demonstrate the photocatalytic decomposition of water. Further potential of TiO_2 photocataysis was investigated in other fields, in 1985 Matsunaga et al., investigated the potential of TiO_2 photocatalysis as an antibacterial potential. Over recent years there has been rapid extensive research in the application of TiO_2 in treatment methods.

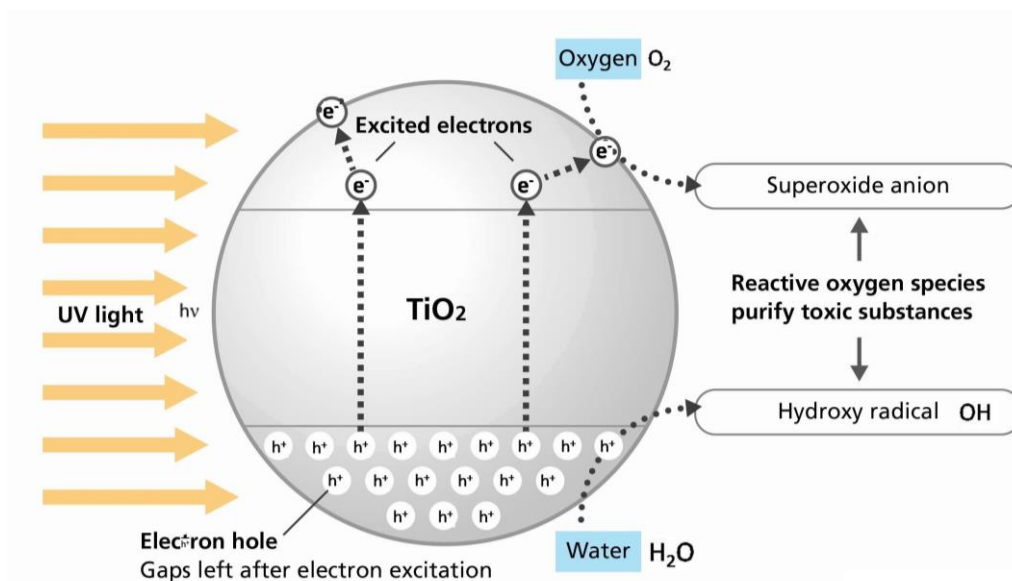


Figure 1.4: Photocatalytic oxidation with the use of TiO_2 photocatalyst

TiO_2 ability to degrade PAHs is made possible by the generation of hydroxyl radicals (OH^\bullet) which in turn due to their high oxidation energy degrades the PAH. UV light that is adsorbed onto the surface of TiO_2 (figure 1.4) generates electrons (e^-) in the conduction band and holes (h^+) in valence band (equation 1.1). The conduction band electrons (e^-) then reacts with oxygen (O_2) to generate superoxide (O_2^-) (equation 1.2) and the valence band holes (h^+) reacts with adsorbed water (OH^-) to form hydroxyl radical (OH^\bullet) (equation 1.3). Superoxide (O_2^-) can also react with H^+ to form hydroperoxyl radical (HO_2^\bullet) (equation 1.4). PAHs are oxidised by the superoxide (equation 1.5) and hydroxyl radicals (OH^\bullet) (equation 1.6)



1.5.2. Photocatalytic application in water treatment

Chemical oxidation processes have been widely used in the chemical remediation of PAHs in water (Rocha et al., 2013; Sanches et al., 2011; Veignie et al., 2009; Sponza and Oztekin 2010; Shemer and Linden 2007). Direct and indirect oxidation have been investigated for the degradation of PAHs in water. The production of carcinogenic halogenated hydrocarbons as intermediates during the oxidation process has provided some limitation to the use of oxidants like chlorine (Rubio et al., 2014).

Photocatalysts such as TiO_2 , SiO_2 and Al_2O_3 have been widely used for the degradation of PAHs in water (Wen et al., 2003). Previous work (Woo et al., 2008; Wen et al., 2003, Antoine et al., 2007) investigated the use of TiO_2 for the remediation of PAHs, however, there were limitations as a result of the introduction of reagents such as methanol and acetone, which slowed the degradation process. This research work focuses on the photocatalytic degradation of PAHs with titanium dioxide photocatalyst (Degussa P25) eliminating the use of the reagents which reduces the rate of degradation.

1.6 Photocatalytic photoreactor

Photoreactors are designed to achieve maximum efficiency by utilizing the photocatalyst type, size and distribution of photocatalyst either as a suspension or immobilized on an inert surface. The pollutant type, photoreactor temperature, reaction mechanism and irradiation source are other factors that influence the photoreactor performance. Recent researchers have focused on the design and construction of photoreactors for heterogeneous photocatalysis due to its wide application in solving major problems such as water treatment, microorganism destruction, cancer cell inactivation, biomass conversion, chemical synthesis and cancer cell inactivation (Lawton et al., 2003, Grieken et al., 2009, Graham et al.,

2010, Leelavathi et al., 2013, Fotiou et al., 2015., Zhang et al., 2015, He et al., 2015, Mahadik et al., 2017, Amiri et al., 2017.,)

Heterogeneous photocatalysis in a photocatalytic reactor creates an environment allowing photons generated from the irradiation source to interact with the photocatalyst leading to the photodegradation of the pollutant thereby allowing for a controlled study of the photocatalytic kinetics process and the identification of intermediates. An ideal photocatalysis environment is created when specific conditions are met as highlighted in table 1.5. When well managed and optimized of all conditions will result in achieving a high photodegradation efficiency.

	Parameter	Methods to which parameters are achieved
1	Sufficient irradiation source	Generated from a light source such as UV lamp
2	High mass transfer	Agitation of sample with the use of mechanical stimulants such as a magnetic stirrer and aeration by adding oxygen
3	Effective distribution of UV light through the reactor	The use of UV reflective materials and also effective positioning of UV light source
4	Effective temperature regulation	Utilize the use of cooling medium such as fan
5	Maximum UV contact with photocatalyst	The use of transparent and UV penetrable reactor vessels
6	Optimal photocatalyst loading	Detailed investigation on the photocatalyst loading that will yield significant photodegradation

Table 1.5: Condition to promote effective Photocatalysis

The efficiency of the photocatalytic reactor is dependent on the cross-sectional area contact between the photocatalyst and the pollutant. It has been seen from published literature that two widely used methods for the catalyst-pollutant interaction has

been used: suspended photocatalyst and photocatalyst immobilised onto an inert surface (Bouchy and Zahraa, 2003, Bickley et al., 2005, Graham et al., 2010, Edwards et al., 2008, McCullagh et al., 2011, Hu et al., 2015, Fotiou et al., 2015, Trandafilović et al., 2017).

1.6.1 Suspended photocatalyst reactor

Suspended photocatalyst reactors are reactors whereby powder or nanoparticles photocatalyst are added to the reactor vessel containing the polluted water. The polluted water in the photoreactor is then agitated either mechanically or by using air and then irradiated using a light source for the photocatalytic process to occur (figure 1.5).

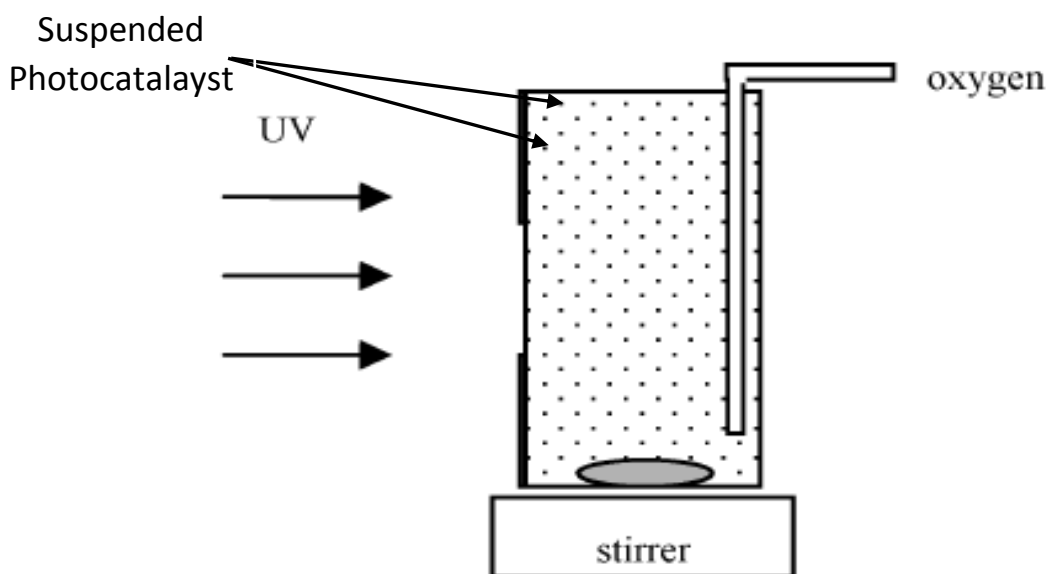


Figure 1.5: Model of suspended photocatalyst reactor agitated mechanically and by air

Suspended photocatalyst reactors are the most widely used conventional photoreactors (Wang et al., 2004, Robertson et al., 2005, Yang and Li 2007, Malato et al., 2009, Cheng et al., 2010). In an effort to achieve high efficiency of the reactors, various researchers have optimized the operational parameters of the photocatalytic reactor. Nishio et al., 2011, investigated the effect of the irradiated

light intensity and photocatalyst (ZnO) loading in the degradation of Orange II. A suspended photocatalytic reactor was designed and constructed using Pyrex glass in a cylindrical reactor with an inner diameter of 8 cm and height of 55 cm. Three UV fluorescent lamps of 15 W placed around the reactor at a distance of 2.5 cm were used to irradiate light unto the reactor. During the investigation it was found that the rate of degradation of the Orange II increased with an increase in light intensity and an optimal efficiency was achieved at a photocatalyst loading of 1000 mg L^{-1} . Subramanian et al., 2010, investigated the degradation of phenol by optimizing the operational conditions such as TiO_2 photocatalyst loading between 1 g dm^{-3} – 8 g dm^{-3} and light illumination mode: continuous or periodic. The conclusion was drawn that the illumination mode did not have a significant effect on the degradation but an increase in photocatalyst loading increased the degradation rate and an optimal degradation efficiency was achieved at a photocatalyst loading of 7 g dm^{-3} . McCullagh et al., 2011, further investigated a novel slurry continuous flow reactor for the photocatalytic degradation of methylene blue (MB) using pellet TiO_2 photocatalyst. High surface area of TiO_2 was investigated alongside various loadings of TiO_2 . Irradiation time of 60 minutes was investigated at TiO_2 loadings of $30 - 200 \text{ g L}^{-1}$. Results showed a complete degradation of MB over the loading range and irradiation time with a high degradation of 98% at TiO_2 loading of 30 g L^{-1} achieved.

1.6.2 Immobilized photocatalyst reactor

Immobilized photocatalyst reactors are photoreactors in which the photocatalyst is immobilized onto a fixed surface either by physical or chemical bonds (figure 1.6) (Dijkstra et al., 2001(a), Kimura et al., 2003, Adams et al., 2013). Its major advantage over the suspended photocatalyst reactor is that it eliminates any secondary treatment process involving the recovery of suspended TiO_2 particles (discussed further in chapter 4). In addition, it allows for the reusability of the

immobilized catalyst surface in several cycles (Dijkstra et al., 2001(b), ChO et al., 2005, Mascolo et al., 2007, Gaya et al., 2008). Limitations on immobilized reactors are their low area-to-volume ratio of the catalyst surface area to the pollutant. Nevertheless, a well-designed photoreactor can help manage this limitation and in the long run reduce their influence on efficiency of the photoreactor. This therefore has created much attention on the design and optimization of the photoreactors elements to maximize photodegradation efficiency (Minero et al., 2006, Morales-Torres et al., 2012, Zhang et al., 2012, Tang et al., 2013). Major emphasis has been focused on factors such as TiO_2 surface thickness, illumination source and light intensity to maximize the design of immobilised TiO_2 photoreactor for maximum efficiency (Chong et al., 2010)

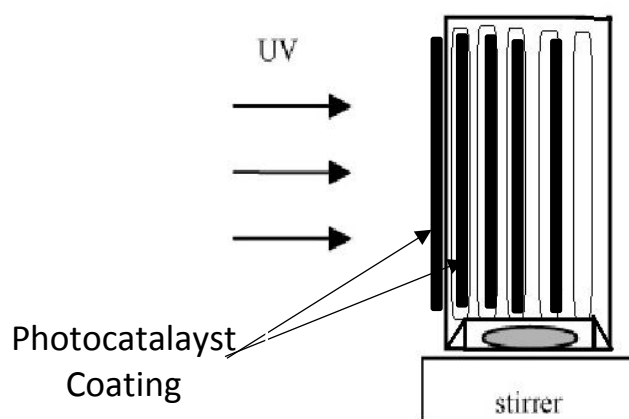


Figure 1.6: Model of immobilized photocatalyst reactor agitated mechanically.

Photocatalyst immobilization is governed by the principle of coating a photocatalyst on an inert surface. The mode of coating, type of coating gel material and coated surface area been used has an influence on the photodegradation of the pollutant. Various published literature has demonstrated how each of these factors can influence photodegradation. Rebah et al., 2017 showed the influence of coating gels on the photodegradation of Indigo carmine by the use of two different coating gels.

Two gels: one of TiO₂ aerogel made up of anatase crystalline structure and prepared at 300 °C and 100 bars pressure, while the second coating gel TiO₂ xerogel made up of anatase and brookite prepared at 200 °C and ambient pressure were investigated. Results showed that the rate constant of TiO₂ aerogel was greater than that of TiO₂ xerogel showing the influence the coating gel has on photodegradation. Coated surface area over the range of 30 m² g⁻¹ to 380 m² g⁻¹ has also been investigated in efforts to influence the photodegradation with results showing an increase in rate constant when surface area increases (Liang et al., 2010, Zhang et al., 2008 & Mascolo et al., 2007)

The coating has also been used in different photoreactors by various researchers in the remediation of pollutants in water. Sapizah et al., 2012, investigated the inactivation of *Escherichia coli* in wastewater using a fixed bed photoreactor by immobilizing TiO₂ onto the inner wall and glass rings. Results showed 80% of the *Escherichia coli* population inactivation in the wastewater. Behnajady et al., 2004, also investigated the degradation of Acid Red 27 (AR27) in water using a tube photoreactor where TiO₂ was immobilized onto four glass tubes and were interconnected using polyethylene tubes. A linear degradation of AR27 was achieved with an increase in light intensity.

1.6.3 Suspended and Immobilized photocatalyst reactor comparison

In order to ascertain the best method for the remediation of pollutants in water using a photoreactor, comparison of both suspended and immobilized TiO₂ photoreactors is essential and has been carried out by various researchers to determine the most efficient method. Dijkstra et al., 2004, in the degradation of formic acid investigated the efficiency of two similar tubular photoreactors with one having suspended TiO₂ and the other with TiO₂ immobilized onto its surface. Results showed that using equal

amount of TiO_2 in both cases resulted in a similar removal efficiency for both systems. Further to this, Ochuma et al. carried out a similar investigation using photonic efficiency to ascertain the most efficient remediation method for photodegrading 1,8-diazabicyclo[5,4,0]undec-7-ene (DBU) using suspended TiO_2 and immobilized TiO_2 . TiO_2 immobilized onto the foam monolith had equal mass to that suspended in water which was 21.78 g L^{-1} . Results showed that the spray coated TiO_2 foam achieved higher efficiency compared to that of the suspended TiO_2 . High efficiency was promoted due to the larger surface area exhibited by the foam monolith created for the immobilized TiO_2 . Li et al. studying the photodegradation of phenol also compared the efficiency of suspended TiO_2 and TiO_2 immobilized on quartz glass plate. The experimental model for both cases was independent of the reactor configuration and size but the photocatalytic efficiency was the same per unit illuminated TiO_2 area for both cases. Suspended TiO_2 achieved a much higher efficiency, as high as 9 times more than immobilized TiO_2 .

It can therefore be seen that the reactor design type or catalyst matrix used has a significant impact on the efficiency of the photoreactor. The medium of coating photocatalyst onto an inert surface, catalyst loading and type of pollutant to be remediated has a significant influence on the photoreactor degradability performance.

1.7. Scope and Aim of research

1.7.1. Scope

The scope of this research investigates two approaches in the removal of PAHs from water. The treatment method investigated in this research involved the adsorption and advanced oxidation process. A flow chart seen in figure 1.7 shows a sequence of investigation carried out in each remediation method which lead to the derivation of a more suitable remediation method.

Biopolymer (chitosan) was used in a coagulation-flocculation process to adsorb PAHs present in water and was further investigated by comparing powder chitosan and dissolved chitosan at different contact times. Recent research has used biopolymers such as chitosan to adsorb pollutants such as metals but little research has been carried out for the removal of PAHs in water. Further to this photocatalysis was also investigated for the degradation of PAHs in water. TiO_2 photocatalyst (Degussa P25) of nano size particles at different concentrations was investigated to determine the rate at which PAHs degrade over a period of time. A novel photo reactor was also developed with TiO_2 immobilized on glass tubes to investigate the degradation of PAHs. UV light intensity was varied to optimize the maximum efficiency of the photo reactor

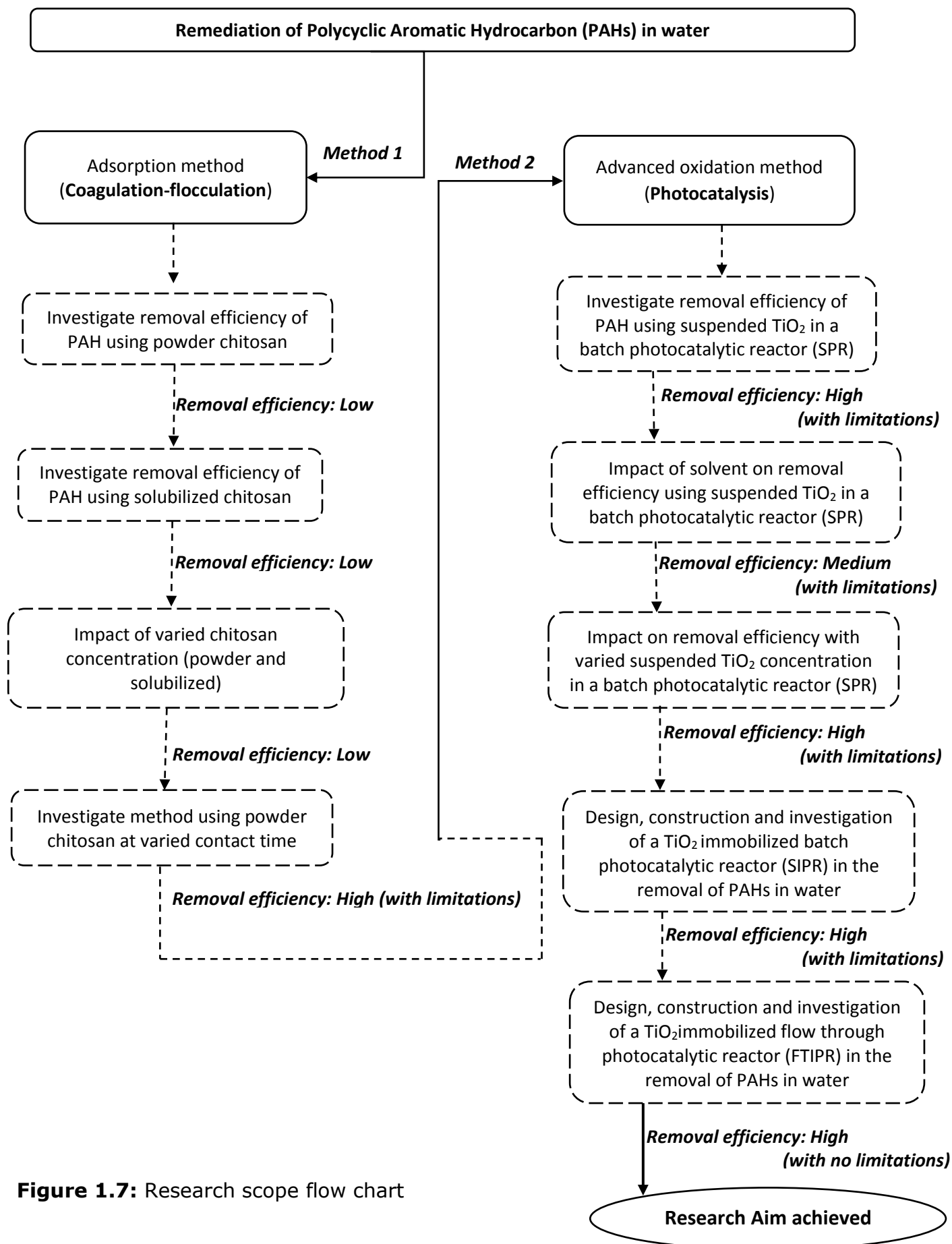


Figure 1.7: Research scope flow chart

1.7.2. Aim of Research

The aim of this research is to establish a method for the treatment of polycyclic aromatic hydrocarbon (PAHs) in water. Two methods have been assessed namely: coagulation-flocculation using chitosan (biopolymer) and photocatalysis, an advanced oxidation process.

The objectives needed to achieve this are:

- Identification and quantification of polycyclic aromatic hydrocarbons (PAHs) in water using a HPLC-UV method.
- Investigate the removal of PAHs in water using chitosan and a coagulation-flocculation method
- Investigate the photocatalysis of PAHs in synthetic water with further optimization of removal method in a constructed flow through reactor.

The major focus is on Polycyclic aromatic hydrocarbons (PAHs) remediation in produced water focusing on 18 EPA polycyclic aromatic hydrocarbons (PAHs) classified as high priority. The PAHs of major concern are those classified as carcinogenic to humans.

1.7.3. Structure of the thesis

This thesis is made up of five chapters comprising a detailed literature review of the research title, research findings represented in results formats (tables and graphs) which are critically reviewed against related literature and explained in a detailed discussion section. The latter part of the thesis gives a summary of the research undertaken which includes the contribution to knowledge.

Chapter 1, which is the introductory chapter, gives a detailed literature review on the research area, highlighting areas of similar past research carried out with a historical research and technological development. It also includes a background on water

pollution from produced water source, current remediation technology and types of legislative limits and control set by different countries. Polycyclic aromatic hydrocarbon the pollutant investigated in this research was also discussed in detail, with a detailed background, environmental impact and discharge limit regulation. Chitosan a biopolymer and TiO_2 a photocatalyst were introduced as a method of environmental remediation in a coagulation-flocculation and photocatalysis treatment method respectively highlighting similar area of research done over the years.

Chapter 2 investigated the analytical system used in the research, which includes: choice of most suitable analytical system used, justification of analytical system, quantification and identification of the 16 EPA priority polycyclic aromatic hydrocarbon. This chapter investigated using a theoretical approach and experimental results to determine the analytical system integrity alongside validation of result.

Chapter 3 investigated the remediation of polycyclic aromatic hydrocarbon (PAHs) in water using coagulation-flocculation treatment method. Chitosan a biopolymer was used as an adsorbent to adsorb the PAHs present in synthesized water. Powder and solubilized chitosan were investigated to determine the most effective removal method. The effect of chitosan-PAHs contact time on the adsorption rate of PAHs was also investigated.

Chapter 4 investigated the use of a static photoreactor which involved the use of suspended TiO_2 particles to establish its ability to photodegrade PAHs. The photocatalytic degradation rate of naphthalene, phenanthrene and fluorene was investigated to establish the efficiency of the photodegradation method. This was carried out when present alone and in a mixture of other PAHs in water. The TiO_2 loading was also investigated in this chapter.

Chapter 5 involved the design and development of a novel flow through immobilized photocatalytic reactor. A batch immobilized photoreactor was first developed and the coated glass tubes of the reactor were optimized with an effective sol gel for coating. The optimized TiO₂ coated glass tubes in the batch photoreactor were then applied into the design and construction of the novel flow through photocatalytic reactor. Further optimization was carried out on the novel flow through photocatalytic reactor by varying parameters such as UV light intensity, irradiation distance, and photoreactor configuration. PAHs spiked in synthetic sea water were then investigated to determine the performance of the novel flow through photocatalytic reactor in remediating it.

CHAPTER 2

2.0. METHOD DEVELOPMENT

2.1. Introduction

The method of analysis, extraction and sampling of the analyte is critical in achieving the precise results required. Protocols developed take into account instrumental sensitivity, high efficiency and low analytical errors to attain results required. Major studies focuses on a specific compound in a specific medium not taking into account the overall process of the different matrix involved in the protocol. A critical review therefore has to be carried out on the protocol used to determine if it takes into account all the different methods of the analytical system from sampling to extraction and quantification. Therefore the accuracy of an analytical system is determined by the sampling method and analyst quantification steps. A propagation of error over experimental stages can be carried and add impact on subsequent stages thereby affecting the accuracy of the results, therefore it is important to select the best method in each experimental stage in order to accommodate any error.

2.1.1. Analytical quantification system

The sampling and quantification method employed for a specific analyte is dependent on the state of the analyte and also the form in which the analyte is present in a substance. PAHs can occur as an analyte in water, air and soil. This research focuses on polycyclic aromatic hydrocarbon (PAHs) in water. In water PAHs occur both in dissolved and suspended state, PAHs dissolved in water will be focused on in this research as that is the state in which it is present in discharged produced water.

2.1.2. Sampling Integrity

Sampling integrity can be influenced by physical, chemical and biological factors in the pollutant matrix. Integrity of sampling can be maintained by employing the appropriate sampling apparatus, storage container and mode of sample preservation. Sampling of pollutants such as PAHs which are hydrophobic and volatile in nature when present in water can be lost in air or onto surface. This therefore requires to be sampled in a controlled way such as; pre-stored in a sealed container, regulated temperature range and sampled using glass apparatus to reduced sample loss and maintain sampling integrity. The sampling method when sampling over a stipulated sampling time is vital for sampling of compounds volatile in nature such as PAHs. Therefore it is required to critically review the sampling and analytical method for the analyte to evaluate the most effective method in order to minimize error, sample losses and maintain a high sampling integrity.

2.2. PAHs extraction and sampling in water

This is dependent on the type of water. The water type such as sea water and fresh water can be determined from the water sampling point source. This research focuses on methods suitable for PAHs present in produced water discharged into the environment for the oil and gas industry, the water type will be taken in terms of produced water which has undergone primary treatment but still contains a significant concentration of PAHs.

Various methods of improving PAHs extraction and sampling have been studied. King et al.,2003, employed the use of solid phase micro-extraction (SPME) in quantifying PAHs in porewater samples collected from Mersey Estuary, UK, using sorption of specific PAHs on a selected fibre and desorption directly to GC-MS. High linearity was only achieved up to 10 ppm with limitation due to the fibre exposure time of the

sample and also the use of agitation impacted significantly on the sampling integrity over 10 ppm.

Martinez et al., 2004, employed the use of solid phase extraction (SPE) to improve PAHs extraction in water using 8 different sorbents and extracting PAHs from groundwater and quantified in GC-MS. C₁₈ sorbent achieved the highest recovery of 16 PAHs while polymeric sorbents achieved the lowest recovery of 3 PAHs. Overall 35 to 113% of the 16 PAHs were recovered using C₁₈ and of this naphthalene and acenaphthene were the least recovered, with a 42% loss in benzo[a]pyrene, benzo[ghi]perylene, indeno[1,2,3-cd]pyrene and dibenzo[a,h]anthracene.

Pena et al., 2009, used ionic liquid based dispersive liquid-liquid extraction (IL-DLLME) to extract 18 PAHs from 9 water sources; ultrapure water, tap water, bottled water, fountain water, well water, rainwater, two sources of river water, treated wastewater and raw wastewater from a wastewater treatment (WWTP) plant in Galicia. Ionic liquid 1-octyl-3-methylimidazolium hexafluorophosphate was used in the dispersive liquid-liquid extraction (DLLME) in high performance liquid chromatography (HPLC) with a fluorescence detector (flu), with 90.3% -103.8% recovery of 18 PAHs achieved.

Extraction and pre-concentration of PAHs in water is often essential in analytical determination of PAHs in water. Limitation of the number of PAHs recovered and the concentration losses has been seen to be a major limiting factor, therefore critical review is required in choosing the type of extraction and pre-concentration method in quantification of the PAHs.

In this research treatment method validation was first carried out on a water matrix with pure water containing PAHs only, after treatment method validation a more complex water matrix was then used with high salt to simulate sea water matrix which would be typical in produced water.

2.2.1 Justification of analytical system

Previous studies have shown various analytical quantification instrument methods that can be used for the analysis of PAHs (Raza et al., 2018; Ivanice et al., 2017; Santos et al., 2016; Menezes et al., 2011; Dianne et al., 2006). Gas chromatography mass spectrometry, flame ionization detection (GC-MS/FID) and High Performance Liquid Chromatography (HPLC-UV) have proven to be the two most predominant analytical quantification instruments used in analysing polycyclic organic hydrocarbons (PAHs). Each of these techniques has its advantages and limitations depending on the desired outcome.

High Performance Liquid chromatography (HPLC) with UV detector

There are early reports of HPLC methods used as an analytical tool in quantifying an analyte in the 1970s with a report published on the use of HPLC with a UV detector in a normal-phase isocratic method in 1977 in quantifying nicotine and cotinine in urine. It was not until the 1980s that reversed-phase HPLC was used and was first reported in 1981 in quantification of tobacco alkaloids. Its ability to separate polar and non-polar compounds, analytically detect a compound without destruction and its non-thermal degradation of the analyte promoted the use of the method over a wide range of analyte quantification. It was not until the 1990s that HPLC was extensively used in the quantification of analytes in water samples. High Performance Liquid Chromatography (HPLC) is an advanced method of liquid chromatography (LC). It has the same principle as that of liquid chromatography (LC), liquid-solid chromatography (LSC) and liquid-liquid chromatography (LLC). Its advantage over this other method is its high sensitivity.

HPLC technique focuses on the concentration measurement of both semi volatile and volatile compounds. Unlike GC which requires the complete volatilization of the

compound, HPLC only requires the compound to be dissolved in a solvent which is compatible with the separation solvent used in the mobile phase. This technique is used widely for quantification of PAHs but the choice of the detector is limited to the PAHs quantified.

HPLC employs the use of a column governed by a nonpolar column packed with a polar mobile phase. PAH samples are injected into this column where they are separated. This then follows through the selected UV detector which shines lights at a specific wavelength which is called the excitation wavelength. Light is then reemitted by the PAH at a much higher wavelength called the emission wavelength depending on the molecular structure of the PAH. The absorbed light is then measured. Using calibrated known PAHs standards, the absorbed light can then be quantified into concentration. Each of the PAHs are then quantified and identified using specific retention times. HPLC-UV is preferable due to its fast speed during sample analysis. Less analytical steps gives room for high integrity by reducing possibility of analytical errors.

2.3. Experimental methods and materials

2.3.1. Material

Analytical standard of a 18 PAHs mixture at 2000 ppm concentration (in benzene:dichloromethane solution) was supplied by sigma Aldrich containing; Naphthalene, Acenaphthylene, 1-methyl naphthalene, 2-methyl naphthalene, Acenaphthene, Fluorene, Phenanthrene, Anthracene, Fluoranthene, Pyrene, Benzo(a)anthracene, Chrysene, Benzo(b)fluoranthene, Benzo(k)fluoranthene, Benzo(a)pyrene, Dibenzo(a,h)anthracene. Analytical grade acetonitrile, methanol and acetone were purchased from Fisher Scientific. Deionized water was generated using PURELAB Dispenser (RO) generating ultrapure (18.2 MΩ.cm at 25°C) water.

2.3.2. Method

PAHs identification and quantification in water was carried out in an HPLC-UV system (Waters Alliance® System) consisting of a solvent delivery pump, UV/VIS detector with variable wavelength photo diode array (PDA), an injection valve with an autosampler and a degasser. The HPLC system used Waters Empower PDA software in the collection and analysis of data. The mobile phase consisted of water (mobile phase A) and acetonitrile (mobile phase B) which were supplied to the PAH column (5 μ m 4.6 x 250mm) at a pre-set gradient (table 2.1) by the solvent delivery pumps. All solvents are initially degassed prior to the start of analysis and degasser maintains these conditions throughout the sample analysis. Standard AOAC 973.30 U.S EPA PAHs identification method was adopted in the analysis of 18 EPA PAHs. This method was employed due to its fast analytical identification and quantification method producing detailed information. In all experiments, triplicate sample of 1 mL were taken to test the repeatability of the experimental results.

The experimental setup employed in this research involved design of a protocol to establish a method for the quantification and identification of PAHs in water. Analytical PAHs standards were prepared at various concentrations and analysed by HPLC UV system. HPLC system was optimized by the selection of right column type, system operating conditions and type of mobile phase to get the best result. The protocol was used in quantifying pre-treatment concentration and post treatment concentration of PAHs present in water.

2.3.3. Method validation

Validation of methods is essential in the justification of the results obtained through this method and for protocols which have been developed based on the results from this method. The validation was carried out using established validation parameter

such as linearity, precision, robustness, limit of detection (LOD) and limit of quantification (LOQ).

Linearity:

A calibration curve was obtained from the plot of a standard PAHs concentration range (4000, 2000, 1000, 500, 125, 62.5 and 50 ppb) against the peak area thereby obtaining a linear regression equation (appendix A). A correlation coefficient (R^2) of 0.9 – 0.9999 was obtained thereby showing a good linear regression. A validated method is required to have a correlation coefficient of between 0.9 and above (Ludwig Huber 2007).

Precision:

A measure of the precision of the method was determined by the repeatability of standard PAHs concentration carried out in the HPLC system. This was carried out in triplicate and analysed on the same day. It was subsequently done in future days to determine any precision variation. Percentage relative standard deviation (%RSD) was the parameter used in measuring the precision by the comparison of concentration of the triplicate standard PAHs sample. A lower %RSD shows a better precision. In this research the precision was tested over a concentration range of 4000, 2000, 1000, 500, 125, 62.5 and 50 ppb carried out in triplicate for each concentration.

Limit of detection (LOD) and Limit of quantification (LOQ):

This validation parameter is vital as this gives the detection and quantification ability of the method. LOD and LOQ are theoretically calculated using a signal to noise ratio

of 3 and 10. LOD of an individual PAH shows the minimum concentration that can be detected by this method while LOQ is the minimum amount that can be quantified.

2.3.3.1. PAHs Identification

A solution of 18 PAHs (1 ppm) was prepared as follows: PAHs (2000 ppm, 10 μ L) was added to acetone (4.9 mL). From this solution, 0.25 mL was sampled and added to acetonitrile (9.75 mL) achieving 1 ppm concentration of 18 PAHs , 1.5 mL sample was then transferred into a 2 mL HPLC vial and analysed using HPLC-UV system under standard HPLC conditions (table 2.1) to identify the retention time of the individual components of the 18 PAHs.

Operating parameter	Values			
HPLC Column	Water PAH Column 5 μ m 4.6 x 250 mm			
Flow rate	1.5 mL/min			
Injection	20 μ l			
Column temperature	30°C			
UV wavelength range	254 – 400 nm			
Sample quantification wavelength	220 nm			
Mobile Phase A	Water (Deionized water)			
Mobile Phase B	Acetonitrile			
Sample run time	35 minutes			
Gradient	Time	Mobile Phase A (%)	Mobile Phase B (%)	
	5	50	50	
	20	0	100	
	28	0	100	
	32	50	50	
	35	50	50	

Table 2.1: HPLC-UV operating conditions for the quantification and identification of PAHs in water

In order to establish a method for the quantification of PAHs in water, seven concentrations of 18 polycyclic aromatic hydrocarbon (PAH) were prepared (4000, 2000, 1000, 500, 125, 62.5 and 50 ppb) and analysed using HPLC-UV. This was

carried out under standard HPLC-UV conditions. Seven point calibration curves were generated by plotting peak area against concentration (appendix 1). The calibration curve generated for each PAH was used to generate a linear regression equation. The linear regression equation (equation 2.1) was used to determine the PAHs concentration by using the amount of UV absorbance in the HPLC-UV system. Samples of 1 mL in triplicate were taken for all experiments.

$$Y = MX + C \quad \text{(Equation 2.1)}$$

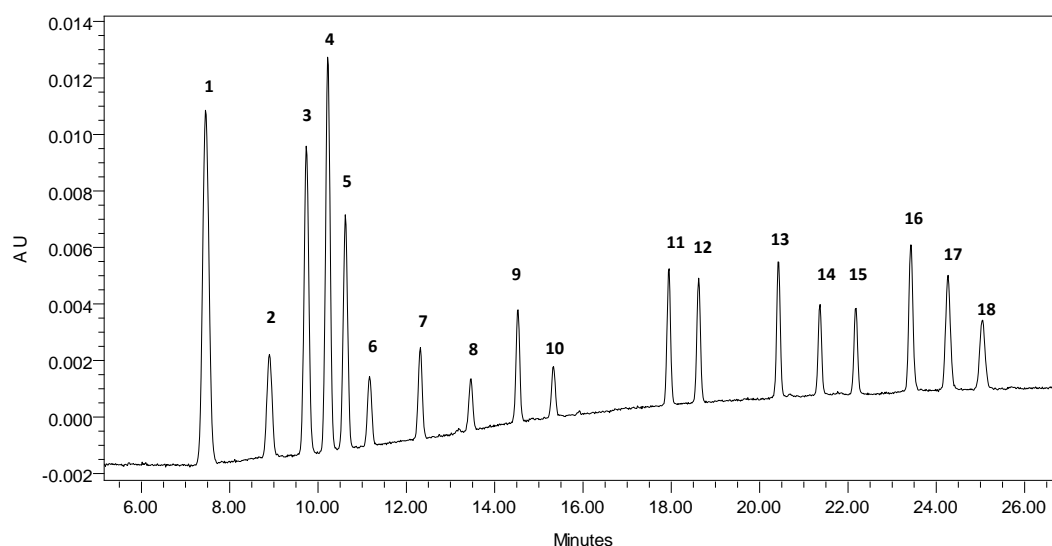
Where X = Concentration of PAHs

Y = UV absorbed

2.4. Result and discussion

2.4.1. Identification of PAHs in water

18 PAHs (1ppm) were identified using analytical HPLC method and represented on a chromatogram (figure 2.1). Each PAH eluted at specific retention time and demonstrating a good separation and resolution (≥ 1.5) between eluted peaks. Each PAH adsorbs at specific UV wavelength (λ_{max}) but was quantified at an optimum wavelength of 220 nm. The polar volatile eluted first before the less volatile PAHs.



1. Naphthalene	10. Pyrene
2. Acenaphthylene	11. Benzo(a)anthracene
3. 1-methyl naphthalene	12. Chrysene
4. 2-methyl naphthalene	13. Benzo(b)fluoranthene
5. Acenaphthene	14. Benzo(k)fluoranthene
6. Fluorene	15. Benzo(a)pyrene
7. Phenanthrene	16. Dibenzo(a,h)anthracene
8. Anthracene	17. Benzo(g,h,i)perylene
9. Fluoranthene	18. Indeno(1,2,3-cd)pyrene

Figure 2.1: 18 EPA PAHs chromatogram showing PAH peaks separated under conditions described in table 2.1

The 18 PAHs were further identified using their unique spectrum generated by the PDA during UV absorbance across a wavelength range of 200 nm – 400 nm. As seen in figure 2.2 and 2.3, naphthalene and phenanthrene can be identified using their max UV absorbance wavelength of 220nm and 250nm respectively which gives them their spectra shape.

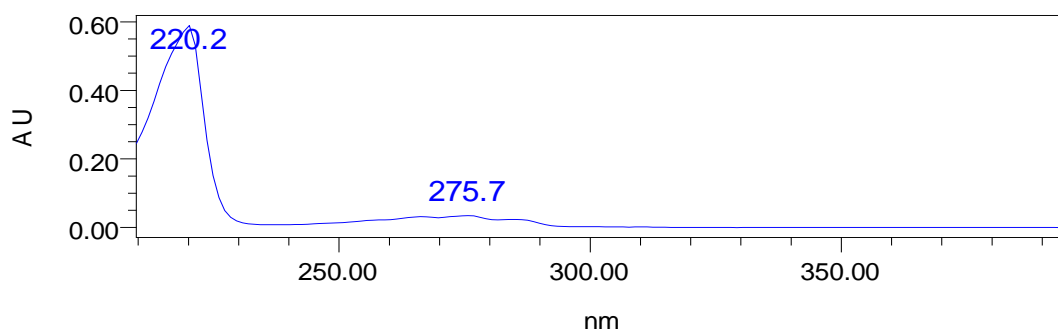


Figure 2.2 : UV adsorption spectra of naphthalene showing max of 220.2 nm

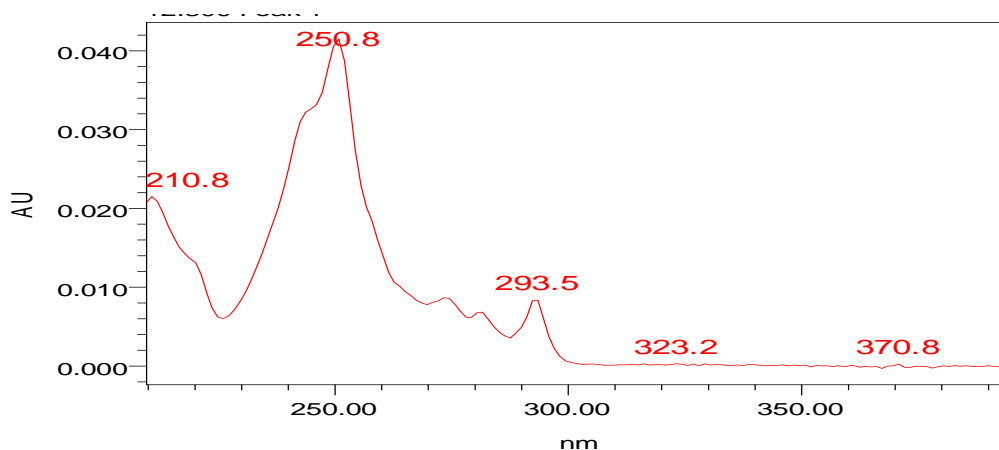


Figure 2.3 – UV adsorption spectra of phenanthrene showing max of 250.8 nm

2.4.2. Effect of UV quantification wavelength on PAH identification

The ability to easily identify the 18 PAHs were investigated using various wavelength. It was observed that at 300 nm wavelength it was easier to identify less polar PAHs which had taller and broader peaks but less easy with more polar PAHs. Naphthalene was not been able to be identified at 300 nm wavelength (figure 2.4).

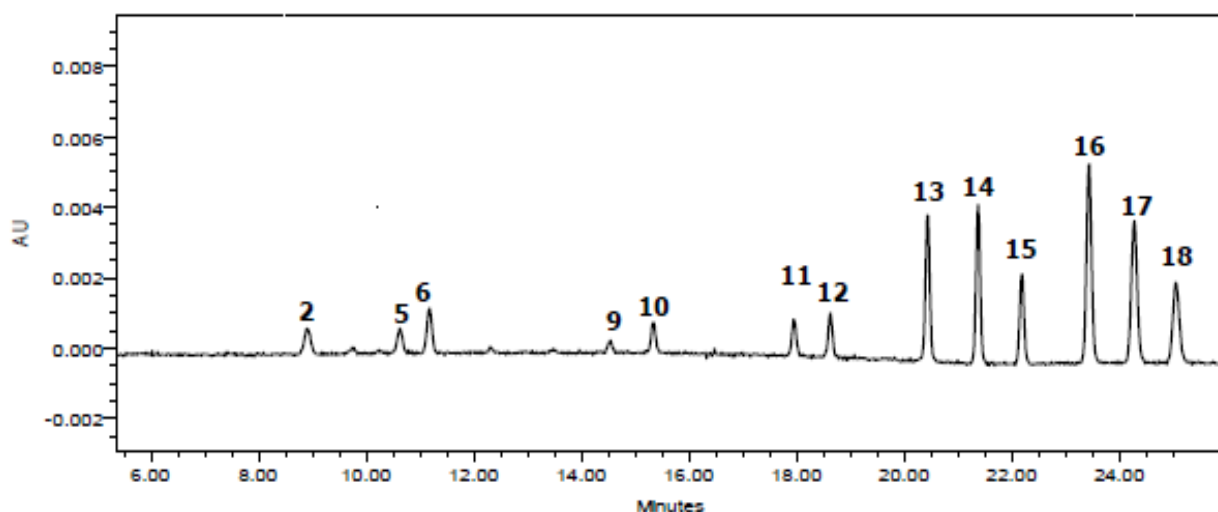


Figure 2.4: Analysis of 18 EPA PAHs by reverse phase chromatogram (1000 ppb) showing the chromatogram at 300 nm

With 254 nm wavelength medium molecular weight PAHs were easily identified based on their taller and peak but heavier PAHs had much smaller peaks making it difficult to identify (Figure 2.5).

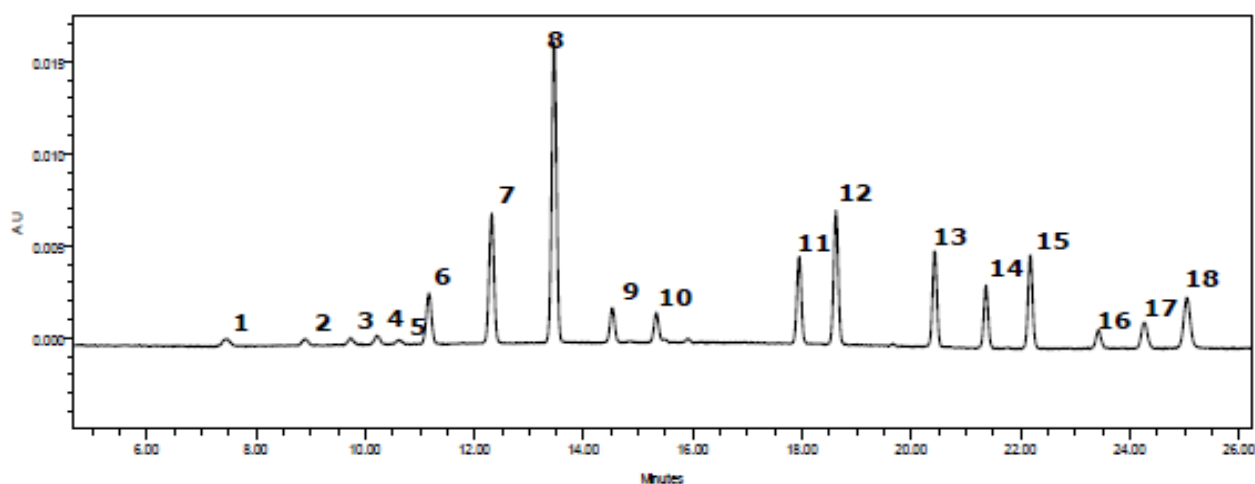


Figure 2.5: Analysis of 18 EPA PAHs by reverse phase chromatogram (1000 ppb) showing the chromatogram at 254 nm

The optimum wavelength of 220 nm was established to be the best wavelength as all 18 PAHs were easily identified giving significant peak height and area (figure 2.6).

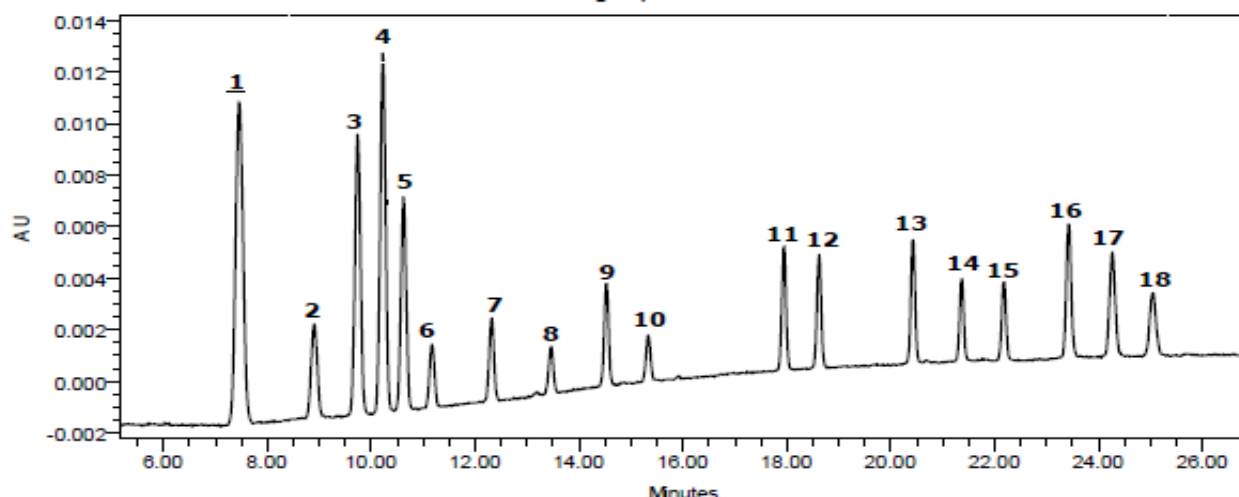


Figure 2.6: Analysis of 18 EPA PAHs by reverse phase chromatogram (1000 ppb) showing the chromatogram at 220 nm

2.4.3. Validation of identification and quantification method

In identification and quantification studies, the efficiency of this process is referred to as resolution value (R_s) as earlier discussed. The resolution value for the method used in this research was investigated using three important factors; capacity factor (k), selectivity factor (α) and column efficiency (n).

Capacity factor (k)

Investigating the capacity factor (k) of the experimental method using the identification of fluoranthene and pyrene in a mixture, a good separation was achieved with capacity factor of 5.7 (figure 2.7, equation 2.2). This falls within the acceptable range for good separation of analyte in a column.

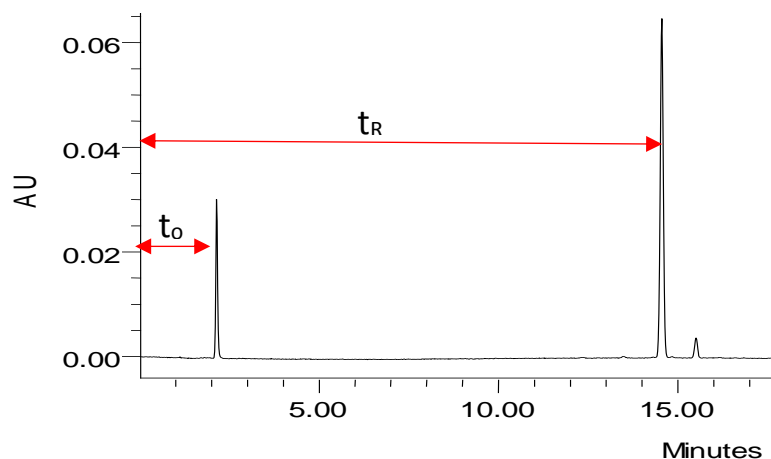


Figure 2.7: Capacity factor calculated for analytical method

$$k = \frac{(T_R - T_0)}{T_0} = \frac{(14.5 - 2.15)}{2.15} = 5.7 \quad (\text{Equation 2.2})$$

Selectivity factor (α)

Selectivity factor was further investigated also for the separation of fluoranthene and pyrene on the chromatogram and a good selectivity (α) of 1.08 was achieved (figure 2.8, equation 2.3). This proves a good separation was achieved and also that no two analytes eluted together. Selectivity factor of all 18 PAHs peaks shown in table 2.2 show a good separation of all analyte on the chromatogram

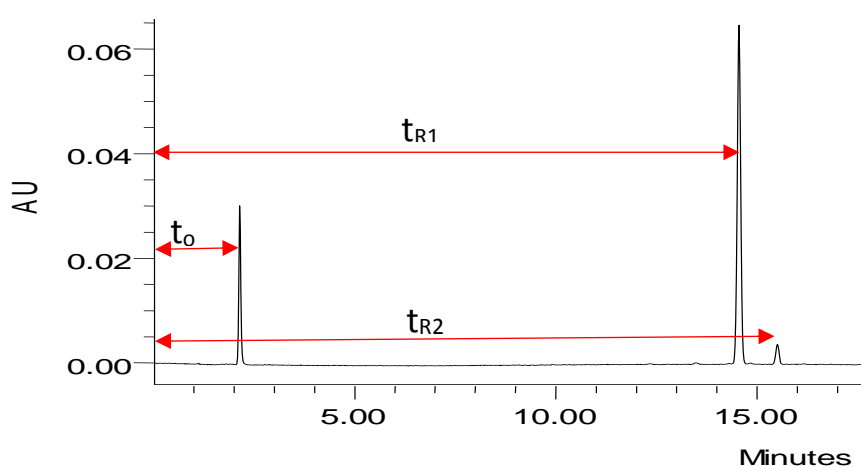


Figure 2.8: Selectivity factor calculated for analytical method

$$\alpha = \frac{k_2}{k_1} = \frac{(t_{R2} - t_0)}{(t_{R1} - t_0)} = \frac{(15.5 - 2.15)}{(14.5 - 2.15)} = 1.08 \quad (\text{Equation 2.3})$$

Column efficiency (*n*)

A high number of 13456 plates is achieved for the 4.6 x 250 mm column used with particle size 5µm (figure 2.9, equation 2.4). This shows a very good efficiency due to the high number of plates and this can further be seen by the narrow peaks obtained for each analyte.

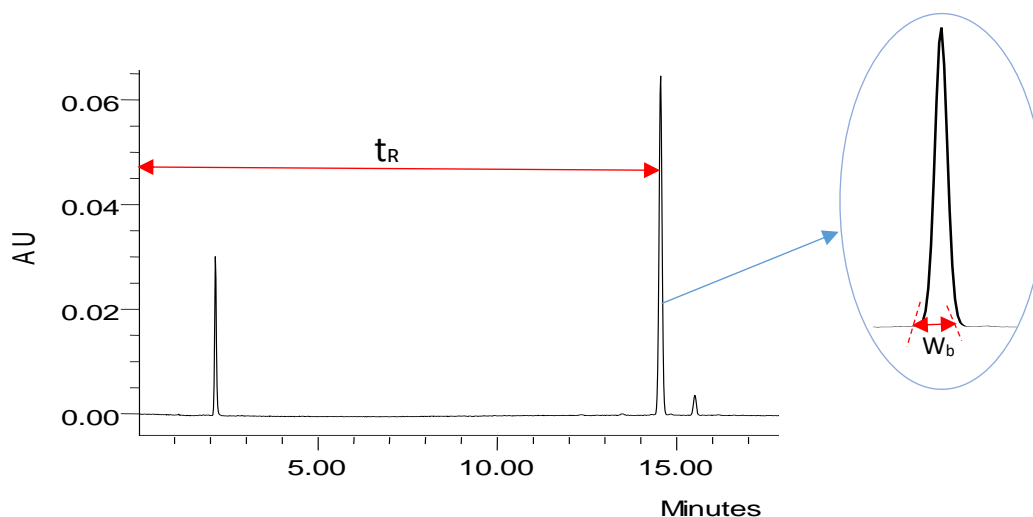


Figure 2.9: Chromatographic column efficiency calculated for analytical method

$$n = 16 \left[\frac{t_R}{W_b} \right]^2 = 16 \left[\frac{14.5}{0.5} \right]^2 = 13456 \quad (\text{Equation 2.4})$$

Resolution value (*Rs*)

The resolution value (*Rs*) investigated employing the capacity factor, selectivity factor and column efficiency in equation 2.10 shows an *Rs* of 1.83. *Rs* greater than 1.5 between the two case study peaks; fluoranthene and pyrene, shows the analyte are separated well enabling for accurate identification and quantification.

	PAH	Capacity factor (k)	Selectivity factor (α)	Column efficiency (n)	Resolution value (Rs)
1	Naphthalene	2.5	1.3	3600	2.5
2	Acenaphthylene	3.2	1.1	5184	1.2
3	1-methyl naphthalene	3.5	1.1	6084	1.4
4	2-methyl naphthalene	3.8	1.1	6724	1.5
5	Acenaphthene	3.9	1.1	7396	1.6
6	Fluorene	4.2	1.1	8100	1.7
7	Phenanthrene	4.7	1.1	9604	1.8
8	Anthracene	5.3	1.1	11664	2.1
9	Fluoranthene	5.7	1.1	13456	2.2
10	Pyrene	6.1	1.2	14884	4.4
11	Benzo(a)anthracene	7.3	1.1	20164	2.8
12	Chrysene	7.7	1.1	22500	3.0
13	Benzo(b)fluoranthene	8.5	1.1	26896	3.3
14	Benzo(k)fluoranthene	8.9	1.1	28900	3.5
15	Benzo(a)pyrene	9.3	1.1	31684	3.7
16	Dibenzo(a,h)anthracene	9.9	1.1	34894	3.9
17	Benzo(g,h,i)perylene	10.3	1.1	37636	4.0
18	Indeno(1,2,3-cd)pyrene	10.6	-	40000	-

Table 2.2 – Capacity factor, selectivity factor, column efficiency and resolution value of HPLC system

$$Rs = \frac{1}{4} \sqrt{n} \times \frac{\alpha - 1}{\alpha} \times \frac{k}{1 + k}$$

$$Rs = \frac{1}{4} \sqrt{13456} \times \frac{1.08 - 1}{1.08} \times \frac{5.7}{1 + 5.7} = 1.83 \quad (\text{Equation 2.5})$$

Further to this the capacity factor, selectivity factor, Column efficiency (n) and resolution value (Rs) was calculated (table 2.2) for the 18 PAHs to determine the overall sustainability of the method.

2.4.4. PAH Quantification

Seven point calibration curves of 18 PAHs were generated by plotting peak area against concentration (appendix 1). As seen for Naphthalene (figure 2.10) the calibration curve generated a good linear regression equation of $y = 575x + 2281$

where y is the UV absorbance and x the concentration. This was also seen in the subsequent PAHs (table 2.3). Correlation coefficient (R^2) was generated for individual calibration curve to determine the calibration linearity (table 2.3). Excellent linearity (0.99994-0.99999) was obtained for all the 18 PAHs with good precision of triplicate injection within 5% RSD. HPLC system of the quantification method was found to be greater than 97% for all 18 PAHs.

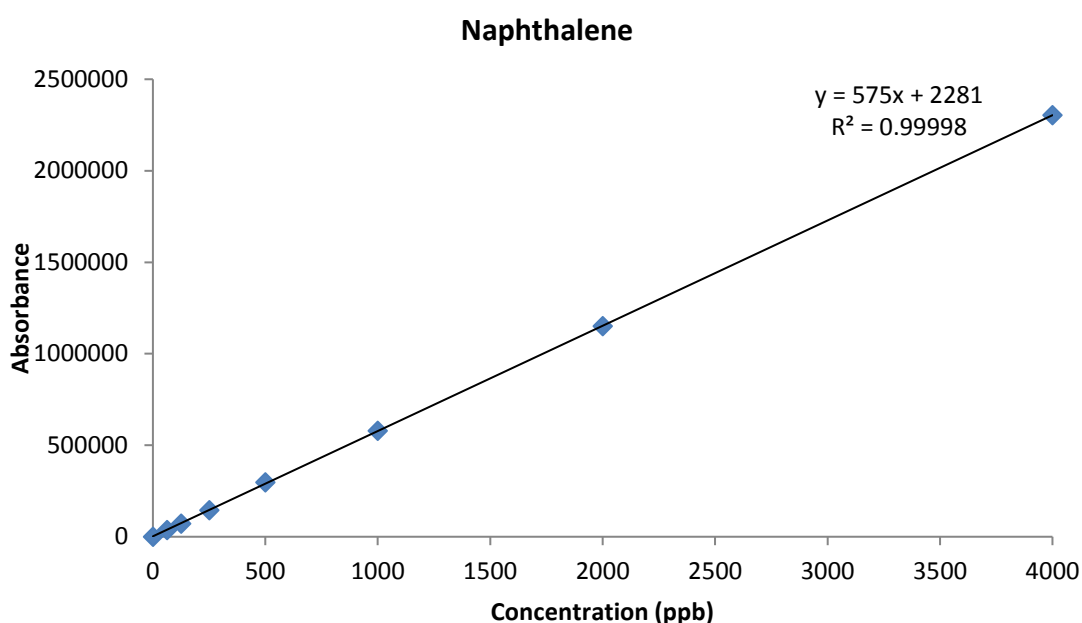


Figure 2.10: Calibration curve for naphthalene. Mobile phase in HPLC-UV system; acetonitrile:water. Flow rate; 1.5 mL/min, UV detection at 220nm. n=3

	PAH	Retention Time	Regression Equation	Linearity (R ²)
1	Naphthalene	6.7	$y = 575x + 2281$	0.99998
2	Acenaphthylene	8.3	$y = 137x - 109$	0.99994
3	1-methyl naphthalene	9.2	$y = 373x + 1847$	0.99999
4	2-methyl naphthalene	9.8	$y = 457x + 1656$	0.99999
5	Acenaphthene	10.2	$y = 263x + 959$	0.99999
6	Fluorene	10.8	$y = 73x + 574$	0.99997
7	Phenanthrene	12.0	$y = 91x + 367$	0.99994
8	Anthracene	13.2	$y = 50x + 215$	0.99999
9	Fluoranthene	14.3	$y = 111x + 373$	0.99999
10	Pyrene	15.2	$y = 51x + 259$	0.99996
11	Benzo(a)anthracene	17.8	$y = 128x + 502$	0.99999
12	Chrysene	18.5	$y = 118x + 456$	0.99998
13	Benzo(b)fluoranthene	20.4	$y = 128x + 279$	0.99999
14	Benzo(k)fluoranthene	21.3	$y = 84x + 224$	0.99997
15	Benzo(a)pyrene	22.1	$y = 82x + 226$	0.99998
16	Dibenzo(a,h)anthracene	23.4	$y = 160x - 38$	0.99998
17	Benzo(g,h,i)perylene	24.2	$y = 147x - 51$	0.99998
18	Indeno(1,2,3-cd)pyrene	25.0	$y = 100x - 349$	0.99996

Table 2.3: HPLC-UV system calibration data for 18 PAHs. Regression equation and linearity generated from calibration curve.

2.4.5. Limit of detection (LOD) and Limit of Quantification (LOQ)

The HPLC-UV method was determined by investigating the minimum concentration that can be detected and quantified by the HPLC-UV system. A signal to noise ratio of 3 and 10 were used to determine the LOD and LOQ (equation 2.6 and 2.7) of the HPLC-UV system at UV detection of 220nm (Huber 2007). The calculated range was between 62.5-250ppb

$$LOD = 3 \times \frac{SD}{\beta} \quad (\text{Equation 2.6})$$

$$LOQ = 10 \times \frac{SD}{\beta} \quad (\text{Equation 2.7})$$

Where:

SD = Standard deviation

σ = Slope of Calibration Curve

The theoretical LOD and LOQ calculated for the 18 PAHs showed that the analytical system could quantify much lower concentration of PAHs. The LOD and LOQ theoretical limit for the 18 PAHs was within a range of 0.50 - 3.92 ppb and 1.66 - 18.87 ppb respectively (table 2.4). This defined the solution concentration limit that was used in this work. The LOD and LOQ falls below the concentration discharge regulator limits which gives the research work the ability to quantify PAHs in the regulatory limit set by the environmental quality under the water framework directive for individual PAHs.

	PAH	LOD (ppb)	LOQ (ppb)
1	Naphthalene	0.50	1.66
2	Acenaphthylene	2.08	6.93
3	1-methyl naphthalene	0.77	2.56
4	2-methyl naphthalene	0.63	2.09
5	Acenaphthene	1.09	3.63
6	Fluorene	3.92	13.08
7	Phenanthrene	3.12	10.40
8	Anthracene	5.66	18.87
9	Fluoranthene	2.56	8.54
10	Pyrene	5.54	18.46
11	Benzo(a)anthracene	2.24	7.46
12	Chrysene	2.41	8.03
13	Benzo(b)fluoranthene	2.23	7.44
14	Benzo(k)fluoranthene	3.40	11.33
15	Benzo(a)pyrene	3.45	11.51
16	Dibenzo(a,h)anthracene	1.78	5.94
17	Benzo(g,h,i)perylene	1.94	6.46
18	Indeno(1,2,3-cd)pyrene	2.84	9.48

Table 2.4: 18 PAHs LOD and LOQ for HPLC-UV system.

2.5. Conclusion

The analytical method development, justification and validation were presented in this chapter. Selection of the most suitable method was determined by critical reviewing of past literature followed by the investigation of the best practice by the optimization of the analytical system when quantifying PAHs. Measures such as percentage relative standard deviation (%RSD) and repeatability tests were used to determine the robustness, accuracy and precision of the analytical method. Justification for the analytical method was carried out by the use of parameters such as capacity factor, selectivity factor, chromatogram column efficiency and resolution value in order to ascertain the reliability of the results. Results produced by the HPLC analytical method were critically analysed and checked using the factors to determine the efficiency of the system. PAHs were identified based on the retention time at which they elute on the HPLC chromatogram and also compared with the spectra generated at that specific retention time. Quantification HPLC conditions (quantification wavelength) were optimized in order to achieve easy and precise interpretation and quantification of results. Calibration of the HPLC analytical system was also carried out in order to achieve consistency in reading over the period of analysis. The regression linear equation derived from the calibration curve is used in quantification of PAHs analysed in the HPLC system. The analytical limits were also investigated using a theoretical approach alongside values from experimental results. The limit of detection (LOD) and limit for quantification (LOQ) were derived from the HPLC analytical system to give the lowest possible value the system can accommodate. The established analytical system was subsequently used in the quantification of PAHs in the remediation of PAHs using chitosan biopolymer in chapter 3 and also in chapter 4 and 5 in quantifying PAHs during the photocatalytic degradation of

PAHs. The HPLC analytical system was able to quantify PAHs below the SEPA legislation limit allowing for the ability to verify if the remediation method investigated was efficient enough to reduce PAHs to required standards.

CHAPTER 3

3.0. POLYCYCLIC AROMATIC HYDROCARBON REMEDIATION USING CHITOSAN

3.1. Introduction

Coagulants are chemicals used in water remediation by destabilizing colloids, particles and organic compounds present in water. Coagulants are generally nontoxic with no effect on humans. In water, they are insoluble with solubility influenced by the water pH level. Coagulant ability in generating coagulation-flocculation greatly depends on its molecular weight and electrical charge. Coagulation-flocculation involves two mechanisms: neutralization of charge and bridging of particles.

Neutralization of charge occurs when the positive charge coagulants attach and interact with the negative charge pollutant surface charge leading to a zero charge on the pollutant surface (figure 3.1). The neutralized pollutant can therefore come together forming a flocs which can be allowed to settle and collect.

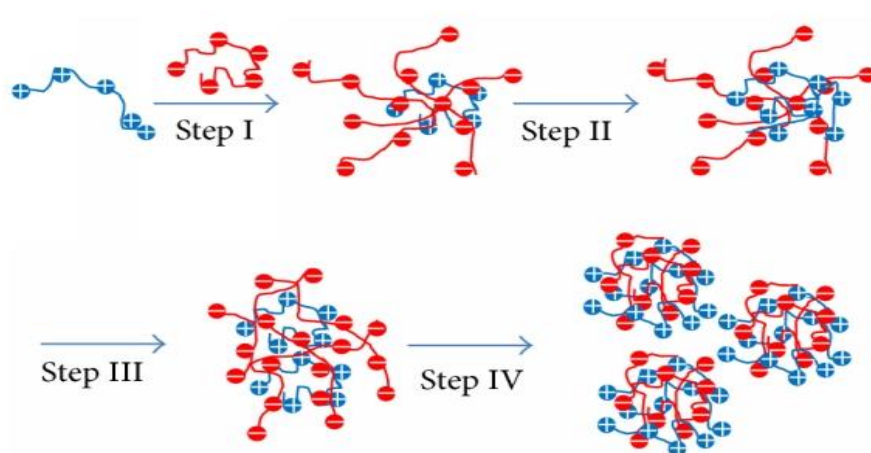


Figure 3.1: Flocs formation through positive and negative charge adsorbent and specie

Bridging of particles occurs when a polymer such as chitosan has the ability to adsorb onto the surface of multiple molecules of a pollutant in water. This thereby forms a large flocs that can be collected leading to the removal of pollutant from water.

3.1.1. Efficiency of Chitosan as a coagulant

Chitosan coagulants have unique characteristics of positive charge as a result of protonation of $-NH_2$. Together with a long chain and polymeric structure, this makes it an effective coagulant. The positive charge of chitosan is a great advantage due to the negative charge many pollutants have in water thereby allowing for the quick interaction between the chitosan and the pollutant in water. The more $-NH_2$ groups present in the molecular structure of chitosan the higher the positive charge. Chitosan is soluble in acidic water but solubility reduces with increased pH level. This can suggest that chitosan is more efficient in neutral pH or higher since insolubility of chitosan encourages the bridging of particles and also charges neutralization. The influence of pH level on the coagulation-flocculation process using chitosan was investigated in this research.

3.1.1.1. Chitosan Structural factor : Influence on treatment efficiency

Established knowledge of the relationship between the structure activities possessed by a material can help in the optimization of its structure to achieve the maximum potential of the material. This applies also to chitosan structure on the coagulation-flocculation process. Chitosan's unique structural characteristic and the in-depth knowledge of its structural relationship has resulted in the wide application of pollutant's removal in water.

The degree of deacetylation (DD) and molecular weight (MW) of chitosan which is directly related to its structure is a major factor that influences the efficiency of

chitosan as a flocculant. The degree of deacetylation directly influences the charge neutralization efficiency while the molecular weight determines the bridging efficiency in coagulation-flocculation process.

An increase in the DD results in the increase in free -NH_2 groups thereby increasing the positive charge of chitosan resulting in an increase in charge neutralization efficiency. This was proven by Huang *et al.*, who investigated the charge density result of chitosan having a DD range of 48% to 86%. The chitosan with different DD which were prepared from deacetylated chitin using NaOH solution showed that chitosan with DD of 48% and 68% resulted in a charge density of 3 meq/g and 6.1 meq/g. Vogelgang *et al.*, also investigated the effect of DD (51% – 99%) on the removal of humic substance and achieved a 10% increase in removal efficiency with an increase of DD from 51% to 99%.

Chitosan with high MW achieves better bridging efficiency compared to that of low MW. This is due to the larger molecular chain conformation when present in water thereby improving the bridging capacity. Nicu *et al.*, investigated using three chitosans of different MW to remove pulp and calcium carbonate and recorded a greater flocculation efficiency with the chitosan of higher MW. Ashmore and Hearn further demonstrated this by comparing chitosan of different MW in the removal of polystyrene latex particles. They were able to prove that flocculation efficiency increased with an increase in chitosan MW.

Studies have shown that DD has a much more significant impact on removal optimization in achieving high treatment efficiency than the impact of MW of chitosan. This was proven by Roussy *et al* who investigated the removal of ink from industrial waste using two chitosan: low MW (8.01×10^4 g/mol) and high MW (3.08×10^5 g/mol) of the same high DD (89.5%). Even though high MW chitosan improved the

removal efficiency, the overall efficiency improvement was not substantial. This shows chitosan structural characteristics can be further optimized through the influence of factors such as pH, dosage, ionic strength, and temperature to increase its treatment efficiency potential.

The impact of pH level on treatment efficiency is influenced based on the DD or MW of chitosan used, which can either promote the treatment efficiency or have a negative impact. Chung *et al.*, showed this by investigating chitosan of the similar high MW (3.0×10^5 g/mol – 6.0×10^5 g/mol) and similar high DD (80% -98%) across a pH level of 3 to 10 and recorded the best removal efficiency for BOD and COD in aquaculture wastewater occurring at low pH level.

3.2. Experimental

3.2.1 Materials and method

Naphthalene (crystal form), phenanthrene (powder) and chitosan (low molecular weight; 50,000 – 190,000 Da) were purchased from Sigma, UK. Acetonitrile, dichloromethane, acetic acid, methanol and acetone were of analytical grade and purchased from Sigma. Deionized water was obtained from a PURELAB deionizer purification system. Other apparatus used were; 100 mL and 500 mL Pyrex bottles, 2 mL HPLC vials, 1.5 mL micro-centrifuge vials, 1 L beaker.

3.2.2 Chitosan as a coagulant in PAH removal in water

A stock naphthalene solution (2000 ppm) was prepared by adding crystal naphthalene (100 mg) into methanol (2 mL). A subsequent dilution of the stock naphthalene (0.1 mL) into methanol (2.4 mL) was carried out. This was also repeated with phenanthrene (100mg). Each of the stocks were spiked in deionized water individually. Spiked water was then produced by adding stock naphthalene (1 mL) into deionized water (800 mL) which was also carried out for phenanthrene separately. Jar batch sample preparation was employed in a closed system in order to reduce the amount of naphthalene and phenanthrene lost to the atmosphere as a result of evaporation.

A jar test was carried out which involved the use of the stock sample of naphthalene in water with the addition of chitosan in the coagulation-flocculation treatment process. Naphthalene and phenanthrene contained in each stock sample individually were investigated using chitosan powder with a concentration range of 12.5, 25, 50, 75, 100, 1000, 10000 and 100000 ppm.

The study of PAHs treatment using chitosan was carried out with the use of chitosan in powder form and also when dissolved in acetic acid. The study investigated the effect chitosan in these two forms has on the removal efficiency of PAHs. Also the settling time was investigated. The investigation was carried out using coagulation-flocculation treatment method.

3.2.2.1 Powder chitosan in removal of PAHs in water

As illustrated in figure 3.3, powdered chitosan of 10, 20 and 40 mg was added into 800 mL of the stock spiked water (containing naphthalene) to attain a concentration of 12.5, 25 and 50 ppm of chitosan respectively. This was then transferred into a flocculator and stirred at 200 rpm for 3 minutes and then 30 rpm for 30 minutes

(figure 3.4). It was then allowed to settle for 30 and 60 minutes (Christophersen *et al.*, 2006) (figure 3.5). A sample was taken from the top 100 mL of the treated water surface into a 2 mL HPLC vial and then quantified using HPLC-UV. Percentage removal efficiency was then calculated using the concentration of naphthalene in water before and after the treatment.

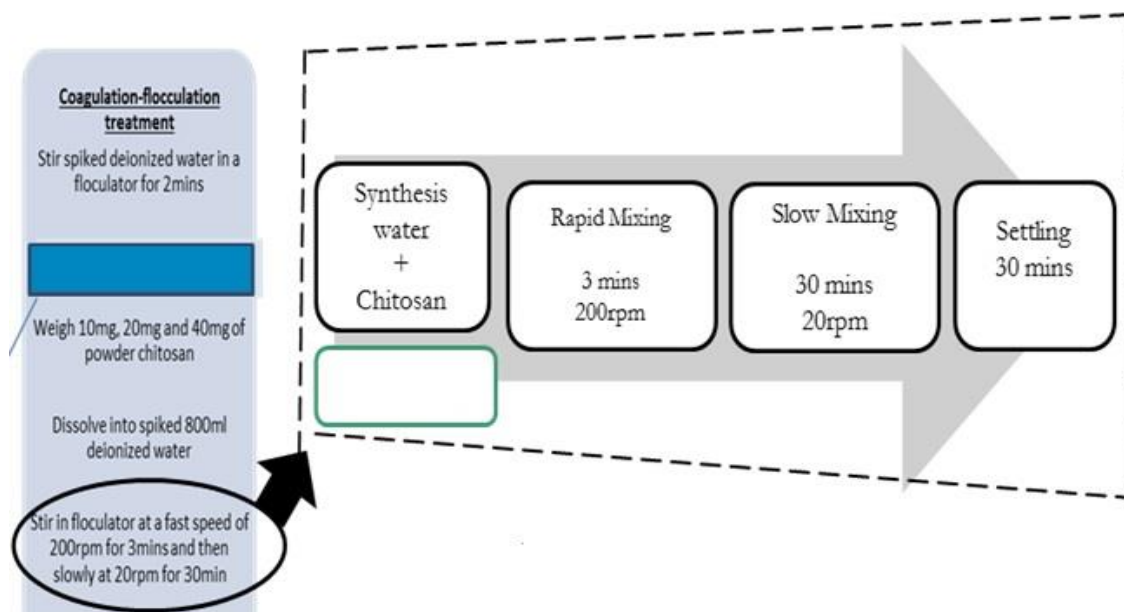


Figure 3.3 – Experimental protocol for powder chitosan for the adsorption of PAHs in water



Figure 3.4 : Experimental setup of Coagulation-flocculation method



Figure 3.5 : Chitosan settled in naphthalene solution

3.2.2.2 Solubilized chitosan in removal of PAHs in water

As illustrated in figure 3.6, chitosan solution (in 1% (v/v) acetic acid), 5000 ppm, 2 mL and 4 mL was transferred individually into 800mL of spiked water (containing naphthalene) to attain a concentration of 12.5 ppm and 25 ppm respectively. Further to this 4 mL of 20000 ppm chitosan solution (in 1% (v/v) acetic acid) was transferred into 800 mL of deionized water to attain a concentration of 100 ppm (figure 3.6). Subsequent concentrations of 1000, 10000 and 100000 ppm of chitosan in water were prepared and used. This was also carried out using the water spiked with phenanthrene. The coagulation-flocculation treatment method used with chitosan powder was also adopted for chitosan in dissolved acetic acid. The percentage removal efficiency was subsequently determined.

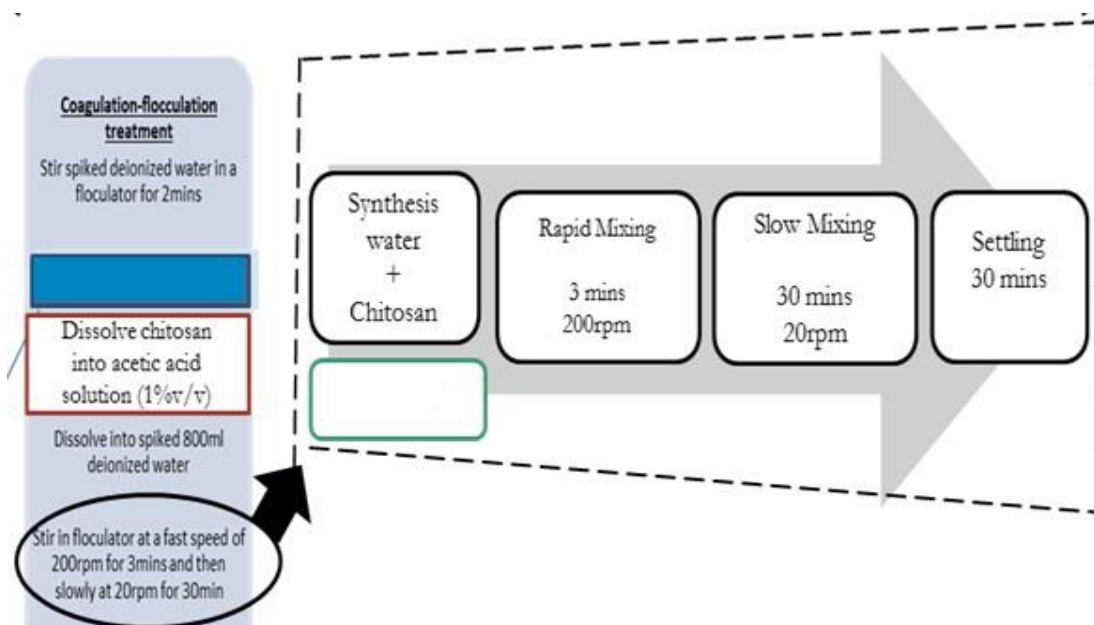


Figure 3.6 – Experimental steps using solubilized chitosan for the adsorption of PAHs in water

3.2.2.3 Effect Contact time has on PAHs removal efficiency

The contact time for the formation of the flocs in the coagulation-flocculation treatment method was investigated for powder chitosan. The contact time was varied: 0.1, 1, 24, 72 and 120 hrs and the efficiency was investigated. The results were then compared with results reported in published literature.

3.3. Results and discussion

3.3.1. Effect of Powder chitosan on the removal of naphthalene in water

The evaluation of naphthalene removed by powder chitosan was found to have removed very little pollutant (figure 3.7). A removal efficiency of 7.9%, 8.1% and 6.5% was attained for powder chitosan concentration of 12.5, 25 and 50 ppm respectively at settling-contact time of 30 minutes. Results of the sorption experiment showed that powder chitosan at varied concentrations did not exhibit

high sorption and removal efficiency towards the removal of naphthalene in water. This could be as a result of the low miscible nature of powder chitosan when directly introduced into water. This limits the mass transfer by the accumulation of the PAHs onto the surface of the chitosan surface which reduces its sorption ability. Another influence can be as a result of the chitosan particle size. Zheng *et al.*, 2010 show this effect particle size has on sorption equilibrium drawing the conclusion that the smaller the particle size of a substance the lower the sorption.

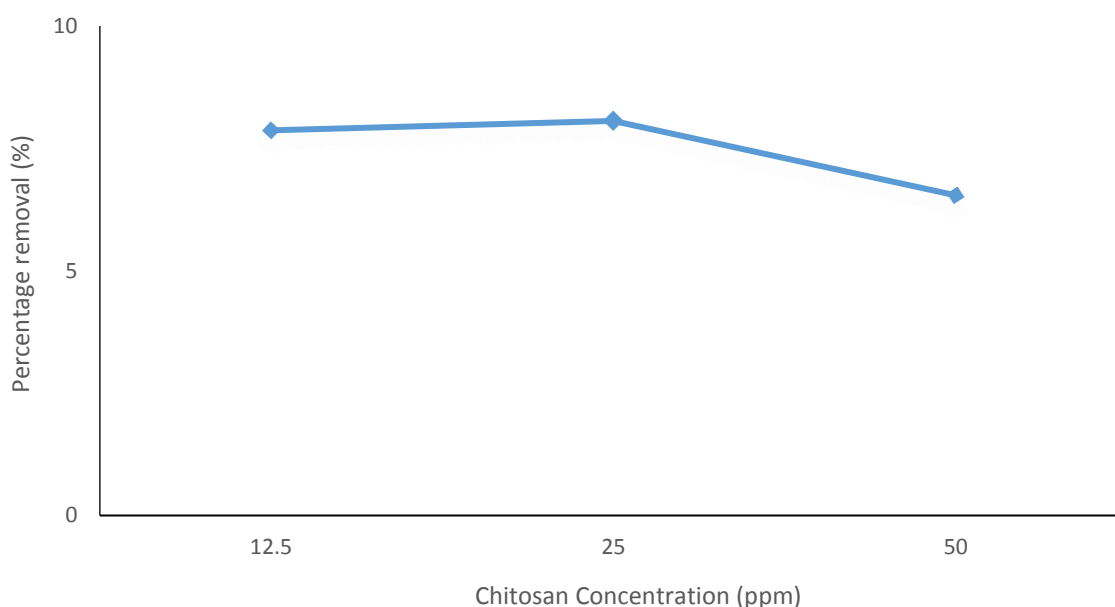


Figure 3.7: The effect of powder chitosan (12.5, 25 and 50ppm) on the removal of Naphthalene in water

The results here were compared with similar investigations published in literature using other adsorbants in remediating PAHs. Oleszczuk *et al.*, (2015) investigated the removal of naphthalene with the use of Biochar in aqueous solution. Due to the high surface area and porous structure of biochar, a higher sorption was attained thereby achieving a 57% removal of naphthalene. The limitation to this is the

secondary treatment of the biochar which is not biodegradable like chitosan. Further to this Hale *et al.* (2012) also investigated the removal of naphthalene in pore water from contaminated soil using activated carbon. Compared to results from this chitosan experiment a much high sorption was also attained. A removal efficiency of 67% was achieved which is attributed to the high surface area of activated carbon (300 m²/g – 3000 m²/g)

Comparing the results of chitosan other adsorbents showed chitosan used in powder form did not show any significant effect in the removal of naphthalene. Therefore further investigation needed to be carried out in order to increase the mass transfer between the PAHs and chitosan. Increasing the miscibility of PAHs to aid the mass transfer was investigated.

3.3.2. Effect of solubilized chitosan on the removal of naphthalene in water

Evaluation of solubilized chitosan was found to have little effect on naphthalene removal (Figure 3.8). It shows the treatment efficiency when using solubilized chitosan (in 1%w/w acetic acid) as an absorbent in a coagulation-flocculation treatment process of naphthalene and phenanthrene at settling-contact time of 30 minutes. The solubilized chitosan showed similar results as when used in a powder form. At chitosan concentration 12.5 ppm a naphthalene removal efficiency of 5% was achieved. In an effort to further optimize the remediation, high concentrations of chitosan at 25, 50, 75, 100, 1000, 10000 and 100000 ppm were investigated to determine the potential impact on naphthalene removal efficiency. It was observed that no significant changes occurred with the increase in chitosan concentration as chitosan concentration of 100000ppm still maintained a low removal efficiency of 6%.

The results from the investigation of phenanthrene removal show a slightly better removal efficiency of 15% at chitosan concentration of 12.5 ppm. This can be

attributed to the hydrophobic character of phenanthrene compared to that of naphthalene. Phenanthrene is more hydrophobic for water than naphthalene thereby giving it a greater tendency to be easily adsorbed by the chitosan. These results were compared with Yakout *et al* (2013) who investigated the removal of naphthalene, phenanthrene and pyrene using low-cost activated carbon. Their results showed that phenanthrene and pyrene had higher removal efficiency compared to naphthalene due to their higher hydrophobicity. The recorded removal efficiency sequence was naphthalene < phenanthrene < pyrene.

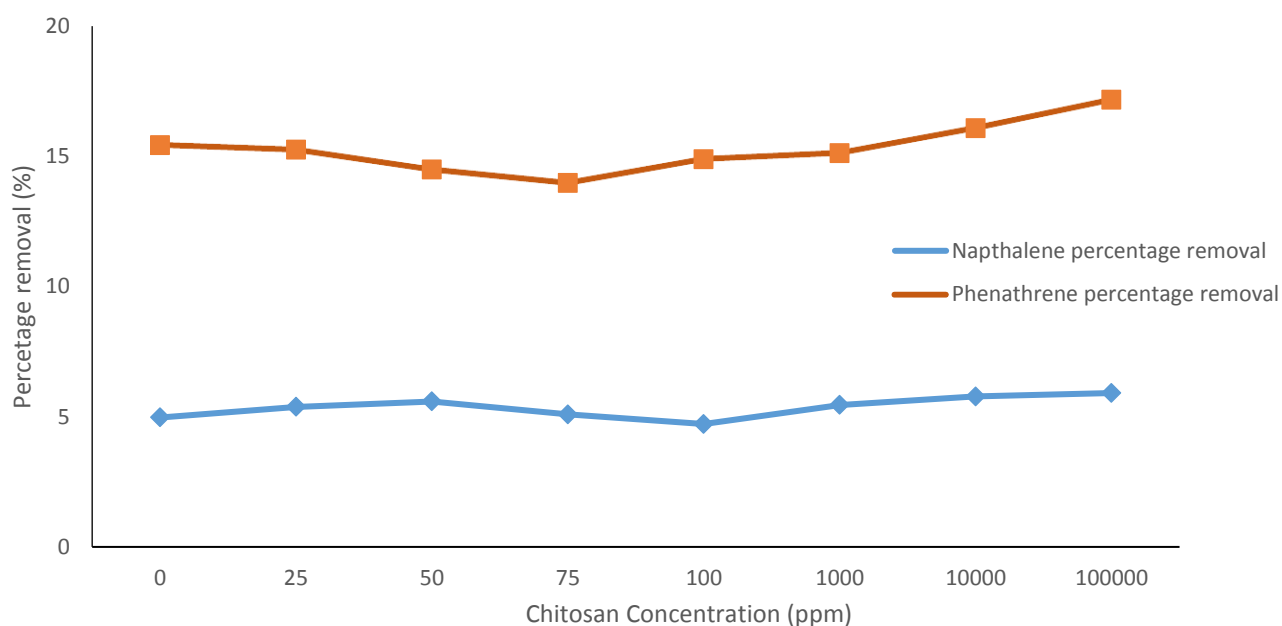


Figure 3.8: The effect of chitosan on the removal of Naphthalene and phenanthrene in deionized water

3.3.3 Effect of settling time of naphthalene and phenanthrene removal using powder chitosan

In effort to optimize the remediation method, the settling-contact time were investigated for 12.5 ppm and 25 ppm chitosan concentration. Contact time of 0.5, 24, 48 and 120 hours were investigated to determine the influence on the removal efficiency. As illustrated in figure 3.9, the removal efficiency for naphthalene at contact time of 0.5, 24, 48 and 120 hours were 10%, 44%, 58% and 88% respectively when 12.5ppm of chitosan was used. Also at chitosan concentration of 25 ppm, naphthalene attained a removal efficiency of 11%, 46%, 66% and 88% at contact time of 0.5, 24, 48 and 120 hours respectively.

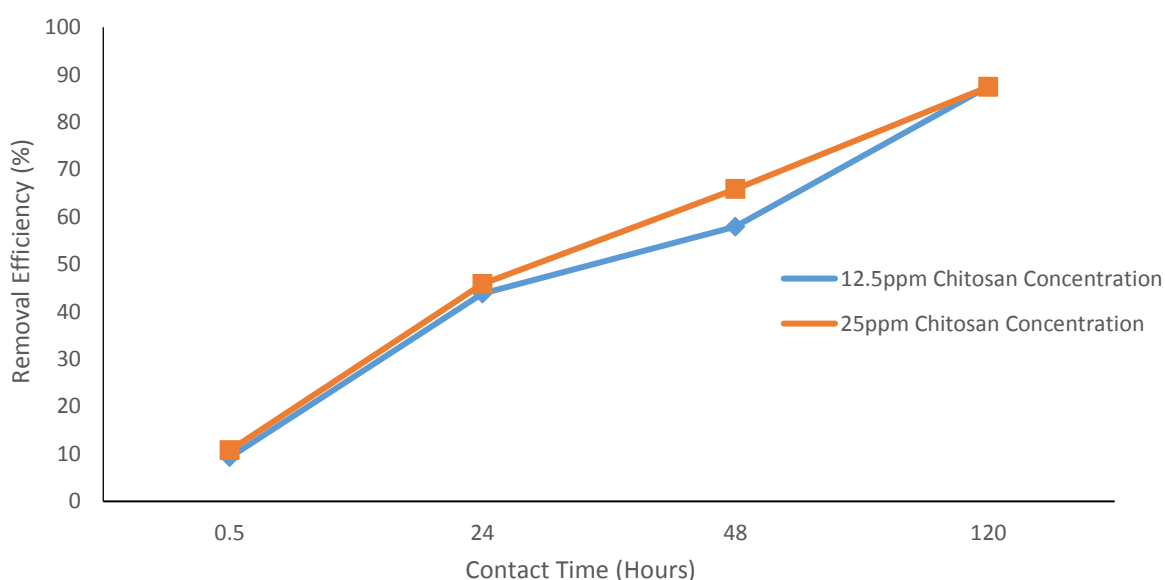


Figure 3.9: The effect of chitosan (1.25 and 2.5ppm) on the removal of Naphthalene in deionized water at settling time: 0.5, 24, 48 & 120 hours.

Figure 3.9 shows the removal efficiency of naphthalene using powder chitosan at various contact times. The results show that an increase in contact time subsequently increased naphthalene removal efficiency. At 120 hours contact time a removal efficiency of 88% was achieved. Contact time has been reported to improve the

adsorption of species onto adsorbent. Yakout *et al.*, (2013) investigated this in the study of adsorption of naphthalene, phenanthrene and pyrene onto low cost activated carbon. Results from the investigation shows removal efficiency increased by 22% for the 3 PAHs when contact time was increased by 24 hours. Also Yuan *et al.*, (2010) in the investigation of PAHs adsorption from water using porous carbon showed that that removal efficiency increased with contact time. Naphthalene one of the PAHs investigated showed an increase to 98% removal efficiency when contact time was increase by 160 hours.

Comparison of results from published literature and experimental results shows that the contact time improves the removal efficiency of PAHs from water. The long contact time allows for the positively charged chitosan to interact longer with the negatively charged PAHs which allows for the formation of more flocs of chitosan and PAHs.

3.4 Conclusion

The adsorption of PAHs onto chitosan in a coagulation-flocculation removal process was investigated here. Chitosan in powder form used as an adsorbent showed little removal effect on naphthalene. A maximum removal efficiency of 8.1% was attained with a chitosan concentration of 25 ppm at a contact time of 30 minutes. The removal efficiency did not show any improvement when the concentration of chitosan was increased to 50 ppm. The surface area of chitosan limited the sorption ability over a short contact time. When compared with other adsorbents in published literature, a much higher sorption was attained with respect to their higher surface area.

Further steps were carried out in optimizing the coagulation-flocculation method, chitosan was solubilized in acetic acid in order to increase the miscibility with the

PAHs in water. The results demonstrated similar findings as to that of the powder chitosan with recorded naphthalene removal efficiency of 5% at chitosan concentration of 25 ppm. A better phenanthrene removal efficiency of 15% was achieved at chitosan concentration of 25 ppm, which was attributed to the hydrophobic nature of phenanthrene. An increase in chitosan concentration showed an increase in the removal efficiency of both naphthalene and phenanthrene when solubilized in acetic acid.

Contact time was investigated to improve removal efficiency. The contact time was investigated using powder chitosan at chitosan concentration of 12.5 ppm and 25 ppm. A significant improvement on the removal efficiency was attained with an increase in contact time, an 88% naphthalene removal was attained at 120 hours contact time. It was demonstrated that chitosan concentration had no influence on the removal efficiency with an increase in contact time.

The focus of this research, which is to remove PAHs from water, was achieved using the coagulation-flocculation method but with a major limitation of treatment time. The method demonstrated that an average of 5 days (160 hours) is required to remediate PAH in water to required legislative limits. In an industrial application this is not practical as the remediation time is very long. In an effort to achieve a more practicable method, a change in approach was required. Thus, with intense literature review a practicable approach was investigated, with the emphasis on photocatalysis. This was fully investigated in chapter 4 and 5.

CHAPTER 4

4.0. PHOTOCATALYSIS DEVELOPMENT FOR THE REMEDIATING OF PAHs

4.1. Introduction

The research aim is to develop a method for the remediation of PAHs in water as they are of significant concern in produced water from the oil and gas industry. To achieve this, a suspended photocatalytic reactor (SPR) was investigated in the photodegradation of PAHs with the use of TiO_2 as the photocatalyst. The remediation method was further optimized to achieve high degradation efficiency of PAH.

Established methods have been published by various researchers on the design of conventional reactors for water treatment with some successfully used in industry (Yaping *et al.*, 2006, Reguero *et al.*, 2013). The complexity of photocatalytic reactors on the other hand has seen limited advancement as more advanced processes are involved in photoreactor design. Processes such as irradiation source, photoreactor material selection and photocatalyst deployment and optimization requires detailed investigation and method optimization.

Photocatalytic reactors have been designed by researchers to remediate pollutants in water with suspended TiO_2 used due to its favourable characteristics such as low cost, low environmental impact, good mass transfer and high photoactivity (Haoran *et al.*, 2015). Research has been carried out in the use of suspended TiO_2 to photodegrade PAHs in water but with limitations, such as solvent impact on degradation rate, secondary treatment of TiO_2 after water treatment (i.e catalyst

removal), TiO₂ stickiness on photoreactor surface and solubility of PAHs in water, all of which have impacted on the advancement of this method (Zhang et al.,2011).

This research takes into account these limitations by optimizing the remediation method to eliminate and manage such limitations in order to achieve high degradation efficiency.

4.2. Photocatalysis method design and development

4.2.1 Basis of design

The basis of the reactor design is to design a system that can effectively remediate PAHs in water to required legislative standards within a short period of time. Conceptualization and definition of the design criteria and material which is a fundamental aspect of the reactor design was first conducted before the construction and testing of the photocatalytic reactor. The design of the photocatalytic reactor involves a three step-by-step process involving the optimizations of various processes.

1st Stage:

Design of a protocol for the preparation of PAHs in water without the aid of any solvents alongside to manage the limitation of PAHs low solubility in water. Solvents have been seen to impact on the degradation rate of pollutants which will be discussed later in the chapter.

This was followed by investigating the photodegradation of three PAHs: naphthalene, phenanthrene and fluorene of different chemical structures (table 4.1) present individually in ultra-pure water in order to determine the individual degradation rate without any internal influence or competition. This involved the

design of a photocatalytic reactor setup in which the degradation of the three PAHs was carried out

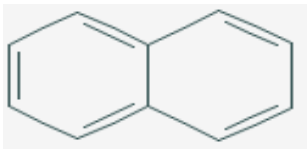
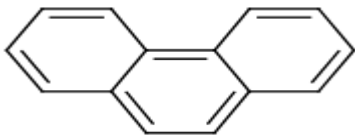
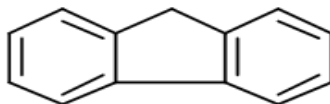
PAH	Solubility in water (ppm)	Chemical structure
Naphthalene	31.60	
Phenanthrene	1.60	
Fluorene	1.99	

Table 4.1 – Chemical structure of Naphthalene, phenanthrene and fluorene

Photocatalytic reactor material selection is also critically evaluated to prevent any loss of PAHs through the wall of the photocatalytic reactor. A control test is also carried out to validate that no losses occur. A final test is carried out to ensure that direct photolysis does not occur and the degradation is due to only photocatalysis

This stage established the method of photodegrading three PAHs: Naphthalene, phenanthrene and fluorene in water and ensuring no factors impact on the degradation rate.

2nd Stage:

Once the method to degrade the three PAHs was established and the individual degradation rate was established, the three PAHs: Naphthalene, phenanthrene and fluorene present together in ultra-pure water were then

investigated to determine the influence each PAH has on the degradation rate of the other. This was vital as the PAHs will mostly exist together naturally in water.

3rd Stage:

The final stage investigated the management of TiO₂ used in the photocatalytic process in order to minimize the amount used. This was carried out to manage the level of TiO₂ produced after the water treatment in order to minimize secondary treatment of TiO₂.

The TiO₂ loading was optimized by investigating the influence various TiO₂ concentrations have on the degradation rate of naphthalene and evaluating the ideal TiO₂ loading that will maintain a high efficiency and low loading.

4.2.2 Theoretical governing equations

In the photocatalytic degradation of polycyclic aromatic hydrocarbons (PAHs), the investigation was carried out based on the assumption that there was no mass transfer limitation, chemical reaction occurs in the liquid-liquid interface and there was a perfect stirring in the reactor. Based on this assumption, the reaction rate was employed as a measure for determining the photoreactor efficiency.

Rate of Reaction

The pseudo-first-order kinetics referred to as the rate of reaction was used as a measure to determine the rate of degradation of PAHs. The rate equation (4.1) is therefore expressed in terms of the reaction rate and concentration.

$$\frac{\ln [C_0]}{\ln [C]} = -Kt \quad (\text{Equation 4.1})$$

where; C_0 is represented as the initial concentration at time 0 minutes just after the dark adsorption, C is the concentration at specific sampling time interval over the degradation rate period and K is the rate constant.

Using regression analysis, $\ln[C]$ plotted against irradiation time is used to determine the pseudo-first-order rate constant (K) as seen in equation 4.2 and 4.3 derived from equation 4.1.

$$\ln[C] - \ln[C_0] = -Kt \quad (\text{Equation 4.2})$$

$$\ln[C] = (-K)t + \ln[C_0] \quad (\text{Equation 4.3})$$

The rate constant (K) gives the rate of degradation of PAHs over a period of time and it is expressed in terms of degradation per time. The rate constant was determined for each photodegraded PAH investigated (appendix B).

4.3. Experimental

The three design and development stages for the photocatalytic degradation of three PAHs in water were described below with the optimization in a step-by-step process and a comparison made with other published literature.

4.3.1. Analytical materials and methods

Titanium dioxide (TiO_2) powder (P25) (Phase ratio – anatase: rutile; 3:1, average size: anatase: 85% and rutile: 25%) was also purchased from Degussa. Analytical grade acetonitrile, methanol and acetone were purchased from Fisher Scientific. Deionized water was generated using PURELAB Dispenser (RO) generating ultra-pure ($18.2 \text{ M}\Omega\cdot\text{cm}$ at 25°C) water.

4.3.2. PAH preparation

As highlighted in stage 1 of photocatalytic reactor design and development (section 4.2), naphthalene was not prepared with the aid of a solvent. Naphthalene solution was prepared using a dissolution process involving vigorous stirring in water alone. Naphthalene crystal (15mg) was added to 150 mL of deionized water in a 250 mL Pyrex glass bottle. Due to the low solubility of naphthalene in water, the solution was vigorously stirred with a magnetic stirrer for 32 hours to allow complete dissolution of the naphthalene crystal. The Pyrex bottle was capped during the stirring time to prevent any loss of naphthalene. A further dilution of the naphthalene solution was carried out in order to attain the concentration within the HPLC calibration range of 4000 ppb to 60 ppb (section 2.3.3). This was done by diluting 2 mL of the standard naphthalene solution into 98 mL of deionized water in a 100 mL Pyrex bottle in order to achieve a concentration of 2 ppm falling within the calibration range.

Various published literature have prepared naphthalene solution in different ways by pre-dissolving it in a solvent (acetone, methanol and dichloromethane) in an effort to increase the solubility of naphthalene in water. Woo *et al.*, in the study of the photocatalytic degradation of naphthalene, phenanthrene, anthracene and benzo[a]anthracene prepared naphthalene in water with the addition of 16% w/w of acetone to increase solubility of each PAH in water. Other published literature such as Felix *et al.*, 2014 in the study of the photocatalytic degradation of Naphthalene using periwinkle shell ash; Agarry *et al.*, 2013, in the study of photocatalytic removal of naphthalene from aqueous solution, and Chang *et al.*, 2004 during the adsorption of naphthalene on zeolite from aqueous solution all used methanol in the preparation of naphthalene in an effort to increase the solubility of naphthalene in water. This has also been seen for other PAHs preparation such as phenanthrene (Woo *et al.*, Gupta *et al.*, 2016) and fluorene (Beltran *et al.*, 2005). With photocatalysis the use

of solvents for PAH preparation impacts on the degradation rate due to the competition since OH radicals are non-selective. The effect of this will be further seen in an experimental work seen in section 4.7 of this chapter

4.3.3 Photocatalytic reactor design and setup

The photocatalytic reactor design setup and development involved the design of a TiO_2 suspended photocatalytic reactor (SPR) (figure 4.2) desired to achieve high degradation efficiency by the optimization of the design parameters such as UV light intensity, photoreactor material and photocatalyst loading. Figure 4.3 illustrates the photocatalysis experimental set-up of a SPR which involves a 4-stage remediation and analysis process.

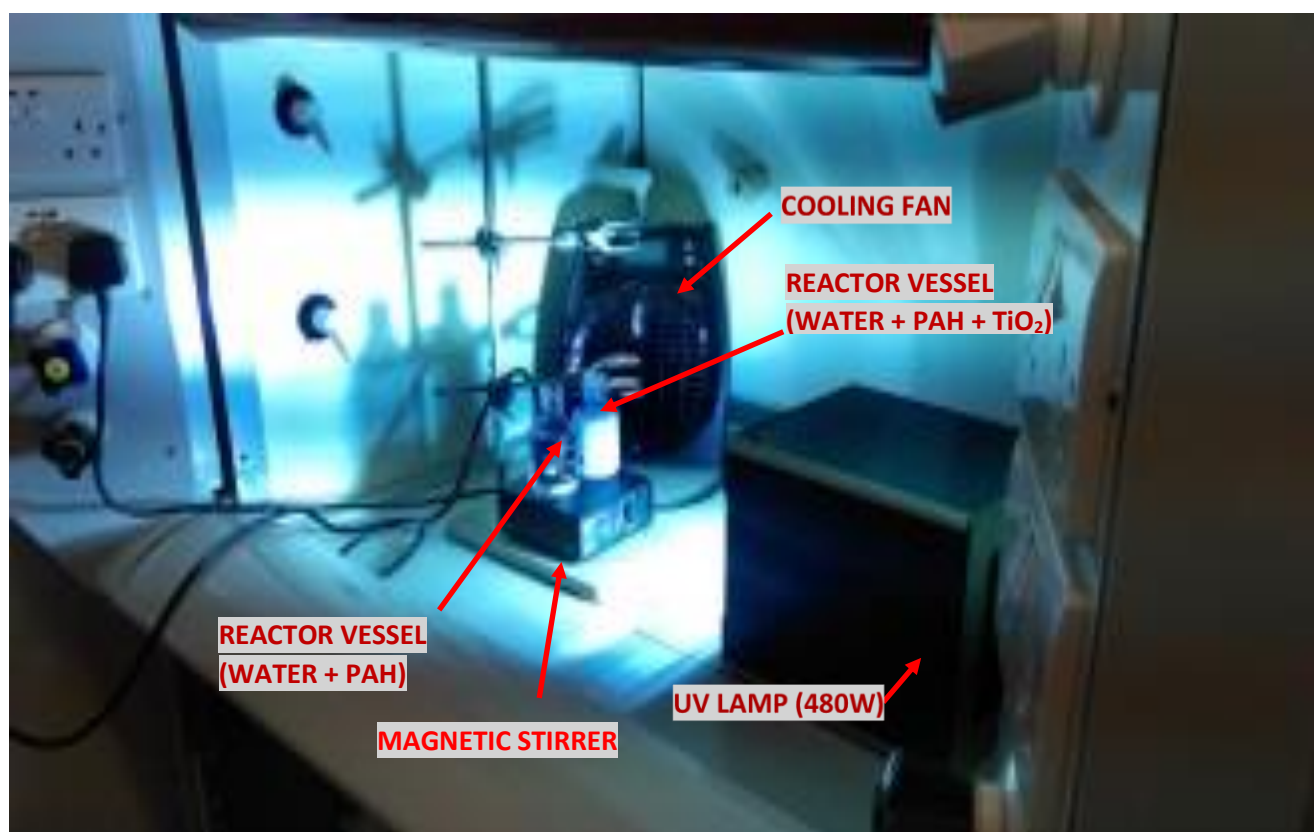


Figure 4.2: Photocatalysis degradation of PAHs alongside the test control

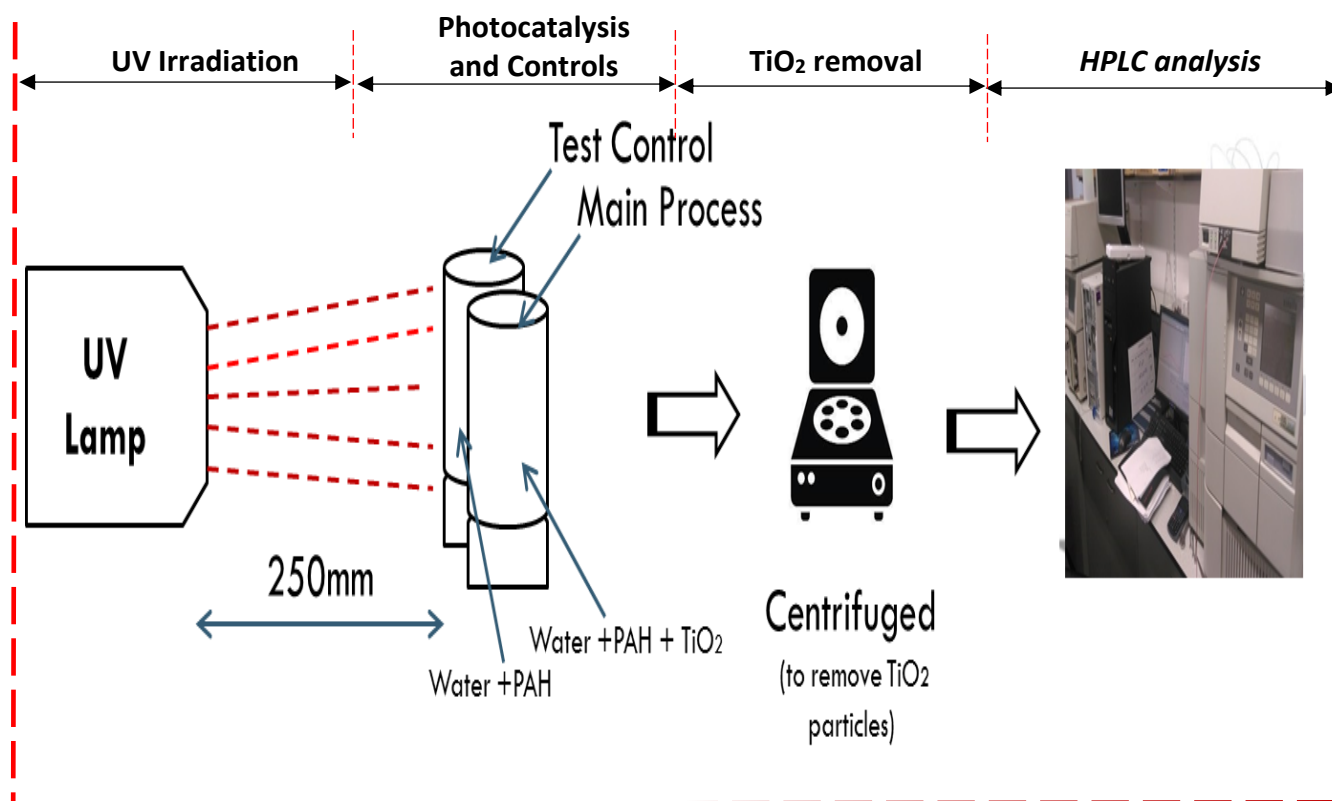


Figure 4.3: Reactor setup of suspended TiO₂ photoreactor

1st Stage: UV Irradiation

The design stage involved the use of a UV xenon lamp (480 W UVASpot lamp, Dr Hönle UK, spectral output 330-450 nm) (figure 4.4) to generate UV light which was irradiated onto one side of the photoreactor. A reflective aluminium surface was used on the other side to rebound the UV light rays to the other side of the reactor to achieve similar reflection of light throughout the reactor. At this stage when the UV light was irradiated onto the TiO₂ particle, the photon in the UV light excites the electrons from the valence band to the conductance band thereby generating electrons and holes (equation 4.4).



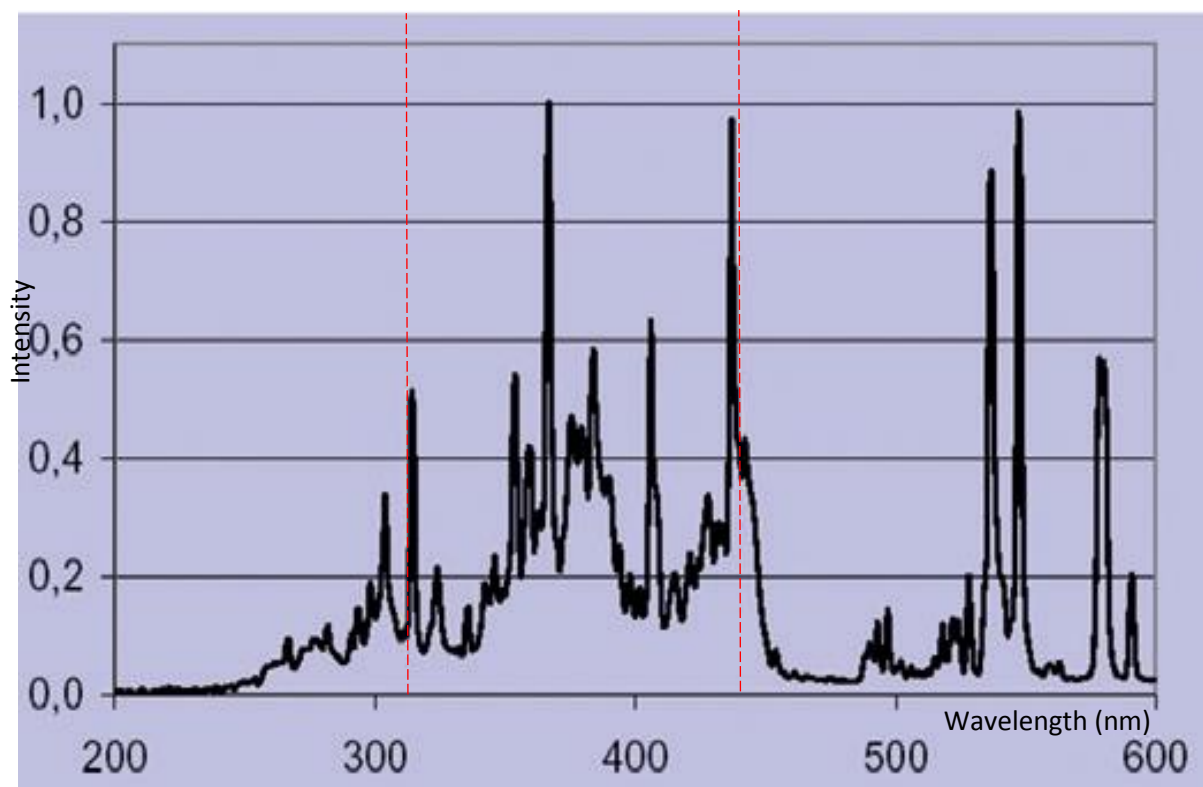


Figure 4.4: 480 W UVASpot 400 lamp, Dr Hönle UK, emission spectrum

2nd Stage: Photocatalysis and Controls setup

A 150 mL pyrex glass beaker serving as the reactor vessel was placed at a distance of 250 mm from the light source and on a magnetic stirrer (figure 4.3). The photoreactor vessel was made of glass in order to allow for the penetration of the UV light ($> 360\text{nm}$) into the PAH-water solution and also to prevent loss of PAH by sticking on the reactor vessel wall. The photocatalysis experimental set-up involved the use of three reactor vessels; one to investigate the photocatalytic degradation rate, the other to investigate direct photolysis and the third reactor used as a test control for dark adsorption.

At this stage of photocatalysis the electrons and holes produced react with OH^- and O_2 to produce OH radicals (OH^\bullet) and superoxide anions (O_2^-) (Equation 4.5 and 4.6). The hydroxyl radicals then react with the PAHs to form intermediates (Equation 4.7)



3rd Stage: TiO_2 removal

A centrifuge was used to separate TiO_2 particles from the treated water sample. 1 mL Subsamples was taken after the photocatalytic degradation and transferred into 1.5 mL micro-centrifuge vial and then centrifuged for 5 minutes at a speed of 13000 rpm. The supernatant was then transferred into a glass HPLC vial preventing the carryover of TiO_2 particle.

4th Stage: HPLC analysis

The established analytical method discussed in Chapter 2 was integrated into the design to quantify the PAH concentration at every stage of the investigation. PAH concentration prior to dark adsorption and after dark adsorption was quantified using the HPLC system and also samples taken at intervals of 1, 2, 3, 4, 5, 6, 8, 10, 12, 14, 16 and 20 minutes of irradiation time (Pestana., 2012).

4.3.4 Photocatalysis procedure

Photocatalytic degradation of naphthalene, phenanthrene and flourene were investigated using the photocatalytic reactor design. Naphthalene was used as a model PAH and the established method was subsequently used for phenanthrene and

fluorene. Naphthalene was used in initial studies due to its ability to easily dissolve in water when compared to the other 17 PAHs giving it a wide concentration range to monitor the degradation rate. Another reason is in discharged water naphthalene occurs in the highest concentration compared to other PAHs (Lair *et al.*, 2008, Jing *et al.*, 2014) thereby imposing a possible greater health impact..

The PAH solution of interest was transferred into the reactor vessel (100 mL). In one reactor vessel UV light was radiated onto the PAH containing 100 mg of TiO₂ particles to determine the effect of photocatalysis. The PAHs solution with suspended TiO₂ was stirred continuously to achieve good mass transfer of the pollutant onto the surface of the photocatalyst. Stirring continuously helped to achieve a homogenous dispersion of TiO₂ so it is distributed evenly and promotes oxygenation.

Into the second reactor containing the PAH without TiO₂ particles, UV light was irradiated with the same photon flux as the first reactor to determine the effect of direct photolysis. This was to ensure that degradation of PAH observed was only occurring as a result of photocatalysis.

The third reactor vessel containing PAH and 100 mg of TiO₂ was not exposed to UV light to determine the dark adsorption. Dark adsorption was carried out for the first 30 minutes prior to the photocatalytic degradation process which involved stirring of the suspended solution in the dark to allow for the adsorption of PAH onto the TiO₂ particles.

A cooling fan equipped with a thermostat was also used to maintain the temperature at room temperature at 21 °C±2 as the UV lamp generates heat.

4.4 Results and Discussion

4.4.1 Photocatalytic degradation of Naphthalene

The photocatalytic degradation in one of the photocatalytic reactor vessels containing naphthalene (1800 ppb) and 100 mg of suspended TiO_2 is shown in figure 4.4. The naphthalene- TiO_2 solution was allowed to equilibrate in the dark prior to exposure to UV light. The results show two steps of preliminary results, one of dark adsorption and the other the photocatalytic degradation.

A rapid degradation of naphthalene over 20 minutes achieved a 99% degradation efficiency (figure 4.4). Within 5 minutes, 764 ppb of naphthalene was seen to be degraded. A rate constant (k) of naphthalene was achieved at $2.09 \times 10^{-1} \text{ min}^{-1}$. In the case of the discharge legislative limits in the North Sea, the concentration limit set at 130 ppb by SEPA (SEPA WAT-SG-53., 2018) was achieved. Nelf *et al.*, 2011, in an investigation to the concentration of naphthalene in the North Sea recorded a peak concentration of 394 ppb. This method was able to achieve a removal of 764 ppb of naphthalene which is sufficient in bringing the concentration below the legislative limits. The performance of the TiO_2 in degrading naphthalene was attributed to the presence of OH° radicals generated during the photocatalysis process between the UV light and TiO_2 .

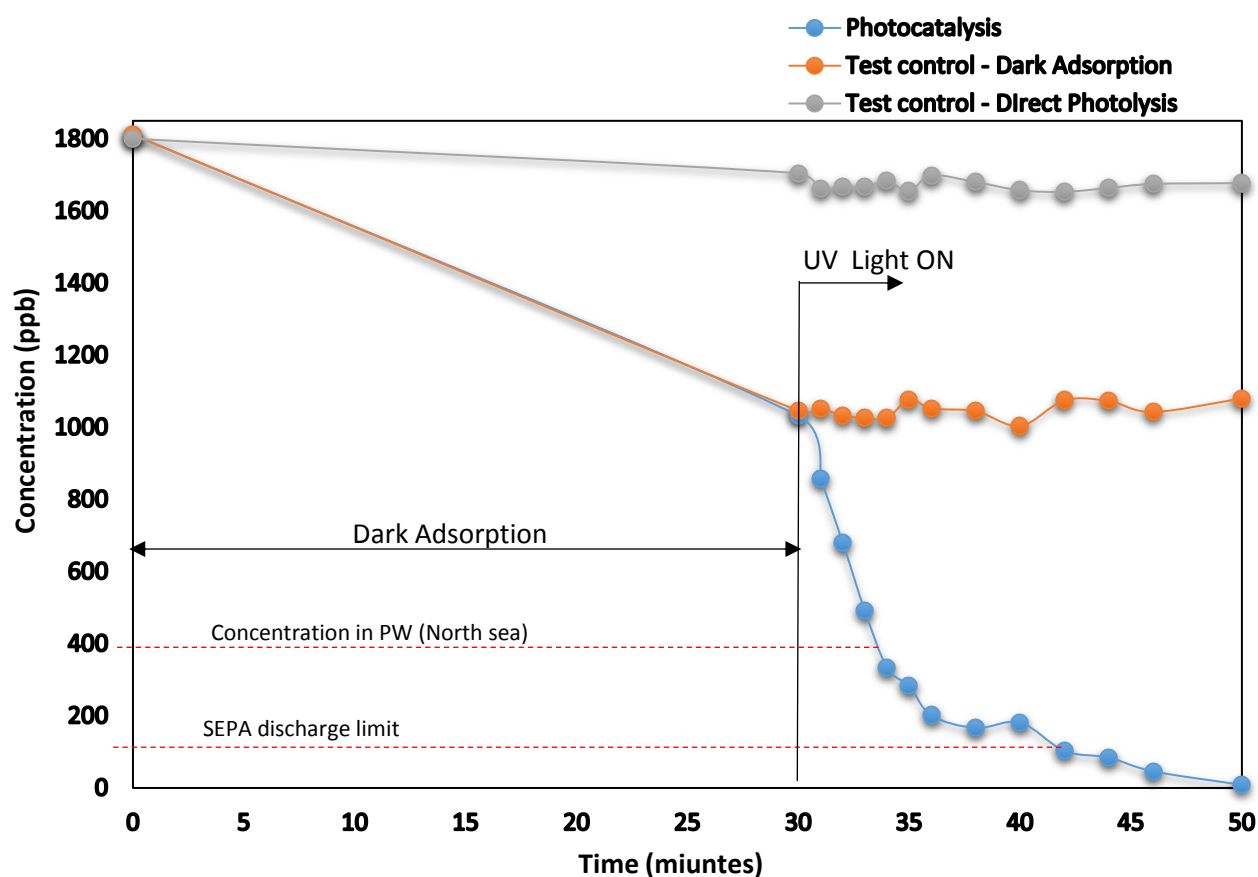


Figure 4.4: Photocatalytic degradation of naphthalene; (1)Under UV light & TiO₂ (2)Under UV light & No TiO₂ (3)No UV light& TiO₂. TiO₂ :1000ppm

When compared with the findings by Weng *et al.*, 2012, in the degradation of naphthalene using suspended TiO₂, a rate constant of 2.19×10^{-3} was achieved over a 12 hr irradiation time which showed a much slower rate of degradation. One limitation to Weng *et al.*, 2012, photocatalytic degradation method was the use of dichloromethane (DCM) during the preparation of naphthalene. DCM slows down the rate of degradation as DCM reacts with the oxygen present in the water sample. DCM's reaction with water produces intermediate species such as CO, HCl, CCl₄ which degrades CO₂ and H₂O (Borisch *et al.*, 2004). This in turn thereby reduces the amount of hydroxyl radicals that can be generated to degrade naphthalene. It therefore does not give a true value of the rate of degradation of naphthalene. This research

accounts for this limitation by ensuring no solvent is used during the preparation of the PAHs in water. The influence of solvent is discussed further in section 4.7.

Test control – Dark Adsorption

Figure 4.4 illustrates the adsorption of naphthalene onto the suspended TiO_2 in the first 30 minutes of dark adsorption. A reduction of 47% of naphthalene was recorded. No further decrease in naphthalene was seen after the 30 minutes dark adsorption period showing that equilibrium was achieved between water phase and TiO_2 . It can therefore be concluded that the dark adsorption has attained its equilibrium at 30 minutes as no further loss of naphthalene by adsorption was observed. When compared with published literature, Antoine *et al.*, 2007 in the study of naphthalene degradation in water by heterogeneous photocatalysis also achieved dark adsorption equilibrium at 30 minutes even though a much higher TiO_2 loading of 2500 ppm was used when compared to 1000 ppm used in this research.

Test control - Direct photolysis

Due to the knowledge that some substances can undergo direct photolysis a control test was carried out to ensure that the degradation achieved during the process is solely promoted by the presence of photocatalyst. The second reactor vessel containing the naphthalene solution but no TiO_2 went through the same process where it was stirred in the dark for 30 minutes and irradiated with UV light and sub-sampled at the same time intervals. Results shown in figure 4.4 show no direct photolysis occurred over a 20 minutes irradiation time. This shows that photons produced by UV light even at high light intensity are not sufficient enough to break down the PAH but with the aid of a photocatalyst this can be achieved.

4.4.2. Photocatalytic degradation of Phenanthrene

The results from the model PAH (naphthalene) showed the ability of TiO_2 to photodegrade one of the 18 EPA PAHs (section 4.6.1) with the use of UV light. As a result of this, further investigation was carried out using the same method to investigate the photocatalytic degradation of phenanthrene. Phenanthrene was selected due to its more complex chemical structure (table 4.1). The influence of a more complex structure will give an indication of the broader applicability of the method for degrading similar PAHs which have a similar 3 aromatic rings chemical structure.

The photocatalytic degradation of phenanthrene (800 ppb) using TiO_2 (1000 ppm) is shown in figure 4.5. As seen with naphthalene, during an illumination period of 5 minutes phenanthrene also degraded rapidly with a rate constant of $4.25 \times 10^{-1} \text{ min}^{-1}$, degrading 170 ppb of phenanthrene achieving a 99% degradation efficiency. When compared with naphthalene where 760 ppb was degraded over the same 5 minute period, the results show that degrading naphthalene is more favourable than phenanthrene. This is attributed to the presence of more aromatic rings of phenanthrene making it harder to break than that of naphthalene with 2 aromatic rings. When compared with the required USEPA discharge legislative limit, in the North Sea at peak concentration 32 ppb of phenanthrene was recorded in produced water. USEPA discharge limit for phenanthrene which is 1.7 ppb shows that this method can degrade phenanthrene below the legislative limit (USEPA 440/5-86-001).

Figure 4.5 also shows the dark adsorption stage with 630 ppb of phenanthrene adsorbed onto TiO_2 surface (1000 ppm). This is lower than that recorded for naphthalene as phenanthrene is a bulkier compound, which results in lesser amount adsorbed onto the surface of TiO_2 .

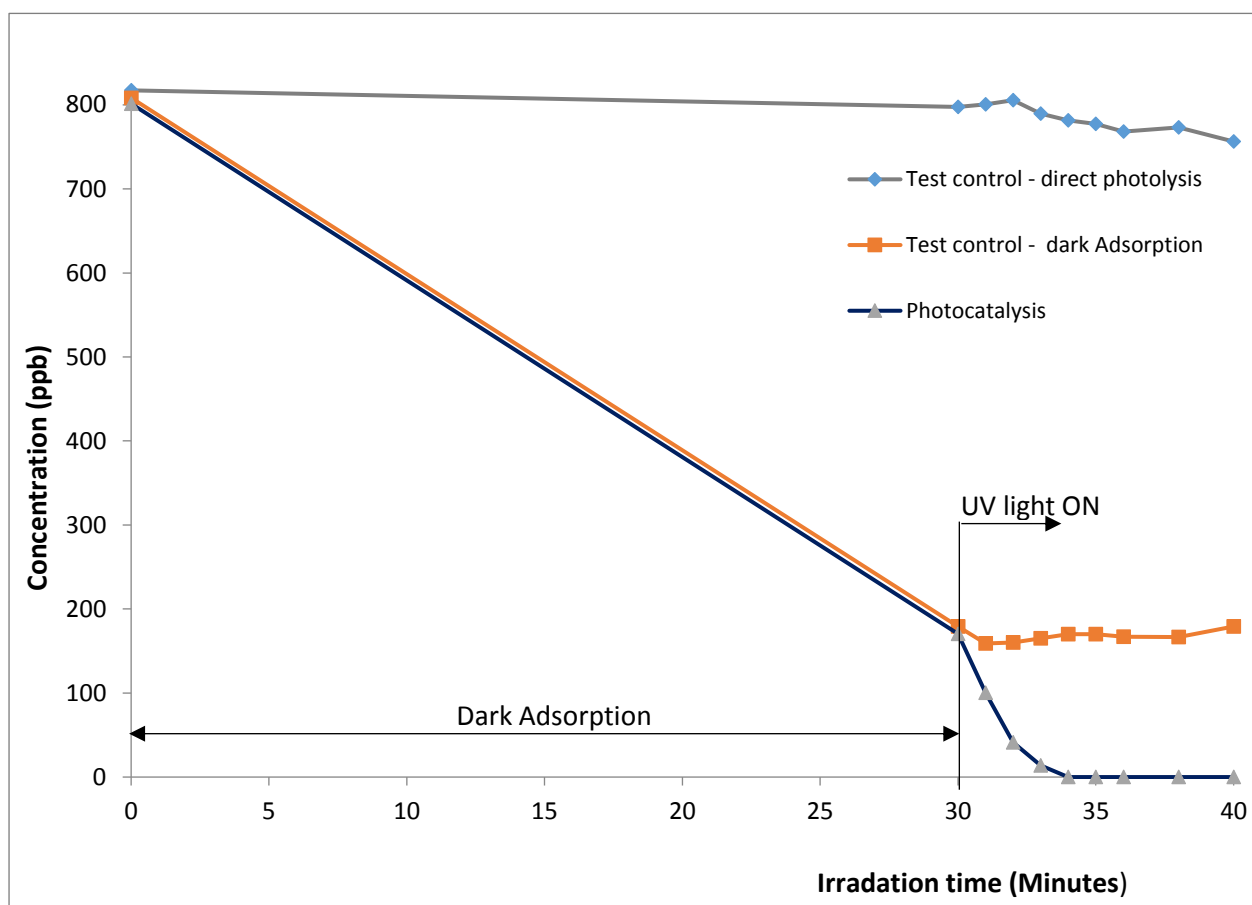


Figure 4.5: Photocatalytic degradation of phenanthrene; (1)Under UV light & TiO_2 (2)Under UV light & No TiO_2 (3)No UV light& TiO_2 . TiO_2 :1000 ppm

Test Controls – Dark adsorption and direct photolysis

The same test controls as carried out for the model PAH; naphthalene, was also carried out for phenanthrene. Phenanthrene attained dark adsorption equilibrium at 30 minutes similar to that of naphthalene. This was also seen in other published literature by Zhang *et al.*, 2011 in the study of heterogeneous photocatalytic degradation of phenanthrene in surfactant solution, with adsorption equilibrium also attained at 30 minutes with 760ppb adsorbed with a TiO_2 of 2000 ppm. Similar results were achieved in the direct photolysis test control for naphthalene and phenanthrene with no significant degradation recorded over the 50 minute test period.

4.4.3. Photocatalytic degradation of Fluorene

A third PAH; fluorene was selected to further establish the ability of the system to photocatalyse the 18 EPA PAHs using the established method. Fluorene's chemical structure was a reason for the selection of this PAH. Fluorene has a similar structure to that of phenanthrene having 3 aromatic rings but consists of 2 benzene rings with a middle weak carbon 9, whereas phenanthrene has 3 benzene rings which are coplanar. This structure is unique to some specific PAHs such as flurothrene, benzo(*k*)flurothrene and benzo(β)flurothrene. Understanding the photocatalytic degradability of the fluorene structure will give an insight to the way similar PAHs may degrade.

Fluorene was prepared using the same dissolution process (section 4.5.2) as that of naphthalene by dissolving crystal fluorene in deionized water for 32 hours to achieve a stock sample of 1300 ppb.

Figure 4.6 illustrates the photocatalytic degradation of fluorene (1300 ppb) using TiO₂ (1000 ppm). A rapid degradation was also observed for fluorene over 20 minutes achieving a 99% degradation efficiency with a rate constant of $1.8 \times 10^{-1} \text{ min}^{-1}$. Fluorene (278 ppb) was rapidly degraded over a 5 minutes irradiation time. The presence of the weak carbon 9 made it much easier to degrade it when compared to similar 3 aromatic ring PAH (Phenanthrene). The weak carbon 9 makes it easy for the reaction of the OH[°] to easily degrade it. The photodegradation ability between the three PAHs can be seen in the order of naphthalene > fluorene > phenantharene (table 4.2). The chemical structural CH bond and available free site played a significant role in increasing the degradation rate. The more the CH bond the less easy it is to photodegrade and also the more the free site available the easier it is to photodegrade.

Comparing the amount of fluorene present in produced water (21.7 ppb) with the required USEPA discharge limit (6.15 ppb), it can be seen that the designed photoreactor can reduce concentration to required limits.

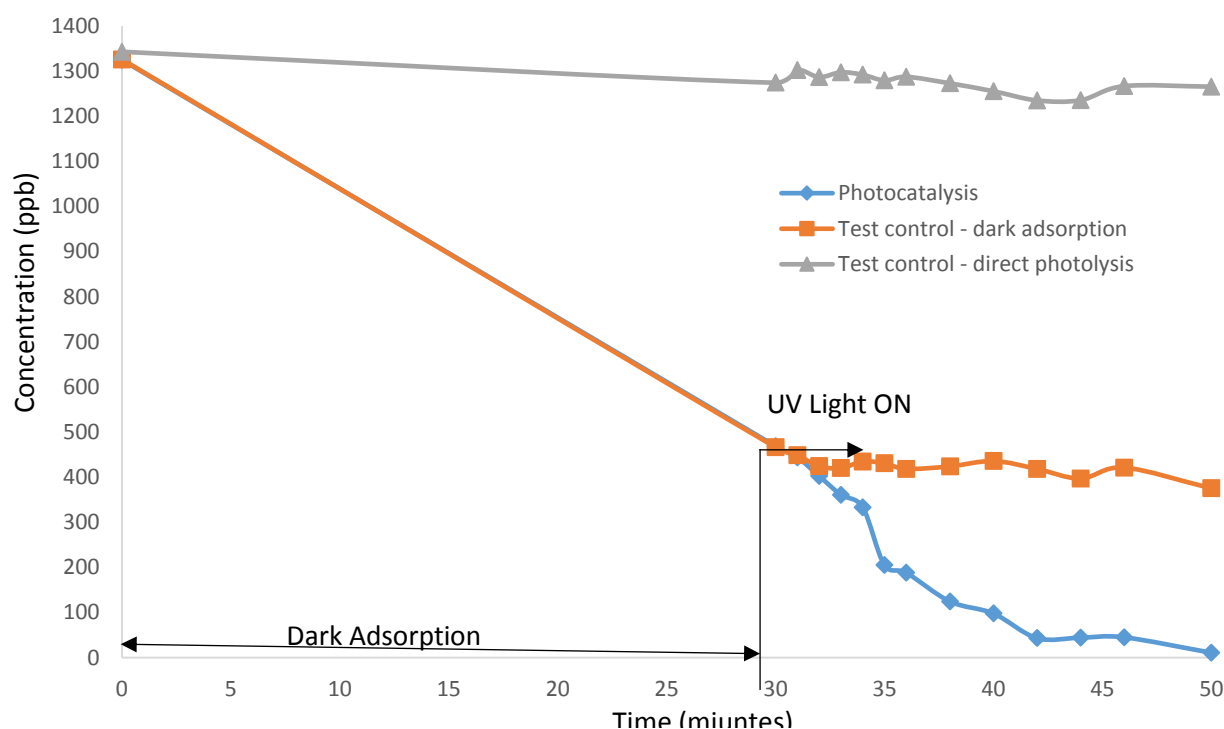


Figure 4.6: Photocatalytic degradation of fluorene; (1)Under UV light & TiO_2 (2)Under UV light & No TiO_2 (3)No UV light& TiO_2 . TiO_2 :1000 ppm

PAHs	Rate Constant (k) (10^{-1} min^{-1})	Concentration photodegraded (5 minutes irradiation) (ppb)	Concentration reduction required to meet limit (ppb)	Aromatic rings
Naphthalene	2.09	764	289.3	2 benzene rings
Phenanthrene	4.25	278	30.3	3 benzene rings
Fluorene	1.85	171	15.55	2 benzene rings with one weak carbon 9

Table 4.2: Rate constant, degradation time and degradation efficiency of naphthalene, phenanthrene and fluorene in suspended TiO_2

4.5 Photocatalytic degradation effect on multiple PAHs in water

Generally, species do not degrade at the same rate when present alone in water compared to when present with other competing chemical species. As a result of this, further investigation was carried out to determine the influence on the degradation rate of each PAH when present in water with other PAHs. An investigation of this was carried out using a PAH sample containing naphthalene, fluorene and phenanthrene prepared using the dissolution process involving vigorous stirring as highlighted in section 4.5.2. Naphthalene, fluorene and phenanthrene dissolved in deionized water to achieve a concentration of 1600, 600 and 160 ppb respectively was prepared. The photocatalysis of each PAH was determined and comparison made with their degradation when present alone in water. Previous studies (section 4.6) established that PAHs are not degraded by direct photolysis in this experimental setup, hence this test was not carried out for this investigation. Dark adsorption on the other hand was investigated to determine the amount each PAH adsorbed prior to illumination and the competition between the PAHs during this process.

The photocatalytic degradation rate of naphthalene, phenanthrene and fluorene when present together in water did change (figure 4.7). It can be observed for naphthalene that the rate of degradation is slower when present in the mixture than when present alone in water. This can be seen in the rate of reaction with naphthalene having $2.09 \times 10^{-1} \text{ min}^{-1}$ rate constant when alone in water and $1.21 \times 10^{-1} \text{ min}^{-1}$ when present in the mixture. These results agreed with the result of investigation carried out by Liu *et al.*, 2016 in the study of the effect of water matrix on photocatalytic degradation of PAHs. The results showed that PAHs rate constant reduces with increased water matrix complexity containing more PAHs than those with lesser PAHs.

It can also be seen (table 4.3) that the dark adsorption of a mixture (404 ppb) is much less than when alone in water as the three PAHs are competing to be adsorbed onto the TiO_2 particle at the same time.

The photocatalytic degradation rate (figure 4.7) showed that naphthalene is the dominating PAH having the highest concentration that is dark adsorbed and displaying highest rate constant. The chemical structure of naphthalene promotes this as it has the least amount of aromatic rings making it easier to be adsorbed onto TiO_2 thereby leading to it being easily photodegraded.

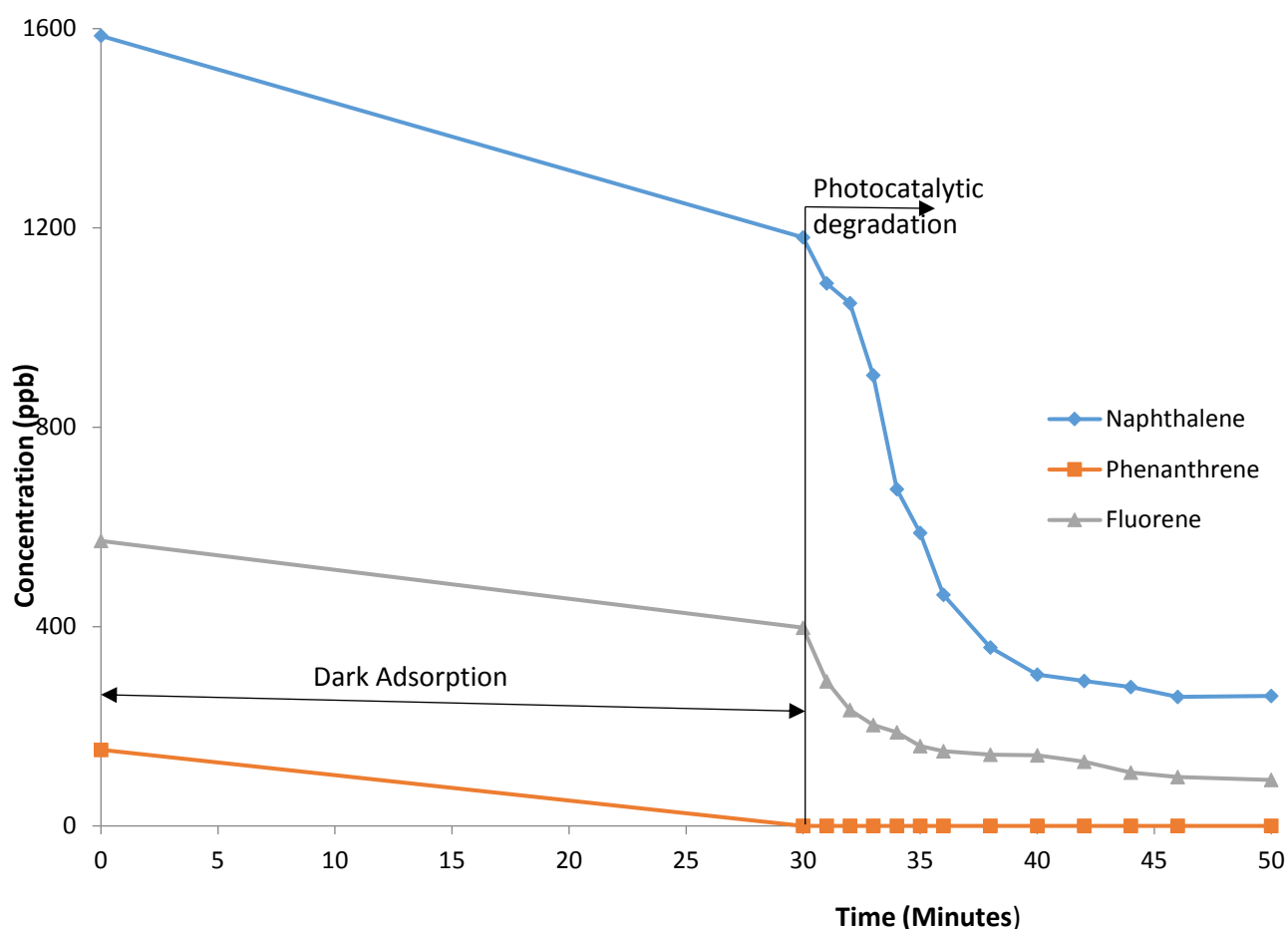


Figure 4.7: Photocatalytic degradation of naphthalene, phenanthrene and fluorene; (1) Under UV light & TiO_2 : 1000ppm

PAHs		Rate constant ($\times 10^{-1} \text{ min}^{-1}$)	Amount photodegraded (in 5 minutes) (ppb)
Naphthalene	In mixture	1.21	593
	Alone	2.09	764
Fluorene	In mixture	0.63	237
	Alone	1.83	171

Table 4.3: Photodegradation of naphthalene and fluorene, and dark adsorption.

4.6 Effect of Acetone on PAH photocatalytic reaction rate

Acetone, a solvent that is miscible with water helps to increase the solubility of PAHs in water. This has been commonly seen in published literature in order to provide a wider concentration range for experimental work. The effect of solvent was therefore investigated to determine the impact on the degradation rate of the PAHs. Naphthalene and phenanthrene were used as model PAHs as they both have significantly different chemical structures which are 2 and 3 aromatic rings respectively and each has a different solubility in water.

4.6.1 Naphthalene and phenanthrene preparation in acetone

Preparation of naphthalene and phenanthrene solution was carried out as follows; 10 mg of naphthalene and 10 mg phenanthrene was added to 10 mL of acetone in a 25 mL Pyrex glass bottle individually.

To the naphthalene solution (0.35 mL), 99.65 mL of deionized water was added to it to attain a concentration 3500 ppb. A high concentration was attained due to the pre-dissolution of naphthalene in acetone. As for phenanthrene, 0.25 mL of pre-dissolved phenanthrene in acetone was dissolved into 99.75 mL deionized water to attain a phenanthrene concentration of 2500 ppb.

Evaluation of photocatalytic degradation was determined as before (section 4.2), the same procedure was carried out in investigating the photocatalysis, dark adsorption and direct photolysis. The same TiO₂ loading of 1000 ppm was also used in this study.

4.6.2 Influence of solvent on photocatalytic degradation

The effect of solvent (acetone) on the photocatalytic degradation of naphthalene was determined (figure 4.8). A much slower degradation was observed in the first 5 minutes of irradiation time when compared with results achieved in the absence of acetone (section 4.6.1; figure 4.4). A recorded 456 ppb concentration loss of naphthalene with acetone and 764 ppb of naphthalene alone in water was achieved. The 40% reduction seen in the presence of acetone is due to the reaction between acetone and the generated OH radical which aids photocatalytic degradation. Published literature by Caralp *et al.*, 2006 in the study of the reaction between acetone with OH radical has proven that there is a reaction between the two species as seen in equation 4.8 and 4.9. This shows the presence of a competition between acetone and naphthalene to use the generated OH radical in degrading themselves.



Also in published literature by Talukdar *et al.*, 2003 in the study of reactions between acetone and OH[•] can be seen the production of acetyl radicals. This further confirms that the presence of acetone reduces the number of OH radicals available to degrade naphthalene.

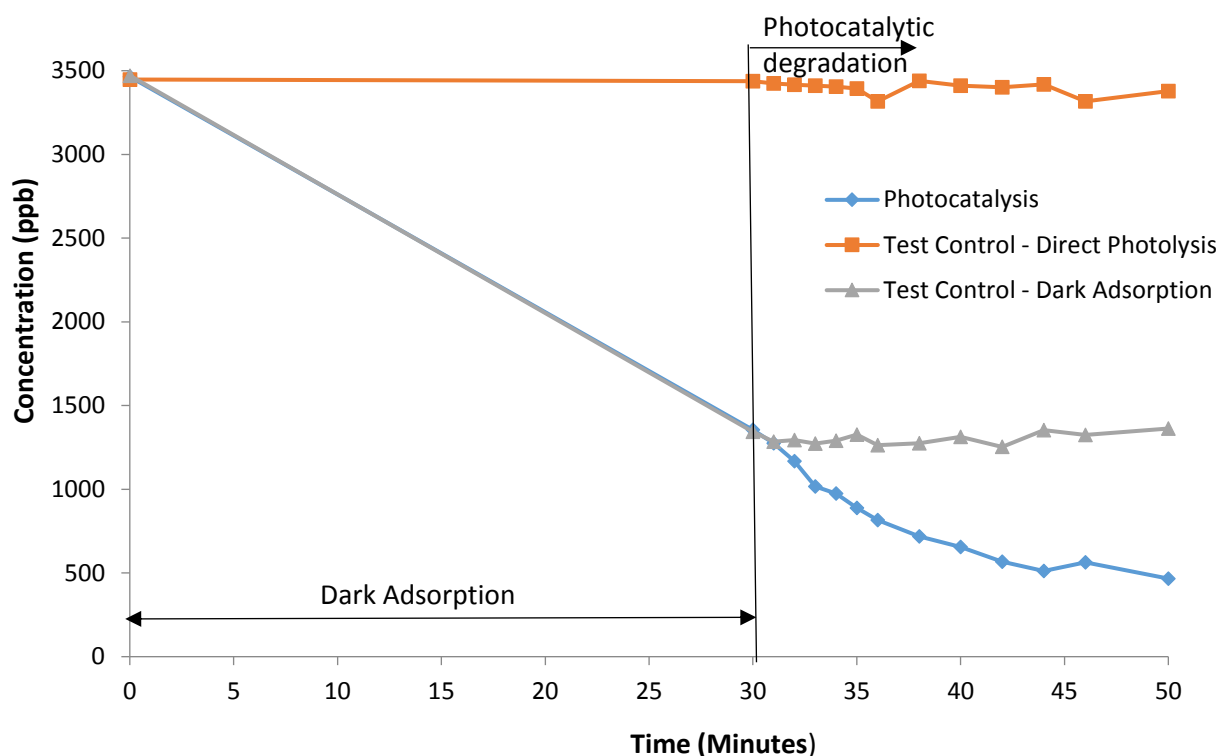


Figure 4.8: Photocatalytic degradation of naphthalene in acetone; (1)Photocatalysis (2)Photolysis (3)Dark Adsorption. TiO_2 loading:1000 ppm

Illustrated in figure 4.9 is the effect of acetone on the degradation of phenanthrene. It is also observed that degradation of phenanthrene was much slower in the presence of acetone than in the absence of acetone. A 25% reduction was seen in the presence of acetone. The lower percentage reduction between phenanthrene and naphthalene can be attributed to the more complex structure of phenanthrene as there are more aromatic rings present making it difficult to degrade.

Acetone influence on the degradation of PAHs is due to its reaction with OH radical. Other published work such as Ma *et al.*, 2001 in the study of photodegradation of chlorinated aromatic dye in non-ionic surfactant solution has seen an increase in the rate of degradation of the dye due to the addition of acetone and NaBH_4 which aids the generation of hydrogen which is used to degrade the dye. This therefore shows

that detailed investigation has to be carried out to determine of use of solvents in photocatalysis as this can impact on the true photodegradation results of species.

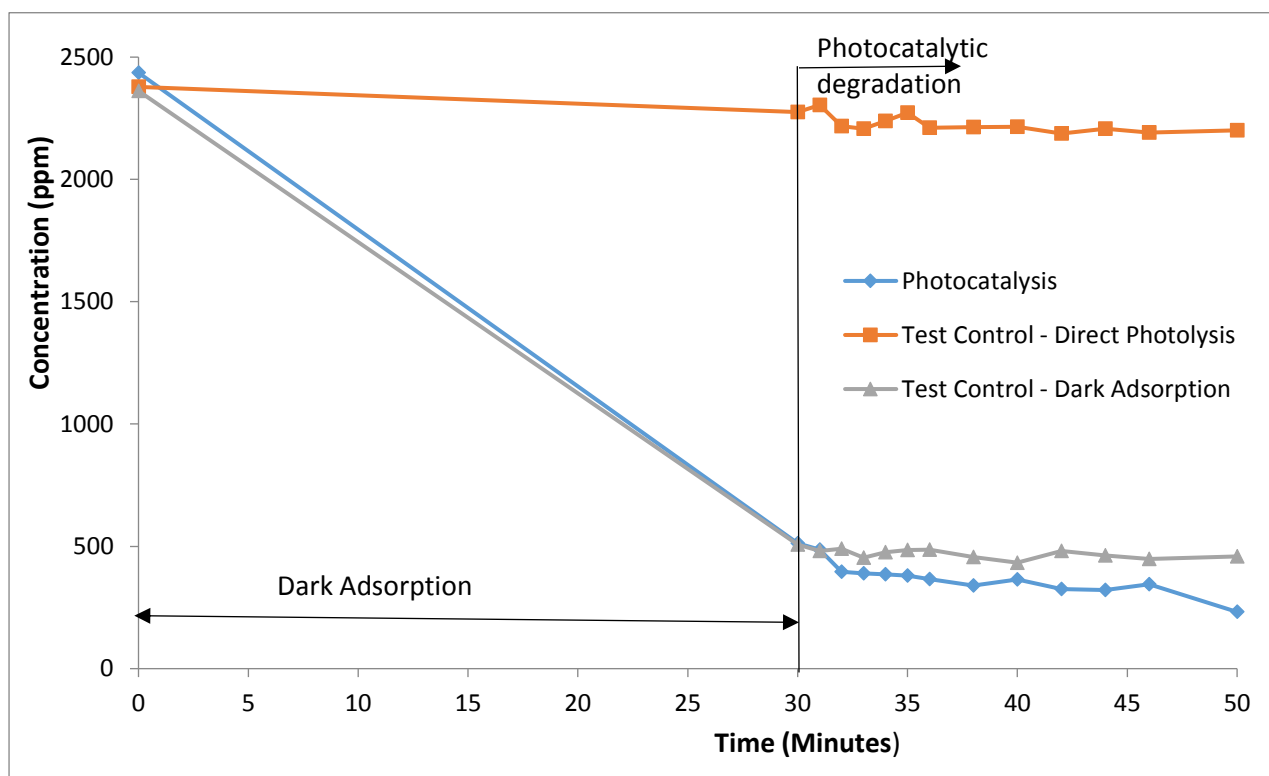


Figure 4.9: Photocatalytic degradation of phenanthrene in acetone; (1)Photocatalysis (2)Photolysis (3)Dark Adsorption. TiO_2 loading:1000 ppm

4.7 Effect of TiO_2 loading on photocatalysis

The effect of TiO_2 loading on photocatalysis was investigated using phenanthrene as a model PAH. Phenanthrene was selected due to its more complex chemical structure when compared with naphthalene and fluorene and also because it has a stronger CH bond.

The first order rate constant (k) at TiO_2 loading of: 200, 400, 600, and 1000 ppm was investigated to determine the photocatalytic degradation optimal value. The amount of dark adsorption at each TiO_2 loading was also investigated to determine

the influence it has on the rate constant (k). The adsorption site present on the TiO_2 surface has been investigated to promote the increase in dark adsorption.

The rate constant (k) (figure 4.10) achieved in the photocatalytic degradation of phenanthrene over a TiO_2 loading of: 200, 400, 600, and 1000 ppm. It was observed that an increase in TiO_2 loading increases the rate constant (k) showing that at higher TiO_2 loading, phenanthrene will photodegrade quicker. Antoine *et al.*, 2007 in the investigation of photocatalytic degradation of naphthalene in water, also investigated the effect of TiO_2 loading on naphthalene at TiO_2 loading range of 1000 – 4000 ppm. It was also observed that naphthalene behaved in a similar way with rate constant increasing with an increase in TiO_2 loading. Also Vahid *et al.*, 2013 in the optimization of the photocatalytic degradation of naphthalene using TiO_2 particles investigated the influence of TiO_2 loading on rate constant. It was observed that an increase in TiO_2 loading increases the rate constant of naphthalene. The rate constant (K) increase can be attributed to the fact that by increasing the TiO_2 loading the number of reactive site areas also increased thereby promoting the generation of OH radical which degrades the PAH.

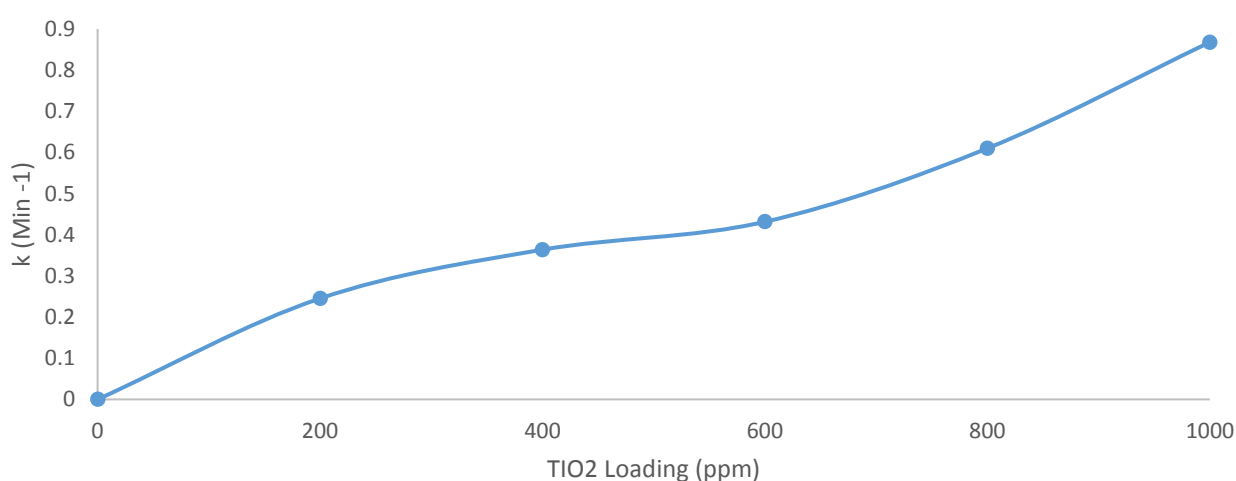


Figure 4.10: Rate Constant of phenanthrene at TiO_2 loading: 1000, 800, 600, 400 and 200 ppm

4.8 TiO₂ particle limitation to photocatalysis

TiO₂ as a photocatalyst has shown great potential in the photocatalytic remediation of PAHs in water. Its low-cost, low environmental impact and high photoactivity has made it promising in water purification. However, with all this significant advantage there is a major drawback in the application of this method in an industrial scale due to the required post-recovery of TiO₂ particles from the treated water. The TiO₂ particles which are still present in the treated water require further separation as they cannot be discharged with the water into the environment.

In an effort to overcome this major challenge research has investigated possible solutions. Immobilization of TiO₂ has been seen to be a solution to this limitation. Published research has shown that this limitation can be overcome by immobilization of TiO₂ onto inert surfaces. Mascole *et al.*, 2007 in the photodegradation of methyl red dye was able to photodegrade methyl red dye by immobilizing TiO₂ onto the inner walls of a cylindrical glass photoreactor in photocatalytic process. Also Gad-Allah *et al.*, 2007 investigated the photoactivity of immobilized TiO₂ in the photocatalytic degradation of methyl orange and was able to degrade methyl orange.

Other pollutants such as phenol (Sylwia *et al.*, 2012, Mozia *et al.*, 2012, Marissa *et al.*, 2014) has been photodegraded using immobilized TiO₂. As a result of this, further works were carried out to investigate the degradation of PAHs using immobilized TiO₂ as seen in chapter 5.

4.9 Conclusion

This chapter presents the development of a method for the photocatalysis of PAHs. The concept behind the design was to create an ideal environment for the photocatalysis process involving the effective radiation of UV light in generating

photons which creates holes and electrons by the TiO_2 particles. The holes and electrons reacting with H_2O and H_2 generates OH radicals which helps in degrading the PAH.

The photoreactors were used in a photocatalytic process to photodegrade naphthalene, phenanthrene and fluorene. When present alone in water a much more rapid photodegradation rate was observed for each PAH with naphthalene, phenanthrene and fluorene having a rate constant of $2.09 \times 10^{-1} \text{ min}^{-1}$, $4.25 \times 10^{-1} \text{ min}^{-1}$ and $1.85 \times 10^{-1} \text{ min}^{-1}$. Further investigation when the three PAHs (naphthalene, phenanthrene and fluorene) are present in the water sample together was also carried out with results showing a slower but steady degradation rate for each of the PAHs. The rate constant for naphthalene and fluorene under this condition achieved were $1.21 \times 10^{-1} \text{ min}^{-1}$ and $0.63 \times 10^{-1} \text{ min}^{-1}$

The effect of solvent on the degradation rate was shown with the used of acetone which was introduced into the photocataytic process during the preparation of the PAH sample. The rate constant was evaluated to determine the photocatalytic degradation performance. The results showed that the rate constant reduced significantly when acetone was present. Naphthalene and fluroene, recorded a 40% and 25% reduction in rate constant respectively. This showed the significant effect solvent has on the degradation rate of PAHs supporting the avoidance of solvents during solution preparation.

TiO_2 loading influence on the degradation rate was investigated using phenanthrene as a model PAH. TiO_2 loading within the range of 200p – 1000 ppm was investigated. Results showed an increase in TiO_2 loading results and an increase in the rate constant of phenanthrene hence future studies will attain to ensure high catalyst loading.

Limitation encountered with the SPR was due to the need of post-recovery of the TiO_2 particles after the water has been treated. This has limited the use of this treatment method in applying it to the industry. A proposed effective method for overcoming this challenge is by the use of immobilized TiO_2 onto inert surface. This therefore has led to the investigation of TiO_2 immobilized photoreactor which is seen in chapter 5.

CHAPTER 5

5.0. DESIGN AND DEVELOPMENT OF A NOVEL PHOTOCATALYTIC REACTOR FOR PAH PHOTOCATALYSIS

5.1. Introduction

Photocatalytic reactors are designed based on the deployed state of the photocatalyst. There are mainly two configurations used in the design of the photoreactor for water treatment which includes: photoreactor having suspended photocatalyst (as discussed in chapter 4) and a photoreactor having photocatalyst immobilized on an inert surface either in a batch system or a continuous flow system (Chong *et al.*, 2010). The latter is being investigated in this chapter for the remediation of PAHs in water.

The limitation encountered with the suspended photocatalyst reactor in chapter 4 which requires additional downstream TiO₂ recovery resulted in the further investigation of immobilized photocatalyst photoreactor. In chapter 1 (section 1.6.2) the literature review discusses the performance of immobilized photocatalyst photoreactor in remediating pollutants. Immobilized photocatalytic reactor application in pollutants treatment has been employed by various researchers over the years yielding high removal efficiency (Brucato *et al.*, 1997, Puma *et al.*, 2001(a), Alfano *et al.*, 2008, Puma *et al.*, 2008(b), Romero *et al.*, 2009, Imoberdorf *et al.*, 2010, Vahid *et al.*, 2014).

Photocatalyst immobilization is the major principle employed in immobilized photocatalytic reactor. This involves the coating of a photocatalyst on an inert surface. Various researchers have investigated the influence coating photocatalyst (TiO₂) on various materials such as glass, alumina, stainless steel, silica gel and

activated carbon has on the degradation rate of pollutants (Zhang *et al.*, 2004, Khatamian *et al.*, 2012, Wang *et al.* 2012, Wang *et al.*, 2013, Ahmed *et al.*, 2011, Li *et al.*, 2012). Glass has been seen to promote UV illumination as it allows for the easy penetration of UV light onto the coated photocatalyst (Wang *et al.*, 20102, Adams *et al.*, 2014).

Photocatalyst immobilized photoreactors are mainly designed in two major ways, either in a batch system or a continuous flow system. This study investigated both systems whereby the batch immobilized photocatalytic reactor is used as a preliminary work for the development of the flow through immobilized photocatalytic reactor. The former: the batch immobilized photocatalytic reactor system involved the detailed optimization of the photocatalytic reactor performance with the development of an effective TiO₂ sol gel for the coating of the glass tubes to achieve high degradation rate. TiO₂ sol gel for the glass tube coating is the key parameter in the photocatalytic reactor optimization process. Flow through photocatalytic reactor system has been investigated by various researchers (Jung *et al.*, 2007, Augugliaro *et al.*, 2005, Molinari *et al.*, 2001, Sapajaree *et al.*, 1999, Camera-Roda and Santarelli, 2007, Mozia *et al.*, 2009) and has been seen to yield a high removal rate. Mozia *et al.*, 2009 employed the use of a flow through photocatalytic reactor in the investigation of the removal of 32 pharmaceuticals compounds from water achieving a removal efficiency of 70% for 29 compounds and 50% for 3 compounds showing high removal can be achieved with the use of a flow through photocatalytic reactor.

5.2. Immobilised photocatalyst design and development

The investigation into the immobilized photoreactor design was carried out using two different approaches: batch and flow through system with the former being the preliminary foundation for the latter. The two approaches involves:

5.2.1. Stage 1 Design: Static Immobilized Photocatalytic Reactor (SPR)

The first design involved the design of a static immobilized photocatalytic reactor (SIPR) with coated TiO_2 glass tubes packed into the reactor vessel. The design concept was similar to that used in the suspended TiO_2 photoreactor (section 4.2) following the same UV irradiation process and photocatalytic degradation time but with the exception of the reactor vessel configuration and photocatalyst matrix (figure 5.2). The reactor vessel had a capacity of 20 mL and ability to contain 20 glass tubes of 5 mm in diameter and 65 mm in length (figure 5.1). TiO_2 photocatalyst was immobilized onto the glass tubes and the inner walls of the reactor vessel. Two different TiO_2 sol gel methods were used to prepare the sol which was dip-coated and then calcined onto the glass tubes and inner walls of the reactor vessel.



Figure 5.1: SIPR reactor vessel

The method set-up in the 3 stages is similar to that of the SPR: UV light illumination, photocatalysis and sample analysis (figure 5.2). The exception was the TiO_2 removal stage which had been eliminated. The TiO_2 removal stage being the major limitation of the suspended photoreactor, had been eliminated through the immobilization of TiO_2 onto the glass tubes.

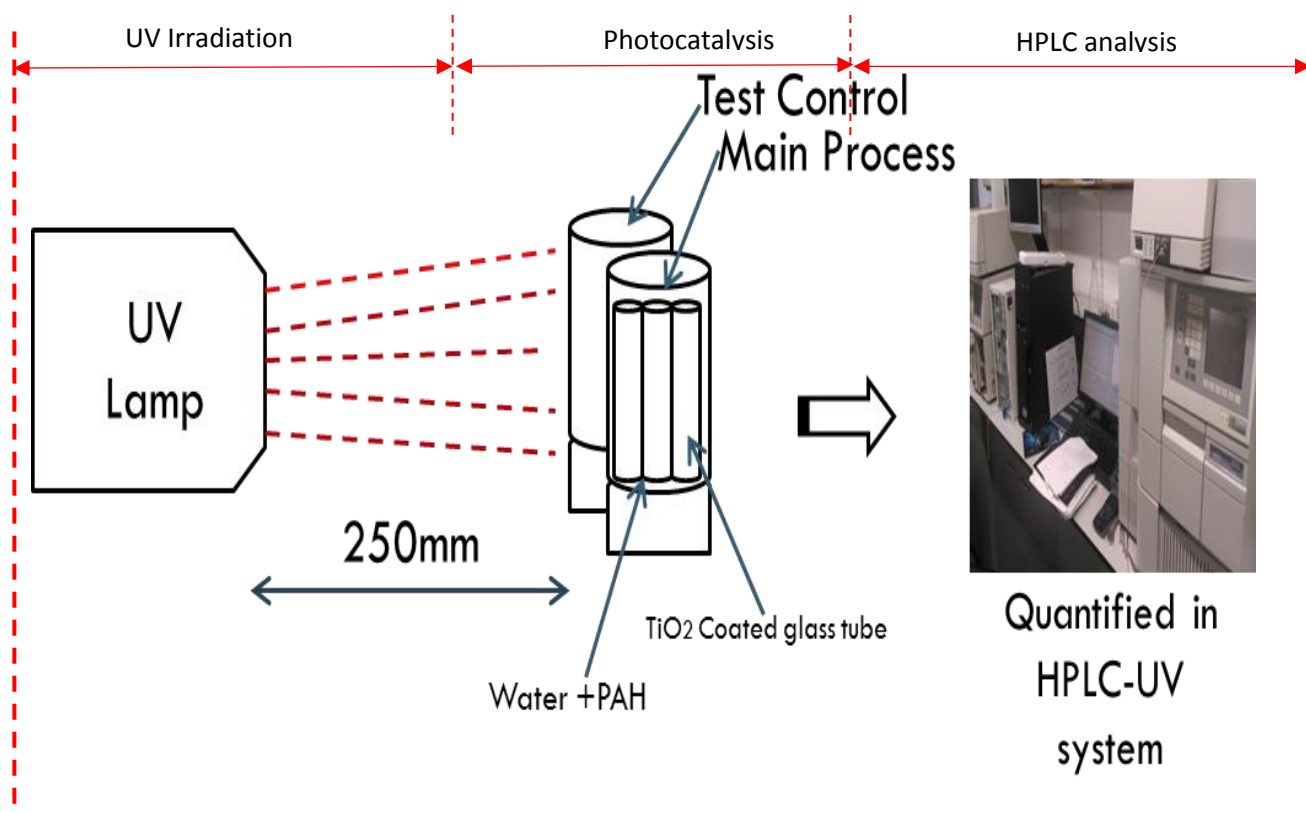


Figure 5.2: SIPR photocatalytic degradation process

5.2.2. Stage 2 Design: Flow Through Immobilized Photocatalytic Reactor (FTIPR)

The optimized design in stage 1 was implemented into the stage 2 design. The second design stage involved the design of a novel flow through immobilized photocatalytic reactor (FTIPR) with coated TiO₂ glass tubes packed into the reactor vessel. This design stage was to enable the easy application of this method to be integrated into the industrial clean-up. The integration of SIPR into the industry is low as this could slow down the treatment flow process which will involve batch treatment units and also impact on the overall treatment time. The stage 2 design can be easily integrated into a flow through pipeline with no impact on the flow process.

The design of the FTIPR was carried out using two different UV irradiation configuration:

- (1) The first involved the use of a high power UV lamp of 480 W with the UV light irradiated on one side of the reactor vessel and reflected at the other side using a reflective surface (figure 5.3 and 5.4).
- (2) The other configuration involved the use of 4 low UV lamps of 50 W arranged at opposite sides of the reactor vessel (figure 5.5 and 5.6).

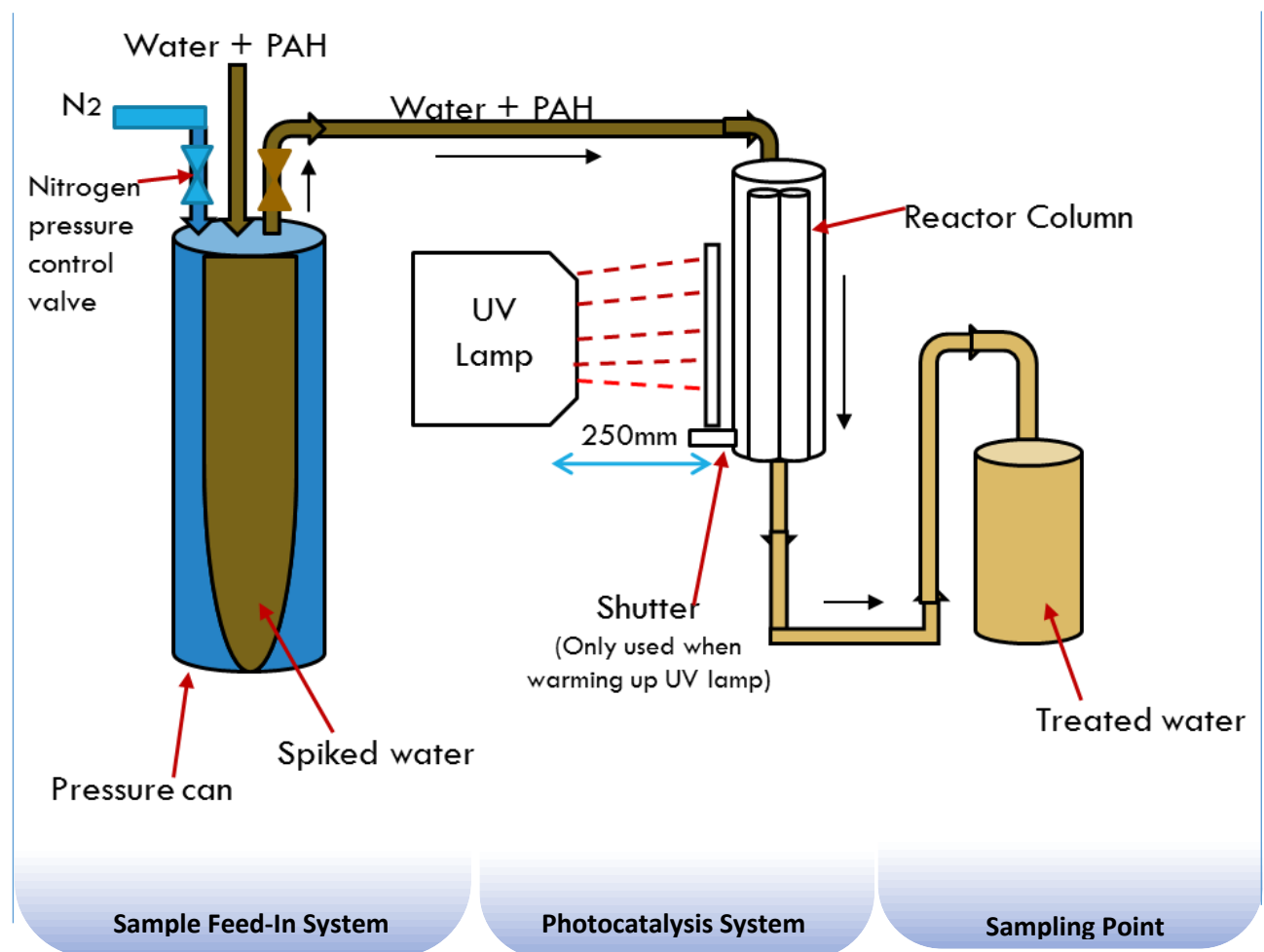


Figure 5.3: Flow process of FTIPR reactor setup using 480 W UV Lamp

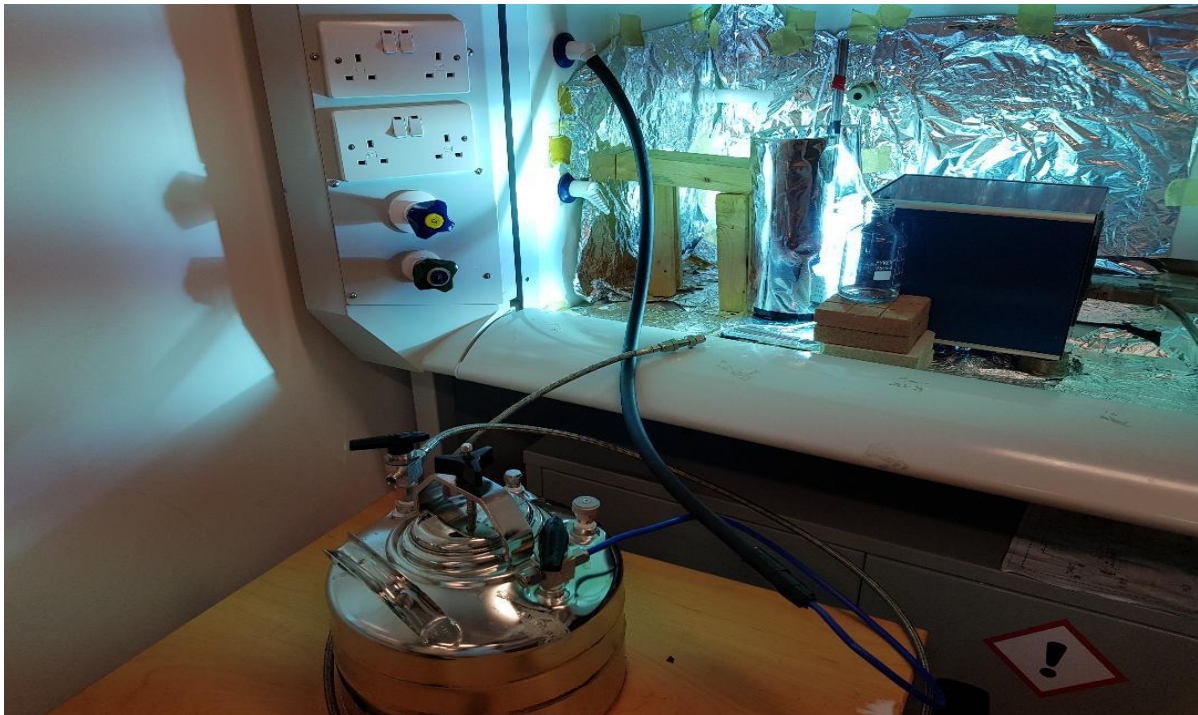


Figure 5.4: Image of FTIPR reactor setup using 480 W UV Lamp

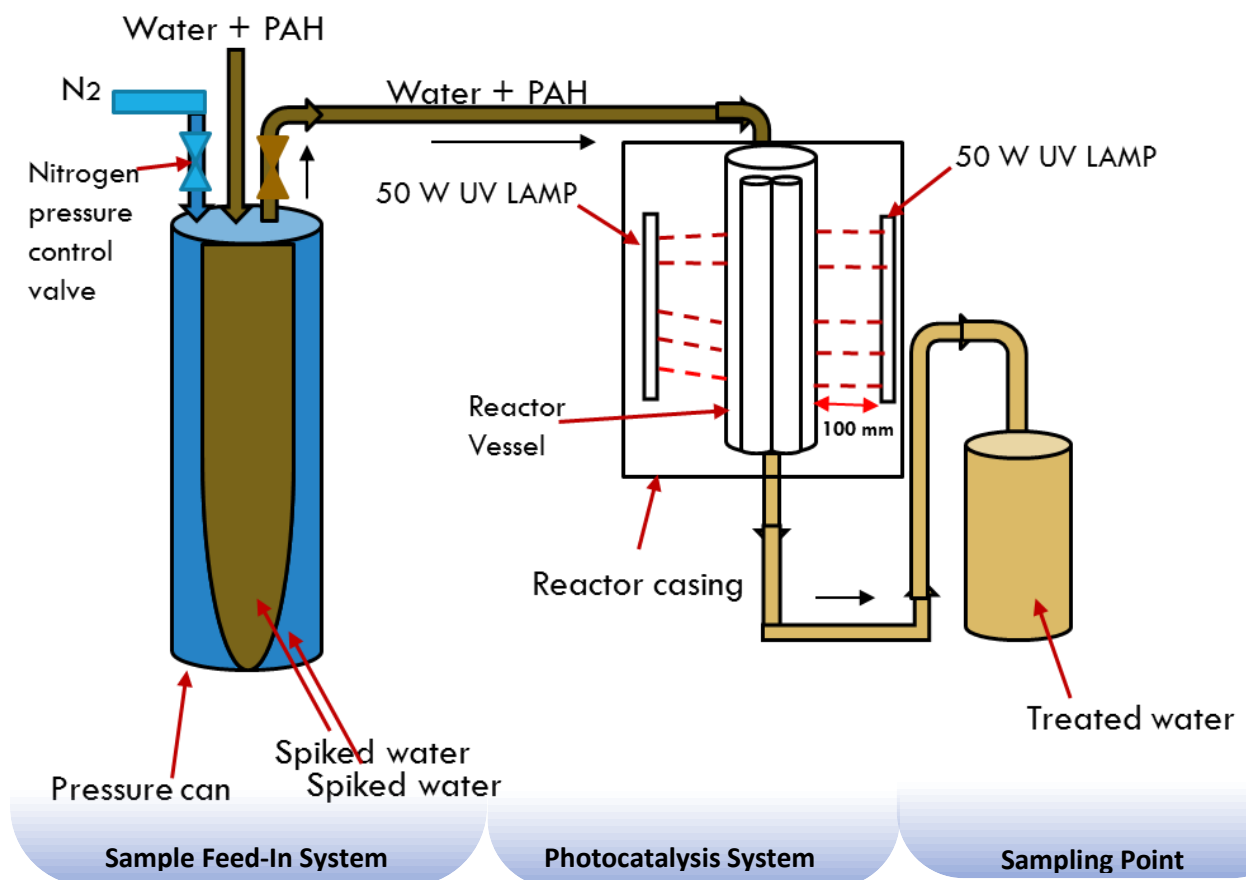


Figure 5.5: Flow process of FTIPR reactor setup using 4 50 W UV Lamp

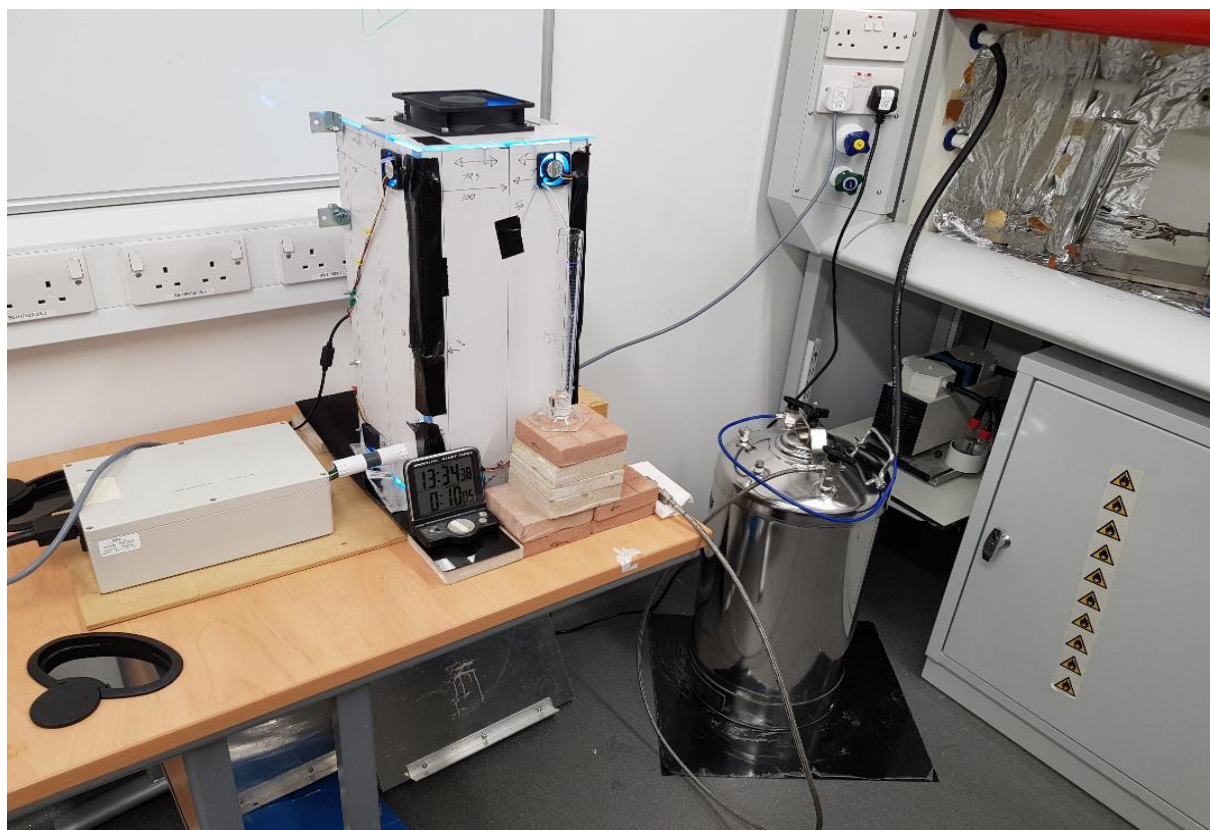


Figure 5.6: Image of FTIPR reactor using four 50 W UV Lamp

5.2.2.1 Flow Through Immobilized Photocatalytic Reactor (FTIPR) design components

The design was grouped into three design components: the sample feed-in system, photocatalysis system and sampling points.

(I) Sample Feed-in system

The selection of the apparatus to feed in PAH into the reactor vessel was determined based on its ability to minimise the loss of PAH through the walls of the apparatus. The most suitable apparatus investigated was made of stainless steel. Stainless steel favourable elemental composition such as Cr gives it such advantage. Cr increases the corrosion resistance of SS thereby preventing any corrosive surface on the SS which will promote the PAH to be lost on it. Various researchers have used stainless

steel material in the design and construction of immobilized photoreactors (Chan *et al.*, 2003, Shang *et al.*, 2003 and Rosas-Barrera *et al.*, 2011).

A pressure can (figure 5.7) made of stainless steel was therefore selected for feeding in the PAH in water into the reactor vessel. Nitrogen was used as a driving force in the pressure can to deliver the water containing dissolved PAH. Nitrogen was selected because it is an inert gas and also it does not have direct contact with the PAHs in the pressure can. This eliminates the need for pumps and pump tubing where the sample can be lost. Stainless steel pressure control valves were also used in both the pressure can liquid outlet line (V_s), nitrogen inlet (V_N) and pressure can cap (C_p). A $\frac{1}{4}$ " PTFE tube was used to transfer the PAH solution from the pressure can to the reactor vessel, as PTFE is also known to show limited adsorption.

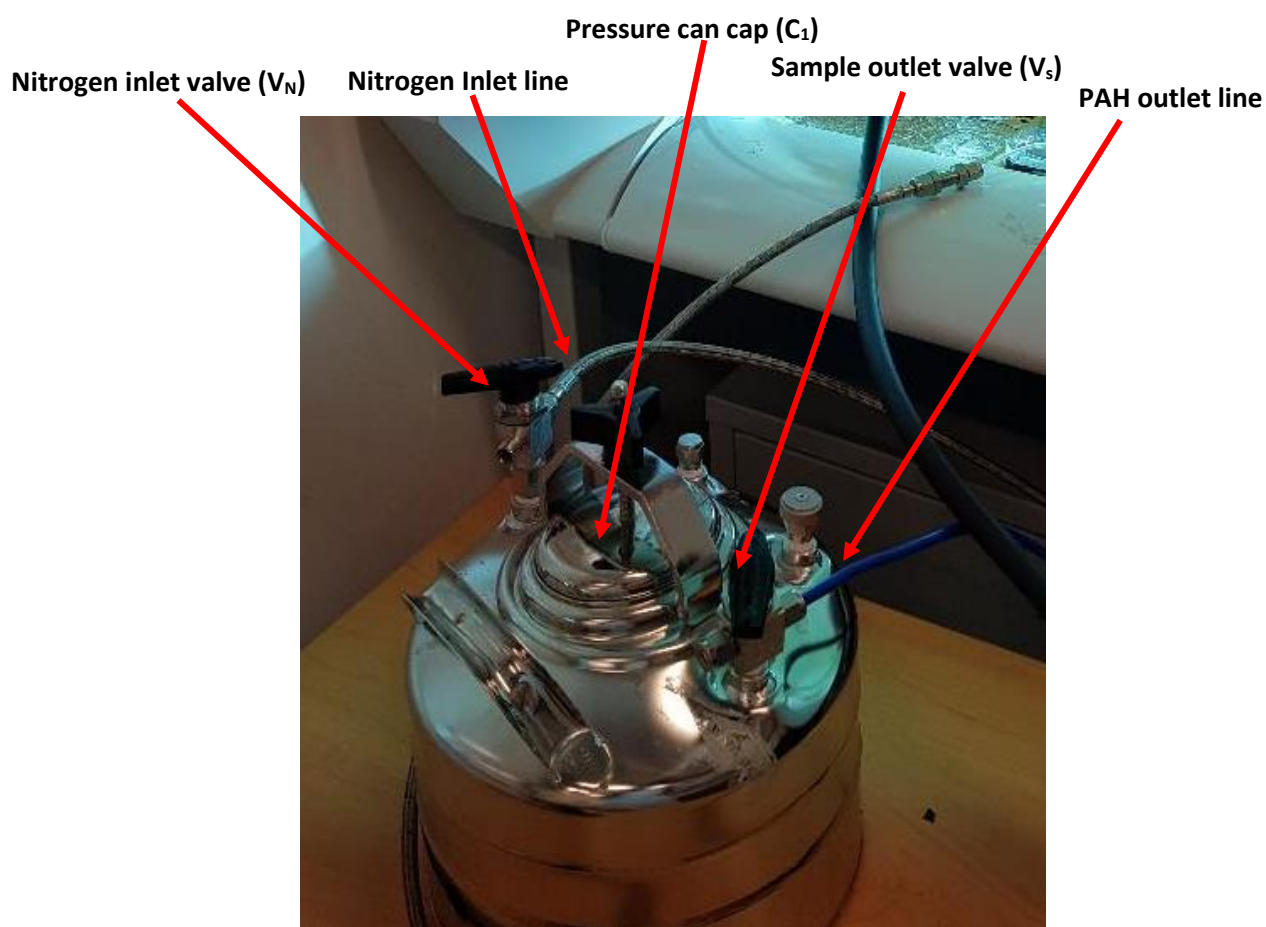


Figure 5.7: Pressure can for driving PAH solution through the reactor

Mode of operation – Pressure can

To operate the pressure can (figure 5.7), nitrogen inlet line control valve (V_N) and sample outlet valve (V_S) were first closed. The pressure can cap (C_P) was then opened and the PAH sample was transferred into the pressure can. C_1 was tightly closed so that the can remains pressurized. V_N was slowly opened to 1/8 opening position and the nitrogen allowed to flow in for 1 minute. The PAH outlet valve (V_O) was slowly opened to 1/8 opening size which then allows the PAH to flow into the reactor vessel through the PTFE pipe.

(II) Stage 2b: Photocatalysis system

The photocatalysis system was made up of two major parts which were the reactor vessel where the photocatalysis reaction occurs and the UV lamp which generates the UV light. A shutter was incorporated to control the UV light.

(a) Reactor Vessel

The FTIPR reactor vessel was made of a clear glass cylindrical tube of 150 mm in height and 50 mm in radius (figure 5.5). It was covered at the top and bottom with a stainless steel cover with a conical inner shape to allow for the even distribution of PAH solution when flowing in through the reactor tubes. The top and bottom cover were further reinforced onto the reactor column by using a secondary stainless steel ring with four enforced screws. The glass allowed for the penetration of the UV light into the reactor chamber and also prevented the loss of PAHs onto the walls of the photoreactor chamber. The top and bottom glass were sealed against the stainless steel plates by using a PTFA sealant to prevent leaks. In literature too, it can be seen that glass and stainless steel materials have been employed in the construction of photoreactors (Well *et al.*, 1997, Rizzo *et al.*, 2006, and Adams *et al.*, 2008). This is

as a result of the materials encouraging full distribution of UV illumination through the sample and limited sample losses that these materials encourage.

A single and double chamber configuration was investigated. This was in an effort to optimize the FTIPR in achieving a higher degradation efficiency by increasing the residence time. A single pass involved the use of one reactor vessel in the photocatalysis process (figure 5.8) while a double chamber involved the use of two identical reactor vessels used in series having the same number of coated tubes (figure 5.9).



Figure 5.8: FTIPR reactor vessel single pass



Figure 5.9: FTIPR reactor vessel double chamber

(b) UV Lamp

To achieve the highest rate of reaction the FTIPR was designed to achieve maximum radiant energy sourced from a UV lamp. As a result of this an external illumination approach was employed in order to increase the photocatalyst surface area per unit of PAH volume reaction ratio. Published literature from Josset *et al.*, 2009 highlighted the limitation encountered in achieving high photocatalyst surface area per volume due to centrally positioning the illumination source.

In the optimization of the FTIPR, two external UV lamps were used: four 50 W UV lamps and a 480 W UV lamp to achieve high rate of degradation of the PAHs. In the optimization process various model configurations of the reactor setup were employed using the UV lamps at varied irradiation distances of 50 and 100 and 250 mm (figure 5.10 – 5.13). A double chamber was also employed in an effort to increase the UV contact time.

The UV lamps were switched on 30 minutes prior to the start of the photocatalysis process to allow the lamps to reach their optimal intensity. The UV light was contained using a shutter to prevent the exposure of the FTIPR to the UV light during this time.

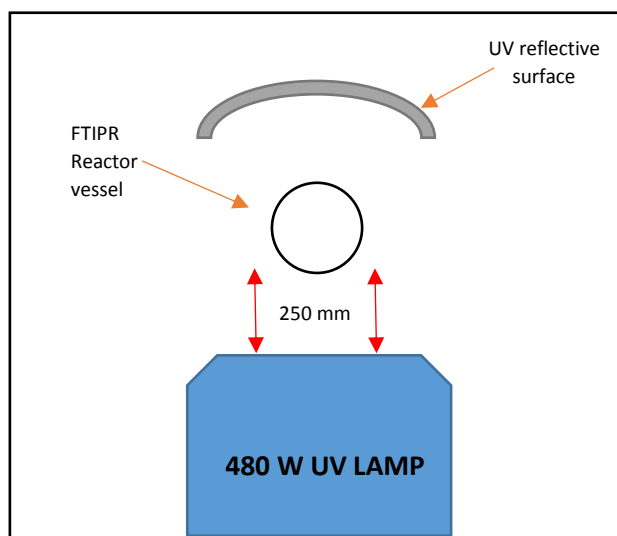


Figure 5.10: UV illumination configuration for 480 W UV LAMP at 250 mm irradiation distance - Model X₁

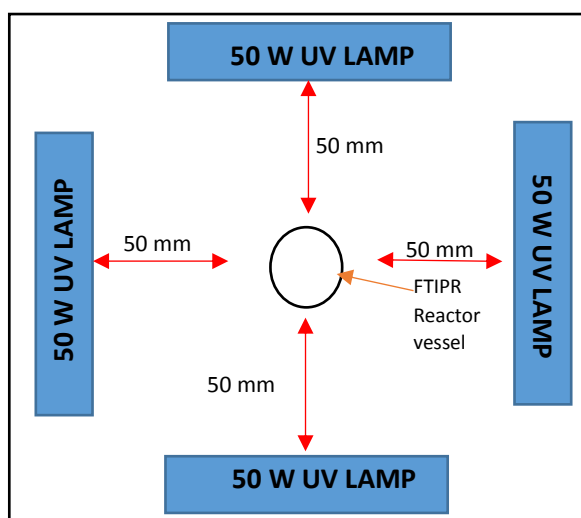


Figure 5.11: UV illumination configuration for four 50 W UV LAMPs at 50 mm irradiation distance - Model X₂

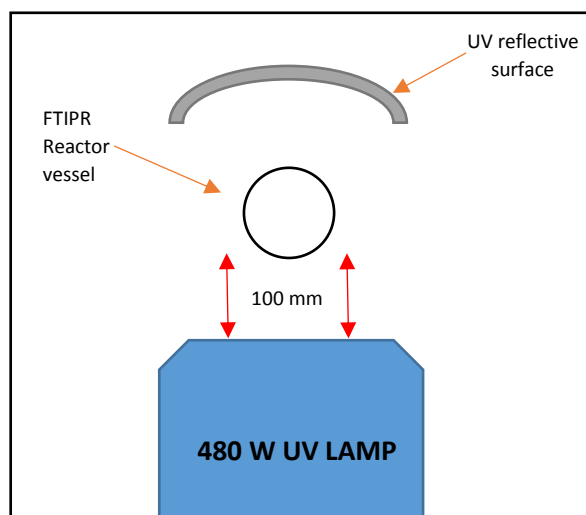


Figure 5.12: UV illumination configuration for 480 W UV LAMP at 100 mm irradiation distance - Model X₃

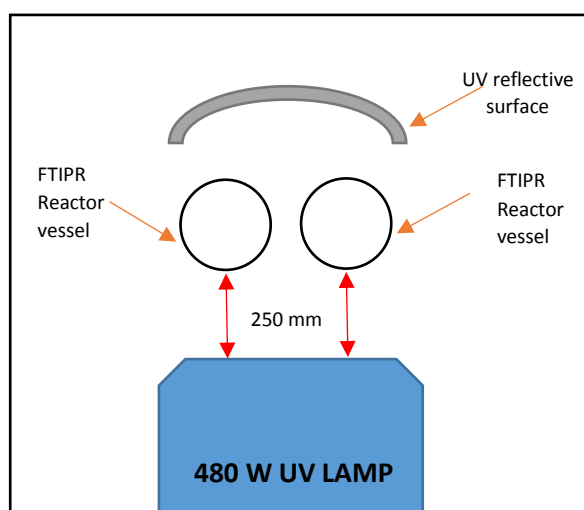


Figure 5.13: UV illumination configuration for 480 W UV LAMP at 250 mm irradiation distance (double reactor chamber) - Model X₄

(III) Sampling point

The treated water was collected from the reactor column using ¼" PTFE tubes directly into the HPLC sample vials. PTFE which also minimized the loss through the walls ensured the desired sampling liquid was maintained, and remained the same at the outlet of the reactor as that which was collected into the vial.

5.3. Sol gel preparation and glass tube coating

5.3.1. TiO₂ sol gel preparation

In the optimization of the TiO₂ sol gel, two sol gel preparation methods were used (figure 5.12). One method (sol gel A) which was employed by Adams *et al.*, 2012 in the preparation of TiO₂ sol gel for a multi tubular photoreactor and the other method (sol gel B) was a modified sol gel preparation method used by Islam *i.*, 2016 in the fabrication of a sol-gel based phenolphthalein encapsulated silica-titania nanomatrix. A higher proportion of titanium isopropoxide and isopropanol was used to attain maximum dissolution of TiO₂ into the sol gel B. The aim was to derive a sol gel which will easily transfer TiO₂ onto the glass tube during the dip coating process.

The two titania sol gels were prepared as follows: For sol gel A glacial acetic acid (4.43 mL) was added to titanium isopropoxide (20 mL). The resulting solution was then added to nitric acid (120 mL). The solution was then heated in a water bath at 80°C for 8 hours (Adams *et al.*, 2012).

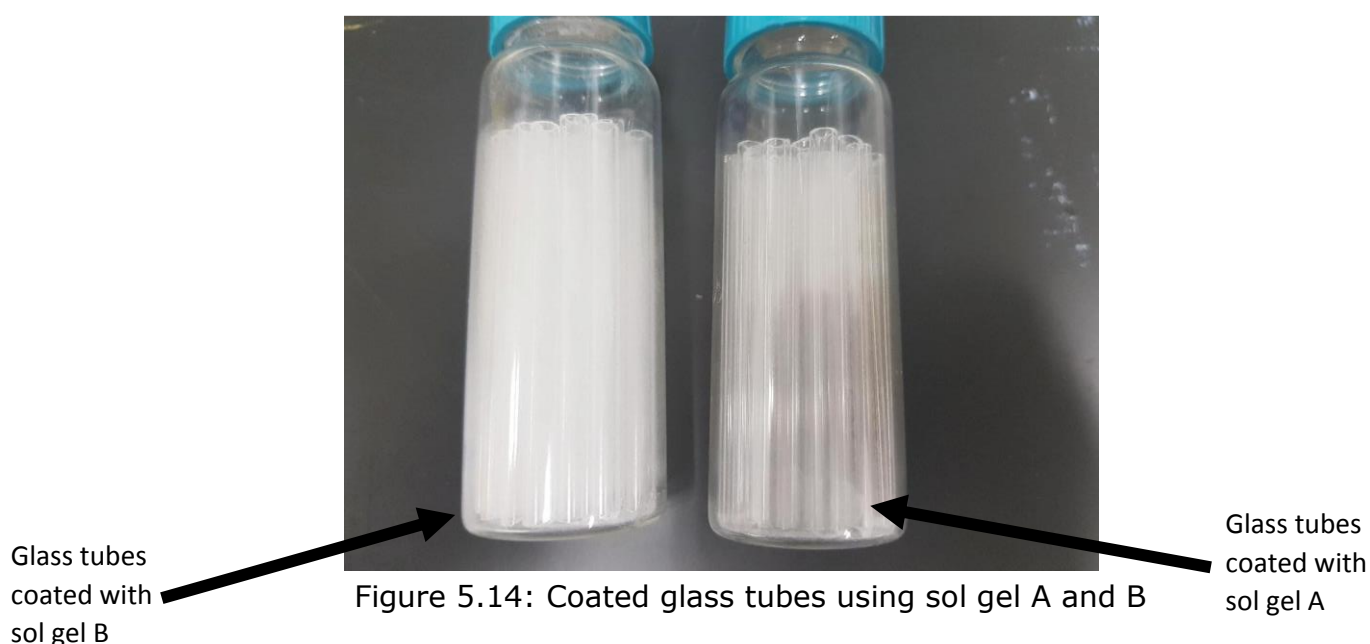
Sol gel B was prepared as follows; titanium isopropoxide (15 mL) was added to isopropanol (10 mL) to produce titanium tetraisopropoxide (TTIP). TTIP (10 mL) was added into a solution containing propanol (10 mL), ultrapure water (10 mL) and nitric acid (2 mL). The solution was stirred at 100°C for 2 hrs. Sol gel A and B both formed a white opaque titania sol gel.

5.3.2. Glass tube coating – Sol gel deposition

TiO₂ sol gels (A and B) were used in the coating of glass tubes. Glass tubes (5 mm diameter), 20 in number were cut to 65 mm in length. The cut glass tubes were first ultrasonically cleaned in decon 90 and rinsed in deionized water. Subsequently the glass tubes were ultrasonically cleaned in acetone and ethanol for 10 minutes and

rinsed in deionized water after which were then dried for 24 hours (Segota *et al.*, 2011). The clean glass tubes were then dip coated in sol gel A or sol gel B and allowed to dry at room temperature for 24 hours. At furnace operating temperature of 450°C the glass tubes were calcined for 30 minutes to allow the formation of the anatase phase (Adams *et al.*, 2013). The anatase phase has been shown by literature to achieve higher photodegradation than rutile phase and calcination above 600°C will result in the formation of the rutile phase (Yung-Fang *et al.*, 2003).

To evaluate the performance of the different sol gel coatings 34 coated glass tubes were transferred into two batch reactor vessels of 25 mm in diameter and 80 mm in height (figure 5.14). One reactor vessel containing glass coated tubes with sol gel A and the other with sol gel B. The inside of the reactor vessel was also coated by pre-filling the glass vessel with the sol gel and emptying it thereby allowing the sol gel to stick onto its inner surface. It was then calcined using the same furnace operating conditions of that used for the glass tubes. At the base of the glass vessel a stainless steel wire mesh was used to create room for a stirrer bar to be added in order to agitate the solution during the experiment.



5.3.4. Characterization of TiO₂ on glass tubes

The characterization of the TiO₂ coated glass surface was carried out to determine the physical properties and surface topography of the coated glass. This was important to determine the amount of titanium dioxide that was coated onto the glass surface. EVO LS10 Zeiss Scanning Electron Microscope (SEM) was used in characterizing the coated glass surface giving a detailed surface topography and cross sectional thickness of the coating.

Two glass tubes were selected from each coated glass tube set coated with either sol gel A and sol gel B. To fracture the glass tubes they were wrapped in a cotton sheet in order to prevent broken glass from scattering and to prevent the chipping off of the TiO₂ coating during the hammering impact. Each broken fragment was placed on an SEM stud and analysed using Scanning Electron Microscope (SEM) to estimate the size and distribution of the TiO₂ particles. The x-ray analysis of the inner and cross-sectional area of the glass tube was analysed.

5.3.5 Photocatalytic Procedure

Two batch photoreactors containing tubes coated with sol gel A and sol gel B were both tested to determine their photocatalytic performance. Naphthalene was used as a model PAH for the preliminary investigation with further investigation using phenanthrene and flourene. Two reactors were filled with coated glass tubes while the third reactor was filled with uncoated glass tubes. As investigated with the previous method for suspended TiO₂, UV light was irradiated onto the two reactors with one containing PAH solution and TiO₂ coated glass tubes and the other containing PAH solution and uncoated glass tubes. The third reactor filled with TiO₂ coated glass tube was not exposed to UV light. Sampling followed the same procedure as that described for suspended TiO₂ with the exception of the use of a centrifuge, which was

not necessary as the TiO_2 was coated onto the glass tubes hence did not require removal.

5.4 SEM/EDXA analysis of TiO_2 coated glass

The TiO_2 coating on the glass tube surface was investigated using Scanning Electron Microscope (SEM) and Energy-dispersive X-ray Spectroscopy (EDXA). The SEM image showed the surface morphology of the coated glass tube when coated with sol gel A and B and also that of the uncoated glass tube.

Figure 5.16 and 5.17 illustrate the surface morphology of TiO_2 immobilized glass tubes coated with sol gel A and B respectively. The results show the presence of TiO_2 coated on the surface when compared with the SEM image (figure 5.15) of the uncoated glass tubes. The surface morphology of the glass coated with sol gel B showed a more even distribution of the TiO_2 coating compared to that of glass coated with sol gel A. These results can be attributed to the higher density of sol gel B compared to that of A. Sol gel with higher density tend to be evenly distributed onto the surface of a medium during the dip coating stage. This was also proven by Sharif *et al.*, 2008 in characterization of TiO_2 coated on nanotubes using a different sol gel method. The results of the investigation showed a more even distribution of TiO_2 onto the nanotubes with the sol gel of a higher density than that of lower density sol gel.

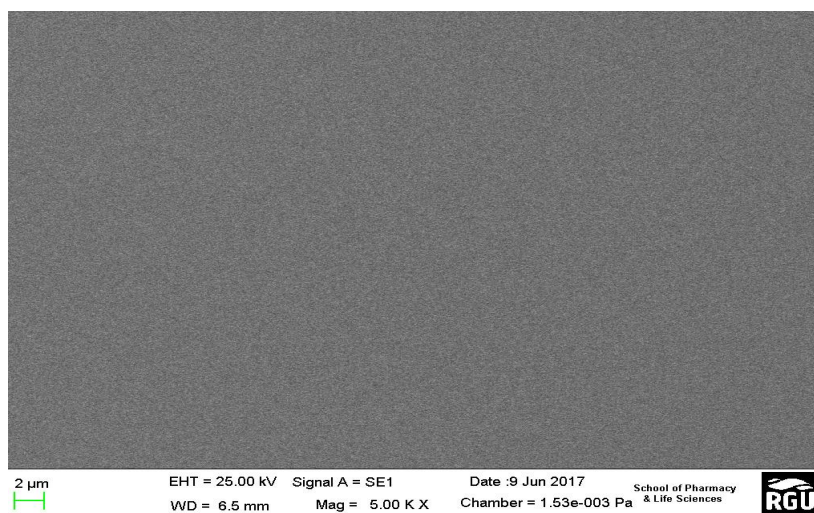


Figure 5.15: SEM image of uncoated glass tube surface

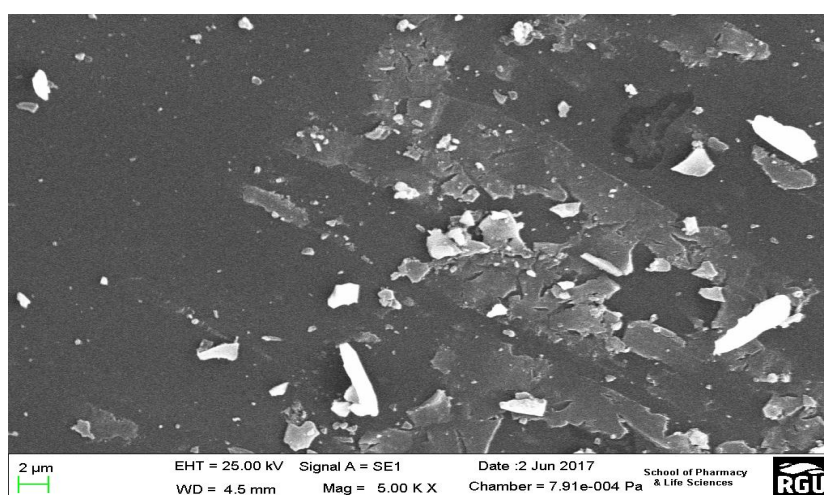


Figure 5.16: SEM image of coated glass tube surface coated using TiO_2 sol gel A

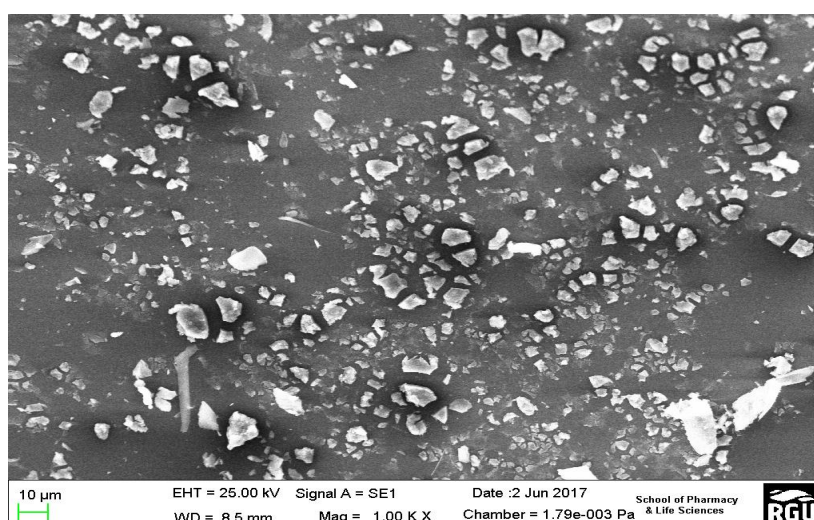


Figure 5.17: SEM of coated glass tube surface coated using TiO_2 sol gel B

Elemental analysis

Elemental analysis was investigated using an Inca system, Oxford Instruments Energy Dispersive X-ray spectroscopy (EDAX) to quantitatively analyse the immobilized TiO₂.

The results illustrated in table 5.1 from the EDAX analysis showed various elements that are exhibited by the glass tube. The results agree with literature on the elements of glass (Matthias 2006). The presence of Ti as an additional element confirming the presence of immobilized TiO₂ in both coated glass tubes. Comparing the results shown by the EDAX image of sol gel A on figure 5.18 and sol gel B on figure 5.19, it can be seen that sol gel B has a higher amount of Ti present on the coated glass tubes surface than that of sol gel A. Table 5.1 shows the weight percentage of Ti confirming the presence of more Ti on the glass tubes coated with sol gel B compared to that of sol gel A.

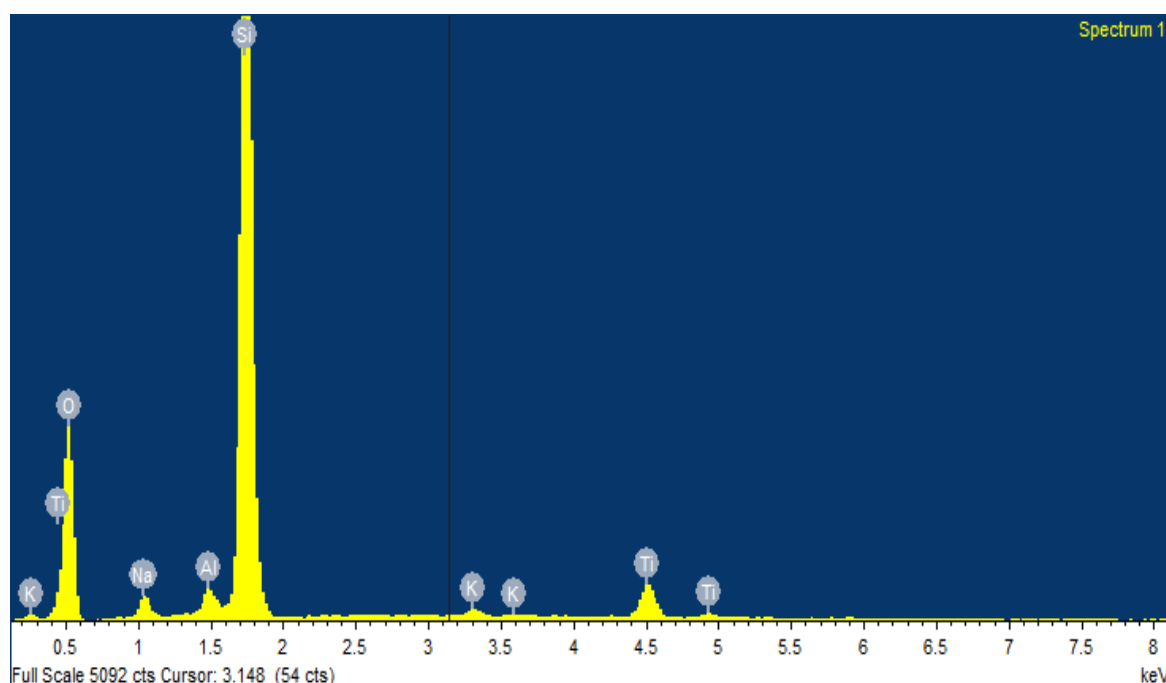


Figure 5.18: EDAX spectrum confirming the presence of Titanium & oxygen on the glass surface when coated with sol gel A

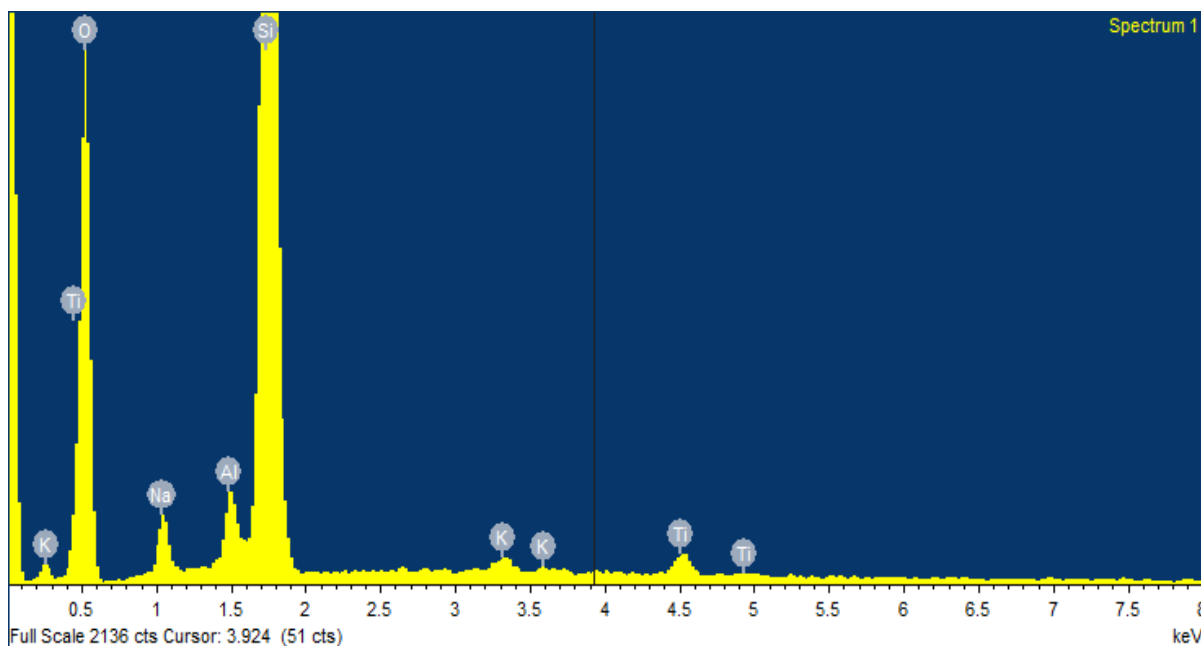


Figure 5.19:EDAX spectrum confirming the presence of Titanium & oxygen on the glass surface when coated with sol gel B

Elements	Weight %	
	Sol gel A	Sol gel B
Ti	0.24	0.96
Oxygen (O)	9.99	32.48
Sodium (Na)	0.38	1.34
Alumina (Al)	0.26	0.70
Silica (Si)	8.82	22.17
Potassium (K)	0.11	0.25

Figure 5.1: Elemental properties and weight % of glass coated with TiO₂

5.5 Naphthalene photocatalysis using SIPR

Figure 5.20 illustrates the photocatalytic degradation of naphthalene by SIPR coated with sol gel A and B. The results showed that there was a significant amount of photocatalytic activity in the degradation of naphthalene with the use of SIPR. In the comparison of the two reactors immobilized with sol gel A and B, results showed the

rate of photocatalytic degradation of naphthalene using reactor coated with sol gel B to be more rapid than that coated with sol gel A. A rate constant of 0.71×10^{-1} and $0.84 \times 10^{-1} \text{ min}^{-1}$ was achieved for sol gel A and sol gel B attaining a degradation efficiency of 72% and 77% respectively (table 5.2). This is expected as preactor of sol gel B has more TiO_2 present on the coated tubes as illustrated in the surface morphology in section 5.4.1

The photocatalytic activity of the suspended TiO_2 photoreactor and the TiO_2 immobilized photoreactor were investigated by the comparison of the rate of degradation of naphthalene. Results in section 4.6.1 for the suspended TiO_2 showed a much more rapid degradation of naphthalene having a rate constant of $2.09 \times 10^{-1} \text{ min}^{-1}$ compared to that of the immobilized photoreactor which showed a rate constant of $0.84 \times 10^{-1} \text{ min}^{-1}$. This can be attributed to less interaction of naphthalene with the immobilized TiO_2 . The result is acceptable since there is a 41% difference in rate constant as the advantage of avoiding the secondary treatment (catalyst removal) of TiO_2 has been eliminated. Further optimization of the immobilized TiO_2 in a more complex flow through photoreactor can increase degradation rate. Similar results have been achieved by other researchers in the comparison of performance between suspended TiO_2 photoreactor and immobilized photoreactor. Ling *et al.*, 2004 compared the performance of suspended TiO_2 photoreactor and immobilized TiO_2 photoreactor in the photocatalytic degradation of phenol. Results achieved showed that suspended TiO_2 performed better with a faster degradation rate when compared with immobilized TiO_2 having an increase of 17% in photocatalytic degradation efficiency.

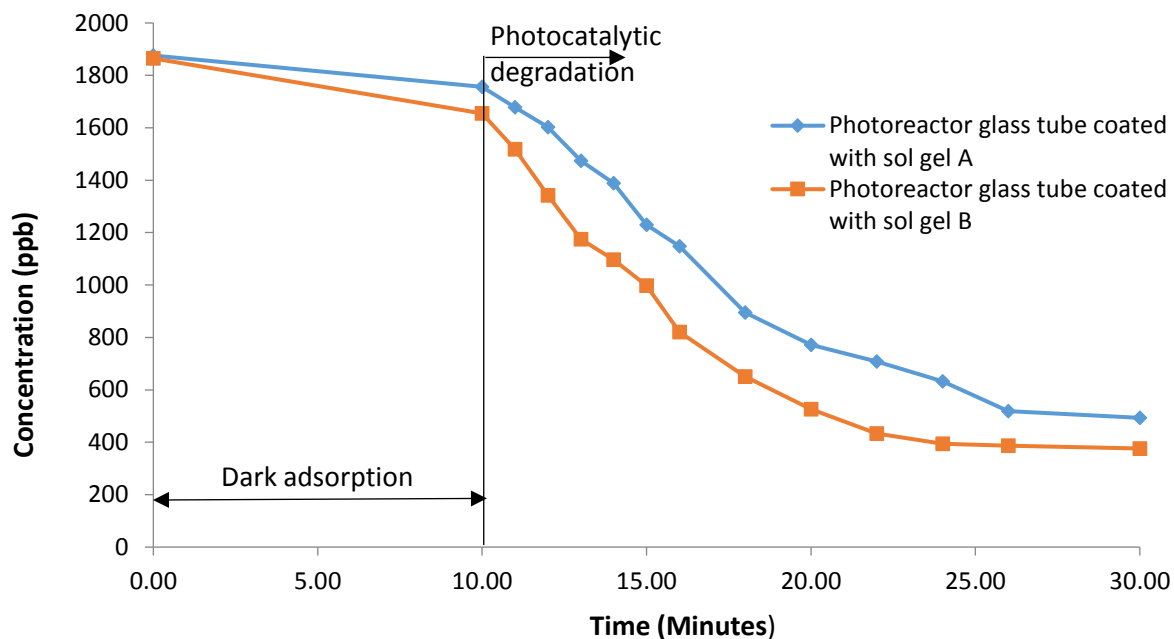


Figure 5.20: Photocatalytic degradation of naphthalene in immobilized photoreactor (1)Sol gel A (2)Sol gel B.

5.6. Phenanthrene photocatalysis using SIPR

The investigation was extended to evaluate the degradation of phenanthrene. In section 4.6.2 it was seen that the differing structure of phenanthrene has a direct influence on the rate of degradation hence it was used to investigate the SIPR.

Figure 5.21 shows the photocatalytic degradation of phenanthrene in an immobilized TiO_2 photoreactor when coated with sol gel A and B. SIPR with sol gel B recorded a more rapid degradation of phenanthrene compared to that of photoreactor with sol gel A. A rate constant of $0.91 \times 10^{-1} \text{ min}^{-1}$ and $1.12 \times 10^{-1} \text{ min}^{-1}$ was recorded for sol gel A and B attaining a photocatalytic degradation efficiency of 86% and 91% respectively (table 5.2). In comparison with SPR, (section 4.6), SPR achieved a higher rate constant of $4.25 \times 10^{-1} \text{ min}^{-1}$ than SIPR with rate constant of $1.12 \times 10^{-1} \text{ min}^{-1}$. This rate constant is still acceptable as this has the ability to reduce phenanthrene concentrations to required legislative limits. With a case study in the North Sea and

recorded phenanthrene concentration in produced water, a 29.3 ppb reduction is required to meet SEPA discharge limit (SEPA WAT-SG-53 2018). The immobilized TiO_2 photoreactor has the ability to photodegrade 124 ppb phenanthrene over a 5 minutes period thereby meeting the legislative limits.

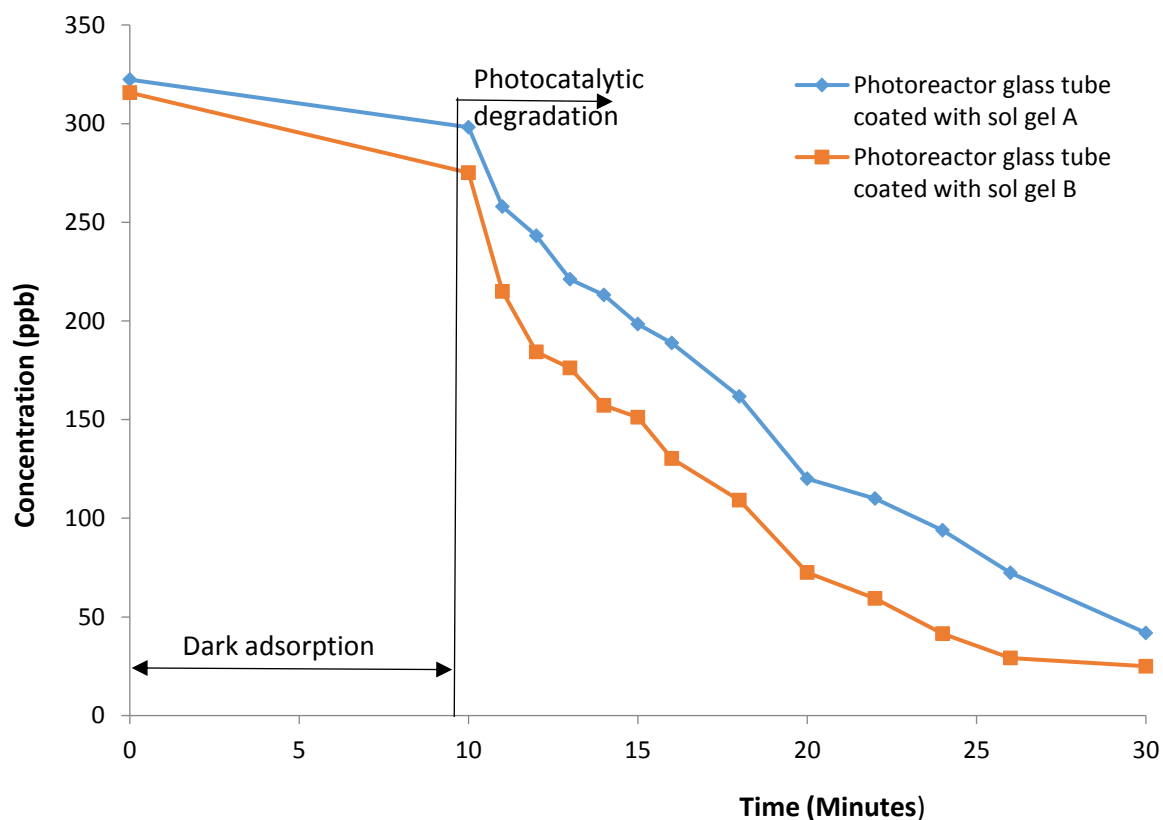


Figure 5.21: Photocatalytic degradation of phenanthrene in immobilized photoreactor (1)Sol gel A (2)Sol gel B.

Phenanthrene chemical structure also played a role in achieving faster degradation than that of naphthalene. Since the photocatalysis followed the same phenomenon (section 4.5.3; stage 2) for suspended TiO_2 in the interaction with the generated OH radicals. Similar results have been seen in published literature by Bo *et al.*, 2016 in the investigation of the water matrix on the photocatalytic degradation of naphthalene and phenanthrene using immobilised TiO_2 photocatalyst. In all the four

different water matrix investigated it was recorded that phenanthrene achieved a higher rate constant than naphthalene confirming phenanthrene degrades faster.

The coated glass tubes were closely packed in the reactor vessel in order to increase the mass transfer between immobilized catalyst and the PAH which can help achieve higher degradation efficiency. Vella *et al.*, 2010 showed this in modelling of TiO₂ immobilized on quartz wool in a packed bed photoreactor in photocatalytically degrading formic acid. Results show higher degradation of formic acid with a closely packed bed than that of a loosely packed bed.

5.7. Fluorene photocatalysis using SIPR

Fluorene, a third PAH was also investigated using SIPR. The photocatalytic degradation of fluorene is illustrated in figure 5.22. The results showed a rapid degradation with a rate constant of $0.55 \times 10^{-1} \text{ min}^{-1}$ and $0.78 \times 10^{-1} \text{ min}^{-1}$ for sol gel A and B attaining a photocatalytic degradation efficiency of 77% and 83% respectively (table 5.2). As seen with naphthalene and phenanthrene, the photoreactor coated with sol gel B achieved greater degradation than that with sol gel A. This further confirms the presence of more TiO₂ on glass tubes coated with sol gel B. Also the TiO₂ suspended photoreactor achieved a greater rate constant. Discharge limits of 6.15 ppb by USEPA in comparison with concentration required to be remediated in North Sea was also met for fluorene using SIPR.

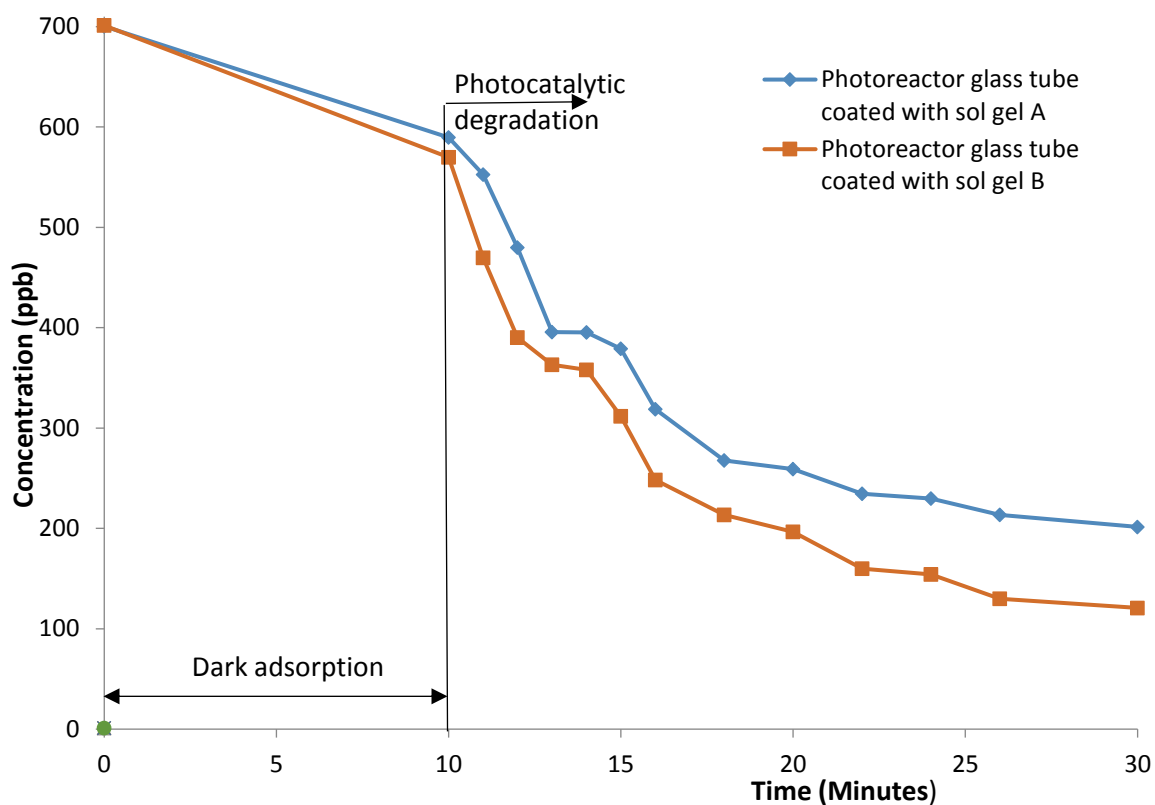


Figure 5.22:Photocatalytic degradation of fluorene in immobilized photoreactor (1)Sol gel A (2)Sol gel B.

Titanium dioxide coated glass tubes	Rate Constant (k) (10^{-1} min^{-1})		Degradation efficiency (%)	
	Sol gel A	Sol gel B	Sol gel A	Sol gel B
Napthalene	0.71	0.84	72	77
Phenanthrene	0.91	1.12	86	91
Fluorene	0.55	0.78	77	83

Table 5.2: Rate constant and degradation efficiency of naphthalene, phenanthrene and fluorene in SIPR using titania sol gel A and B

5.8. Effect on multiple PAHs photodegradation using SIPR

As investigated for the SPR (section 4.7), three PAHs: naphthalene, phenanthrene and fluorene prepared in water were photocatalytically degraded using SIPR. The influence the mixture of compounds had on the degradation rate was evaluated.

Figure 5.23 illustrates the photo catalytic degradation of the three PAHs naphthalene, phenanthrene and fluorene in a SIPR. The comparable results of the three PAHs: when present alone in water and when present with other PAHs showed a slower rate of degradation. The recorded rate constant of naphthalene, phenanthrene and fluorene when present together in water were $0.62 \times 10^{-1} \text{ min}^{-1}$, $0.90 \times 10^{-1} \text{ min}^{-1}$ and $0.67 \times 10^{-1} \text{ min}^{-1}$ respectively which equates to 23%, 20% and 15% less when alone in water. This confirms the similar results obtained for the SPR with low rate constant observed for PAH when present in a mixture of other PAHs. This is attributed to the catalyst available, surface area and competition for produced OH radicals

The rate constant achieved with the PAHs together in water is still acceptable as the rate constant achieved is sufficient to reduce each PAHs to required legislative limits in the case of North Sea. Based on the results obtained for the photocatalytic degradation of the PAH over a 5 minutes period, the concentration of naphthalene, phenanthrene and fluorene that were degraded were 219 ppb, 136 ppb and 106 ppb. When compared with the amount required to be degraded to meet the SEPA and USEPA limits, it can be seen that the SIPR is able to degrade the PAHs to the required limits.

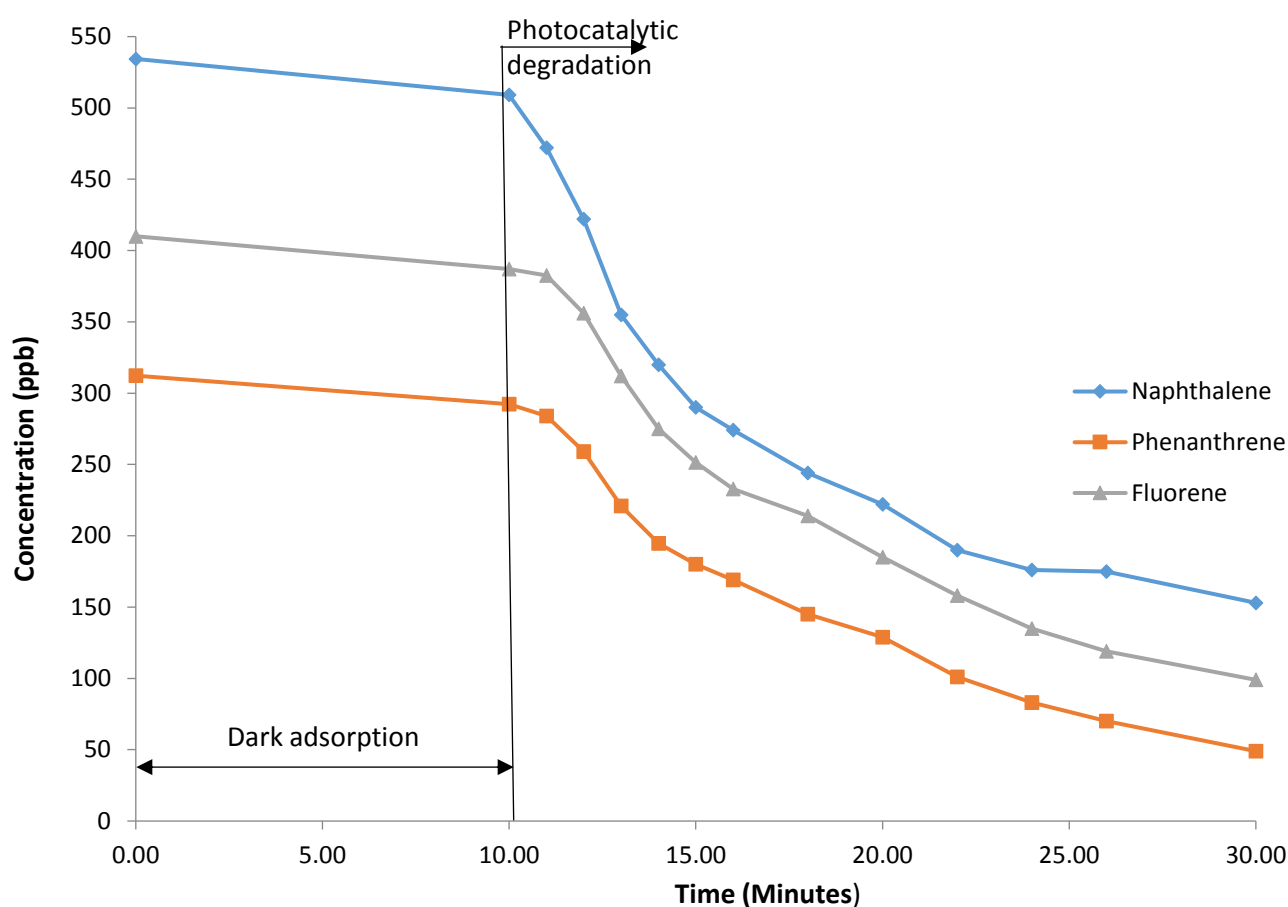


Figure 5.23: Photocatalytic degradation of naphthalene, phenanthrene and fluorene; (1) Under UV light & TiO_2 , TiO_2 : 100 mg, water: 100 mL.

5.9. FTIPR photoactivity testing and optimization of naphthalene photocatalysis

A four-stage optimization process was carried out in the testing of the performance of the FTIPR. Photocatalytic degradation efficiency was used as a measure to quantify the performance of the FTIPR. Naphthalene was employed as a model PAH during the testing and optimization stage. Once an established method was achieved, it was applied to phenanthrene and fluorene. Sampling was carried out at every 60 minutes interval with a total sampling time of 120 minutes in a continuous flow process to confirm the consistency in treatment over time. The optimized method ensured

effective mass transport of the PAH onto the coated glass tube surface by reactor vessel configuration. Also the effect of utilization of UV source to achieve maximum UV irradiation by the use of reflective surfaces to distribute the UV round the reactor vessel. All reaction conditions were kept at room temperature. Table 5.2 highlights the operating conditions of the FTIPR and every optimization stage

Condition	Photoreactor design conditions
Stage 1 – C ₀	Test control : Coated tube and No UV ray
Stage 2 - PC ₁	480W UV lamp and UV ray distance 250mm
Stage 3 – PC ₂	4 - 50W UV lamp and UV ray distance 50mm
Stage 4 – PC ₃	480W UV lamp and UV ray distance 100mm
Stage 5 – PC ₅	480W UV lamp and UV ray distance 100mm (double reactor chamber)

Table 5.2: Stages involved in photocatalytic reactor optimization and degradation efficiency

1st Stage - Test control (C₀)

The first stage with results illustrated in figure 5.24 involved a controlled test carried out by passing naphthalene through the FTIPR without the irradiation of UV light. FTIPR configuration with a single reactor pass was employed. No reduction in naphthalene concentration was observed over a 120 minutes testing period (table 5.3). This showed no loss of naphthalene occurred through the sample container (pressure can) or the wall of the reactor vessels. Test controls are frequently used as seen in published literature (Vezzoli et al., 2013, Chen et al., 2015, Leblebici et al., 2015) in a photoreactor investigation to ensure no loss of species occurs and also for validity of subsequent results. With no naphthalene loss at this stage the

subsequent stages in the optimization in the photocatalysis process (PC_1 , PC_2 , PC_3 & PC_4) of naphthalene was investigated as shown stages 2-5.

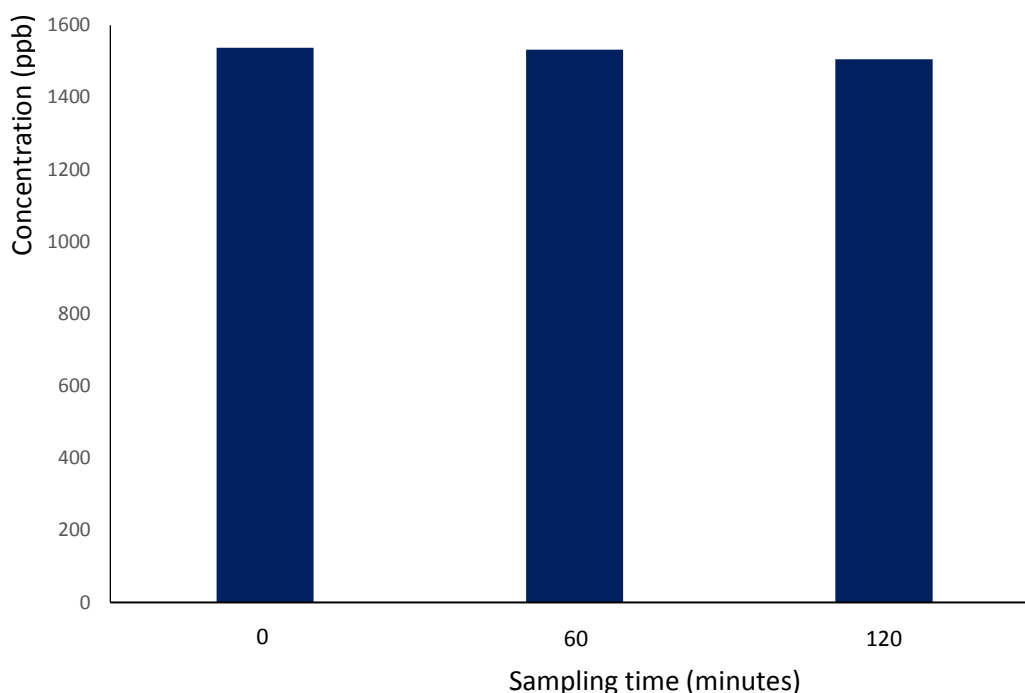


Figure 5.24: Test control of naphthalene in the presence of immobilized TiO_2 and absence of UV light in FTIPR

Condition	Photoreactor design conditions	System loss
Stage 1 – C_0	Test control : Coated tube and No UV ray	0

Table 5.3: Stage 1 involved in FTIPR optimization showing system loss

2nd Stage – Photocatalysis (PC_1)

At this stage the photocatalysis of naphthalene was investigated in the FTIPR by introducing naphthalene (1550 ppb) through the Model X_1 FTIPR (figure 5.10). The UV lamp was kept at a distance of 250 mm from the reactor vessel. Figure 5.25 illustrates the photocatalytic degradation through the Model X_1 FTIPR. A photocatalytic degradation efficiency of 20% (table 5.4) was attained at 60 minutes of sample flow through the Model X_1 FTIPR. The photocatalytic degradation efficiency

remained constant with an additional sample flow through of 60 minutes. This confirms that the introduction of UV light is the key factor in the degradation of naphthalene when compared with results achieved in C₀ stage with no naphthalene loss. The low efficiency can be attributed to the minimized utilization of the UV irradiation. An improvement in irradiation has been seen to increase photocatalytic degradation efficiency. Hassan *et al.*, 2010 in the investigation of the photocatalytic degradation of nitro and chlorophenol using TiO₂ showed the effect UV irradiation distance has on degradation. An increase of 40% degradation efficiency was achieved when the UV irradiation distance was reduced by 60 mm. The reduction in irradiation will increase the light intensity thereby exciting the immobilized TiO₂ which generated more holes and electrons used for the generation of more OH radicals. The FTIPR performance was further optimized by varying the irradiation distance in stage 3 of the photocatalysis process (PC₂)

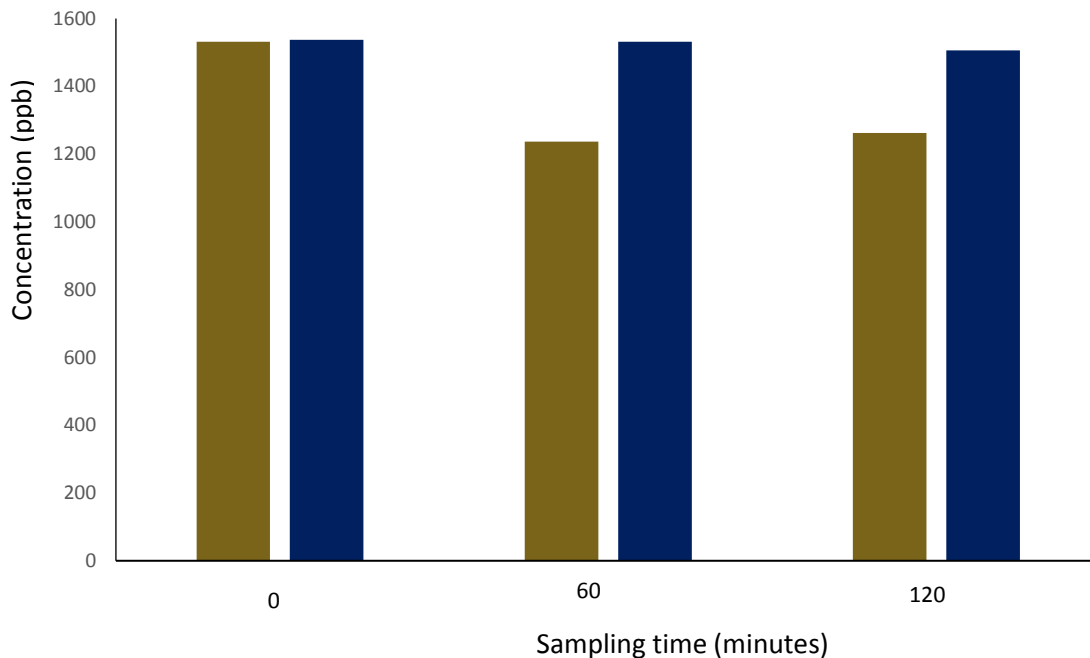


Figure 5.25: Photocatalytic degradation of naphthalene in Model X₁ FTIPR. Photoreactor conditions: UV lamp: 480 W and irritation distance: 250 mm

Condition	Photoreactor design conditions	Degradation efficiency (%)
Stage 1 – C ₀	Test control : Coated tube and No UV ray	0
Stage 2 – PC ₁	480W UV lamp and UV ray distance 250mm	20

Table 5.4: Stage 1-2 involved in FTIPR optimization showing degradation efficiency

3rd Stage – Photocatalysis (PC₂)

In effort to increase the FTIPR photocatalytic degradation efficiency, Model X₂ FTIPR (figure 5.11) was employed thereby reducing the irradiation distance from 250 mm to 50 mm and using also four UV lamps with a 50 W output which surrounded the reactor on all sides in an effort to maximize UV irradiation. As illustrated in figure 5.26, the results showed an increase in the photocatalytic degradation efficiency of naphthalene to 28% (table 5.5). The little improvement of 8% in photocatalytic degradation efficiency can be attributed to the reduction in irradiation distance. The use of four 50W UV lamps could have limited any further increase in the degradation efficiency as this would have cancelled the positive impact the shorter irradiation distance could have had. An improved energy efficiency for better removal can also be seen, although as a low energy: four 50 W lamps compared to the 480 W can still achieve a significant amount of photocatalytic degradation. In the next stage of optimization (PC₃) the use of a shorter irradiation distance and high UV lamp was therefore employed.

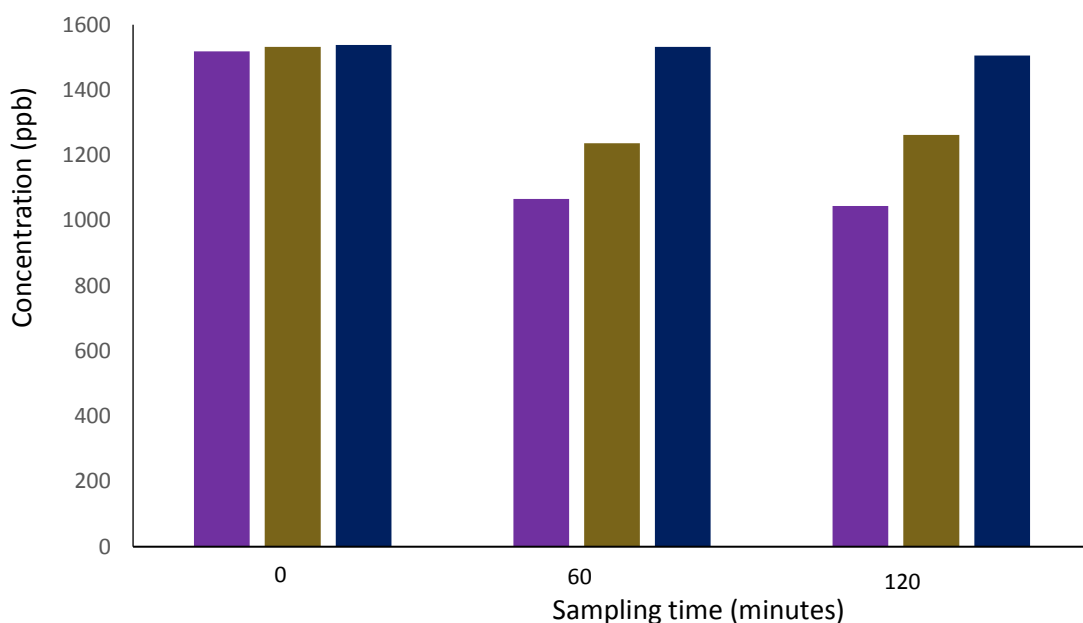


Figure 5.26: Photocatalytic degradation of naphthalene Model X₂ FTIPR. Photoreactor conditions: UV lamps: four 50 W and irradiation distance: 50 mm

Condition	Photoreactor design conditions	Degradation efficiency (%)
Stage 1 – C ₀	Test control : Coated tube and No UV ray	0
Stage 2 – PC ₁	480W UV lamp and UV ray distance 250mm	20
Stage 3 – PC ₂	4 - 50W UV lamps and UV ray distance 50mm	28

Table 5.5: Stage 1-3 involved in FTIPR optimization showing degradation efficiency

4th stage – Photocatalysis (PC₃)

Further optimization was carried out on the FTIPR using the Model X₃ FTIPR with an irradiation distance of 100 mm (figure 5.12). The effect of the Model X₃ FTIPR at 100 mm in the degradation of naphthalene is shown in figure 5.27. The results showed a significant increase to 58% photocatalytic degradation efficiency. This can be attributed to the high energy produced by the UV lamp as a result of the reduced irradiation distance (100 mm) added with the high UV lamp power (480 W) used

which generates more photons for the generation of more holes and electrons by the immobilized TiO_2 .

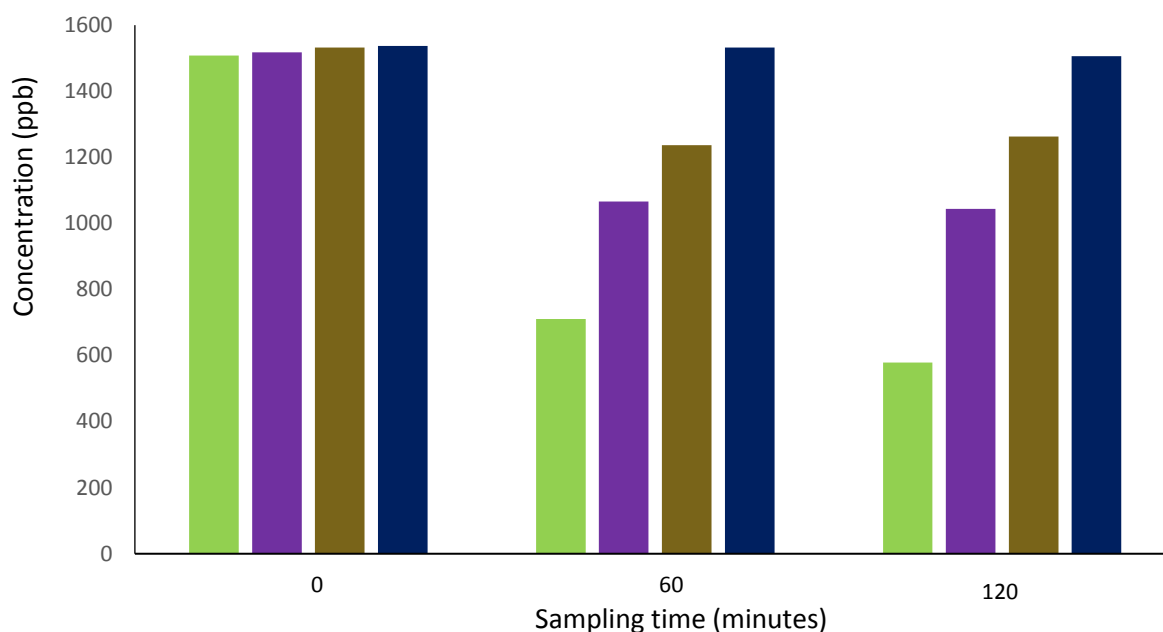


Figure 5.27: Photocatalytic degradation of naphthalene in Model X₃ FTIPR Photoreactor conditions: UV lamp: 480 W and irradiation distance: 100 mm.

Condition	Photoreactor design conditions	Degradation efficiency (%)
Stage 1 – C ₀	Test control : Coated tube and No UV ray	0
Stage 2 – PC ₁	480W UV lamp and UV ray distance 250mm	20
Stage 3 – PC ₂	4 - 50W UV lamps and UV ray distance 50mm	28
Stage 4 – PC ₃	4800W UV lamp and UV ray distance 100mm	58

Table 5.6: Stage 1-3 involved in FTIPR optimization showing degradation efficiency

5th Stage – Photocatalysis (PC₄)

A final optimization was carried out by increasing the residence time between the UV irradiation and naphthalene sample. Natalia *et al.*, 2010 showed in an investigation

into the photocatalytic degradation of toluene using a TiO₂ immobilized photoreactor that a three times increase in residence time increased the degradation efficiency by 60%. This principal was therefore employed by the use of two identical reactor chambers.

Model X₃ FTIPR was optimized by increasing residence time from 6.3 mL min⁻¹ to 12.6 mL min⁻¹ by using a double chamber reactor vessel configuration at irradiation distance of 100 mm. This involved the use of two identical reactor vessels connected in series. As illustrated in figure 5.28, a much higher photocatalytic degradation efficiency of 83% was achieved (table 5.7). High photocatalytic degradation efficiency was achieved as the Model X₄ FTIPR design fully utilized the key photocatalysis parameters by maximizing the irradiation energy and residence time. The established design of the Model X₄ FTIPR at irradiation distance of 100 mm was further used in the investigation of the photocatalytic degradation of phenanthrene and fluorene.

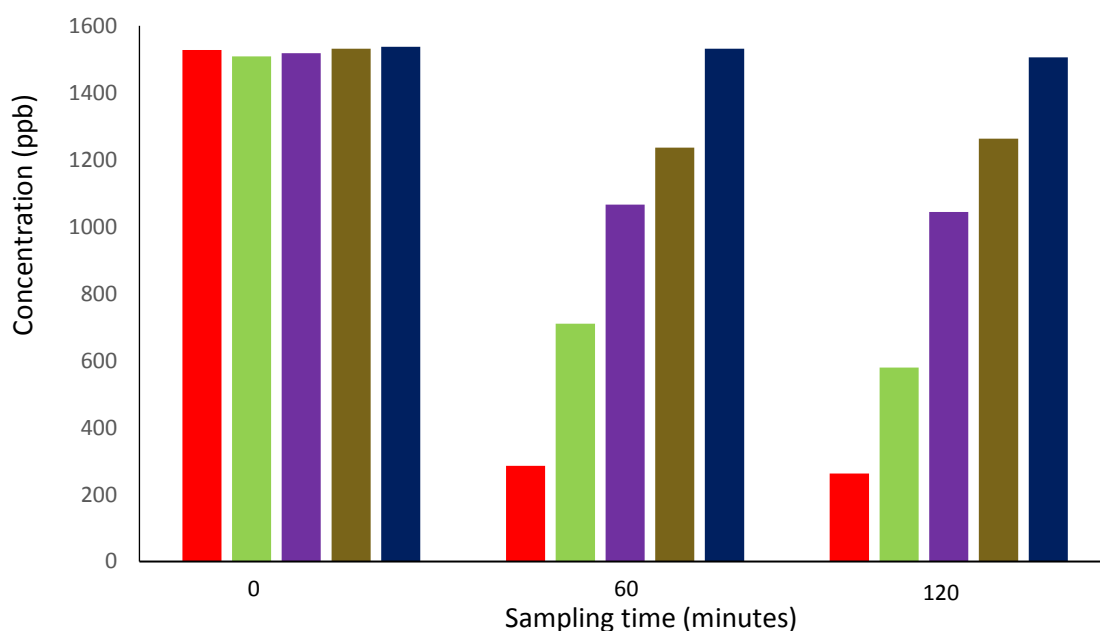


Figure 5.28: Photocatalytic degradation of naphthalene Model X₄ FTIPR. Photoreactor conditions: UV lamp: 480 W and irritation distance: 100 mm , double chamber

Condition	Photoreactor design conditions	Naphthalene Removed (ppb)	Degradation efficiency (%)
Stage 1 – C ₀	Test control : Coated tube and No UV ray	0	0
Stage 2 – PC ₁	480W UV lamp and UV ray distance 250mm	269	20
Stage 3 – PC ₂	4 - 50W UV lamps and UV ray distance 50mm	452	28
Stage 4 –PC ₃	4800W UV lamp and UV ray distance 100mm	798	58
Stage 5 –PC ₄	480W UV lamp and UV ray distance 100mm (2 stage)	1242	83

Table 5.7: Stage 1-5 involved in FTIPR optimization showing degradation efficiency

5.10. Model X₄ FTIPR for photodegrading phenanthrene and fluorene

The established design of the Model X₄ FTIPR was used to investigate the photodegradation of phenanthrene and fluorene when each is present alone in water. The model PAH: naphthalene demonstrated the ability of the FTIPR in generating sufficient OH radicals through the excitation of electrons in the immobilized TiO₂ photocatalyst from sufficient irradiation source. This also can be seen in the investigation of Model X₄ FTIPR photodegradation ability of phenanthrene and fluorene. Figures 5.29 and 5.30 illustrate the photodegradation of phenanthrene and fluorene respectively. A high degradation rate of 92% and 88% was achieved for phenanthrene and fluorene respectively.

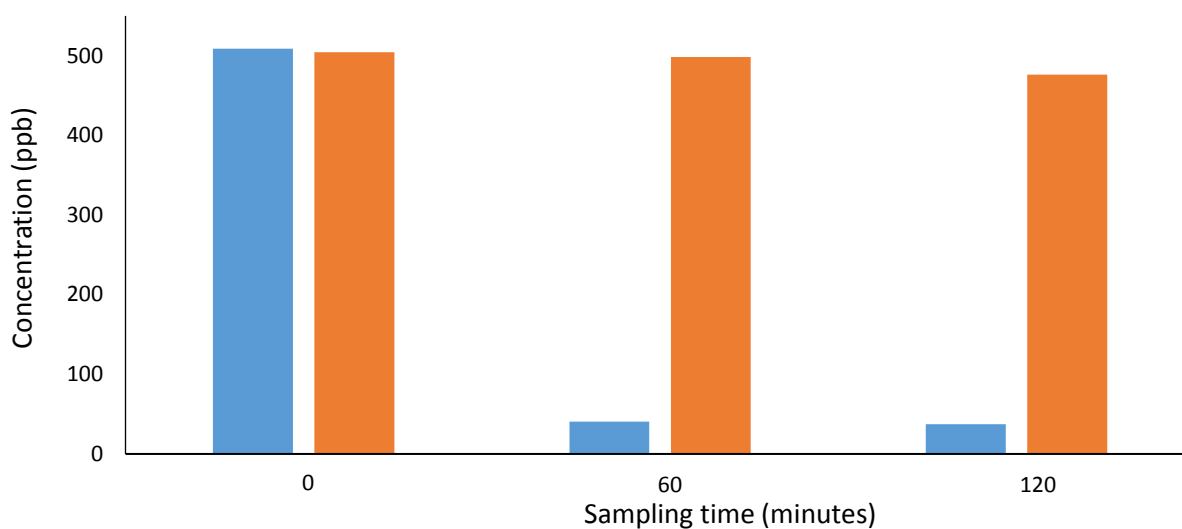


Figure 5.29: Photocatalytic degradation of phenanthrene (blue) in Model X₄ FTIPR with control test (orange)

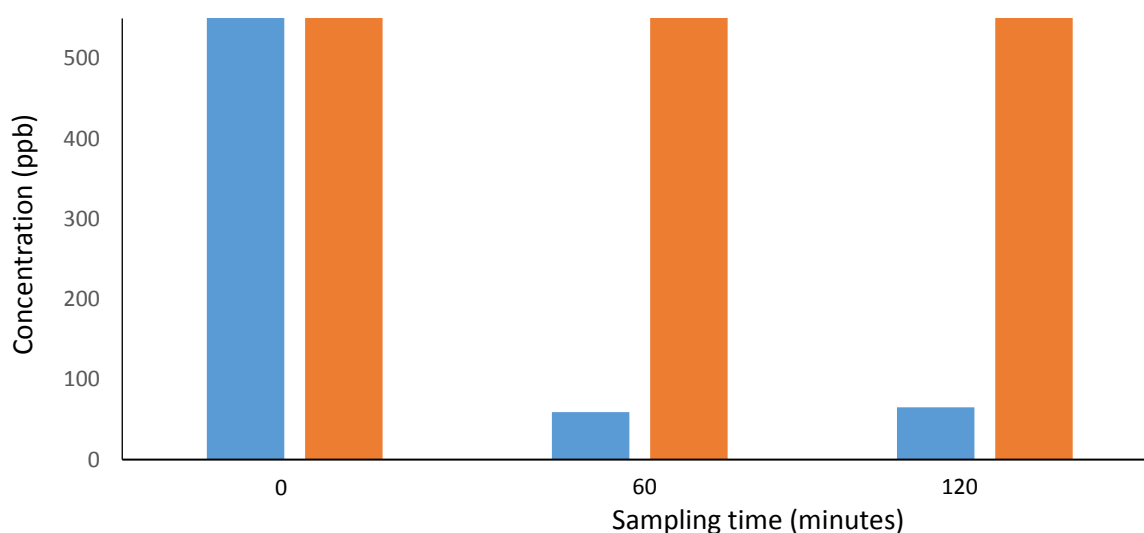


Figure 5.30: Photocatalytic degradation of fluorene (blue) in Model X₄ FTIPR with control test (orange)

5.11. Model X₄ FTIPR photodegradation of three PAHs

As investigated with the suspended photoreactor and BIPR, the effect each PAH has on each other when present together in water was investigated with the FTIPR. Naphthalene (1100 ppb), phenanthrene (710 ppb) and fluorene (200 ppb) present in water was passed through the optimized Model X₄ FTIPR. Illustrated in figure 5.31 is

the result of the photodegradation of naphthalene, phenanthrene and fluorene. Naphthalene photodegradation efficiency remained constant at 84% as when present alone in water and with other PAHs (table 5.8). This signifies naphthalene's dominating ability in the competition of acquiring sufficient OH radicals to maintain its maximum photodegradation efficiency.

Also illustrated in figure 5.31 phenanthrene and fluorene showed significant photodegradation when present together with naphthalene in water. A photodegradation efficiency of 77% and 69% was achieved for phenanthrene and fluorene respectively (table 5.8). A reduction in photodegradation efficiency of 16% and 21% was recorded for phenanthrene and fluorene. This drop in efficiency is sufficient to meet the required legislative standards as set by the SEPA for discharge limit in the North Sea. The degradation efficiency recorded for naphthalene (84%), phenanthrene (77%) and fluorene (69%) achieved a removal of 909 ppb, 539 ppb and 162 ppb respectively.

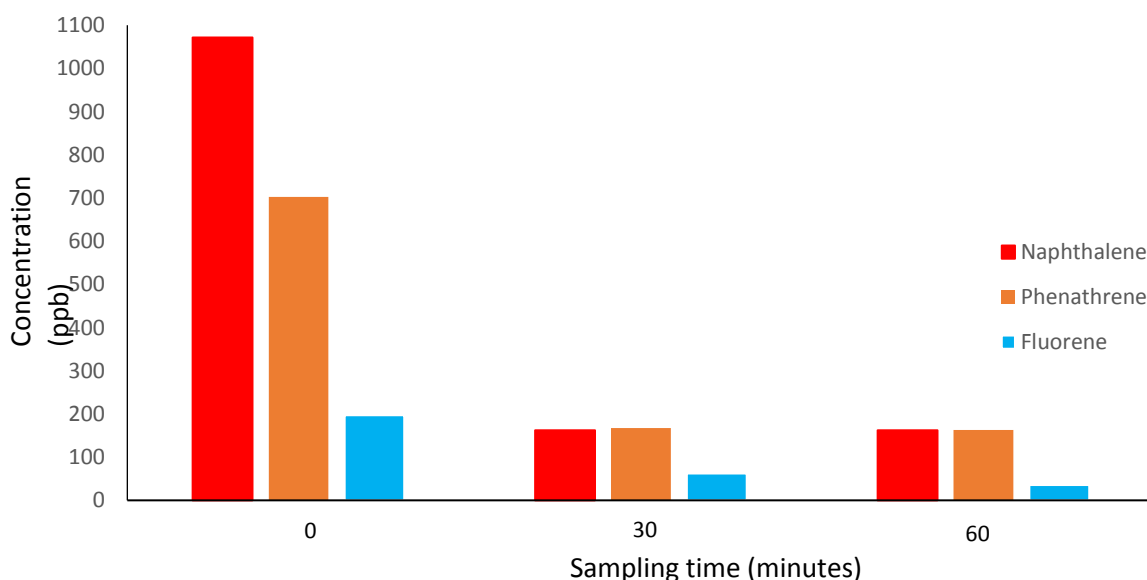


Figure 5.31: Photocatalytic degradation of naphthalene, phenanthrene, fluorene in a mixture; immobilized TiO_2 and UV light (480 W and 100 mm), double reactor chamber

	Degradation efficiency (%)		
	Naphthalene	Phenanthrene	Fluorene
Alone	83	92	88
In mixture	84	77	69

Table 5.8: Naphthalene, phenanthrene and fluorene photodegradation efficiency using FTIPR

5.12. Photocatalysis of PAH in sea water

Photocatalytic removal of pollutants has seen major focus on removal from distilled water but extensive studies have not been carried out on pollutants from seawater. Seawater being one of the major mediums in which water pollution occurs either through human error factor such as oil spill or discharge of effluent from industries requires much attention.

Seawater was therefore synthesized using the most suitable salt, having close elemental composition to that of natural seawater. As seen in table 5.9, instant ocean commercial salt has close elemental composition to that seen in North Pacific Ocean. Instant ocean commercial salt was used to synthesize seawater.

Salts	Elemental composition (mM)	
	Instant ocean	North Pacific
Chloride (Cl ⁻)	521	550
Sodium (Na ⁺)	462	470
Sulfate (SO ₄ ²⁻)	23	28
Magnesium (Mg ²⁺)	52	53
Calcium (Ca ²⁺)	9.4	10.3
Potassium (K ⁺)	9.4	10.2
Strontium (Sr ²⁺)	0.19	0.09

Table 5.9: Ionic elemental composition of instant ocean salt and north pacific

Synthesized seawater preparation

Seawater was synthesized from a salt mixture purchased from Instant Ocean. Instant ocean salt which has similar ionic elemental composition to that found in natural seawater was used. Synthesized seawater was prepared by the dissolution of instant ocean salt mixture (100 g) into 10 L of deionized water. This was then stirred rigorously for 1 hour to allow for the full dissolution of the salt.

5.12.1. FTIPR Photodegradation of Naphthalene in seawater.

The photocatalytic behaviour of PAHs in seawater was investigated with the use of naphthalene as a model PAH. Naphthalene in seawater was used in the Model X₄ FTIPR during the investigation.

Naphthalene (13 mg) was added into the synthesized seawater (10 L) and then vigorously mixed for 72 hours to allow for it to be fully dissolved into the seawater. Naphthalene concentration of 1200 ppb was attained. This preparation method also

took into account the effect solvent has on photocatalysis as highlighted in section 3.2 by preparing naphthalene in the absence of any solvent.

Figure 5.32 illustrates the photocatalytic removal of naphthalene present in seawater. Results showed a photodegradation efficiency of 60% was still achieved, degrading 755 ppb of naphthalene. The reduction of 24% photodegradation efficiency can be attributed to the seawater ions reacting with the OH radical. Seawater ions such as chloride (Cl^-), sodium (Na^+) and sulfate (SO_4^{2-}) reacts with the OH radicals generated which limits the amount of available OH radical to degrade naphthalene. Joseph *et al.*, 2004 in the investigation of chloride ion influence on rate of degradation, showed the reaction that occurs between chloride (Cl^-) and OH radicals as seen in equation 5.1.



Recent photocatalytic reduction studies done of pollutants in seawater has also seen similar photodegradation efficiency. In a published study by Yasser *et al.*, 2016 in the photodegradation of nitrate in seawater using TiO_2 , a 69% photodegradation efficiency was attained. The reduced degradation efficiency was thought to be as a result of the salts reacting with the OH radical therefore impeding any increase in degradation efficiency. Yasser *et al.* in an effort to cancel the salt effect employed the use of formic acid as a hole scavenger to generate more OH radicals to achieve the photodegradation efficiency attained.

The photodegradation efficiency attained for naphthalene is sufficient when compared with the amount required to meet SEPA discharge limit. This shows the robustness of the Model X₄ FTIPR to degrade naphthalene in seawater.

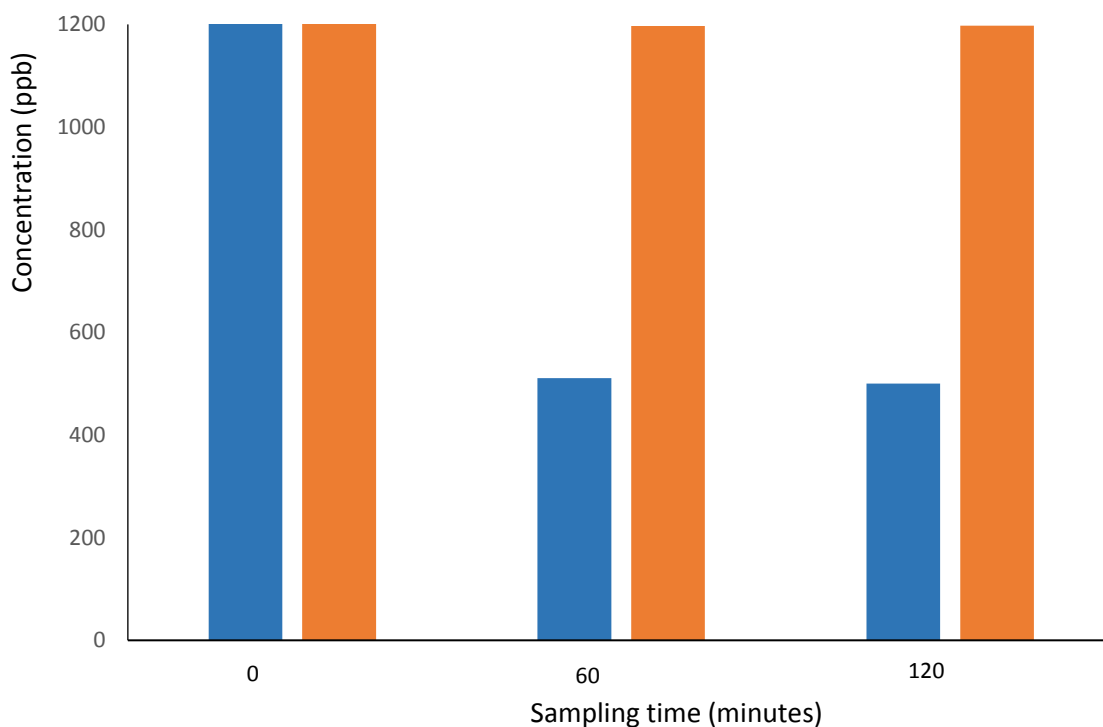


Figure 5.32: Photocatalytic degradation of naphthalene (blue) in seawater using Model X₄ FTIPR and test control (orange)

5.12.2. FTIPR Photodegradation of 7 PAHs in seawater.

Seven PAHs: Naphthalene (600 ppb), Acenaphthylene (600 ppb), 1-methyl naphthalene (500 ppb), 2-methyl naphthalene (400 ppb), Acenaphthene (550 ppb), Fluorene(400 ppb), and Phenanthrene (200 ppb), which are soluble in seawater and within the quantification range were investigated using the Model X₄ FTIPR. The photodegradation of individual PAHs when present with multiple PAHs together in seawater is shown in figure 5.33. Results show all 7 PAHs photodegraded with degradation efficiency highlighted within the range of 77% to 99% with an exception of acenaphthylene with a 20% degradation efficiency (table 5.10). This can be attributed to the tightly packed CH bond and aromatic ring it possesses giving it a very limited free site to allow the OH radicals to attach to and photodegrade it.

Similar results on the difficulty of photodegrading acenaphthylene have been recorded in published literature: Zhao-hui *et al* 2015, in the investigation of the photodegradation of PAHs classified acenaphthylene as an indeterminate photocatalytic degradable PAH thereby not having an established photodegradable ability. This was also confirmed by Francisco *et al.*, 2010 in the investigation of the photodegradation of acenaphthylene with results showing a low photodegradation efficiency of 33%. The low degradation efficiency was only overcome when the UV irradiation was combined with ozonation in conjunction with hydrogen peroxide resulting in a much higher efficiency of 95%.

This therefore shows with the exception of acenaphthylene that the designed Model X₄ FTIPR is robust enough in photodegrading individual PAHs at high photodegradation efficiency with little influence when present with other PAHs and also the added composition of salt present in water. This shows the robustness of the Model X₄ FTIPR in the application in the industry as it overcomes a limitation which may impact the treatment process time.

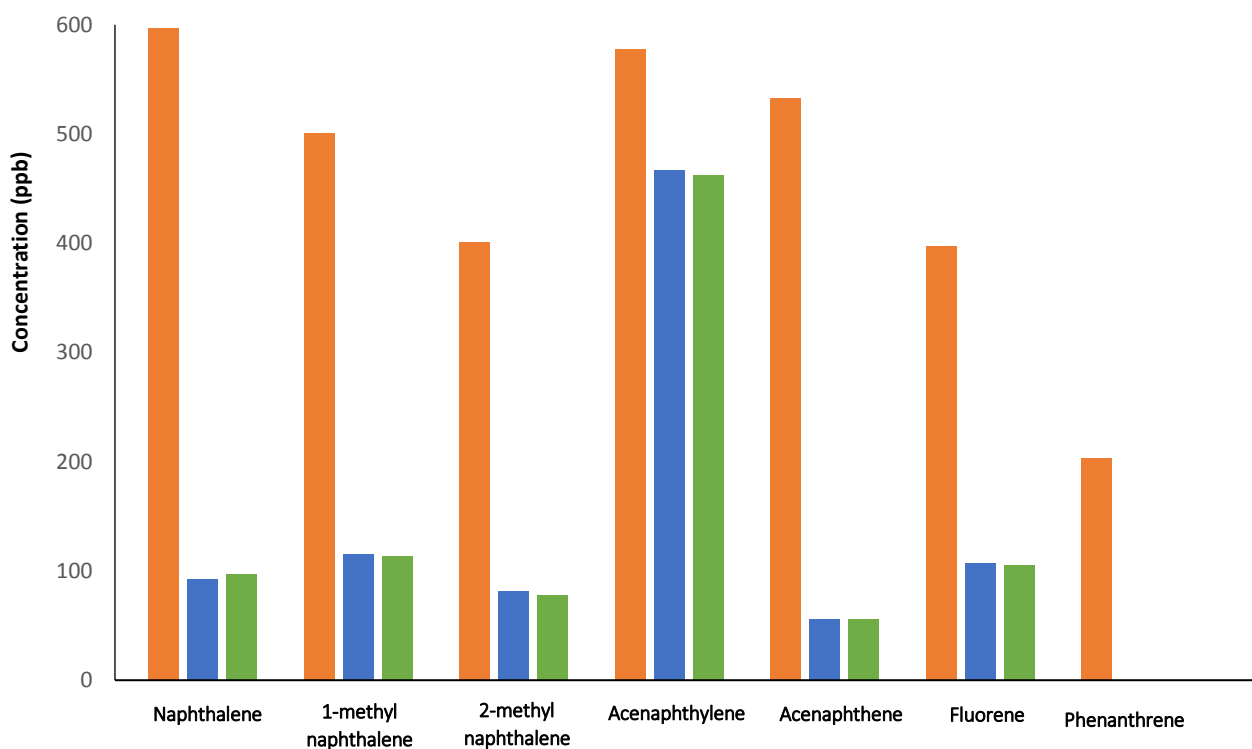


Figure 5.33: Degradation of 7 PAHs in seawater using Model X₄ FTIPR. Initial concentration: orange, 1st sampling (60 minutes): blue, 2nd sampling (120 minutes): green

	Photodegradation efficiency (%)						
	Naphthalene	1-methyl naphthalene	2-methyl naphthalene	Acenaphthylene	Acenaphthene	Fluorene	Phenanthrene
Seawater	84	77	79	20	89	72	99

Table 5.10: 7 PAHs photodegradation efficiency using Model X₄ FTIPR

5.13. Conclusion

The performance of the SIPR and FTIPR in comparison to the suspended TiO_2 photoreactor was discussed in this chapter. The investigation into the SIPR and FTIPR as an alternative to the suspended TiO_2 photoreactor was carried out due to the management issues imposed by suspended TiO_2 . The requirement for secondary treatment of TiO_2 from the treated water imposes more impact on the treatment system. This also can result in the increase of energy consumption for the treatment system required for the TiO_2 removal unit, which in turn requires an additional process. The SIPR and FTIPR system eliminate all these limitations by the proper management of the TiO_2 which is solved by coating it on glass tubes. The SIPR, a prototype for the development of FTIPR, employed the use of the glass tubes closely packed in the photoreactor to eliminate mass transport issues encountered by immobilized photocatalyst reactors. SIPR also employed two coating sol gels which were investigated and optimized in order to maximize the amount of TiO_2 that is coated onto the glass tubes. Three PAHs: naphthalene, phenanthrene and fluorene were investigated using the immobilized TiO_2 photoreactor to determine their rate of degradation when present alone in water and also in a mixture with the three PAHs.

The design and construction of a novel FTIPR shows the ability of UV light to photodegrade PAHs by the optimization of photocatalysis parameters. The preliminary works which were first carried out using suspended TiO_2 showed a significant remediation of the PAHs in water with the highest degradation efficiency of 99% recorded for phenanthrene over a 5 minutes irradiation period. Subsequently due to the limitation of using TiO_2 particles that includes secondary treatment for the removal of TiO_2 , TiO_2 immobilized on glass tubes was employed.

The novel FTIPR investigation using different TiO_2 sol gel achieved significant degradation of the PAH with sol gel B degraded the PAH much faster than sol gel A. The coated glass tubes were characterised using SEM showing the surface topography with the EDAX showing the glass elemental component. SEM and EDAX confirmed the glass tubes were sufficiently coated with TiO_2 . Glass tube coated with sol gel B had more TiO_2 coated onto the surface than that coated with sol gel A. The optimized glass tube coating was applied into the design of the novel FTIPR. The novel FTIPR was designed to minimize PAH loss both on the reactor surface and also on other auxiliary units. The FTIPR design was optimized through a five stage optimization process by the modification of parameters such as UV light intensity, residence time and irradiation distance. The established design and method were then used to degrade PAHs in ultrapure water with a recorded degradation efficiency as high as 92% for phenanthrene. Further to this the photoreactor performance was tested using PAHs present in synthesized seawater. A degradation efficiency of 60% was also achieved for naphthalene in seawater. In a mixture with 7 PAHs in seawater, a high photodegradation efficiency was maintained at a range of 77% to 99% with the exception of acenaphthylene with a 20% photodegradation efficiency.

This therefore shows the practicability in the application of the novel FTIPR in the remediation of PAHs in seawater in the industry.

CHAPTER 6

6.0. CONCLUSION, CONTRIBUTION AND RECOMMENDATION FOR FUTURE WORK

6.1. Conclusion

The scope of this research was to provide a method for the remediation of polycyclic aromatic hydrocarbons (PAHs) in water. The objective of the research was the investigation of two PAHs remediation processes: coagulation-flocculation and photocatalysis towards achieving the scope of this research. The coagulation-flocculation investigation involved the use of chitosan a biopolymer in powder and solubilized form in an optimized batch system. In contrast, photocatalysis investigation involved the use TiO_2 a photocatalyst in the development of a photoreactor. The objectives were driven toward achieving high efficiency within a limited time and less remediation process.

An analytical system for the quantification of the 18 EPA PAHs was developed, justified and validated to determine the robustness of the system. Ensuring correct interpretation and accuracy of results was essential and was validated using the capacity factor, selectivity factor, chromatogram column efficiency and resolution value.

The batch system developed for the coagulation-flocculation method investigated the chitosan loading and contact time for the removal of naphthalene and phenanthrene. Results showed no significant removal of naphthalene using chitosan powder loading of 12.5, 25 and 50 ppm with maximum removal efficiency of 8% at 25 ppm and 30 minutes contact time. Using solubilized chitosan (in 1% w/w acetic acid) at chitosan loading range of 25ppm – 100000ppm a low removal efficiency of 7% and 17% was still achieved for naphthalene and phenanthrene respectively at chitosan loading

100000 ppm and contact time of 30 minutes. The higher removal efficiency of phenanthrene was attributed to the high hydrophobic nature. Further optimization using the powder chitosan by increasing contact time achieved a higher removal efficiency for naphthalene. Contact time range of 30 minutes to 120hrs at chitosan loading of 25 ppm achieved a removal efficiency of 88% at 120 hours contact time. These results confirm the ability of chitosan to adsorb PAHs but within a much longer time frame.

The removal efficiency did not show any improvement when the concentration of chitosan was increased to 50 ppm. The surface area of chitosan limited the sorption ability over a short contact time. When compared with other adsorbents in published literature, a much higher sorption was attained with respect to their higher surface area.

Further steps were carried out in optimizing the coagulation-flocculation method, chitosan was solubilized in acetic acid in order to increase the miscibility with the PAHs in water. The results demonstrated similar findings to that of the powder chitosan with recorded naphthalene removal efficiency of 5% at chitosan concentration of 25 ppm. A much better phenanthrene removal efficiency of 16% was achieved at chitosan concentration of 25 ppm which was attributed to the hydrophobic nature of phenanthrene. An increase in chitosan concentration showed no significant impact on increasing the removal efficiency of both naphthalene and phenanthrene when pre solubilized in acetic acid.

Contact time was investigated to improve the removal efficiency. The contact time was investigated using powder chitosan at chitosan concentration of 12.5 ppm and 25 ppm. A significant improvement on the removal efficiency was attained with an increase in contact time, with 88% naphthalene removal attained at 120 hours

contact time. It was demonstrated that chitosan concentration had no influence on the removal efficiency with an increase in contact time.

The objective of the research which requires the removal of PAHs in a timely manner for proper integration into the industry was not attained at this stage. For industrial application implementation of this remediation method is not practicable as 5 days (120 hours) treatment time will impact on cost through slow process time and higher energy usage.

A remediation alternative was the development of a method for the photocatalysis of PAHs. TiO_2 photocatalyst was investigated in suspended and immobilized form applied in a three reactor design: suspended photocatalytic reactor (SPR), static immobilized photocatalytic reactor (SIPR) and flow through immobilized photocatalytic reactor (FTIPR). Photocatalysis parameters investigated and optimized in the development and construction of the novel FTIPR included: UV irradiation source, irradiation distance, photocatalyst mode of application, photocatalyst loading and residence time. An investigation into factors that could compromise the true removal efficiency was carried out on solvents application and presence of multiple PAHs.

SPR utilized the use of suspended TiO_2 in a photoreactor. The SIPR configuration employed the use of a 480 W UV lamp, TiO_2 loading of 1000 ppm and irradiation time of 20 minutes. The results showed three major observations. Firstly, the ability of TiO_2 to photodegrade PAHs with photodegradation efficiency of 99%, achieved for naphthalene, phenanthrene and flourene. Secondly, when investigating the effect of solvents, it was established that acetone compromised the degradation efficiency reducing the efficiency by 40% and 25% for naphthalene and phenanthrene respectively. This was attributed to the acetone reacting with the generated OH

radicals thereby limiting the available OH radicals for degrading the PAH. Thirdly, I established the influence TiO₂ loading has on the rate of degradation. TiO₂ loading range 200 ppm – 1000 ppm showed an increase in degradation efficiency with an increase in TiO₂ loading. The SPR attained high degradation efficiency but with limitation of post-recovery of the TiO₂ particles which require additional treatment. The requirement for further post-removal of TiO₂ particles creates limitation in industrial application as additional cost, energy and longer treatment time is required. This therefore led to the development and construction of SIPR.

SIPR design is governed around proper management of the TiO₂ particle which is the major limitation to SPR. SIPR was designed and constructed as a prototype for the optimization of FTIPR. SIPR utilized the immobilization of TiO₂ onto glass tubes in a batch system thereby eliminating the TiO₂ post-recovery stage. The SIPR showed a successful photodegradation of PAHs with a photodegradation efficiency of 77%, 91% and 83% attained for naphthalene, phenanthrene and flourene respectively. As a result of the promising results achieved, the TiO₂ immobilized glass tubes were therefore applied and integrated into the FTIPR

FTIPR integrated the SIPR design in a flow through process. The design target was the easy and practicable implementation of SIPR in an industrial treatment application. The ability to easily retrofit the FTIPR into a flow through system overcomes the limitations encountered by the SPR and SIPR. The FTIPR was fully optimized on a 5 stage process (section 5.6) by varied photocatalysis parameters such as UV lamp energy, irradiation distance and residence time. The optimized FTIPR photocatalytic performance showed a significantly high photodegradation efficiency on PAHs. Photodegradation efficiency of 83%, was achieved for naphthalene when photodegraded in ultra-pure water and 60% when photodegraded in seawater.

6.2 Contribution

Significant contributions in the remediation of PAHs in water have been achieved and reported in this thesis. Photocatalysis remediation process through the development of a novel FTIPR has played a major role in the body of contribution.

6.2.1 Experimental approach

The first contribution made in this research was discussed in chapter 4 (section 4.7), shown in the experimental impact of solvents on the degradation rate constant of PAHs. The experimental approach was carried out in the absence of any solvent. The results which gives the true rate constant of the PAH as solvent slows the rate of degradation indicates the novelty in the experimental approach, which is not accounted for in the literature.

6.2.2 Optimizing of TiO₂ immobilized on glass tube

Another contribution captured in chapter 4 involved the development of an efficient photocatalytic glass tube immobilized with an optimized TiO₂ sol gel. The glass tubes showed a high photocatalytic efficiency under UV light in the photodegradation of PAHs. The ability to immobilize a large amount of TiO₂ onto the glass tubes to promote high photodegradation was a significant contribution in the research.

6.2.3 PAH photocatalytic efficiency

In chapter 4 and 5, the investigation in the combined effect of multiple PAHs presence in water on the photodegradation rate on individual PAHs was carried out. Results in this study outline how individual PAHs compete for OH radicals to be photodegraded. This is important for understanding the photocatalytic behaviour of individual PAHs.

6.2.4 FTIPR design

A flow through immobilized photoreactor (FTIPR) which utilized the effective mass transfer of a close packed TiO_2 immobilized glass tubes was a significant contribution highlighted in chapter 5 in the remediation of PAHs. The novel FTIPR was first conceptualized in a prototype SIPR which followed intensive optimization leading to the design and construction of FTIPR. A high photodegradation efficiency attained for remediating PAHs in water and seawater indicates the novelty of the FTIPR. The easy integration of FTIPR into industrial application makes it a valuable remediation method.

6.3 Recommendation for future works

The objectives of this research have all been met with the design and construction of a novel FTIPR for the remediation of PAHs. Looking ahead in the recommendation for future works, the scaling up of the FTIPR in an effort to implement on industrial scale can be developed. Limitations such as post-recovery of TiO_2 which is a major challenge in the field of photocatalysis has been overcome by the FTIPR therefore allowing for the easy integration.

Also as the concept behind photocatalysis is adhered to in the FTIPR, future investigative work can be carried out on the photodegradation of other pollutants in water which can show promising results. The FTIPR is designed to allow for the remediation of dissolved pollutants in water.

REFERENCES

- ADAMS, M., SKILLEN, N., MCCULLAGH, C. AND ROBERTSON, P.K., 2013. Development of a doped titania immobilised thin film multi tubular photoreactor. *Applied Catalysis B: Environmental*, 130, pp.99-105.
- ADHAM, S., HUSSAIN, A., MATAR, J.M., DORES, R. AND JANSON, A., 2013. Application of membrane distillation for desalting brines from thermal desalination plants. *Desalination*, 314, pp.101-108.
- AGARRY, S.E., OGUNLEYE, O.O. AND AWORANTI, O.A., 2013. Biosorption equilibrium, kinetic and thermodynamic modelling of naphthalene removal from aqueous solution onto modified spent tea leaves. *Environmental technology*, 34(7), pp.825-839.
- AHMED, M.H., KEYES, T.E., BYRNE, J.A., BLACKLEDGE, C.W. AND HAMILTON, J.W., 2011. Adsorption and photocatalytic degradation of human serum albumin on TiO₂ and Ag-TiO₂ films. *Journal of Photochemistry and Photobiology A: Chemistry*, 222(1), pp.123-131.
- AMIRI, O., MIR, N., ANSARI, F. AND SALAVATI-NIASARI, M., 2017. Design and fabrication of a high performance inorganic tandem solar cell with 11.5% conversion efficiency. *Electrochimica Acta*, 252, pp.315-321.
- BAGHERI, M., ROSHANDEL, R. AND SHAYEGAN, J., 2018. Optimal selection of an integrated produced water treatment system in the upstream of oil industry. *Process Safety and Environmental Protection*, 117, pp.67-81.
- BARROW, E. AND TARPLEE, I., 2017. Rigging the Odds against Climate Change. In *SPE Offshore Europe Conference & Exhibition*. Society of Petroleum Engineers.
- BELTRÁN, F.J., RIVAS, F.J., GIMENO, O. AND CARBAJO, M., 2005. Photocatalytic enhanced oxidation of fluorene in water with ozone. Comparison with other chemical oxidation methods. *Industrial & engineering chemistry research*, 44(10), pp.3419-3425.
- BHUPANDER, K., VERMA, R. G., GAUR, R., SHARMA, C. S., & AKOLKAR, A. B., (2014). Validation of HPLC method for determination of priority aromatic hydrocarbon (PAHs) in waste water and sediments. *Advanced applied science*, 5(1), 201-209.

BORISCH, J., PILKENTON, S., MILLER, M.L., RAFTERY, D. AND FRANCISCO, J.S., 2004. TiO₂ photocatalytic degradation of dichloromethane: an FTIR and solid-state NMR study. *The Journal of Physical Chemistry B*, 108(18), pp.5640-5646.

CAMUS, L., BROOKS, S., GERAUDIE, P., HJORTH, M., NAHRGANG, J., OLSEN, G.H. AND SMIT, M.G.D., 2015. Comparison of produced water toxicity to Arctic and temperate species. *Ecotoxicology and environmental safety*, 113, pp.248-258.

CARALP, F., FORST, W., HÉNON, E., BERGEAT, A. AND BOHR, F., 2006. Tunneling in the reaction of acetone with OH. *Physical Chemistry Chemical Physics*, 8(9), pp.1072-1078.

CHANG, C.F., CHANG, C.Y., CHEN, K.H., TSAI, W.T., SHIE, J.L. AND CHEN, Y.H., 2004. Adsorption of naphthalene on zeolite from aqueous solution. *Journal of colloid and Interface Science*, 277(1), pp.29-34.

CHO, I.H., PARK, J.H. AND KIM, Y.G., 2005. Oxidative degradation and toxicity reduction of trichloroethylene (TCE) in water using TiO₂/solar light: comparative study of TiO₂ slurry and immobilized systems. *Journal of Environmental Science and Health, Part A*, 40(5), pp.1033-1044.

CHONG, M.N., JIN, B., CHOW, C.W. AND SAINT, C., 2010. Recent developments in photocatalytic water treatment technology: a review. *Water research*, 44(10), pp.2997-3027.

CHONG, M.N., JIN, B., CHOW, C.W. AND SAINT, C., 2010. Recent developments in photocatalytic water treatment technology: a review. *Water research*, 44(10), pp.2997-3027.

CHOQUETTE-LABBÉ, M., SHEWA, W.A., LALMAN, J.A. AND SHANMUGAM, S.R., 2014. Photocatalytic degradation of phenol and phenol derivatives using a nano-TiO₂ catalyst: Integrating quantitative and qualitative factors using response surface methodology. *Water*, 6(6), pp.1785-1806.

CRINI, G. AND BADOT, P.M., 2008. Application of chitosan, a natural aminopolysaccharide, for dye removal from aqueous solutions by adsorption processes using batch studies: a review of recent literature. *Progress in polymer science*, 33(4), pp.399-447.

DANESHVAR, N., RABBANI, M., MODIRSHAHLA, N. AND BEHNAJADY, M.A., 2004. Kinetic modeling of photocatalytic degradation of Acid Red 27 in UV/TiO₂ process. *Journal of Photochemistry and Photobiology A: Chemistry*, 168(1-2), pp.39-45.

DE LAAT, J., LE, G.T. AND LEGUBE, B., 2004. A comparative study of the effects of chloride, sulfate and nitrate ions on the rates of decomposition of H₂O₂ and organic compounds by Fe (II)/H₂O₂ and Fe (III)/H₂O₂. *Chemosphere*, 55(5), pp.715-723.

DIJKSTRA, M.F.J., BUWALDA, H., DE JONG, A.W.F., MICHORIUS, A., WINKELMAN, J.G.M. AND BEENACKERS, A.A.C.M., 2001. Experimental comparison of three reactor designs for photocatalytic water purification. *Chemical Engineering Science*, 56(2), pp.547-555.

DIJKSTRA, M.F.J., MICHORIUS, A., BUWALDA, H., PANNEMAN, H.J., WINKELMAN, J.G.M. AND BEENACKERS, A.A.C.M., 2001. Comparison of the efficiency of immobilized and suspended systems in photocatalytic degradation. *Catalysis Today*, 66(2-4), pp.487-494.

DORES, R., HUSSAIN, A., KATEBAH, M. AND ADHAM, S., 2012. Advanced water treatment technologies for produced water. In *Proceedings of the 3rd Gas Processing Symposium* (pp. 102-109).

EDWARDS, C., GRAHAM, D., FOWLER, N. AND LAWTON, L.A., 2008. Biodegradation of microcystins and nodularin in freshwaters. *Chemosphere*, 73(8), pp.1315-1321.

FAKHRU'L-RAZI, A., PENDASHTEH, A., ABDULLAH, L.C., BIAK, D.R.A., MADAENI, S.S. AND ABIDIN, Z.Z., 2009. Review of technologies for oil and gas produced water treatment. *Journal of hazardous materials*, 170(2-3), pp.530-551.

FOTIOU, T., TRIANTIS, T.M., KALOUDIS, T. AND HISKIA, A., 2015. Evaluation of the photocatalytic activity of TiO₂ based catalysts for the degradation and mineralization of cyanobacterial toxins and water off-odor compounds under UV-A, solar and visible light. *Chemical Engineering Journal*, 261, pp.17-26.

FOTIOU, T., TRIANTIS, T.M., KALOUDIS, T., O'SHEA, K.E., DIONYSIOU, D.D. AND HISKIA, A., 2016. Assessment of the roles of reactive oxygen species in the UV

and visible light photocatalytic degradation of cyanotoxins and water taste and odor compounds using C-TiO₂. *Water research*, 90, pp.52-61.

GAD-ALLAH, T.A., KATO, S., SATOKAWA, S. AND KOJIMA, T., 2007. Role of core diameter and silica content in photocatalytic activity of TiO₂/SiO₂/Fe₃O₄ composite. *Solid State Sciences*, 9(8), pp.737-743.

GAYA, U.I. AND ABDULLAH, A.H., 2008. Heterogeneous photocatalytic degradation of organic contaminants over titanium dioxide: a review of fundamentals, progress and problems. *Journal of Photochemistry and Photobiology C: Photochemistry Reviews*, 9(1), pp.1-12.

GRAHAM, D., KISCH, H., LAWTON, L.A. AND ROBERTSON, P.K., 2010. The degradation of microcystin-LR using doped visible light absorbing photocatalysts. *Chemosphere*, 78(9), pp.1182-1185.

GUIBAL, E. AND ROUSSY, J., 2007. Coagulation and flocculation of dye-containing solutions using a biopolymer (Chitosan). *Reactive and functional polymers*, 67(1), pp.33-42.

GUPTA, H., 2016. Photocatalytic degradation of phenanthrene in the presence of akaganeite nano-rods and the identification of degradation products. *RSC Advances*, 6(114), pp.112721-112727.

HALDIMANN, M., 2006. *Fracture strength of structural glass elements* (No. THESIS_LIB). EPFL.

HU, Y., SONG, X., JIANG, S. AND WEI, C., 2015. Enhanced photocatalytic activity of Pt-doped TiO₂ for NO_x oxidation both under UV and visible light irradiation: A synergistic effect of lattice Pt⁴⁺ and surface PtO. *Chemical Engineering Journal*, 274, pp.102-112.

HUBER, L., 2007. Validation and qualification in analytical laboratories. CRC Press.

HE, X., ARMAH, A., HISKIA, A., KALOUDIS, T., O'SHEA, K. AND DIONYSIOU, D.D., 2015. Destruction of microcystins (cyanotoxins) by UV-254 nm-based direct photolysis and advanced oxidation processes (AOPs): Influence of variable amino acids on the degradation kinetics and reaction mechanisms. *water research*, 74, pp.227-238.

ILYAS, H., QAZI, I.A., ASGAR, W. AND AWAN, M.A., 2011. Photocatalytic degradation of nitro and chlorophenols using doped and undoped titanium dioxide nanoparticles. *Journal of Nanomaterials*, 2011, p.21.

ISLAM, M.M., MASUM, S.M., RAHMAN, M.M., MOLLA, M.A.I., SHAIKH, A.A. AND ROY, S.K., 2011. Preparation of chitosan from shrimp shell and investigation of its properties. *Int. J. Basic Appl. Sci*, 11(1), p.116.

ISLAM, S., BIDIN, N., RIAZ, S. AND NASEEM, S., 2016. Sol-gel based phenolphthalein encapsulated heterogeneous silica-titania optochemical pH nanosensor. *Journal of industrial and engineering chemistry*, 34, pp.258-268.

JOZEF, S., & NADIA A. A., 2010. Production, properties, and some new application of Chitin and Its derivatives. *Food Science and Nutrition*, 43(2), 145-171.

KHATAMIAN, M., HASHEMIAN, S., YAVARI, A. AND SAKET, M., 2012. Preparation of metal ion (Fe^{3+} and Ni^{2+}) doped TiO_2 nanoparticles supported on ZSM-5 zeolite and investigation of its photocatalytic activity. *Materials Science and Engineering: B*, 177(18), pp.1623-1627.

KING, A.J., READMAN, J.W. AND ZHOU, J.L., 2003. The application of solid-phase micro-extraction (SPME) to the analysis of polycyclic aromatic hydrocarbons (PAHs). *Environmental geochemistry and health*, 25(1), pp.69-75.

KIMURA, I., KASE, T., TAGUCHI, Y. AND TANAKA, M., 2003. Preparation of titania/silica composite microspheres by sol-gel process in reverse suspension. *Materials research bulletin*, 38(4), pp.585-597.

LADNER, D.A., SUBRAMANI, A., KUMAR, M., ADHAM, S.S. AND CLARK, M.M., 2010. Bench-scale evaluation of seawater desalination by reverse osmosis. *Desalination*, 250(2), pp.490-499.

LAOUFI, N.A., TASSALIT, D. AND BENTAHAR, F., 2008. The degradation of phenol in water solution by TiO_2 photocatalysis in a helical reactor. *Global NEST Journal*, 10(3), pp.404-418.

LAW, R.J., DAWES, V.J., WOODHEAD, R.J. AND MATTHIESSEN, P., 1997. Polycyclic aromatic hydrocarbons (PAH) in seawater around England and Wales. *Marine pollution bulletin*, 34(5), pp.306-322.

- LAWTON, L.A., ROBERTSON, P.K., ROBERTSON, R.F. AND BRUCE, F.G., 2003. The destruction of 2-methylisoborneol and geosmin using titanium dioxide photocatalysis. *Applied Catalysis B: Environmental*, 44(1), pp.9-13.
- LEE, C.S., ROBINSON, J. AND CHONG, M.F., 2014. A review on application of flocculants in wastewater treatment. *Process Safety and Environmental Protection*, 92(6), pp.489-508.
- LEELAVATHI, A., MUKHERJEE, B., NETHRAVATHI, C., KUNDU, S., DHIVYA, M., RAVISHANKAR, N. AND MADRAS, G., 2013. Highly photoactive heterostructures of PbO quantum dots on TiO₂. *RSC Advances*, 3(43), pp.20970-20977.
- LI, Y., ZHOU, X., CHEN, W., LI, L., ZEN, M., QIN, S. AND SUN, S., 2012. Photodecolorization of Rhodamine B on tungsten-doped TiO₂/activated carbon under visible-light irradiation. *Journal of hazardous materials*, 227, pp.25-33.
- LIU, B., CHEN, B., ZHANG, B.Y., JING, L., ZHANG, H. AND LEE, K., 2016. Photocatalytic degradation of polycyclic aromatic hydrocarbons in offshore produced water: effects of water matrix. *Journal of Environmental Engineering*, 142(11), p.04016054.
- LUO, Z.H., WEI, C.L., HE, N.N., SUN, Z.G., LI, H.X. AND CHEN, D., 2015. Correlation between the photocatalytic degradability of PAHs over Pt/TiO₂-SiO₂ in water and their quantitative molecular structure. *Journal of Nanomaterials*, 2015, p.6.
- MA, C.W. AND CHU, W., 2001. Photodegradation mechanism and rate improvement of chlorinated aromatic dye in non-ionic surfactant solutions. *Water research*, 35(10), pp.2453-2459.
- MA, Z., YIN, X., JI, X., YUE, J.Q., ZHANG, L., QIN, J.J., VALIYAVEETIL, S. AND ADIN, A., 2016. Evaluation and removal of emerging nanoparticle contaminants in water treatment: a review. *Desalination and Water Treatment*, 57(24), pp.11221-11232.
- MAHADIK, M.A., AN, G.W., DAVID, S., CHOI, S.H., CHO, M. AND JANG, J.S., 2017. Fabrication of A/R-TiO₂ composite for enhanced photoelectrochemical performance: solar hydrogen generation and dye degradation. *Applied Surface Science*, 426, pp.833-843.

- MAHMOODI, V. AND SARGOLZAEI, J., 2014. Optimization of photocatalytic degradation of naphthalene using nano-TiO₂/UV system: statistical analysis by a response surface methodology. *Desalination and Water Treatment*, 52(34-36), pp.6664-6672.
- MALATO, S., FERNÁNDEZ-IBÁÑEZ, P., MALDONADO, M.I., BLANCO, J. and Gernjak, W., 2009. Decontamination and disinfection of water by solar photocatalysis: recent overview and trends. *Catalysis Today*, 147(1), pp.1-59.
- MARTINEZ, E., GROS, M., LACORTE, S. AND BARCELÓ, D., 2004. Simplified procedures for the analysis of polycyclic aromatic hydrocarbons in water, sediments and mussels. *Journal of Chromatography A*, 1047(2), pp.181-188.
- MASCOLO, G., COMPARELLI, R., CURRI, M.L., LOVECCHIO, G., LOPEZ, A. AND AGOSTIANO, A., 2007. Photocatalytic degradation of methyl red by TiO₂: Comparison of the efficiency of immobilized nanoparticles versus conventional suspended catalyst. *Journal of Hazardous Materials*, 142(1-2), pp.130-137.
- MASCOLO, G., COMPARELLI, R., CURRI, M.L., LOVECCHIO, G., LOPEZ, A. AND AGOSTIANO, A., 2007. Photocatalytic degradation of methyl red by TiO₂: Comparison of the efficiency of immobilized nanoparticles versus conventional suspended catalyst. *Journal of Hazardous Materials*, 142(1-2), pp.130-137.
- MINERO, C. AND VIONE, D., 2006. A quantitative evaluation of the photocatalytic performance of TiO₂ slurries. *Applied Catalysis B: Environmental*, 67(3-4), pp.257-269.
- MORALES-TORRES, S., PASTRANA-MARTÍNEZ, L.M., FIGUEIREDO, J.L., FARIA, J.L. AND SILVA, A.M., 2012. Design of graphene-based TiO₂ photocatalysts—a review. *Environmental Science and Pollution Research*, 19(9), pp.3676-3687.
- MOUSSAOUI, R., ELGHNIJI, K., BEN MOSBAH, M., ELALOUI, E. AND MOUSSAOUI, Y., 2017. Sol-gel synthesis of highly TiO₂ aerogel photocatalyst via high temperature supercritical drying. *Journal of Saudi Chemical Society*, 21(6), pp.751-760.
- MOZIA, S., BROŽEK, P., PRZEPIÓRSKI, J., TRYBA, B. AND MORAWSKI, A.W., 2012. Immobilized TiO₂ for phenol degradation in a pilot-scale photocatalytic reactor. *Journal of Nanomaterials*, 2012, p.16.

MOZIA, S., BROŽEK, P., PRZEPIÓRSKI, J., TRYBA, B. AND MORAWSKI, A.W., 2012. Immobilized TiO₂ for phenol degradation in a pilot-scale photocatalytic reactor. *Journal of Nanomaterials*, 2012, p.16.

NEFF J, LEEK, DE BLOIS EM (2011) Produced water: overview of composition, fate, and effects. In: Lee k, Neff J editors. Produced water. Environmental risks and advances in mitigation technologies. Springer, London, UK. pp 3-54

PAMPANIN, D.M. AND SYDNES, M.O., 2013. Polycyclic aromatic hydrocarbons a constituent of petroleum: presence and influence in the aquatic environment. In *Hydrocarbon*. InTech.

PENA, M.T., CASAIS, M.C., MEJUTO, M.C. AND CELA, R., 2009. Development of an ionic liquid based dispersive liquid-liquid microextraction method for the analysis of polycyclic aromatic hydrocarbons in water samples. *Journal of Chromatography A*, 1216(36), pp.6356-6364.

PAMPANIN, D.M. AND SYDNES, M.O., 2013. Polycyclic aromatic hydrocarbons a constituent of petroleum: presence and influence in the aquatic environment. In *Hydrocarbon*. InTech.

PAUL, K., ROBIN, V., & JAMES, F., (2005). Management of produced water on offshore oil installations: a comparative assessment using flow analysis.

PESTANA, C.J., 2012. Monitoring and regulating cyanobacterial metabolites (microcystins and geosmin) in aquatic systems.

QUICI, N., VERA, M.L., CHOI, H., PUMA, G.L., DIONYSIOU, D.D., LITTER, M.I. AND DESTAILLATS, H., 2010. Effect of key parameters on the photocatalytic oxidation of toluene at low concentrations in air under 254+ 185 nm UV irradiation. *Applied Catalysis B: Environmental*, 95(3-4), pp.312-319.

RAHIM, S., RADIMAN, S. AND HAMZAH, A., 2012. Inactivation of Escherichia coli under fluorescent lamp using TiO₂ nanoparticles synthesized via sol gel method. *Sains Malaysiana*, 41(2), pp.219-224.

REGUERO, V., LÓPEZ-FERNÁNDEZ, R., FERMOSO, J., PRIETO, O., POCOSTALES, P., GONZÁLEZ, R., IRUSTA, R. AND VILLAVARDE, S., 2013. Comparison of conventional technologies and a Submerged Membrane Photocatalytic Reactor

(SMPR) for removing trihalomethanes (THM) precursors in drinking water treatment plants. *Desalination*, 330, pp.28-34.

RENAULT, F., SANCEY, B., BADOT, P.M. AND CRINI, G., 2009. Chitosan for coagulation/flocculation processes—an eco-friendly approach. *European Polymer Journal*, 45(5), pp.1337-1348.

RIVAS, F.J., BELTRÁN, F.J. AND ACEDO, B., 2000. Chemical and photochemical degradation of acenaphthylene. Intermediate identification. *Journal of hazardous materials*, 75(1), pp.89-98.

ROBERTSON, J.M., ROBERTSON, P.K. AND LAWTON, L.A., 2005. A comparison of the effectiveness of TiO₂ photocatalysis and UVA photolysis for the destruction of three pathogenic micro-organisms. *Journal of Photochemistry and Photobiology A: Chemistry*, 175(1), pp.51-56.

SANDRA, N., DRAGUTIN, P., SKEVIN, D., KLARA, K., & PETER, Z., (2013). Online DACC-HPLC analysis of polycyclic aromatic hydrocarbon in edible oils. *Journal of food technology*, Biotechnology 8(3-4), 74-81.

SCURTU, C.T., 2009. Treatment of produced water: targeting dissolved compounds to meet a zero harmful discharge in oil and gas production.

SHARIF ZEIN, S.H. AND BOCCACCINI, A.R., 2008. Synthesis and characterization of TiO₂ coated multiwalled carbon nanotubes using a sol gel method. *Industrial & Engineering Chemistry Research*, 47(17), pp.6598-6606.

SIAGIAN, U.W., WIDODO, S., WARDANI, A.K. AND WENTEN, I.G., 2018. Oilfield Produced Water Reuse and Reinjection with Membrane. In *MATEC Web of Conferences* (Vol. 156, p. 08005). EDP Sciences.

TALUKDAR, R.K., GIERCZAK, T., MCCABE, D.C. AND RAVISHANKARA, A.R., 2003. Reaction of hydroxyl radical with acetone. 2. Products and reaction mechanism. *The Journal of Physical Chemistry A*, 107(25), pp.5021-5032.

TANG, Y., ZHANG, G., LIU, C., LUO, S., XU, X., CHEN, L. AND WANG, B., 2013. Magnetic TiO₂-graphene composite as a high-performance and recyclable platform for efficient photocatalytic removal of herbicides from water. *Journal of hazardous materials*, 252, pp.115-122.

TRANDAFILOVIĆ, L.V., JOVANOVIĆ, D.J., ZHANG, X., PTASIŃSKA, S. AND DRAMIĆANIN, M.D., 2017. Enhanced photocatalytic degradation of methylene blue and methyl orange by ZnO: Eu nanoparticles. *Applied Catalysis B: Environmental*, 203, pp.740-752.

TURPIN, E., FITTSCHEN, C., TOMAS, A. AND DEVOLDER, P., 2003. Reaction of OH radicals with acetone: Determination of the branching ratio for the abstraction pathway at 298 K and 1 Torr. *Journal of atmospheric chemistry*, 46(1), pp.1-13.

USEPA 440/5-86-001, United States. Environmental Protection Agency. Office of Water Regulations and Standards eds., 1986. Quality criteria for water, 1986 (Vol. 86, No. 1). US Environmental Protection Agency, Office of Water Regulations and Standards.

VAN GRIEKEN, R., MARUGÁN, J., SORDO, C. AND PABLOS, C., 2009. Comparison of the photocatalytic disinfection of E. coli suspensions in slurry, wall and fixed-bed reactors. *Catalysis Today*, 144(1-2), pp.48-54.

VELLA, G., IMOBERDORF, G.E., SCLAFANI, A., CASSANO, A.E., ALFANO, O.M. AND RIZZUTI, L., 2010. Modeling of a TiO₂-coated quartz wool packed bed photocatalytic reactor. *Applied Catalysis B: Environmental*, 96(3-4), pp.399-407.

WANG, J., ZHAO, J., LEI, X. AND WANG, H., 2018. New approach for point pollution source identification in rivers based on the backward probability method. *Environmental Pollution*, 241, pp.759-774.

WANG, K., ZHANG, J., LOU, L., YANG, S. AND CHEN, Y., 2004. UV or visible light induced photodegradation of AO7 on TiO₂ particles: the influence of inorganic anions. *Journal of Photochemistry and Photobiology A: Chemistry*, 165(1-3), pp.201-207.

WANG, M.Q., YAN, J., CUI, H.P. AND DU, S.G., 2013. Low temperature preparation and characterization of TiO₂ nanoparticles coated glass beads by heterogeneous nucleation method. *Materials Characterization*, 76, pp.39-47.

WANG, X., SHI, F., HUANG, W. AND FAN, C., 2012. Synthesis of high quality TiO₂ membranes on alumina supports and their photocatalytic activity. *Thin Solid Films*, 520(7), pp.2488-2492.

WANG, Y., YANG, J., LIANG, J., QIANG, Y., FANG, S., GAO, M., FAN, X., YANG, G., ZHANG, B. AND FENG, Y., 2018. Analysis of the environmental behavior of farmers for non-point source pollution control and management in a water source protection area in China. *Science of The Total Environment*, 633, pp.1126-1135.

WEISMAN, W. ED., 1998. *Analysis of petroleum hydrocarbons in environmental media* (Vol. 1). Amherst Scientific Publishers.

World Health Organization (WHO and UNICEF, 2000. *Global water supply and sanitation assessment 2000 report*. World Health Organization (WHO).

YANG, G.C. AND LI, C.J., 2007. Electrofiltration of silica nanoparticle-containing wastewater using tubular ceramic membranes. *Separation and Purification Technology*, 58(1), pp.159-165.

YANG, H., SHAO, D., LIU, B., HUANG, J. AND YE, X., 2016. Multi-point source identification of sudden water pollution accidents in surface waters based on differential evolution and Metropolis-Hastings-Markov Chain Monte Carlo. *Stochastic environmental research and risk assessment*, 30(2), pp.507-522.

YU, J.G., YU, H.G., CHENG, B., ZHAO, X.J., YU, J.C. AND HO, W.K., 2003. The effect of calcination temperature on the surface microstructure and photocatalytic activity of TiO₂ thin films prepared by liquid phase deposition. *The Journal of Physical Chemistry B*, 107(50), pp.13871-13879.

ZHANG, F., CHENG, Z., KANG, L., CUI, L., LIU, W., XU, X., HOU, G. AND YANG, H., 2015. A novel preparation of Ag-doped TiO₂ nanofibers with enhanced stability of photocatalytic activity. *RSC Advances*, 5(41), pp.32088-32091.

ZHANG, Y., CRITTENDEN, J.C., HAND, D.W. AND PERRAM, D.L., 1994. Fixed-bed photocatalysts for solar decontamination of water. *Environmental science & technology*, 28(3), pp.435-442.

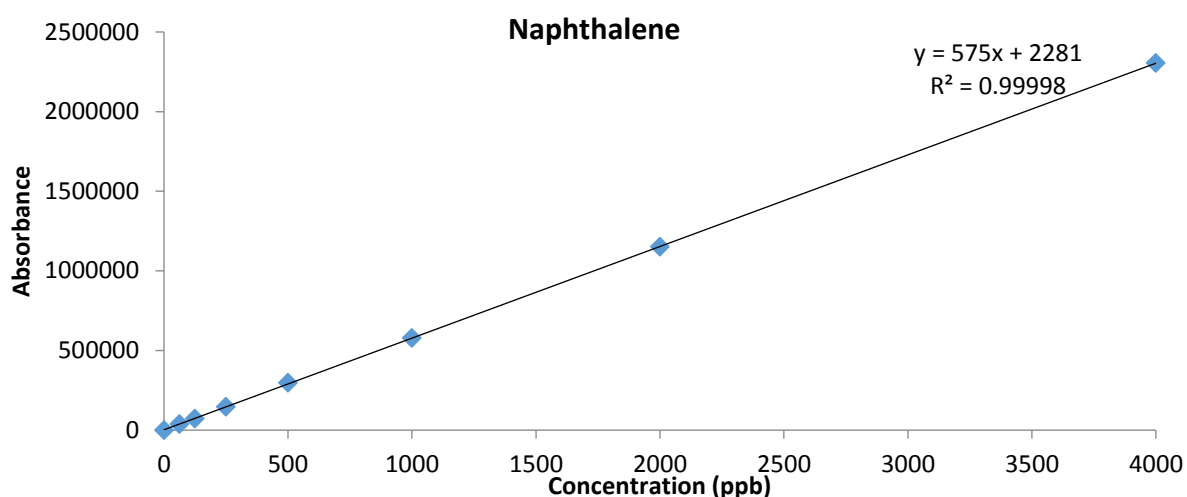
ZHANG, Y., WONG, J.W.C., LIU, P. AND YUAN, M., 2011. Heterogeneous photocatalytic degradation of phenanthrene in surfactant solution containing TiO₂ particles. *Journal of hazardous materials*, 191(1-3), pp.136-143.

ZHANG, Y., ZHANG, N., TANG, Z.R. AND XU, Y.J., 2012. Improving the photocatalytic performance of graphene-TiO₂ nanocomposites via a combined

strategy of decreasing defects of graphene and increasing interfacial contact. *Physical Chemistry Chemical Physics*, 14(25), pp.9167-9175.

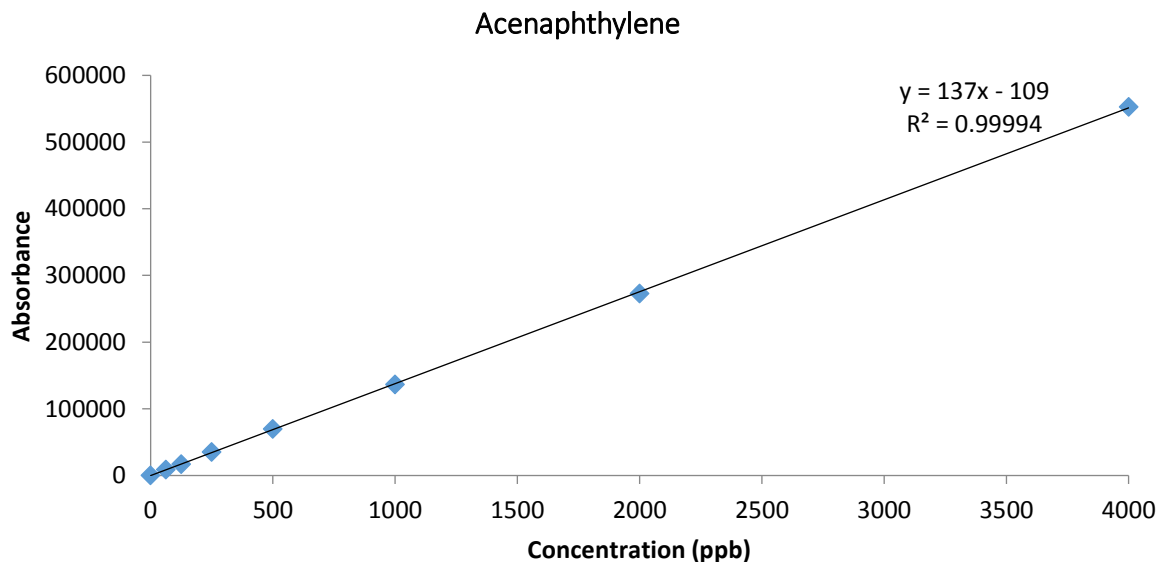
ZHAO, Y., CAO, D., LIU, L. AND JIN, W., 2006. Municipal wastewater treatment by moving-bed-biofilm reactor with diatomaceous earth as carriers. *Water environment research*, 78(4), pp.392-396.

APPENDIX A



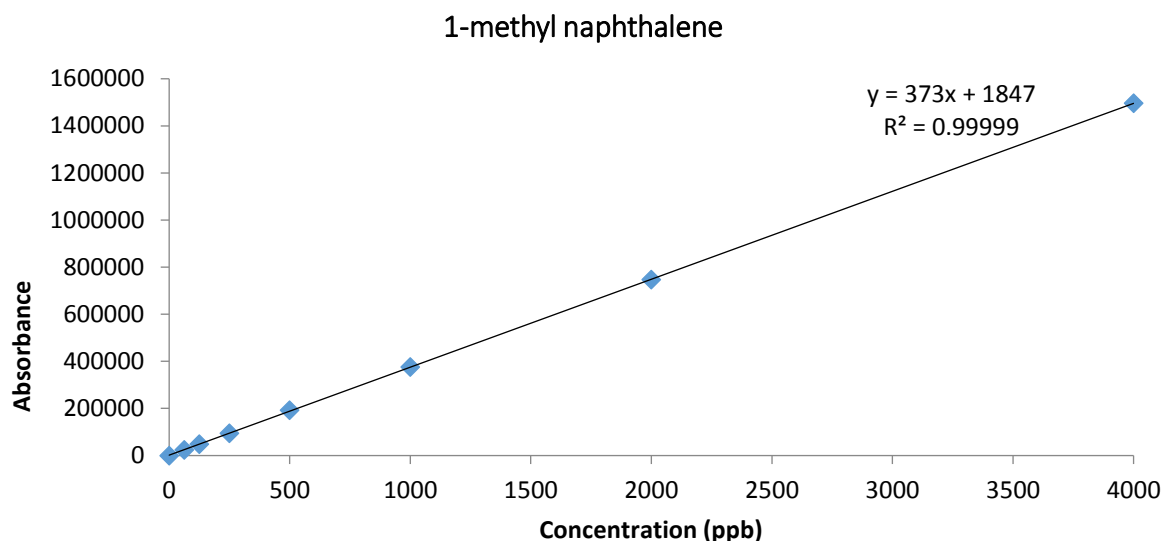
Naphthalene	Concentration (ppb)	62.5	125	250	500	1000	2000	4000
	Absorbance	37189	72094	145896	297328	578227	1150295	2304024

A.1: Calibration curve for naphthalene. HPLC-UV system Mobile phase; acetonitrile:water. Flow rate; 1.5mL/min, UV detection at 220nm. n=3



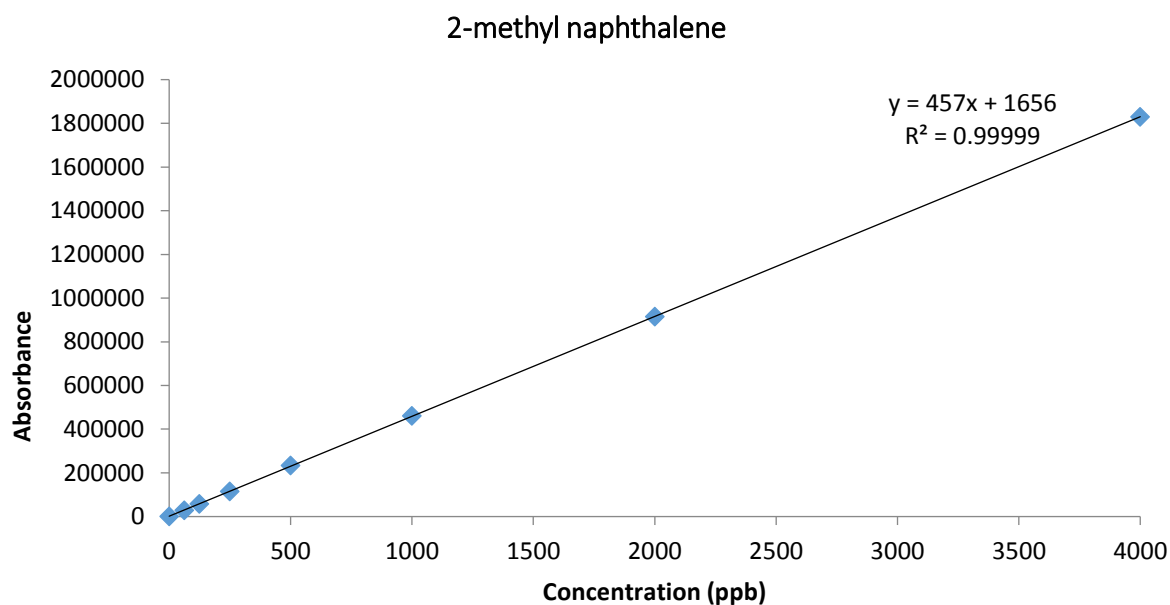
Acenaphthylene	Concentration (ppb)	62.5	125	250	500	1000	2000	4000
	Absorbance	8882	16978	35345	69914	136624	272762	552740

A.2: Calibration curve for Acenaphthylene. HPLC-UV system Mobile phase; acetonitrile:water. Flow rate; 1.5mL/min, UV detection at 220nm. n=3



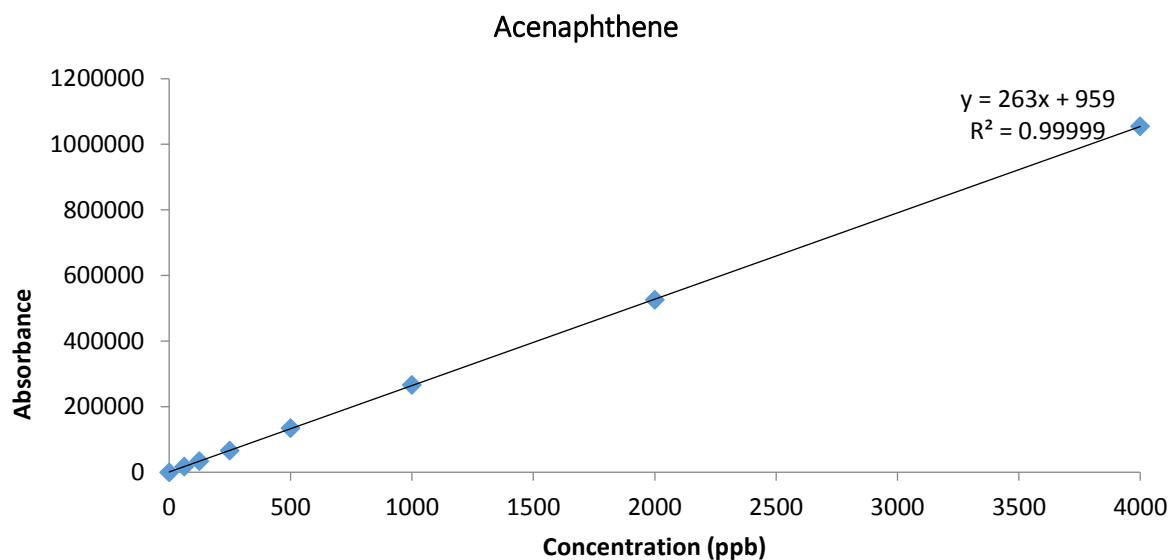
1-methyl naphthalene	Concentration (ppb)	62.5	125	250	500	1000	2000	4000
	Absorbance	24484	47853	94936	192664	376171	747095	1495704

A.3: Calibration curve for 1-methyl naphthalene. HPLC-UV system Mobile phase; acetonitrile:water. Flow rate; 1.5mL/min, UV detection at 220nm. n=3



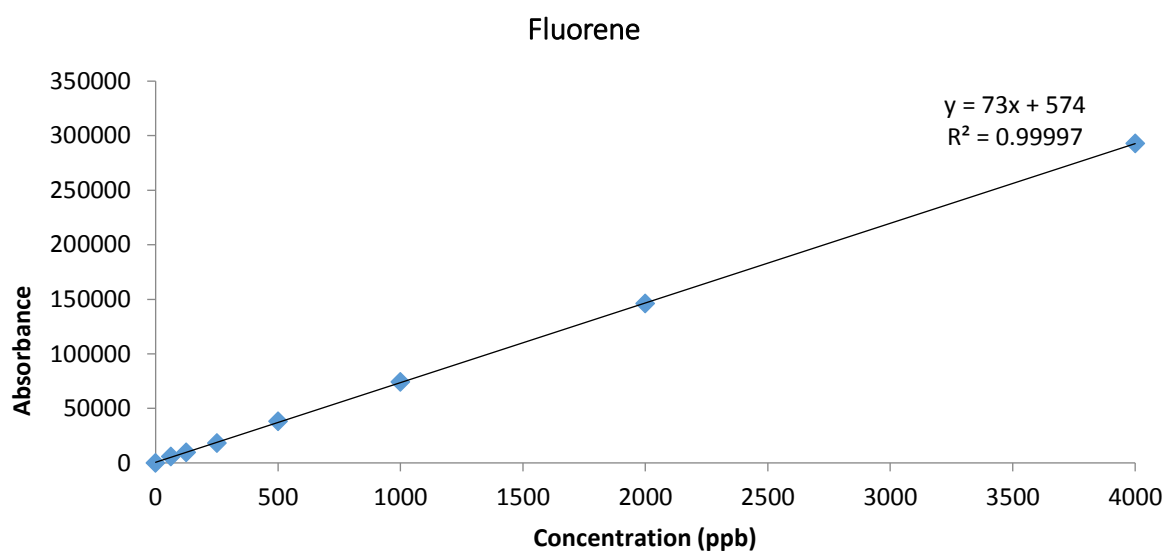
2-methyl naphthalene	Concentration (ppb)	62.5	125	250	500	1000	2000	4000
	Absorbance	28703	58073	115694	233920	460759	914528	1829842

A.4: Calibration curve for 2-methyl naphthalene. HPLC-UV system Mobile phase; acetonitrile:water. Flow rate; 1.5mL/min, UV detection at 220nm. n=3



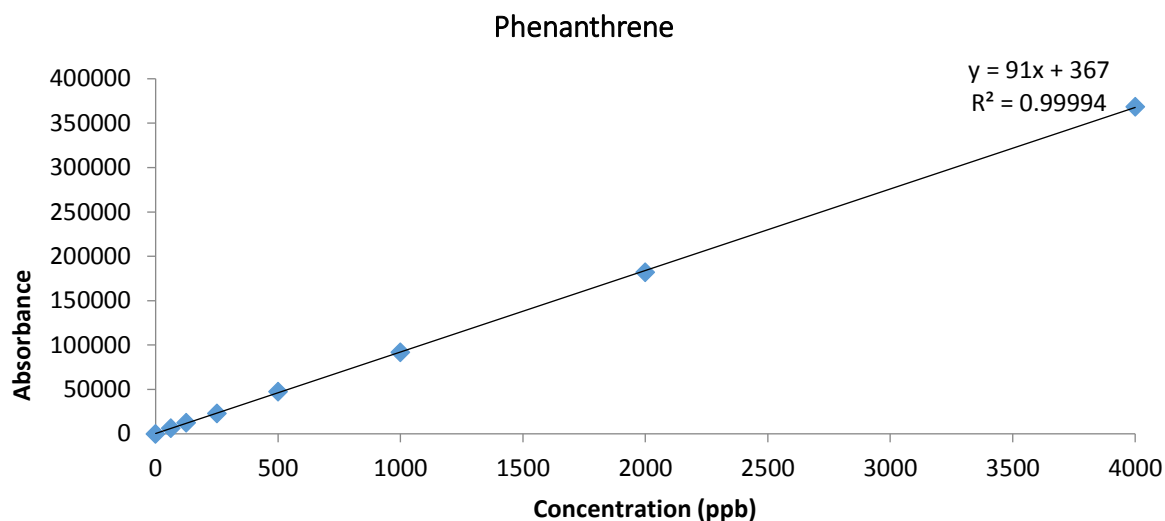
Acenaphthene	Concentration (ppb)	62.5	125	250	500	1000	2000	4000
	Absorbance	17102	33910	66220	134001	266374	525870	1054749

A.5: Calibration curve for Acenaphthene. HPLC-UV system Mobile phase; acetonitrile:water. Flow rate; 1.5mL/min, UV detection at 220nm. n=3



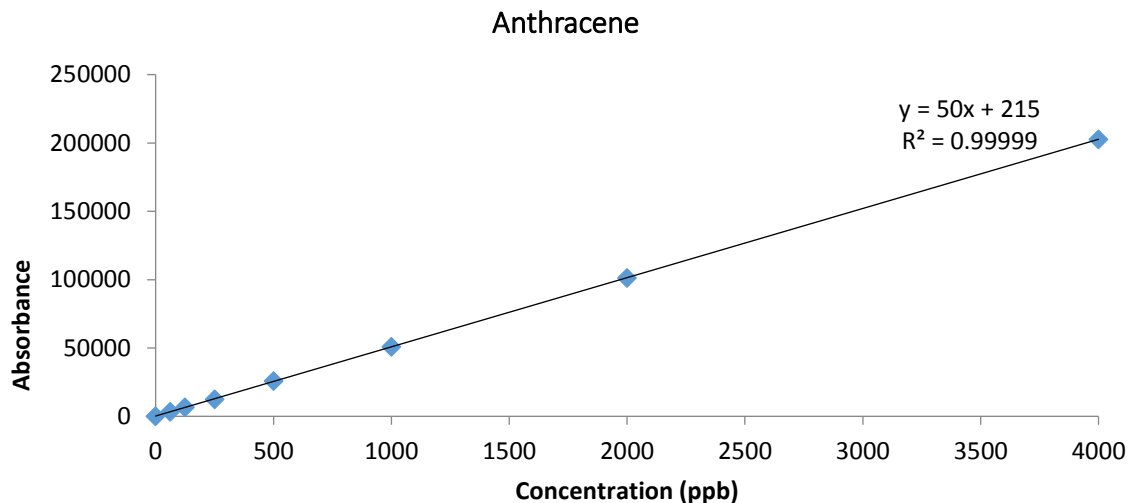
Fluorene	Concentration (ppb)	62.5	125	250	500	1000	2000	4000
	Absorbance	5628	9544	18181	37897	74237	146033	292819

A.6: Calibration curve for Fluorene. HPLC-UV system Mobile phase; acetonitrile:water. Flow rate; 1.5mL/min, UV detection at 220nm. n=3



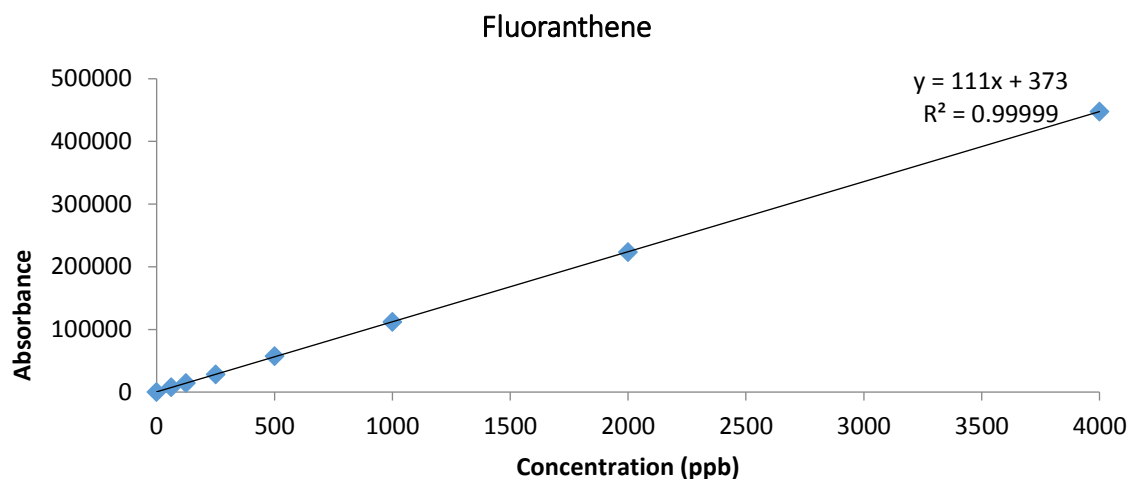
Phenanthrene	Concentration (ppb)	62.5	125	250	500	1000	2000	4000
	Absorbance	6474	12338	23025	47421	91883	182130	368571

A.7: Calibration curve for phenanthrene. HPLC-UV system Mobile phase; acetonitrile:water. Flow rate; 1.5mL/min, UV detection at 220nm. n=3



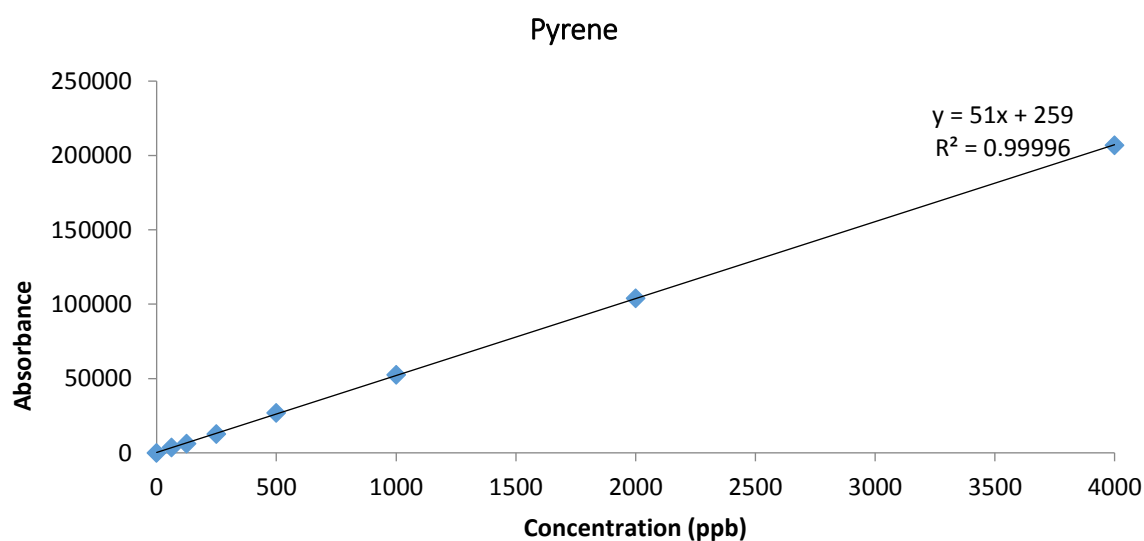
Anthracene	Concentration (ppb)	62.5	125	250	500	1000	2000	4000
	Absorbance	3284	6636	12572	25956	50998	101405	202590

A.8: Calibration curve for anthracene. HPLC-UV system Mobile phase; acetonitrile:water. Flow rate; 1.5mL/min, UV detection at 220nm. n=3



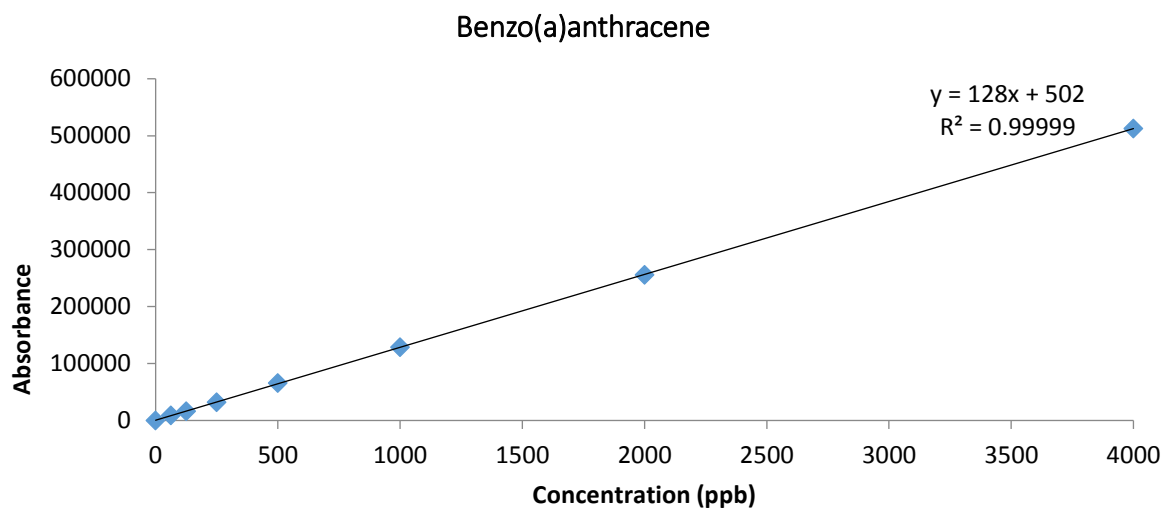
Fluoranthene	Concentration (ppb)	62.5	125	250	500	1000	2000	4000
	Absorbance	7606	14378	28054	57114	112222	223243	447932

A.9: Calibration curve for fluoranthene. HPLC-UV system Mobile phase; acetonitrile:water. Flow rate; 1.5mL/min, UV detection at 220nm. n=3



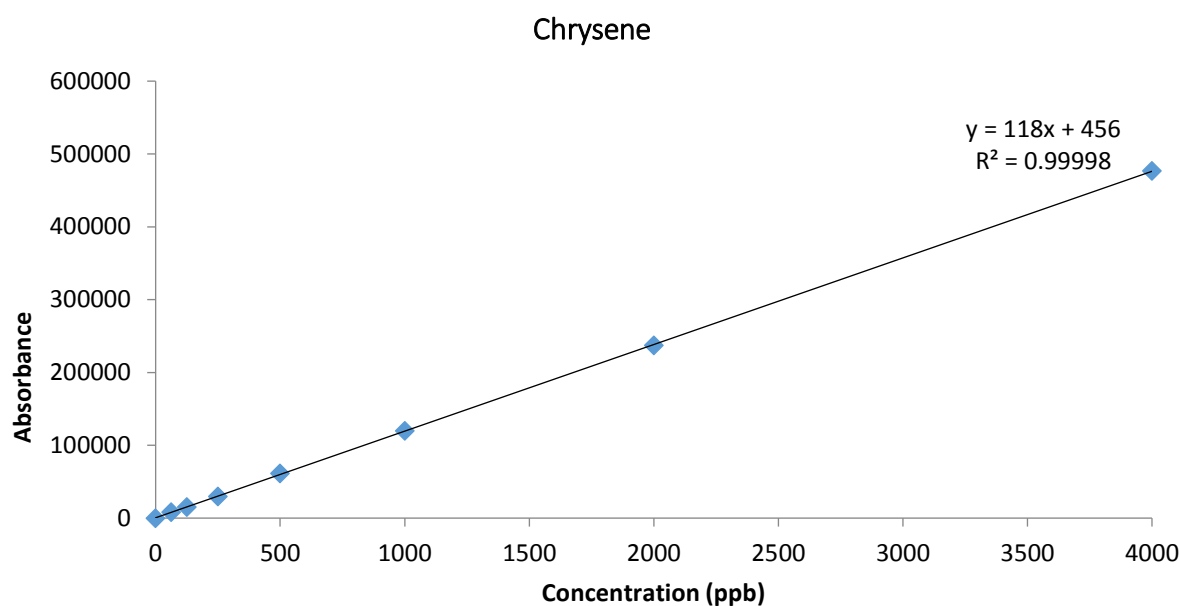
Pyrene	Concentration (ppb)	62.5	125	250	500	1000	2000	4000
	Absorbance	3547	6285	12610	26825	52579	104022	206898

A.10: Calibration curve for pyrene. HPLC-UV system Mobile phase; acetonitrile:water. Flow rate; 1.5mL/min, UV detection at 220nm. n=3



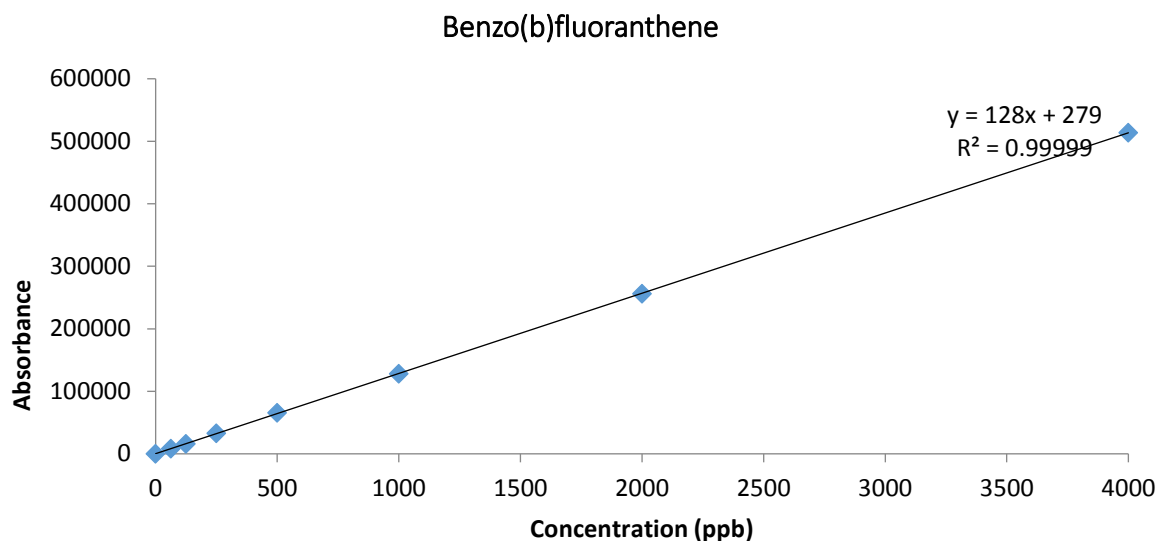
Benzo(a)anthracene	Concentration (ppb)	62.5	125	250	500	1000	2000	4000
	Absorbance	8748	16330	32035	65722	128837	255601	512748

A.11: Calibration curve for Benzo(a)anthracene. HPLC-UV system Mobile phase; acetonitrile:water. Flow rate; 1.5mL/min, UV detection at 220nm. n=3



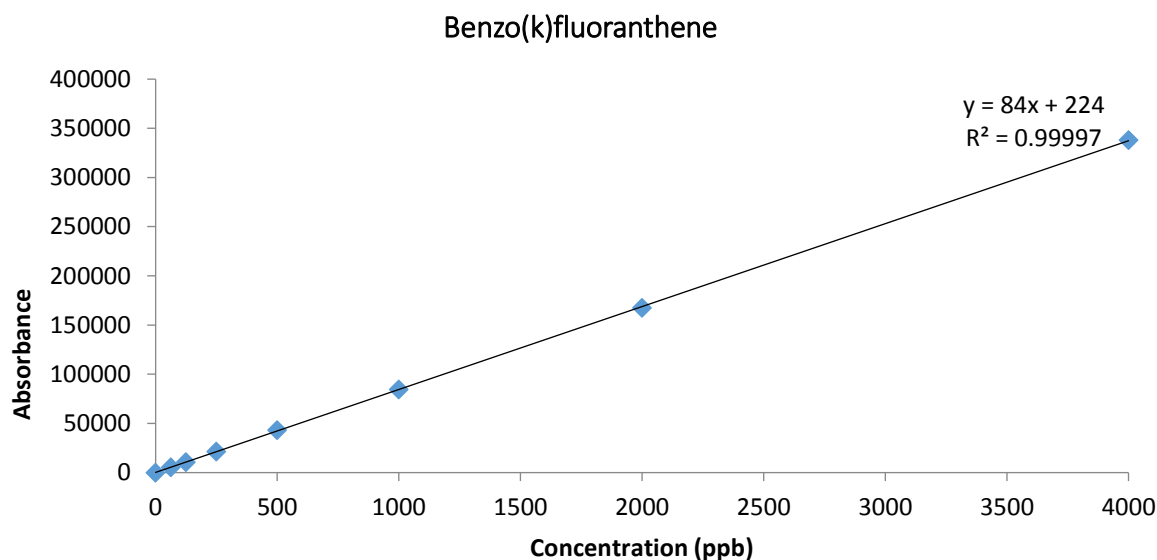
Chrysene	Concentration (ppb)	62.5	125	250	500	1000	2000	4000
	Absorbance	8111	15163	29798	61206	119712	237136	476585

A.12: Calibration curve for Chrysene. HPLC-UV system Mobile phase; acetonitrile:water. Flow rate; 1.5mL/min, UV detection at 220nm. n=3



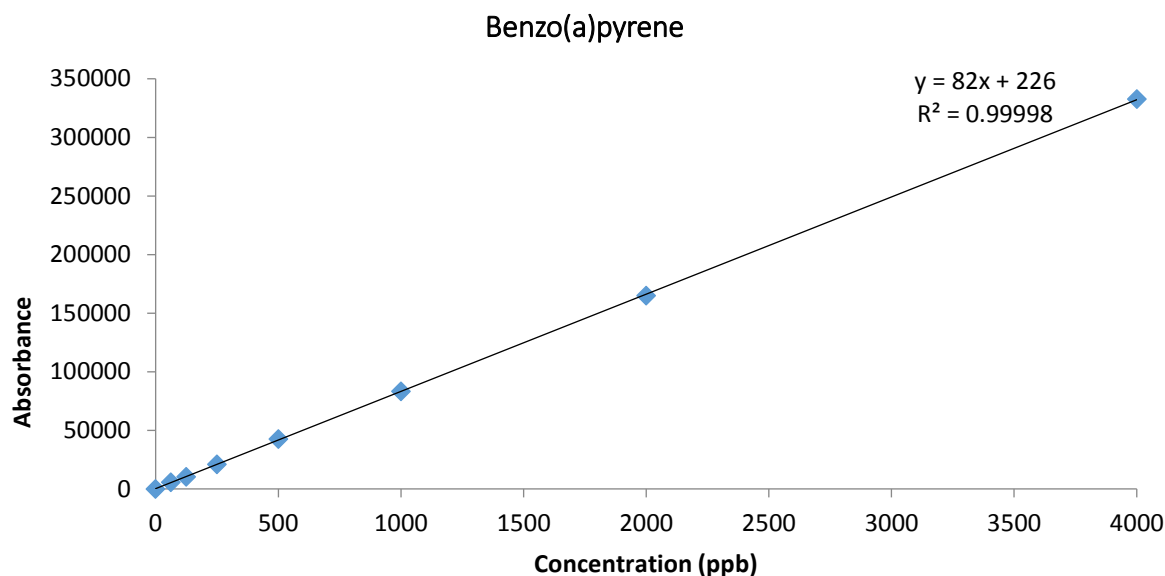
Benzo(b)fluoranthene	Concentration (ppb)	62.5	125	250	500	1000	2000	4000
	Absorbance	8387	15916	32743	65429	128274	256117	513894

A.13: Calibration curve for Benzo(b)fluoranthene. HPLC-UV system Mobile phase; acetonitrile:water. Flow rate; 1.5mL/min, UV detection at 220nm. n=3



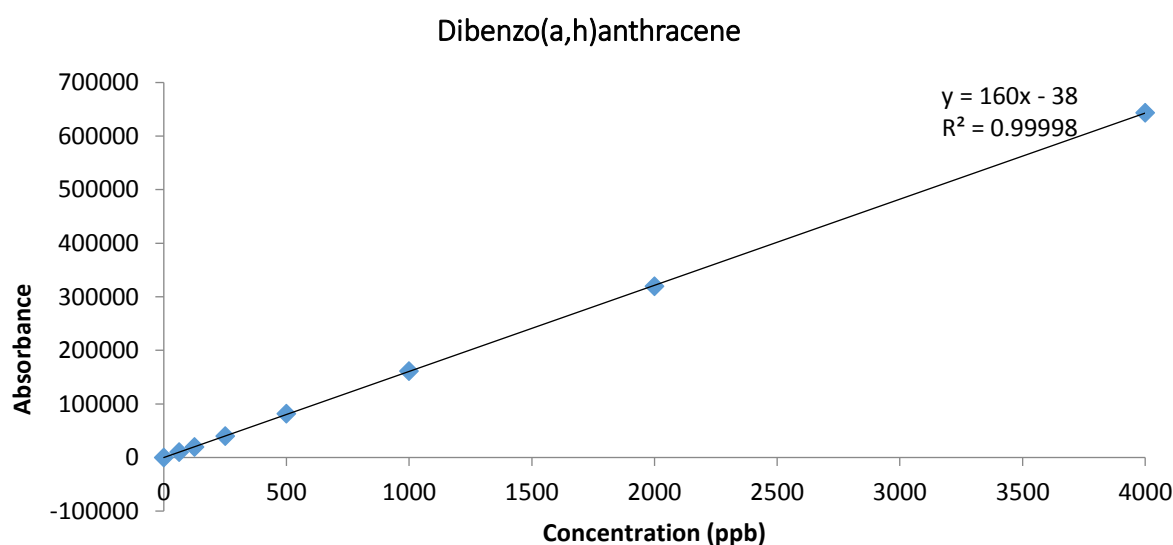
Benzo(k)fluoranthene	Concentration (ppb)	62.5	125	250	500	1000	2000	4000
	Absorbance	5474	10668	21464	43280	84642	167355	337935

A.14: Calibration curve for Benzo(k)fluoranthene. HPLC-UV system Mobile phase; acetonitrile:water. Flow rate; 1.5mL/min, UV detection at 220nm. n=3



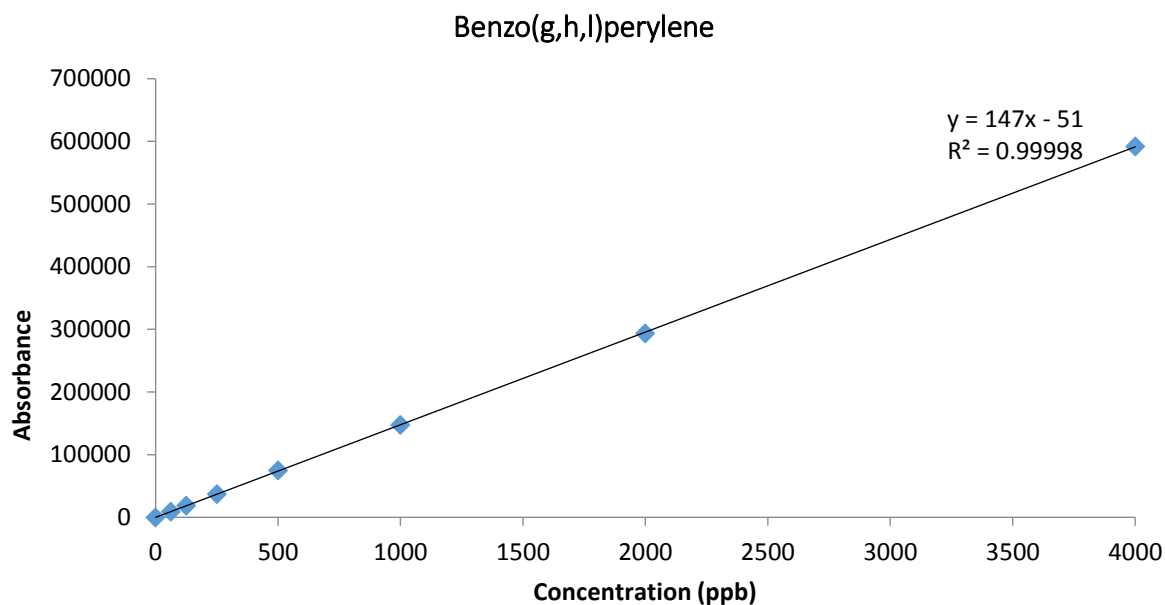
Benzo(a)pyrene	Concentration (ppb)	62.5	125	250	500	1000	2000	4000
	Absorbance	5614	10390	21005	42479	83331	165064	332579

A.15: Calibration curve for benzo(a)pyrene. HPLC-UV system Mobile phase; acetonitrile:water. Flow rate; 1.5mL/min, UV detection at 220nm. n=3



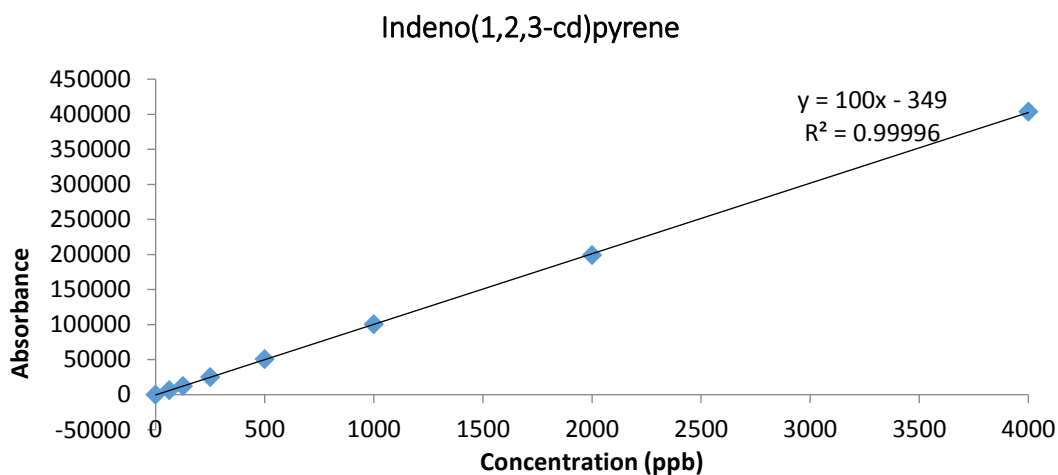
Dibenzo(a,h)anthracene	Concentration (ppb)	62.5	125	250	500	1000	2000	4000
	Absorbance	9967	19511	40187	81634	161119	319583	643668

A.16: Calibration curve for dibenzo(a,h)anthracene. HPLC-UV system Mobile phase; acetonitrile:water. Flow rate; 1.5mL/min, UV detection at 220nm. n=3



Benzo(g,h,i)perylene	Concentration (ppb)	62.5	125	250	500	1000	2000	4000
	Absorbance	9069	18500	36944	75013	147686	293720	592160

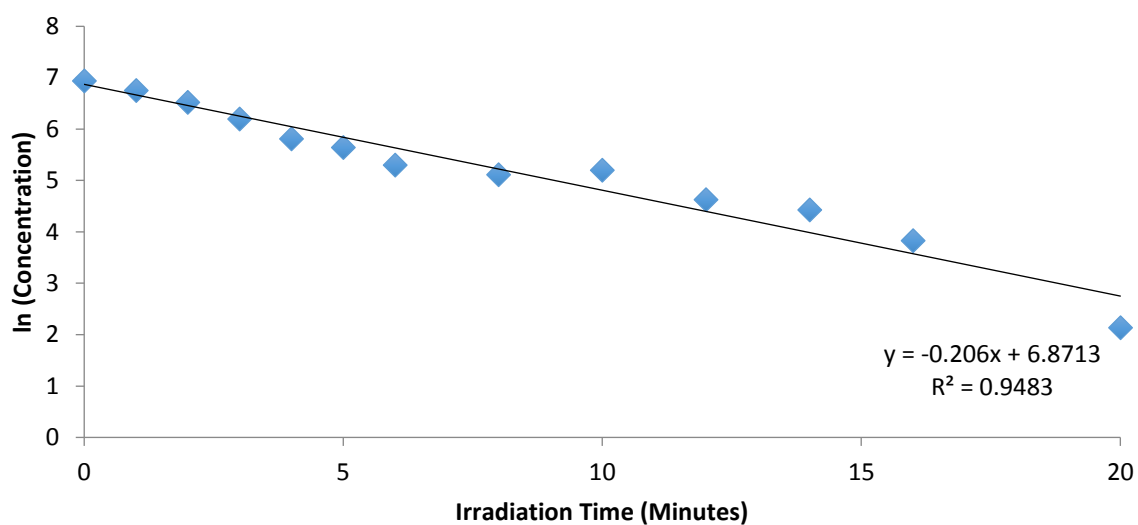
A.17: Calibration curve for Benzo(g,h,i)perylene. HPLC-UV system Mobile phase; acetonitrile:water. Flow rate; 1.5mL/min, UV detection at 220nm. n=3



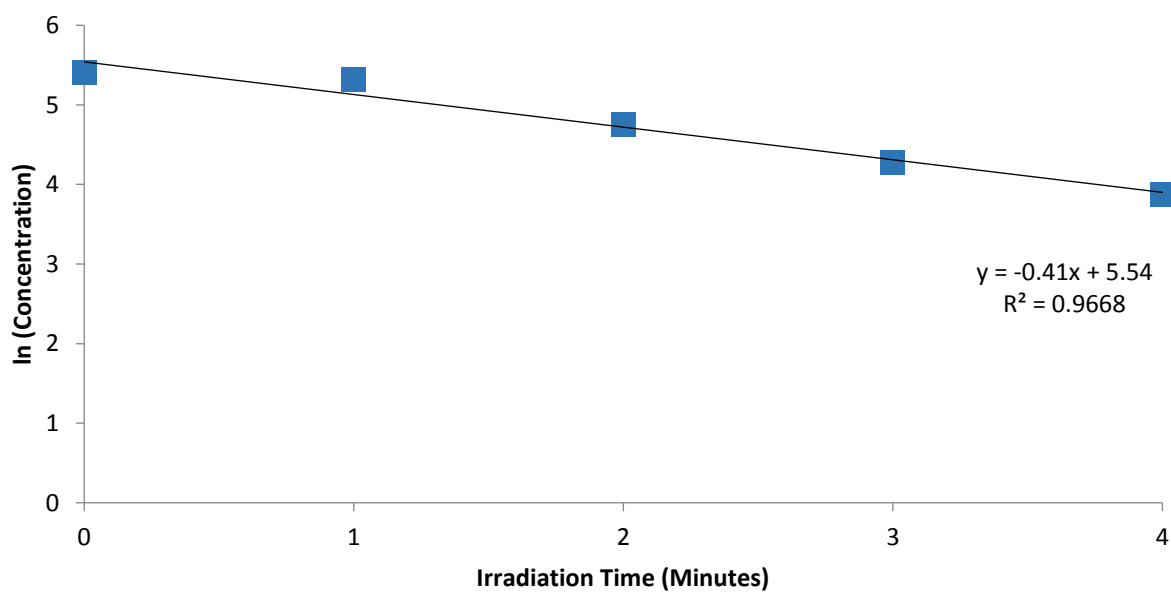
Indeno(1,2,3-cd)pyrene	Concentration (ppb)	62.5	125	250	500	1000	2000	4000
	Absorbance	6389	12075	24893	50427	100170	199113	403324

A.18: Calibration curve for Indeno(1,2,3-cd)pyrene. HPLC-UV system Mobile phase; acetonitrile:water. Flow rate; 1.5mL/min, UV detection at 220nm. n=3

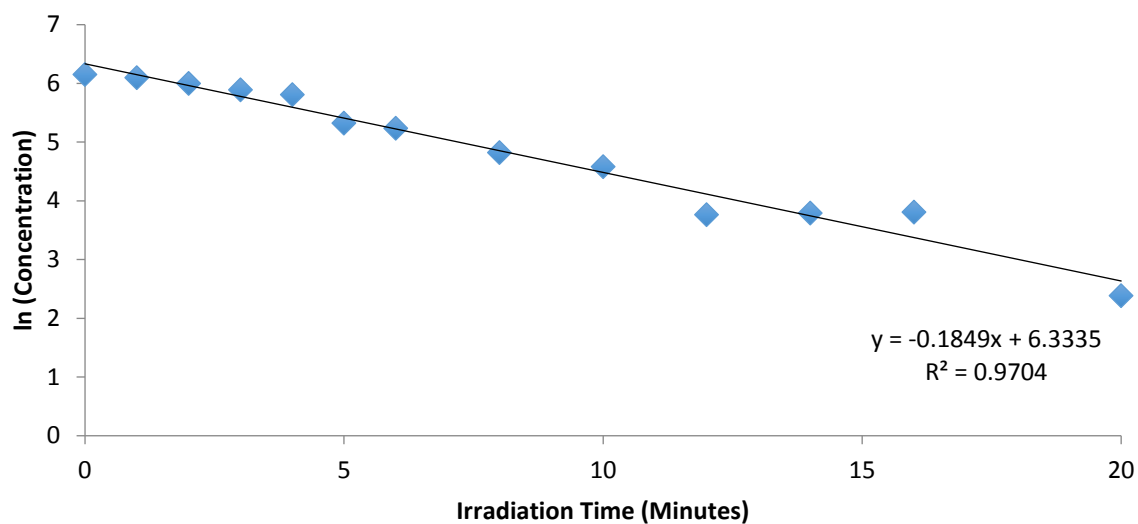
APPENDIX B



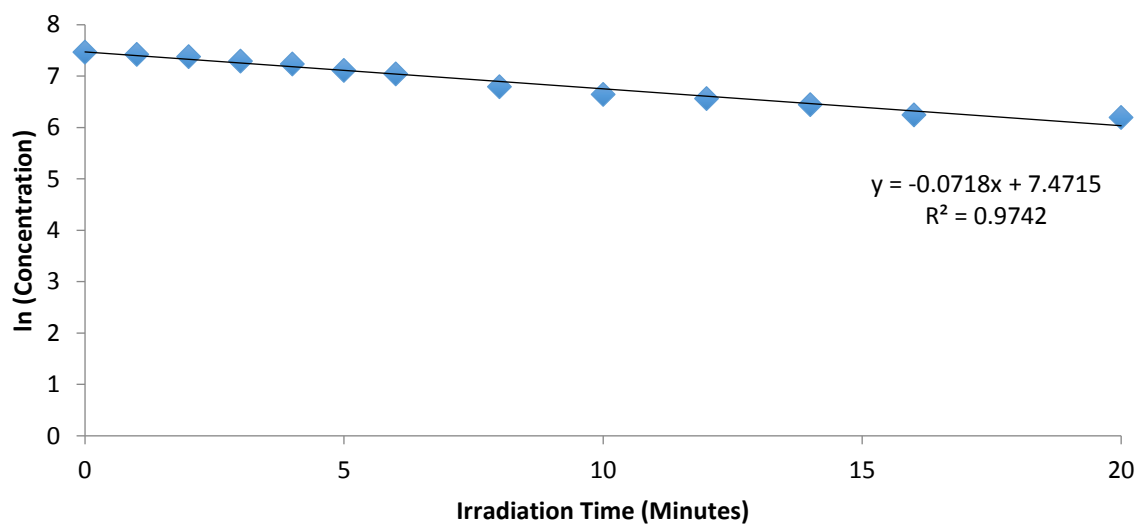
B.1: Pseudo-first-order reaction for the photodegradation of Naphthalene alone in water in SPR



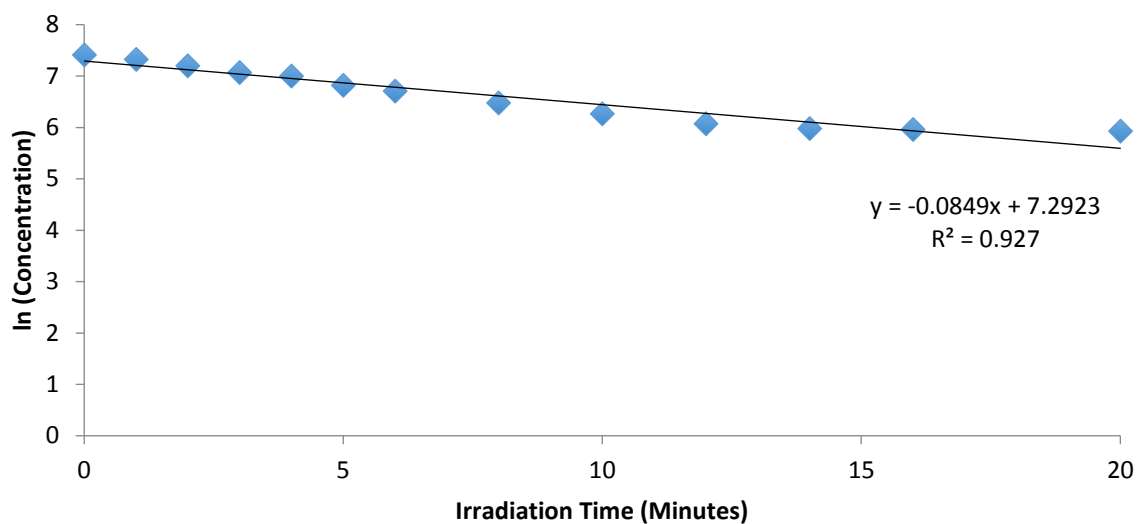
B.2: Pseudo-first-order reaction for the photodegradation of phenanthrene alone in water in SPR



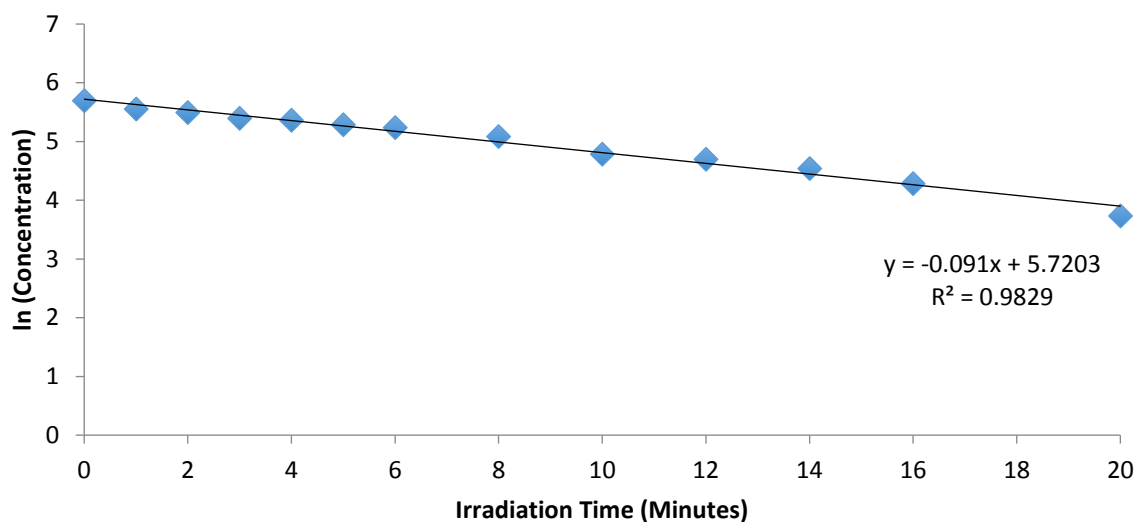
B.3: Pseudo-first-order reaction for the photodegradation of fluorene alone in water in SPR



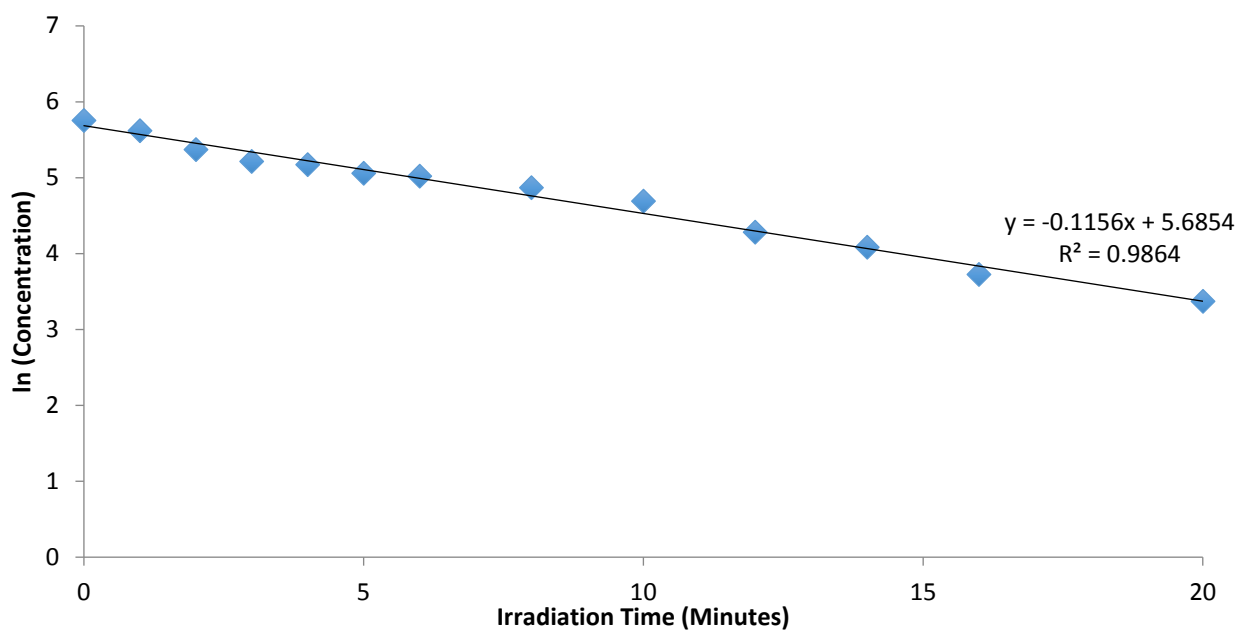
B.4: Pseudo-first-order reaction for the photodegradation of naphthalene in SIPR using TiO_2 sol gel A coating



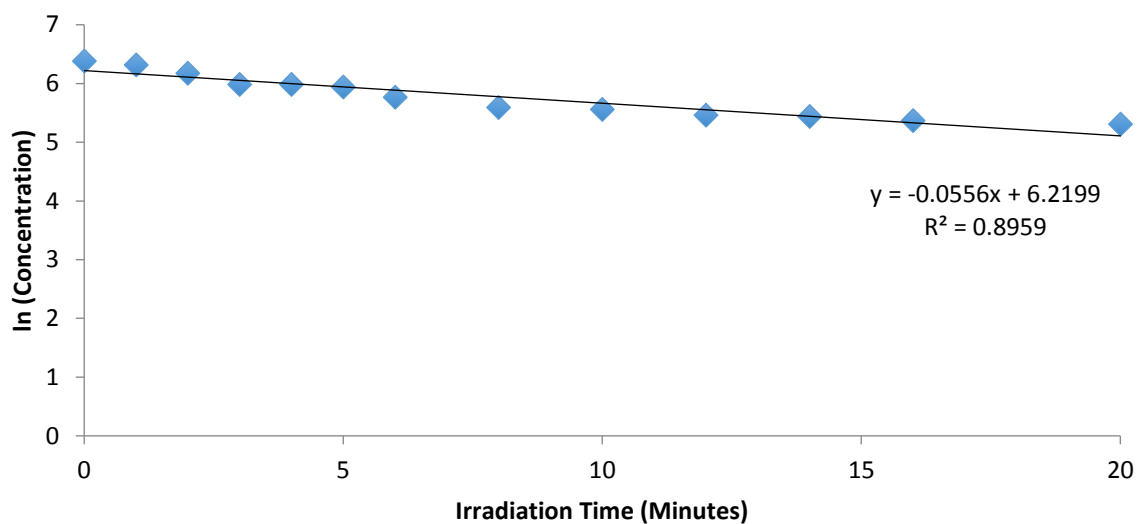
B.5: Pseudo-first-order reaction for the photodegradation of naphthalene in SIPR using TiO_2 sol gel B coating



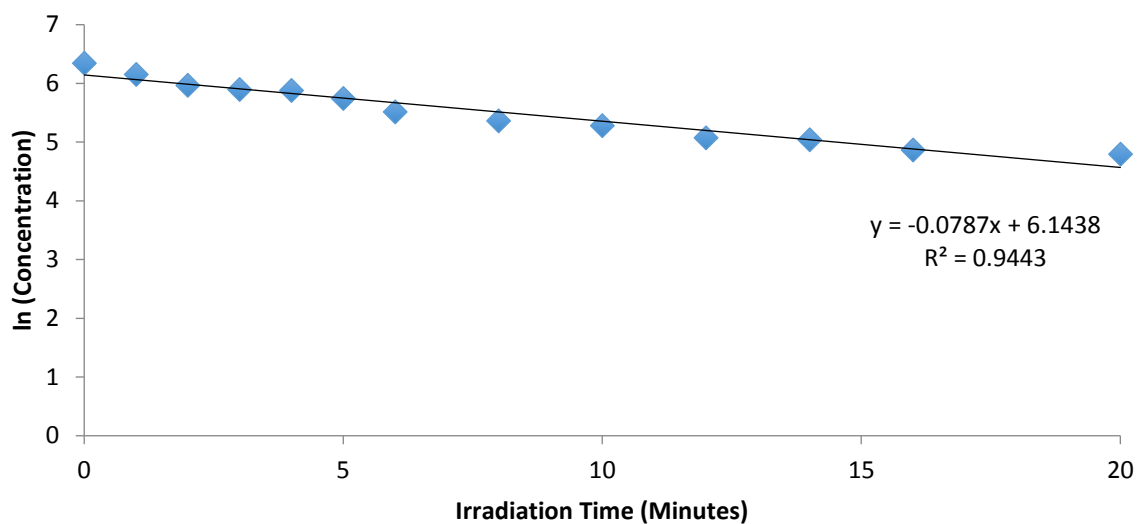
B.6: Pseudo-first-order reaction for the photodegradation of phenanthrene in SIPR using TiO_2 sol gel A coating



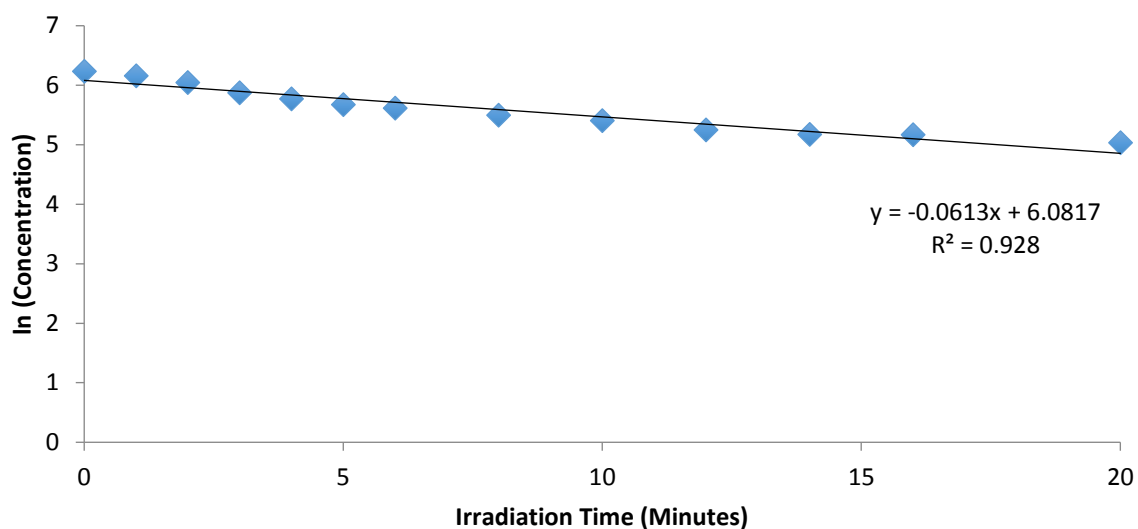
B.7: Pseudo-first-order reaction for the photodegradation of phenanthrene in SIPR using TiO₂ sol gel B coating



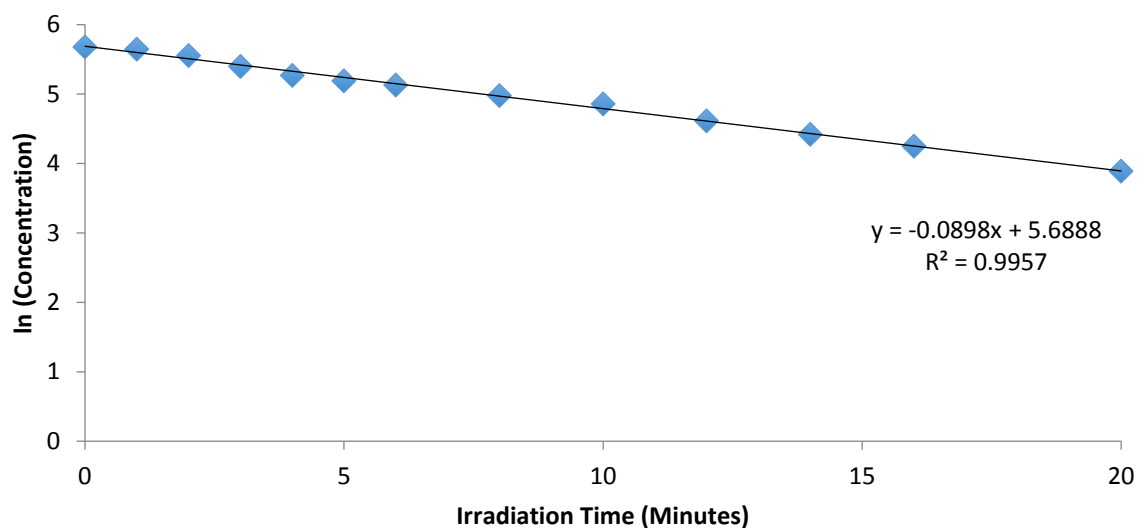
B.8: Pseudo-first-order reaction for the photodegradation of fluorene in SIPR using TiO₂ sol gel A coating



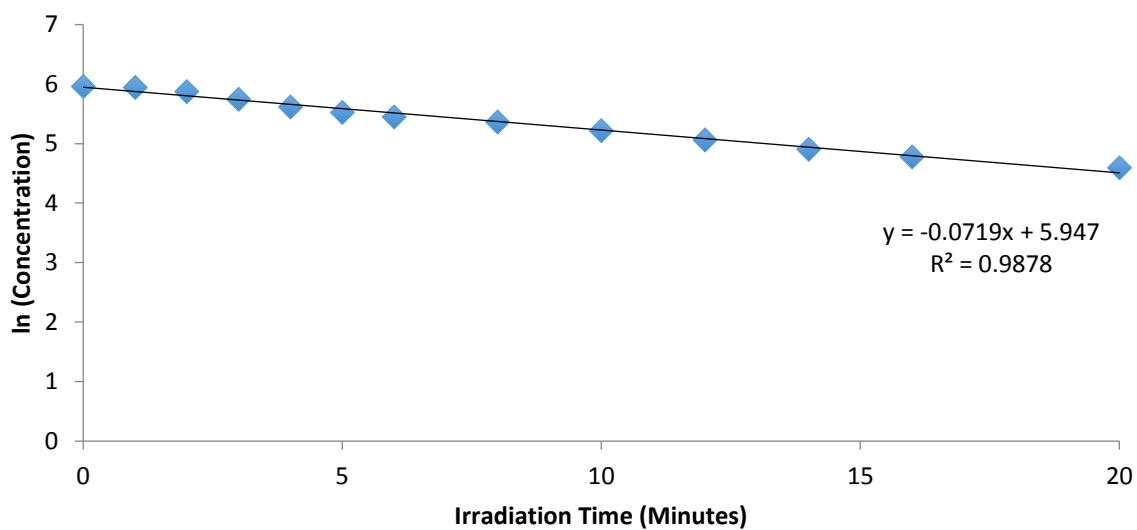
B.8: Pseudo-first-order reaction for the photodegradation of fluorene in SIPR using TiO_2 sol gel B coating



B.9: Pseudo-first-order reaction for the photodegradation of naphthalene in SIPR using TiO_2 sol gel A coating with phenanthrene and fluorene mixed in water



B.10: Pseudo-first-order reaction for the photodegradation of phenanthrene in SIPR using TiO_2 sol gel A coating with naphthalene and fluorene mixed in water



B.11: Pseudo-first-order reaction for the photodegradation of fluorene in SIPR using TiO_2 sol gel A coating with naphthalene and phenanthrene mixed in water